ENVIRONMENTAL GENETICS OF ROOT SYSTEM ARCHITECTURE

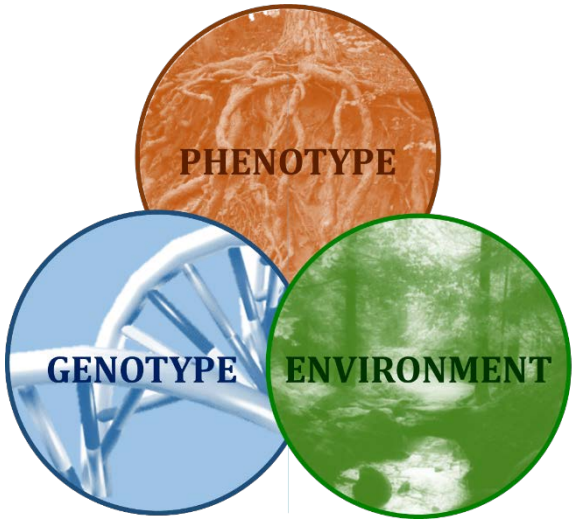

Thesis submitted for the degree of Doctor of Philosophy

by

Fabian Kellermeier

Dipl.-Biol.

Institute of Molecular, Cell and Systems Biology

College of Medical, Veterinary and Life Sciences

University of Glasgow

July 2013

ABSTRACT

The root system is the plant's principal organ for water and mineral nutrient supply. Root growth follows an endogenous, developmental programme. Yet, this programme can be modulated by external cues which makes root system architecture (RSA), the spatial configuration of all root parts, a highly plastic trait. Presence or absence of nutrients such as nitrate (N), phosphate (P), potassium (K) and sulphate (S) serve as environmental signals to which a plant responds with targeted proliferation or restriction of main or lateral root growth. In turn, RSA serves as a quantitative reporter system of nutrient starvation responses and can therefore be used to study nutrient sensing and signalling mechanisms.

In this study, I have analysed root architectural responses of various *Arabidopsis thaliana* genotypes (wildtype, mutants and natural accessions) to single and multiple nutrient deficiency treatments. A comprehensive analysis of combinatorial N, P, K an S supply allowed me to dissect the effect of individual nutrients on individual root parameters. It also highlighted the existence of interactive effects arising from simultaneous environmental stimuli. Quantification of appropriate RSA parameters allowed for targeted testing of known regulatory genes in specific nutritional settings. This revealed, for example, a novel role for *CIPK23*, *AKT1* and *NRT1.1* in integrating K and N effects on higher order lateral root branching and main root angle.
A significant contribution to phenotypic variation also arose from P*K interactions. I could show that the iron (Fe) concentration in the external medium is an important driving force of RSA responses to low-P and low-K. In fact, P and K deprivation caused Fe accumulation in distinct parts of the root system, as demonstrated by Fe staining and synchrotron X-Ray fluorescence. Again, selected K, P and Fe transport and signalling mutants were tested for aberrant low-K and/or low-P phenotypes. Most notably, the two paralogous ER-localised multicopper oxidases LPR1 and LPR2 emerged as important signalling components of P and K deprivation, potentially integrating Fe homeostasis with meristematic activity under these conditions.

In addition to the targeted characterisation of specific genotype-environment interactions, I investigated novel RSA responses to low-K via a non-targeted approach based on natural variation. A morphological gradient spanned the entire genotype set, linking two extreme strategies of low-K responses. *Strategy I* accessions responded to low-K with a moderate reduction of main root growth but a severe restriction of lateral root elongation. In contrast, *strategy II* genotypes ceded main root growth in favour of lateral root proliferation. The genetic basis of these low-K responses was then subsequently mapped onto the *A. thaliana* genome via quantitative trait loci (QTL) analysis using recombinant inbred lines derived from parental accessions that either adopt *strategy I* (Col-0) or *II* (Ct-1).

In sum, this study addresses the question how plants incorporate environmental signals to modulate developmental programmes that underly RSA formation. I present evidence for novel phenotypic responses to nutrient deprivation and for novel genetic regulators involved in nutrient signalling and crosstalk.

TABLE OF CONTENTS

LIST OF TABLES

LIST OF FIGURES

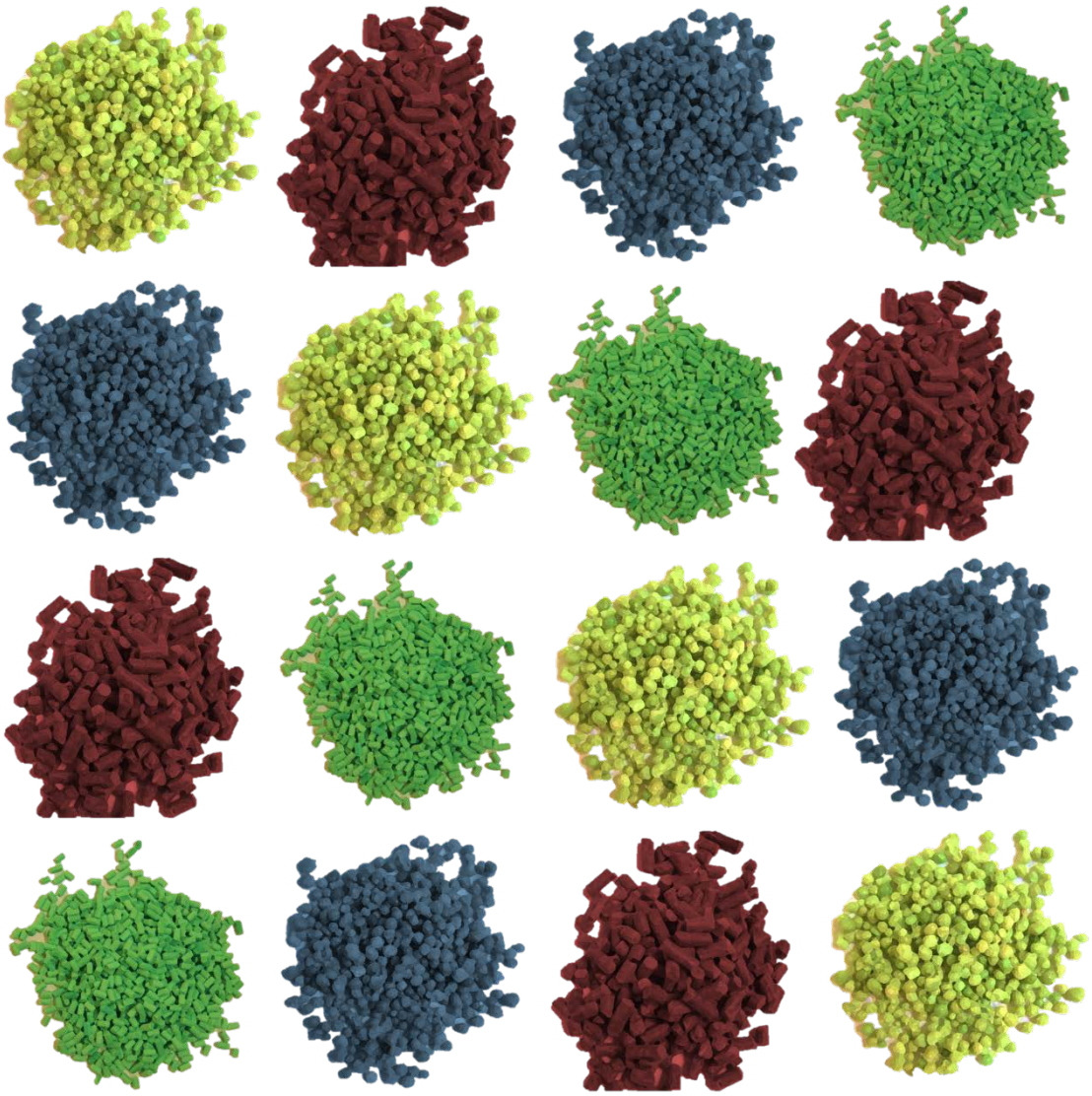

Gott mit dir, du Land der Baywa, deutscher Dünger aus Phosphat.

Über deinen weiten Fluren liegt Chemie von fruah bis spaat.

Und so wachsen deine Rüben, so ernährest du die Sau.

Herrgott, bleib dahoam im Himmi, mir hom Nitrophoskablau.

(Hans Well)

ACKNOWLEDGEMENTS

The Scottish Connection

I would like to thank:

My supervisor Dr Anna Amtmann for entrusting me with a complex project, for keeping me on a long leash working on this project, for all the support along the way and particularly the crucial moments, for giving me the opportunity to develop my research abroad, and particularly for being very understanding when it comes to personal circumstances.

My lab mates who have helped me with all the work on the bench and on the computer, particularly

Dr Giorgio Perrella thanks for answering every silly question, for keeping an eye on my stuff when I was away, for filling out all those online forms, for letting me contribute to your project, and for just being a good buddy and bench neighbour.

Dr Christopher Grefen thanks for all your advice on cloning, for providing vectors and scientific feedback.

Dr Cornelia Eisenach thanks for all the help with technical issues, especially the confocal microscope, for your highly valued feedback and for all those pints (with and without science being involved).

Dr Annegret Honsbein thanks for scientific input and feedback on my writing.

Naomi Donald thanks for all the technical work and advice you have given me, for putting up with my 'clicking-mood' and of course for shining like a princess – inside and outside.

Maria Papanatsiou thanks for keeping an eye on my plants when I was away, for scientific input and feedback on written work.

George Boswell thanks for the long, *scientific* discussions and for technical assistance.

Amparo Ruiz-Prado thanks for sowing, harvesting and keeping my plants as healthy as they could be.

Craig Carr thanks for all your help with plants, PCRs and Blots.

Liz O'Donnell thanks for helping me with plant tissue culture.

My friend (now Dr) Simon Bordage for resetting my clock at lunchtime, for science, non-science and non-sense talk and for strengthening *l'amitié franco-allemande*.

Prof Mike Blatt for hands on support with the microscope and for all the helpful comments on my project.

Prof Peter Dominy for introducing me to ICP-OES.

Dr Pawel Herzyk for microarray analysis.

Prof Hugh Nimmo and Dr Joseph Gray for advice and feedback in panel meetings.

My lab mates again, for making this time at the Bower great fun!

The rest of the Bower Crew for promoting the right work-life balance. Thanks for all the socials, all the quizzes and karaoke nights.

The Bower Football Team for not breaking my leg.

My wife Karin - wouldn't be here without you!

The American Connection

I would like to thank:

Prof. Mary Lou Guerinot for hosting me at Dartmouth College, for valuable input into my project and for inviting me into the hot tub.

Dr Tracy Punshon for taking me along to NSLS Brookhaven and thus enabling me to carry out SXRF experiments, for helping me with data analysis and for critical reading of paper manuscripts.

The Vogls, Sonia, Bob, Lin, Tad and Julie, for being fantastic hosts at the Funny Farm and in Geneva, IL. Thanks for showing us that passion and endurance can indeed make the world a better place – and make you happy. And thanks for organising everything: from cars to concerts.

Heidi Luquer for making me feel welcome – man, I loved that porch!

The Bavarian Connection – De boarisch Klitschn

Ich bin zu tiefstem Dank verpflichtet:

Meinen Eltern Maria und Günter, danke, dass Ihr mich immer in meinen Vorhaben unterstützt habt, in guten wie in turbulenten Zeiten.

Meinem Sohn Franz für die zusätzliche Motivation zum Abschluss dieser Arbeit.

Günni und Assi, für Eure herzliche Aufnahme während der Evakuation und für alle anderen Sachen, die Ihr für uns gemacht habt.

Der Feuerwehr, der Wasserwacht, den Gemeinden Niederwinkling und Mariaposching, dem THW, dem Dammkönig Sigi Heigl und allen anderen Helden vom Polder Sulzbach, die dafür gesorgt haben, dass uns im Juni 2013 das Donauwasser nicht bis zum Hals stand.

Karin, natürlich! Danke, dass Du immer zu mir gehalten hast und mich bei wichtigen Entscheidungen stets unterstützt hast. Danke, dass Du Verständnis aufgebracht hast für all die Zeit, die ich mit meinem Computer verbracht habe. Und danke fürs Korrekturlesen.

And finally: Thanks to **David Sainsbury** and the **Gatsby Foundation** for funding and for providing a fantastically friendly and stimulating academic environment.

AUTHOR'S DECLARATION

I declare that that this dissertation is the result of my own work except where explicit reference is made to the contribution of others. This thesis has not been submitted for any other degree at the University of Glasgow or elsewhere.

Part of this work has been published in the peer-reviewed, scientific journal *Plant Physiology* (chapter 4; Appendix I). Some parts of the methods section have been published as part of a *Methods in Molecular Biology* book edition (Appendix II). A third manuscript dealing with results presented in chapter 3 was in the process of being submitted for peer-reviewed publication by the time of thesis submission.

Fabian Kellermeier

ABBREVIATIONS

bp	base pairs
Ca	calcium
C/N	carbon / nitrogen ratio
EDTA	ethylenediaminetetraacetic acid
ER	endoplasmic reticulum
Fe	iron
FW	fresh weight
K	potassium
kb	kilobases
LR	lateral root
MES	4-morpholinoethanesulfonic acid
Mg	magnesium
MR	main root
N	nitrate
P	phosphate
ROS	reactive oxygen species
RSA	root system architecture
S	sulphate
TRIS	tris(hydroxymethyl)aminomethane

For abbreviations of root architecture parameters please see **Table 5** (Material and Methods section).

1. Introduction

1.1 Root system architecture analysis - tracing the hidden half

1.1.1 The roots of root research

Darwin - what comes to mind when reading this name? Probably 'the father of evolution'. Laying out his thoughts on evolution in *The Origin of Species* is of course what Charles Darwin is best known for. However, the theory of natural selection and adaptation also plays a central role in one of Darwin's other fields of interest: the perception of environmental signals by the plant root system. Indeed, by demonstrating the gravitropic response of root tips, he and his son Francis became 'the fathers of root research' (Darwin and Darwin, 1880; reviewed in Rich and Watt, 2013).

Since then, the root system has drawn the attention of many a plant scientist. In the beginning, roots were dug up and detailed drawings of the extension of root systems throughout the soil were produced (Weaver, 1925). The multitude of shapes encountered gave researchers a first idea on the ecological importance of root system architecture (RSA), the spatial configuration of all parts of the root system. More root scientists followed in those footsteps and made great efforts to bring the complex nature of root architecture from soil to paper, helping others in understanding the interplay of plant and soil as well as plant-plant competition for natural resources belowground (Fig. 1). Unforgotten is the Austrian scientist Lore Kutschera (1917 – 2008) whose '*Wurzelatlas*' (German for '*root atlas*') of central European species was first published in 1960. Still today, this and many follow-up *atlases* with special focus on e.g. crops, grasses or trees are benchmarks in many aspects of RSA research (cf. Fig. 1).

However, root research did not stop at the stage of documenting RSA of species in the wild. Weaver (1925) already contemplated the morphological variation of maize roots grown in two different types of soil. Hoagland and Arnon (1950) devised a soil-free cultivation method, today known as *hydroponics*, which they suggested to be particularly suitable for the study of mineral deficiency. Indeed, 'Hoagland's solution' is still widely used for exactly this purpose today. A landmark study concerned with environmental plasticity of root architecture was performed by Drew (1975) who demonstrated a targeted proliferation of barley secondary roots in nutrient rich patches.

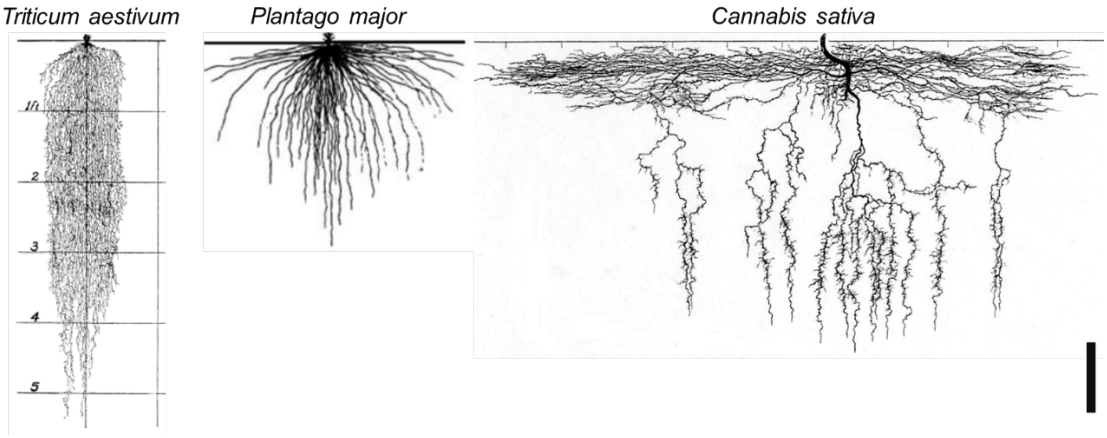

Figure 1: Root architecture phenotypes of three species drawn from plants grown in natural environments.
Images were adapted from Weaver (1925; *Triticum aestivum*) and Kutschera (1960; *Plantago major*, *Cannabis sativa*). Scale bar: 30 cm.

The subsequent breakthrough of modern molecular genetics shifted the research focus more towards the characterisation of root development, and many important components were identified by mutant analysis. However, the study of root responses to the environment equally benefitted from these technical advances. Major findings of this research will be summarized in sections 1.2 to 1.6.

1.1.2 Significance of the root system for plant viability and agriculture

During land plant evolution, root systems have taken on a whole array of important functions. First and foremost, they are the principal organ for water uptake in most non-aquatic plants. In addition to water they also extract essential mineral nutrients from the soil, including nitrate (N), ammonium, phosphate (P), potassium (K), sulphate (S), calcium (Ca), magnesium (Mg) and iron (Fe). Roots also anchor the plant, preventing it from being dislocated by wind, water or other mechanical disturbances. Many genera and families have evolved additional types of roots with specialised functions (Sitte et al., 2002). Some species use roots to colonise new territory by spreading in the subsurface and eventually forming new shoots. Aerial roots enable gas exchange for waterlogged and submerged parts of the plant. And of course in many plant species root organs serve as major storage units and therefore as important components of the human diet, like cassava, carrots or sugar beet.

A key role for environmental plasticity in root development has been diagnosed early on, as it allows the plant to optimise its foraging strategy by modulating its RSA. Significant impact of root architecture on P acquisition was discovered in bean about 20 years ago (Lynch, 1995). Later, selection of RSA traits has been recognized as a major driving force of historical yield increases in maize by raising water use efficiency (Hammer et al., 2008). Improving root growth and architecture of crops was even proposed as a central step to elicit a 'new green revolution' (Den Herder et al., 2010). The authors argue that *all* root research should be intensified, meaning that more knowledge needs to be gained from crops and model species alike.

Studies on the 'lab rat of plant science', *Arabidopsis thaliana* (also referred to as 'Arabidopsis' in the following), are indispensable because of the availability of an incomparable amount of genetic resources, the long experience of handling this species in the lab and the sheer amount of experimental data that are already available. Research on crops on the other hand has the great advantage of offering a direct link to crop improvement in the field. It is also important to note that RSA of dicotyledons like Arabidopsis, cabbage and tomato is quite different from that of monocotyledons which include all agronomically important cereals.

Biotechnological approaches to improve plant vigour and yield by specifically altering the root system are already in place but should be further developed (Ghanem et al., 2011). A traditional 'biotech' example is grafting where scions of one variety are joined with rootstocks of another. This technique is widely used in horticulture (e.g. fruit trees or grapevine) and the underlying physiology of grafted varieties is beginning to be understood (Gregory et al., 2013). However, modern biotechnology is also employed by organ- or tissue-targeted expression of important genes in transgenic plants (Ghanem et al., 2011).

1.1.3 Unearthing the root system: techniques to monitor root system architecture

An obvious constraint when studying roots is their preferred natural occurrence in an opaque, chemically complex environment: the soil. Hence, analysing root architecture for decades meant digging up at least part of the root system and start measuring from there (cf. Weaver, 1925; Kutschera, 1960). This technique is still in use today and is now traded under the name 'shovelomics' (Trachsel et al., 2011). Clearly, once a root system is literally unearthed, considerable damage has been done to it. In most cases that procedure actually marks the starting point as well as the end point of RSA analysis.

One way to overcome this limitation is by uncovering part of the root system in rhizotrons (Neumann et al., 2009). In this method at least one side of a growth container, if not all, are transparent and thus enable monitoring of those roots that touch the inside of the container. In recent years, most studies used a quite different approach: seedlings are grown on transparent, solidified growth media in transparent containers. Root growth in these systems can consequently be followed over time and quantified in non-invasive ways via imaging and subsequent computational image analysis. In the Arabidopsis community, the most widely adopted systems are derived from classic techniques of bacterial culture, i.e. growing seedlings on agar medium in transparent petri dishes. This two-dimensional projection of a 3D root structure onto a surface often makes use of semi-automated imaging tools that generate root trait data in a high-throughput fashion (Armengaud et al., 2009b; French et al., 2009; Brooks et al., 2010; Wells et al., 2012; Clark et al., 2013). However, novel gel tank platforms now also offer ways to collect 3-dimensional root phenotypic datasets (Fang et al., 2009; Iyer-Pascuzzi, 2010; Clark et al., 2011). One striking advantage of both methods is the absolute control of growth media composition.

An alternative solution is given by growth pouches, where roots are grown on a water-absorbing surface medium like paper, unfolded or rolled up into a tube and placed into a container with nutrient solution (Atamian et al., 2012). The probably most sophisticated way of quantifying root architecture in soil without mechanical disturbance is X-ray microcomputed tomography (Mairhofer er al., 2012). Here X-rays penetrate the soil and 3D RSA images are being reconstructed from scanned sections. Although this new technology allows for RSA quantification in a natural scenario, it is currently very expensive and far from high-throughput. Similarly, nuclear magnetic resonance imaging (MRI) and positron emission tomography coupled MRI (MRI-PET) are still at an early stage of development and have so far only been employed to study more functional aspects of water (Van As, 2007) and carbon dynamics (Jahnke et al., 2009).

Luckily, there are many ways to quantify RSA with current technology. The best choice of the system really depends on the research question.

1.2 Root development

In general, a typical dicotyledonous root can be regarded as a cylinder formed of several layers of tissues (only primary growth will be considered in the following; secondary growth in girth employs additional tissues and mechanisms). The outermost boundary is the epidermis which constitutes the root-soil interface (see also Fig. 4 for a longitudinal root section). Underneath lies the cortex and subsequently the endodermis which, due to its ligno-suberic polymers in the cell wall, represents a boundary for apoplastic transport of nutrients and water (Roppolo et al., 2011). Surrounded by the endodermal layer is the central vasculature (a.k.a. the stele) which is composed of phloem, xylem and pericycle.

The whole root structure is formed by the root apical meristem (RAM) which gives rise to undifferentiated stem cells that a) either maintain stem cell status and hence continue to form the RAM or b) differentiate into respective tissues. Root growth by cell division in the RAM is followed by cell expansion in the elongation and differentiation zone. The following sections will briefly summarize current knowledge on the formation and maintenance of the RAM.

1.2.1 Embryonic root development

Root development begins immediately after the oocyte is fertilised and the zygote has started to divide. Coordinated expression domains of several *WUSCHEL*-related homeobox (*WOX*) genes are a central factor in root embryonic patterning (Haecker et al., 2004). WOX transcription factors probably regulate gene expression of developmentally important target genes. However, other so far unknown mechanisms must be at work, since most *WOX* knockouts show no or only moderate morphological aberrations (Haecker et al., 2004).

The bottom part of the embryo, the suspensor (Fig. 2), connects the apical embryo to the maternal tissue. At this stage, basipetal auxin fluxes from the suspensor tip towards the centre of the embryo generate a gradient that is important for hypophysis formation (Friml et al., 2003). Several auxin responsive regulatory proteins are present in the proembryo central cells. Their action specifies the hypophysis which will ultimately become the RAM (Petricka et al., 2012). Amongst them are the transcription factor MONOPTEROS (MP), its interacting repressor the Aux/IAA protein BODENLOS (BDL) and the co-repressor TOPLESS (TPL; reviewed in Perilli et al., 2012). Knockouts of *MP*

and *BDL* completely fail to produce roots. MP itself is not present in the hypophysis but it has recently been shown to activate transcription of the bHLH transcription factor gene *TMO7* (Schlereth et al., 2010). TMO7 then moves into the hypophysis where it is sufficient for stem cell specification. Auxin is still needed for proper hypophysis formation but now flows into the opposite direction (Perilli et al., 2012). Acropetal auxin transport is controlled by MP-induced expression of PIN1 carrier proteins that mediate auxin efflux from the proembryo into the hypophysis (Weijers et al., 2006). Subsequent cell division of the hypophysis gives rise to the quiescent centre (QC) at the base and the columella founder cells at the bottom/apex (Perilli et al., 2012). At this stage, auxin and cytokinin form a relay that determines stem cell identity and differentiation (Müller and Sheen, 2008). Eventually, at heart stage, the main tissues needed to establish and to proliferate the primary root have already been formed (Fig. 2).

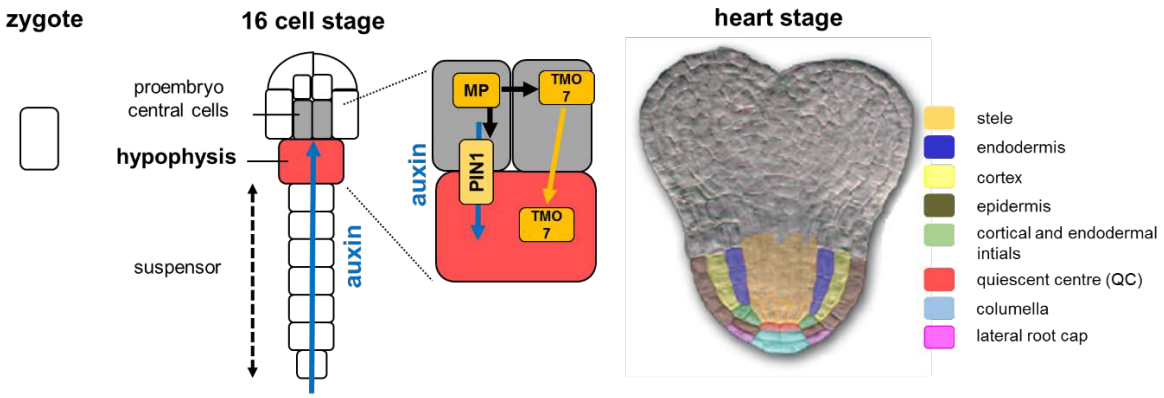

Figure 2: Embryonic root development.
Starting from the zygote, tightly coordinated cell divisions produce the proembryo which is connected to maternal tissue via the suspensor. A basipetal auxin gradient from the suspensor causes a maximum in central cells of the proembryo. Here, the transcription factor MONOPTEROS (MP) activates amongst others *TARGET OF MONOPTEROS 7* (*TMO7*) expression. TMO7 is itself a mobile bHLH transcription factor that moves into the adjacent hypophysis. Together with the auxin gradient now created by PIN1 auxin efflux carriers (expression also controlled by MP), TMO7 specifies the hypophysis which will eventually divide into the quiescent centre (QC) and the columella. At heart stage, embryonic root development has already produced all the main tissues needed for primary root establishment (adapted from Perilli et al., 2012).

1.2.2 Postembryonic root meristem establishment

Maintenance of the apical root meristem still largely depends on an auxin gradient from base to tip. This gradient is formed via the action of PIN efflux carriers (Blilou et al.,

2005). The interplay of several PIN members actually creates an auxin 'loop' in the root apex (Fig. 3A). This loop guarantees an auxin maximum in the QC and adjacent cells of the columella (Kepinski and Leyser, 2005; Grieneisen et al., 2007). Four *PLETHORA* (*PLT*) genes are directly involved in this process, probably acting as a readout of auxin concentrations (Aida et al., 2004; Galinha et al., 2007).

QC stem cell identity is maintained by WOX5, and QC expansion is restricted via CLE40, a CLAVATA3-like peptide, and the receptor kinase ACR4 (Stahl et al., 2009; Fig. 3B). Moreover, SCARECROW (SCR) and SHORTROOT (SHR) maintain and restrict *WOX5* expression in the QC (Helariutta et al., 2000; Sabatini et al., 2003; Sarkar et al., 2007). Recently, the distribution of SCR and SHR in cells surrounding the QC has been shown to be altered by phosphate starvation (Ticconi et al., 2009), linking nutrient supply to root development.

In addition to auxin signalling, auxin-cytokinin crosstalk is crucial for correct RAM size and patterning (Dello Ioio et al., 2008). The pathways summarized above illustrate the importance of maintaining the stem cell niche whilst restricting the meristem size, as patterning and differentiation is needed to produce a root cylinder composed of different tissues with different functions.

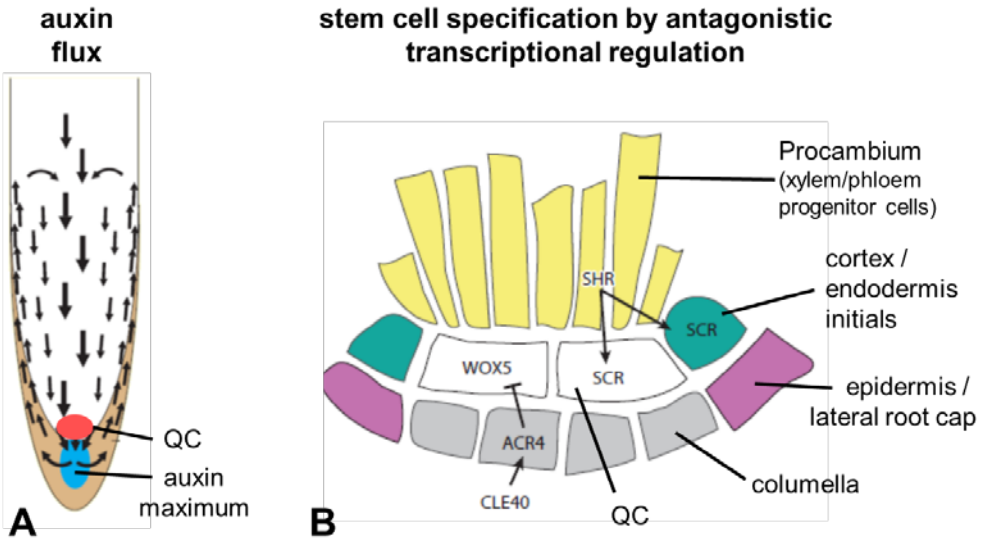

Figure 3: Mechanisms involved in postembryonic root development.
A) An auxin gradient creates an auxin maximum at the root tip via PIN-mediated transport (adapted from Kepinski and Leyser, 2005). **B)** Stem cell specification and RAM maintenance is regulated by several transcription factors, activators and repressors (adapted from Petricka et al., 2012). WOX5 and SCR (SCARECROW) maintain stem cell identity. *SCR* expression is restricted by SHR (SHORTROOT). In addition, ACR4 restricts WOX5. ACR4 is controlled by the CLAVATA3-like peptide CLE40. The signalling

pathways presented here are only a snapshot on a selected subset of factors. Further components are described in the text under section 1.2.3.

Apart from transcriptional activation/repression and protein-protein interaction, another important factor in RAM maintenance and modulation is the cellular redox status (Dunand et al., 2007). Changing the balance of different reactive oxygen species (ROS) was postulated to act as a switch for cellular differentiation. Since many environmental stresses have been shown to involve ROS signalling (Shin and Schachtman, 2007), a direct link between redox signalling and root growth, and hence root architecture formation, might be given. De Tullio et al. (2010) actually propose that ROS signalling is a downstream target of auxin. Moreover, the recently identified gene *UPBEAT1* (*UBP1*) closes the loop between transcriptional regulation and ROS mediated signalling (Tsukagoshi et al., 2010).

1.2.3 Root elongation, differentiation and lateral root branching

Aside of characterising the formation and function of the RAM, equally hard work has been put into unravelling the mechanisms behind root elongation, differentiation and lateral root development. Fig. 4A gives an overview of the tissues forming the apical part of the main root (MR).

Developing roots are typically sub-divided into several root zones. The root cap and the RAM are at the very forefront. Next follows the transition zone where cells are prepared for elongation and differentiation. This zone has been proposed as an important 'nexus' that controls root development as well as environmental responses by generating and modulating the 'auxin fountain' (Fig. 3A) through PIN-mediated transport and PIN-trafficking (Baluska et al., 2010). Moreover, together with the RAM, this is also the site of central vasculature (stele) differentiation into xylem, phloem and pericycle. Radial patterning of the vasculature employs mutually inhibitory crosstalk between auxin and cytokinin signalling pathways (Bishopp et al., 2011).

Subsequently, cells grow to their final length in the elongation zone. In a review article describing the action of phytohormones in the various root zones, Ubeda-Tomas et al. (2012) emphasize the central role of gibberellin (GA) in regulating cell expansion. In fact, GA was shown to be mainly acting on endodermal cell elongation (Ubeda-Tomas et al., 2008). By expression of gain-of-function *gai* DELLA proteins, which are negative regulators in GA pathways, GA signalling in the endodermis was blocked, and this was sufficient to inhibit elongation of the whole primary root. Again, auxin signalling was demonstrated to be involved in elongation responses of epidermal cells (Swarup et al., 2005). However, auxin appears to be mainly acting on gravitropic bending.

Cells acquire their ultimate shape and function in the differentiation zone. The last apical root zone is sometimes also referred to as 'root hair differentiation zone' as this is the site where epidermal cell files form root hairs.

Lateral root (LR) development starts synchronously to other tissue differentiation processes in the 'basal meristem' which is the zone just behind the RAM (Peret et al., 2009). LRs originate from the pericycle, the outermost cell layer of the stele. In dicots like Arabidopsis, only cells of the xylem pole pericycle, i.e. pericycle cells that overlay the xylem, are able to originate LRs whereas in cereals this is done by the phloem pole pericycle (Nibau et al., 2008). Xylem pole pericycle cells advance to G2 phase after they have exited the RAM, meaning that they still possess the ability to further divide (Peret et al., 2009).

An oscillating auxin gradient generates auxin maxima in the basal meristem (Fig. 4B) which in regular intervals primes xylem pole pericycle cells to become lateral root primordia (De Smet et al., 2007). The presence of auxin targets the Aux/IAA repressor IAA14 (aka SOLITARY ROOT 1) for TIR1 or AFB-mediated degradation by the proteasome (Peret et al., 2009), thus activating a pathway that is largely controlled by auxin response factors ARF7 and ARF19 (transcription factors). But auxin not only regulates cell divisions and elongation in the forming lateral root primordium (Fig. 4C). It also ensures locally restricted cell wall modifications of the overlaying main root tissue that enable LR primordia to 'break through' to the surface (Peret et al., 2009). The main gene involved in this response is *LAX3* (Swarup et al., 2008).

It should be noted that other phytohormones such as cytokinin brassinosteroids and ethylene are also part of the LR development machinery (Nibau et al., 2008). Subsequent LR emergence is promoted by further cell division in the LR apical meristem followed by cell elongation, probably employing similar mechanisms as described for the main root. Its high degree of responsiveness to environmental cues like nutrient conditions makes LR development a central process in RSA plasticity (Nibau et al., 2008). This will be examined in more detail section 1.5.

Last not least, integrated experimental work and modelling connected main root bending directly with lateral root formation (cf. also De Smet et al., 2007). Laskowski et al. (2008) showed that waving of the *A. thaliana* (referred to as 'Arabidopsis' in the following) primary root grown on a 2D surface alters cell shape and hence auxin transport patterns which in turn produces an auxin maximum in pericycle cells at the outer side of the bend and consequently triggers LR development as described above. Indeed, the

resulting phenotype is visible at the macroscopic scale, as lateral roots typically emerge at the vertex of main root curves.

In sum, root development relies on a complex gene network and is largely controlled by auxin gradients and signalling. However, many other factors, e.g. cytokinin, other hormones and environmental signals, also play an important role in main and lateral root formation. The following section will now summarize knowledge on one of the root's principal functions: providing the plant with mineral nutrients from the surrounding medium (soil). Subsequently, established sensing and signalling pathways that control physiological and metabolic responses to nutritional cues will be examined in section 1.4. The morphological effect of such signals on root growth and architecture will be introduced in section 1.5.

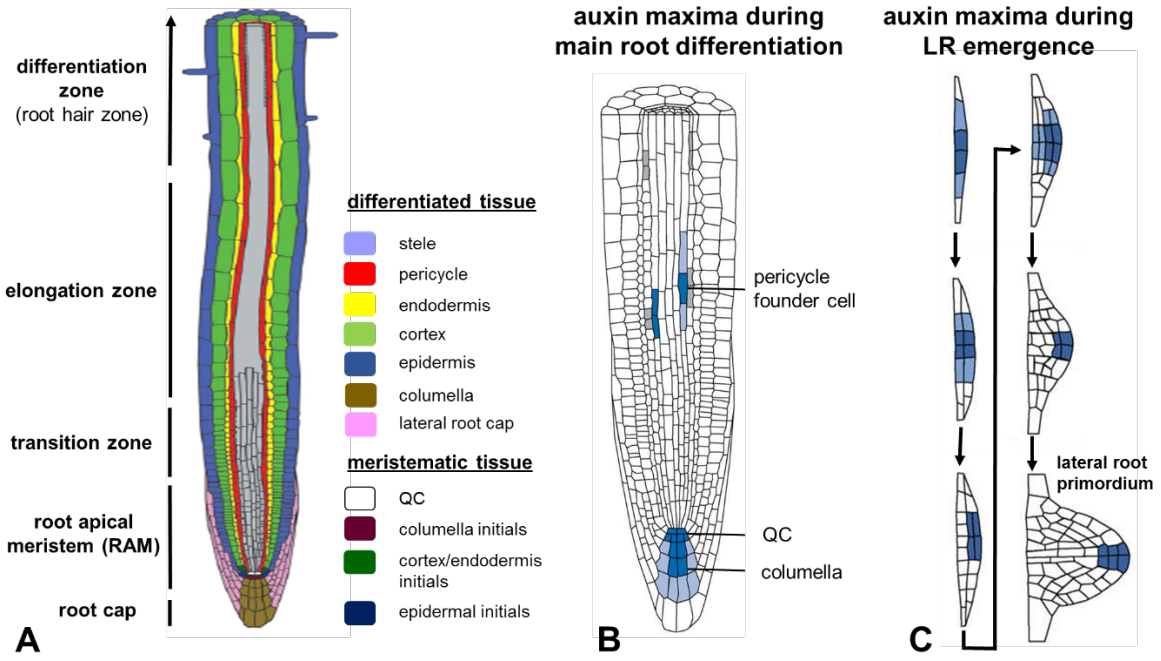

Figure 4: Pattering of the main root and lateral root formation.
A) Zoning and tissue differentiation in the developing main root (adapted from Ubeda-Tomas et al., 2012). **B)** Auxin maxima (in blue) in the pericycle prime individual cells that **C)** develop into lateral root primordia in a specific pattern of cell divisions. An auxin gradient also determines the site of the emerging lateral root tip. B) and C) adapted from Peret et al. (2009).

1.3 Plant mineral nutrition

1.3.1 Relative importance of mineral nutrients

In addition to water and carbon, which is supplied via photosynthesis, plants need a whole range of nutrients for proper metabolism and growth. Most of them are taken up from soil via the root system. Mineral nutrients can be classified into three categories: 1) essential, 2) non-essential but beneficial and 3) detrimental or toxic. In total, 14 minerals have been proposed to be essential for plant nutrition (Table 1; White and Brown, 2010).

Table 1: Critical leaf concentrations of 14 essential elements in plant nutrition.
Critical 'sufficient' leaf concentrations denote the quantified concentration in a diagnostic tissue that allows the plant to produce > 90 % of its maximum yield potential (as per White and Brown, 2010). 'Toxic' concentrations are determined in the same way and refer to the concentrations at which maximum yield is decreased > 10 %. Data is an overview for plant species that are not tolerant to extreme concentrations of specific elements ('non-accumulators'). Values are taken from White and Brown (2010).

	leaf concentration [mg / kg DW]	
Element	**sufficient (adequate)**	**toxic**
Nitrogen	15 - 40	
Potassium	5 - 40	> 50
Phosphorus	2 - 5	> 10
Sulphur	1.0 - 5.0	
Calcium	0.5 - 10	> 100
Magnesium	1.5 - 3.5	> 15
Chlorine	0.1 - 6.0	4 - 7
Iron	50 - 150 $\times 10^{-3}$	> 0.5
Boron	5 - 100 $\times 10^{-3}$	0.1 - 1.0
Zinc	15 - 30 $\times 10^{-3}$	100 - 300 $\times 10^{-3}$
Manganese	10 - 20 $\times 10^{-3}$	0.2 - 5.3
Copper	1 -5 $\times 10^{-3}$	15 - 30 $\times 10^{-3}$
Nickel	0.1 $\times 10^{-3}$	20 - 30 $\times 10^{-3}$
Molybdenum	0.1 - 1.0 $\times 10^{-3}$	1.0

Nitrogen, potassium, phosphorus and sulphur are the four quantitatively most important mineral nutrients. This is not surprising as nitrogen, phosphorus and sulphur are structural components of basic metabolites such as amino acids, nucleotides, phospho- and sulpholipids. They are also part of many regulatory substances, like phytohormones, redox buffers (e.g. glutathione) or energy storage molecules (e.g. ATP, GTP), and many secondary metabolites (Maathuis, 2009).

Potassium (K) on the other hand is not incorporated into any chemical compounds, but it is needed as the main osmoticum for cell expansion and for many physiological processes (e.g. enzyme function, control of stomatal aperture; Amtmann et al., 2006; Aleman et al., 2011). Calcium (Ca) is an important secondary messenger in cellular signalling and hence its cytoplasmic concentration is tightly controlled (Amtmann and Blatt, 2009). Magnesium (Mg) constitutes the central ion in chlorophyll and is essential for energy metabolism and DNA synthesis. Chloride (Cl) acts as an anionic osmoticum, e.g. in stomatal opening and closure (Amtmann and Blatt, 2009), and is of general importance in pH and membrane potential stabilisation (Tejada-Jimenez et al., 2009).

Essential micronutrients are present at much lower concentrations (cf. Table 1: iron to molybdenum). Elements of this group generally fulfil a role as co-factors in enzyme complexes. Iron (Fe) for instance mediates many cellular redox processes as the central ion of heme or Fe-S cluster containing enzymes that are part of the electron transport chain in chloroplasts and mitochondria (Palmer and Guerinot, 2009). Similarly, copper (Cu) also elicits redox activity, e.g. as a co-factor in plastocyanin and multicopper oxidases (Svistoonoff et al., 2007; Palmer and Guerinot, 2009). Manganese (Mn) is needed for oxygen release in photosystem II and for ROS-detoxification in superoxide dismutase (White and Brown, 2010). Two other heavy metals, nickel (Ni) and molybdenum (Mo), are only needed in trace amounts because their function as co-factors is restricted to urease (Ni), sulphite oxidase (Mo), aldehyde oxidase (Mo), xanthine dehydrogenase (Mo) and nitrate reductase (Mo; Tejada-Jimenez et al., 2009). Although it is well established that boron (B) deficiency has a broad range of detrimental phenotypes, and hence B is essential for plant nutrition, it is not well understood how B acts on the molecular level.

The following section will briefly introduce the basics of mineral nutrient transport. In my PhD thesis, I have focussed on nitrogen in the form of nitrate (N), phosphorus in the form of phosphate (P), potassium (K), sulphur as sulphate (S) and iron (Fe). Only transport of these nutrients will be considered. These ionic nutrients will be abbreviated by their respective elemental identifier (see also Table 2).

Table 2: Abbreviations used for nutrients examined in this study.
Please note that letters do *not* abbreviate the chemical element.

nutrient	chemical form	abbreviation
nitrate	NO_3^-	**N**
phosphate	HPO_4^{2-} and $H_2PO_4^-$	**P**
potassium	K^+	**K**
sulphate	SO_4^{2-}	**S**
iron	Fe^{2+} and Fe^{3+}	**Fe**

1.3.2 Mineral transport

1.3.2.1 Nitrate (N) transport

Aside of carbon input via photosynthesis and water uptake, nitrogen in the form of nitrate (here referred to as 'N'; Table 2) is regarded as the most important abiotic factor limiting agriculture in temperate climates (Chapman and Miller, 2011). Nitrate is taken up at the root epidermal plasma membrane via specialised transporters of the NRT1 and NRT2 families (Miller et al., 2009). The two most important members of either group are NRT1.1 and NRT2.1. The putative nitrate transceptor NRT1.1 (aka CHL1) has a dual role as transporter and receptor (hence 'transceptor') and acts with dual affinity for low and high external N concentrations (Liu and Tsay, 2003; Ho et al., 2009; see also 1.4.2).

NRT2.1 encodes a high-affinity transport system (HATS), and consequently its expression is upregulated when external N concentrations are low (Wirth et al., 2007; Chapman and Miller, 2011). It is also rapidly induced when N becomes available after a period of complete N absence (Ho et al., 2009). The NAR2.1 protein has been shown to form a complex with NRT2.1 that is essential for full HATS activity (Wirth et al., 2007; Yong et al., 2010). Recently, it has been verified that posttranscriptional regulation is the main driver of *NRT2.1* / *NAR2.1* HATS function (Laugier et al., 2012). Moreover, NRT2.1 fulfils a role in morphological responses to low nitrate (Remans et al., 2006b; see also section 1.4.2).

The *NRT2.1* / *NAR2.1* system is complemented by *NRT2.4* which is also induced under N deficiency (Kiba et al., 2004). Root-to-shoot transport is mediated by NRT1.5 which loads N into the xylem (Lin et al., 2008). NRT1.9 is a phloem N transporter that

probably controls N remobilisation and redistribution (Wang and Tsay, 2011). Finally, the vacuolar localised NRT2.7 is important for N storage in seeds (Chopin et al., 2007).

Intracellular N homeostasis is regulated by members of the CLC anion/proton antiporter family (Miller et al., 2009). Although the existence of more than one gene has been suggested (Miller et al., 2009), *CLCa* was identified as the first one in this family encoding a nitrate specific vacuolar transporter (De Angeli et al., 2006).

Inside the plant, nitrate is reduced to ammonium and incorporated into amino acids. Consequently, a whole range of amino acid and peptide transporters contributes to nitrogen transport and allocation within the plant. Background knowledge on the latter transporter group is not essential for this thesis. The interested reader shall be referred to a comprehensive list of Arabidopsis nitrate and peptide transporters that has been collated by Tsay et al. (2007).

1.3.2.2 Phosphate (P) transport

In Arabidopsis, five classes of phosphate (P) transporters have been characterised to date (Remy et al., 2012). P uptake from the environment is the function of members of the *PHT1* class (Nussaume et al., 2011). This gene family consist of 9 genes in total and all PHT1 members are P-proton co-transporters. A review by Nussaume et al. (2011) summarises results that show the expression of eight *PHT1* genes (all but *PHT1;6*) in the root hair zone of Arabidopsis. However, PHT1;1 and PHT1;4 are probably the two most important root-localised PHTs since they are responsible for both low- and high-affinity P uptake from the soil (Shin et al., 2004). P limitation is a naturally widely occurring phenomenon and bioavailable P concentrations hardly exceed 10 µM (Nussaume et al., 2011). Hence, high-affinity transport seems to be the physiologically most relevant process. *PHT1;2* and *PHT1;3* are also expressed in roots, but mainly in older parts of the main root and lateral roots (Nussaume et al., 2011). In addition, *PHT1;8* and *PHT1;9* are induced under P starvation and act as high-affinity uptake systems (Remy et al., 2012).

Remobilisation of P from source to sink organs is controlled by PHT1;5 (Nagarajan et al., 2011). Intracellular P-distribution is mediated by transporters of the plastidic P transporter family (Knappe et al., 2003). *PHT3* members encode mitochondrial P translocators (Takabatake et al., 1999). *PHT2;1* and *PHT4* family genes encode chloroplast-located transporters (Versaw and Harrison, 2002; Guo et al., 2008).

1.3.2.3 Potassium (K) transport

K is taken up by a whole range of transporters and channels acting as low-affinity or high-affinity systems. A major contributor to root K uptake is the Shaker-type inward rectifying channel AKT1 (Hirsch et al. 1998; Aleman et al., 2011). Nevertheless, *akt1* knockout mutants grow normally in millimolar (mM) external K concentrations, suggesting that sufficient K is taken up through other transporters. Members of the CHX family, cyclic nucleotide gated channels (CNGC) and glutamate receptor-like channels (GLR) have been proposed to fulfil just that function (Aleman et al., 2011). Growth of *akt1* mutants is strongly impaired in low micromolar (µM) K concentrations ('high-affinity range'), but only if high-affinity transporters are inhibited by ammonium (see below). Uptake capacity for K through AKT1 in these conditions is provided by a very low membrane potential, which provides a driving force for passive, channel-mediated K-uptake even at very low K concentrations.

AKT1 is voltage-gated, meaning that its open probability depends on the membrane potential (Amtmann and Blatt, 2009). As an inward rectifier, its open probability is increased when the membrane is hyperpolarised e.g. in low external K. The voltage sensor domain consists of a charged transmembrane helix that is believed to move in response to changes in membrane potential thus altering the conformation of the channel pore (Dreyer and Blatt, 2009).

K uptake by AKT1 is also regulated by a variety of other processes. First, phosphorylation of AKT1 via the CBL-interacting protein kinase CIPK23 activates AKT1 at low external K concentrations following this sequence: a cytoplasmic Ca-signal promotes binding of CBLs (particularly CBL1 and CBL9) to CIPK23 which then interacts with AKT1 and promotes its phosphorylation (Xu et al., 2006). Dephosphorylation via the phosphatase AIP1 in turn inactivates the channel (Lee et al., 2007). Additionally, AKT1 interaction with the 'silent' channel subunit KC1 negatively regulates AKT1 function (Duby et al., 2008; Wang et al., 2010b). Research in the Blatt Lab at the University of Glasgow has shown that another component is involved in forming a 'tripartite' channel complex needed for native gating properties: the SNARE protein SYP121 (Honsbein et al., 2009). Other Shaker-type channels regulate long-distance K transport in the xylem (SKOR; Gaymard et al., 1998) and guard cell function (GORK; Ache et al., 2000).

In Arabidopsis, high-affinity uptake in roots is mediated by the KT/HAK/KUP transporter family. HAK5 is the main uptake component at very low external concentrations (< 10 µM; Rubio et al., 2008; Qi et al., 2008). Indeed, experiments using the K analogue Rb showed that transport via HAK5 is able to deplete external Rb

concentrations down to about 1 µM (Rubio et al., 2008). Transcriptional regulation of *HAK5* is well documented, most notably a strong upregulation of expression in low-K (Armengaud et al., 2004). However, HAK5 transport is blocked by ammonium (NH_4^+) ions. In the presence of NH_4^+, K uptake at external K concentrations below 50 µM is solely mediated by AKT1 (Rubio et al., 2010).

1.3.2.4 Sulphate (S) transport

Fourteen members, dividing into 5 subclasses, form the SULTR family of sulphate (S) transporters in Arabidopsis (Buchner et al., 2004). These proteins function in both S uptake from the soil as well as S distribution within the plant.

The main components of high-affinity (HA) S uptake from the external medium are SULTR1;1 and SULTR1;2 which are expressed in the root epidermis and cortex (Yoshimoto et al., 2002; Gojon et al., 2009). Albeit their structural similarity, both HA systems appear to be differentially responsive to local and global S supply and demand (Rouached et al., 2008). Nevertheless, local S sensing appears to be the stronger signal for *SULTR1;1* and *SULTR1;2* up-regulation (Hubberten et al., 2012). Moreover, mutant analysis of single and double knockouts revealed an unequal functional redundancy between both transporters (Barberon et al., 2008). To date, the exact role in high- and low-affinity phases of either uptake system in not fully deciphered.

Other members of the SULTR family are responsible for long-range phloem transport (SULTR1;3, SULTR2;1, SULTR2;2; Gojon et al., 2009). SULTR3;5 in contrast, was shown to enhance transport capabilities of SULTR2;1 in low-S conditions but it had none by itself (Kataoka et al., 2004a). Intracellular distribution and S remobilisation from storage vacuoles is achieved by the two tonoplast-localised efflux transporters SULTR4;1 and SULTR4;2 (Kataoka et al., 2004b).

1.3.2.5 Iron (Fe) transport

Fe^{3+} [Fe(III)] is the predominant form of Fe in the soil but it is mainly bound in hardly soluble minerals (Marschner, 1995). Its solubility is increased by release of protons and chelating agents into the rhizosphere (Palmer and Guerinot, 2009). Fe^{3+} is reduced at the apoplastic surface of the plasma membrane via FERRIC REDUCTION OXIDASE 2 (FRO2) to yield Fe^{2+} (Fe(II); Yi and Guerinot, 1996; Robinson et al., 1999) which can subsequently be transported into the plant through its main high-affinity uptake system IRT1 (Vert et al., 2002).

Several transporters tightly control Fe homeostasis at the cell level, amongst others FPN2 and VIT1 that facilitate vacuolar influx (Kim et al., 2006; Morrissey et al., 2009). NRAMP3 and NRAMP4 work in the opposite direction as vacuolar effluxers (Lanquar et al., 2005). Distribution of Fe within the plant demands FRD3 which mobilises Fe by efflux of its chelator citrate into the xylem (Rogers and Guerinot, 2002; Durrett et al., 2007). The FPN2-homolog FPN1 also functions in xylem loading (Morrissey et al., 2009). Efflux of another chelator (nicotianamide) into the xylem is probably the function of YSL-proteins which might help to translocate Fe^{2+} between tissues (Thomine and Lanquar, 2011).

It should be noted, that Fe transporters are often able to transport other heavy metals of similar atomic radius and charge. For instance, IRT1 was shown to transport cobalt (Co^{2+}; Korshunova et al., 1999), zinc (Zn^{2+}; Korshunova et al., 1999) and nickel (Ni^{2+}; Nishida et al., 2011) whereas FPN1 and FPN2 are responsible for root-to-shoot translocation of cobalt (Co^{2+}; Morrissey et al., 2009). In fact, altering the Fe nutritional regime had a profound effect on manganese (Mn^{2+}), Co^{2+} and Zn^{2+} leaf concentrations (see also the 'Fe signature' described in the next section and Fig. 5A; Baxter et al., 2008b). Further information on Fe transport in Arabidopsis is also given in Chapter 6.1 and 7.8.

1.3.3 Putting the elements together – the plant ionome

The composition of all mineral nutrients and trace elements is referred to as the plant *ionome* (Salt et al., 2008). Studying several elements at a time enables researchers to dissect the interdependencies of mineral nutrition in single samples. This is of particular interest when cross-regulation of transport and signalling processes is at the heart of research. Technical advances like inductively coupled plasma (ICP) optical emission spectroscopy (ICP-OES), ICP mass spectrometry (ICP-MS) or synchrotron X-ray fluorescence (SXRF) make these measurements technically and financially accessible to a broad range of scientists (Salt et al., 2008; Punshon et al., 2009).

Usually, ICP-OES and ICP-MS are performed on samples that represent a whole tissue or plant organ like e.g. the leaf (Salt et al., 2008). Baxter et al. (2008b) have successfully employed ICP-MS to define an elemental profile that reflects Fe deficiency in Arabidopsis leaf tissue. Interestingly, Fe itself only plays a minor role but a multivariate system of other elements make up an ionomic 'Fe signature' (marked red in Fig. 5A). ICP-MS has also been used to identify mutants (Lahner et al., 2003) and Arabidopsis natural accessions with altered ionomes (Buescher et al., 2010).

SXRF in contrast is able to resolve the spatial distribution of elements across samples (Fig. 5B; Punshon et al., 2009; Donner et al., 2012). This technique has just recently emerged as a novel tool for ionomic analysis of plants. For instance, Punshon et al. (2012) have mapped multiple elemental abundances to specific tissues inside seeds of Arabidopsis wildtype, *cax1* and *cax3* mutants. Distribution of arsenic in hydrated cowpea (*Vigna unguiculata*) roots was also visualised via SXRF (Kopittke et al., 2012).

In direct comparison, ICP-techniques are cheap, fast and precise and hence enable high-throughput analysis. Yet, they are usually limited by quantifying whole-tissue samples. SXRF enables 2D and 3D spatial imaging of multiple elements at submicron resolution in fixed and living plant tissue. The principal restriction is having access to a synchrotron light source. Consequently, both methods should be regarded as complementary.

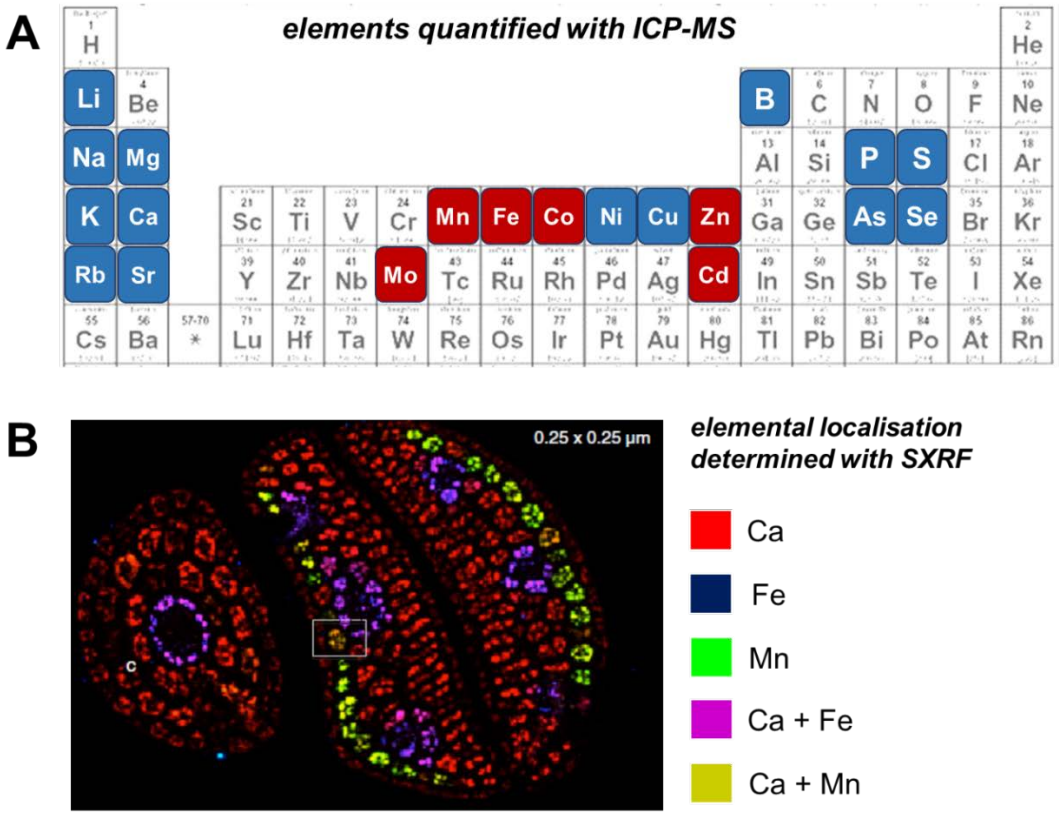

Figure 5: Ionomic analysis with ICP-MS and SXRF.
A) Periodic table of elements highlighting elements that are typically measured in ICP-MS studies. Metals that define the 'Fe signature' (Baxter et al., 2008b) are marked in red, other elements quantified with ICP-MS are marked in blue. **B)** Synchrotron X-ray fluorescence (SXRF) image of a cross-sectioned Arabidopsis wildtype seed showing elemental distributions of Ca, Fe and Mn (adapted from Donner et al., 2012). The pixel resolution is given at the top right corner, i.e. elemental profiles were determined by scanning across the

sample in 0.25 µM steps (both x- and y-axis). The image clearly shows that specialised cells contain Mn and Fe whereas Ca is distributed more or less evenly.

1.4 Nutrient sensing and signalling

1.4.1 General features of nutrient sensing and signalling

To optimally maintain growth, physiology and nutrient homeostasis, plants actively adapt to changes in their environment. Soil/media concentrations serve as a direct environmental cue on the prospects of a plant's nutrient supply. Correspondingly, the root surface is the primary site of nutrient sensing and signalling (Schachtman and Shin, 2007). Environmental sensing might work in two opposite directions, either 'alerting' the plant that unfavourable conditions are about to come or 'informing' it of a newly encountered, rich deposit of valuable resources. In addition to those two extreme ends, it is of course conceivable that several consecutive ranges of concentrations may elicit targeted responses of their own. In fact, nutrient depletion in natural soils can be considered a rather slow process. As a consequence, it is often hard to distinguish whether plants experience a period of (mild) nutrient deficiency or whether they are under (severe) starvation. In the following, I will therefore use the term *starvation* from an outside perspective, i.e. the experimenter starves a plant for certain nutrients via targeted manipulation of its environment.

Similar to other abiotic stresses, timing of nutrient starvation responses is crucial (Schachtman and Shin, 2007). Amongst the quickest reactions to nutrient starvation are transcriptional changes. Accordingly, transcriptional profiling of root responses to nitrate (Wang et al., 2003; Scheible et al., 2004), phosphate (Misson et al., 2005) and potassium (Armengaud et al., 2004) deficiency or re-supply show immediate regulation of whole sets of genes. However, plants are usually transferred from one medium to another, eliciting exactly that 'on–off' response mentioned above.

Deficiency symptoms that gradually develop over time may elicit different patterns of transcriptional activation or repression. Hence, other experiments have focussed on the longer-term transcriptional effects of nutrient starvation for nitrogen (Krapp et al., 2011) or sulphate (Nikiforova et al., 2003). One also has to bear in mind that fast responses are also elicited by many other abiotic and biotic stresses (Schachtman and Shin, 2007). In the case of P starvation it has actually been shown that early transcriptional responses are unspecific, whilst low-P specific responses intensify gradually (Hammond et al., 2003). Another quickly changing factor is the membrane potential which directly responds to fluxes of nutrients and protons across the epidermal plasma membrane (Schachtman and Shin, 2007). At least at the individual cellular level, rapid changes of external nutrient

concentrations are possible, as soil water content may change in an instant altering the availability of minerals in solution.

In addition to timing, the integration of local and systemic signalling pathways is crucial for the overall molecular or morphological output. An elegant way to uncouple local and systemic responses is the experimental split-plate technique which exposes different parts of the root system to different concentrations of nutrients. This approach has led to the identification of a signalling module controlling lateral root proliferation in nitrate rich patches (Zhang and Forde, 1998) and a local phosphate sensor acting at the root apex (Svistoonoff et al., 2007; see also below). However, plants will take into account the complete nutritional status when 'making decisions' on growth and/or physiological adaptations by executing long-range signalling programmes that inform distant plant organs about their current nutritional status (Liu et al., 2009). Often, this feedback depends on the abundance of nutrient assimilates and incorporates phytohormonal signalling pathways (Rubio et al., 2009).

A brief overview of sensing and signalling pathways concerning the macronutrients N, P, K and S will be given in the following sections.

1.4.2 Nitrate signalling

Nitrate (N) is probably the most extensively studied nutrient as far as sensing and signalling are concerned. To date only few nutrient sensors have been identified, such as the stelar K channel SKOR for which gating depends on the apoplastic K concentration (Johansson et al., 2006). A true sensor has also been found for nitrate: NRT1.1 (Ho et al., 2009). This nitrate *transceptor* has dual affinity both in its transport (Liu and Tsay, 2003) as well as its signalling function (Ho et al., 2009). In low-N, NRT1.1 is phosphorylated by CIPK23 (Fig. 6), the same CBL-interacting kinase that activates the K shaker channel AKT1 (Xu et al., 2006). Evidence for a putative calcium signal upstream of CBL-CIPK23-NRT1.1 interactions, generated by nitrate itself or as a consequence of the plant nitrogen status, is so far missing. More is known about the downstream pathways. Phosphorylation at threonine residue 101 was shown to act as the switch for the 'primary nitrate response' which was expressed as the quantitative induction of *NRT2.1* expression (Ho et al., 2009). Using point mutations at other residues, the authors also conclude that the transport function is not required for NRT1.1's signalling properties.

Nitrate signalling mediated by NRT1.1 was shown to elicit several morphological responses. First, nitrate rich patches are colonized by extensive lateral root elongation at

the site of high N. This response requires the MADS box transcription factor ANR1 (Zhang and Forde, 1998) but it has later been shown that NRT1.1 is needed as well, probably acting as the upstream sensor (Remans et al., 2006a). Moreover, NRT1.1 mediated nitrate signalling antagonises the repressive effects of glutamate (Walch-Liu and Forde, 2008) which inhibits main root elongation (Walch-Liu et al., 2006). Again, this response depended on the phosphorylation state at T101. Finally, Krouk et al. (2010) linked nitrate sensing directly to hormonal signalling, as they have demonstrated that NRT1.1 itself acts as an auxin transporter. In their model, the authors propose that presence of nitrate inhibits the auxin transport function of NRT1.1, thus enabling the build-up of an auxin maximum at the lateral root tip that promotes LR elongation into nitrate rich patches. Nevertheless, a more recent study using constitutive and inducible *ANR1* overexpression lines once again strengthened the central role of ANR1 in LR proliferation (Gan et al., 2012).

The high-affinity transporter NRT2.1 also controls phenotypic responses to altered external nitrate concentrations (Remans et al., 2006b). Knockouts of this gene have been shown to respond to low-N conditions with less LR formation but with more LR elongation as the respective wildtype. In fact, whilst a high external carbon (sucrose) to nitrogen ratio (C/N) represses lateral root formation (Malamy and Ryan, 2001), the *nrt2.1* mutant was much less sensitive to this repression (Little et al., 2005). Remans et al. (2006b) explain this with NRT2.1's dual role in nitrate signalling and nitrate provision.

It is true that the systemic nitrogen status plays an important role in plant responses to N deprivation. A recent analysis using a split-root system has identified a core set of 123 genes that differentially responded to local variation in nitrate supply (Ruffel et al., 2011). The authors reported the need for systemic nitrogen signalling mediated by the shoot, as demonstrated via decapitation experiments, and the involvement of cytokinin in this signalling relay.

A higher resolution was achieved by Gifford et al. (2008) who analysed cell-specific N responses via root cell-sorting followed by transcriptional profiling. A major result in their study was the identification of yet another level of regulation performed by micro RNAs. In fact, at least two micro RNAs influence nitrate regulated root architecture by regulating auxin related genes: miR167 targets *ARF8* (Gifford et al., 2008) and miR393 targets *AFB3* (Vidal et al., 2010). Post-transcriptional gene regulation via micro RNAs will also play a role in other nutrient signalling pathways (see P and S signalling below).

Last not least, the nodule inception like protein NLP7 (Castaings et al., 2009), a putative transcription factor, and three other homologous transcription factors of the

LATERAL BOUNDARY DOMAIN family (*LBD37*, *LBD38*, *LBD39*; Rubin et al., 2009), are equally involved in nitrate responses. Although *nlp7* knockouts have been demonstrated to lack induction of *NRT2.1* expression following a nitrate signal, the exact role of these genes in the complex N signalling network has yet to be established.

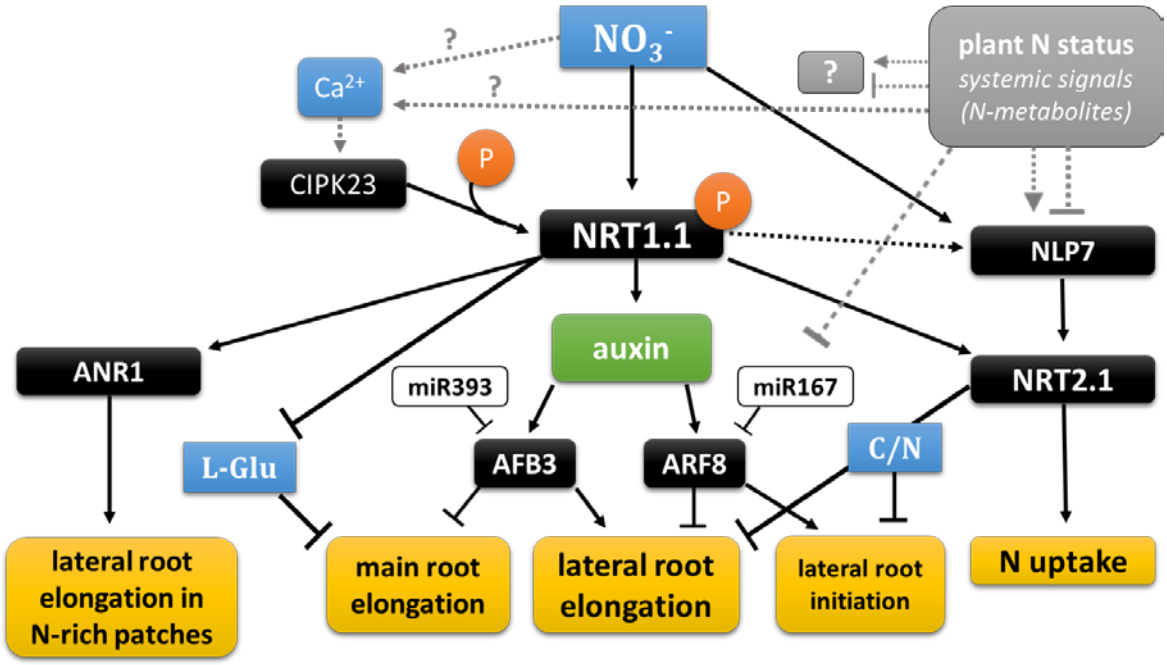

Figure 6: Simplified N signalling network.
Black boxes denote proteins (or genes), white ones micro RNAs and 'P' depicts protein phosphorylation. Phenotypes are shown in yellow boxes, nutrient signals in blue and hormonal signals in green. Grey boxes highlight complex or unknown ('?') signalling pathways. Known links are indicated by solid lines and putative links by dashed lines respectively.

1.4.3 Phosphate signalling

Phosphate (P) starvation elicits strong morphological (e.g. root system architecture, root hair proliferation), metabolic (e.g. anthocyanin accumulation), physiological and transcriptional responses. Fig. 7 depicts a simplified version of the phosphate signalling network presented in the following text.

At the morphological level, main root growth inhibition is a well-known phenomenon of P deprivation (Lopez-Bucio et al., 2002; see also below Chapter 1.5). Three genes have been identified as local regulators of the main root growth response to low-P: the two paralogous multicopper oxidases *LPR1* and *LPR2* (Svistoonoff et al., 2007) and the P5-type ATPase *PDR2* (Ticconi et al., 2009). Split-root experiments have

demonstrated direct low-P sensing at the main root apex mediated by LPR1 and/or LPR2 (Svistoonoff et al., 2007). Consequently, *lpr1* and *lpr2* knockouts were low-P insensitive. In contrast, *pdr2* was hypersensitive to P starvation (Ticconi et al., 2009). Ticconi et al. (2009) speculated that LPR1 and PDR2 function in a common regulatory pathway because their tissue expression domains overlap in the RAM and both proteins localise to the endoplasmic reticulum (see also Chapter 6). The actual function of LPR2 in that respect has not been studied that well. Interestingly, iron was also implicated in the main root response to low-P (Ward et al., 2008; Abel, 2011). It will be interesting to investigate whether there is any overlap between LPR1/LPR2/PDR2 mediated signalling and iron homeostasis (see also Chapters 5 and 6). The genetic bases of other mutants (*lpi1* to *lpi3*; Sanchez-Calderon et al., 2006) that showed insensitivity of main root growth to low-P have yet to be established.

A central gene of P signalling is the small ubiquitin-like modifier (SUMO) E3 ligase *SIZ1* (Miura et al., 2005; Miura et al., 2011). Hence, the *siz1* mutant shows exaggerated main root, lateral root and root hair growth responses to low-P. One study has reported an involvement of SIZ1 in auxin signalling (Miura et al., 2011) possibly altering main and lateral root growth. Earlier, the same core group of researchers has demonstrated that PHR1 is a direct target of SIZ1-mediated SUMOylation (Miura et al., 2005). *PHR1* and its homologue *PHL1* encode MYB transcription factors and are both central regulators of P starvation responses (Rubio et al., 2001; Bustos et al., 2010). Hence, the loss of posttranslational PHR1 modification is at least partly responsible for the *siz1* phenotype. Nevertheless, *SIZ1* appears to have additional functionality exemplified by its involvement in copper tolerance (Chen et al., 2011) and nitrate reductase regulation (Park et al, 2011).

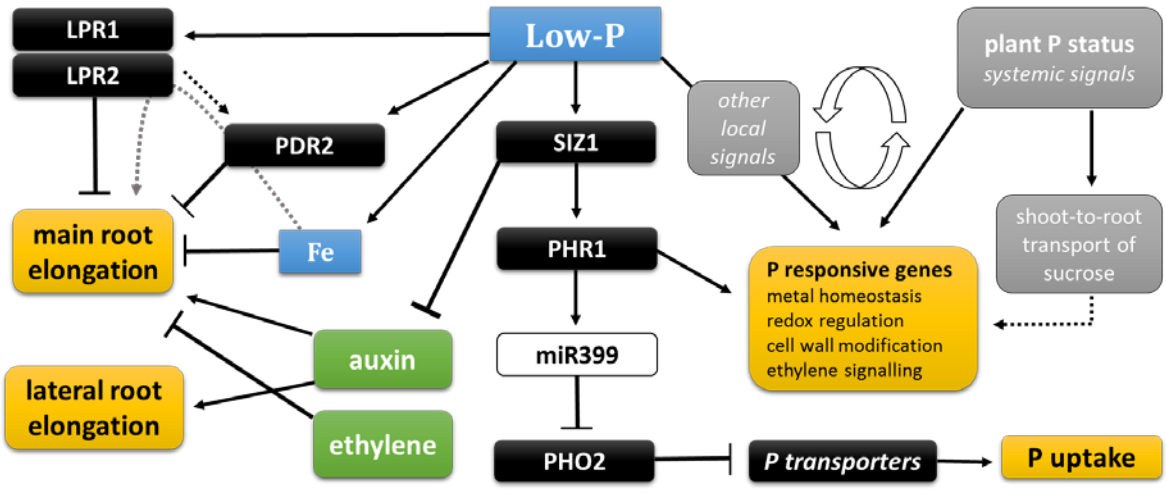

Figure 7: Simplified P starvation signalling network.

Black boxes denote proteins (or genes), white ones micro RNAs and ‘P’ depicts protein phosphorylation. Phenotypes are shown in yellow boxes, nutrient signals in blue and hormonal signals in green. Grey boxes highlight complex or unknown (‘?’) signalling pathways. Known links are indicated by solid lines and putative links by dashed lines respectively.

A particularly interesting downstream target of PHR1 transcriptional activation is miRNA399. This micro RNA is a long-distance signalling molecule that mediates shoot-to-root communication via the phloem (Bari et al., 2006; Pant et al., 2008). In the root, miRNA399 targets the mRNA of *PHO2*, a gene encoding an ubiquitin conjugating enzyme, thus inhibiting PHO2-mediated regulation of phosphate transporter gene expression (Bari et al., 2006).

Transcriptomic responses of local and systemic phosphate starvation were again determined via split-root experiments (Thibaud et al., 2010). Most systemically induced genes (n = 111) were well established components of P sensing, signalling, recycling and recovery. Systemically repressed genes (n = 111) were mainly related to heavy metal homeostasis like Fe and Zn transport and storage. This finding reinforces the interdependence of P and Fe uptake and signalling (Palmer and Guerinot, 2009; Abel, 2011). A much higher number of genes was induced (301 genes) or repressed (240 genes) locally (Thibaud et al., 2010). Apart from transcription factors and genes involved in ethylene signalling, a large part of locally induced genes was also part of metal homeostasis and redox regulation. Locally repressed genes mainly control root development and cell wall modification. The study by Thibaud et al. (2010) not only identified responsive genes but also highlighted the importance of the transcription factor PHR1 in plant-wide responses as promoter sequences of systemically responsive genes were enriched in PHR1-binding motifs.

In addition, sucrose has been identified as a novel mediator of systemic low-P signalling (Hammond and White, 2008; Lei et al., 2011). In fact, disruption of the SUC2 sucrose transporter that loads sucrose into the phloem greatly reduced low-P signalling, whilst *SUC2* overexpression rendered Arabidopsis seedlings hypersensitive to P starvation (Lei et al., 2011). The current model suggests that low P concentrations in the shoot stimulate shoot-to-root transport of sucrose which in turn activates P starvation responses in the root via a so far unknown mechanism (Hammond and White, 2011).

Apart from sugars, a whole range of phytohormones appear to regulate systemic low-P responses, particularly morphological ones, namely auxin (Nacry et al., 2005), cytokinin (Franco-Zorrilla et al., 2002) and ethylene (Ma et al., 2003; Wang et al., 2012a).

1.4.4 Potassium signalling

Since potassium (K) is not metabolised, sensory and signalling systems underlying K supply can be expected to be different from those of nitrate and phosphate (see also Fig. 8). As mentioned above, one of the first responses is the activation of the Shaker-type channel AKT1 via the CBL-CIPK23 network (see section 1.3.2.3: Potassium transport). The membrane potential might be an upstream signal that elicits rapid changes in cytosolic free calcium concentrations. The CBL-interacting kinase CIPK9 has also been shown to act in low-K responses (Pandey et al., 2007). Currently, it is speculated that CIPK9 might phosphorylate a protein that helps to balance cytoplasmic and vacuolar K concentrations, e.g. a K channel (Armengaud and Amtmann, 2007).

Another well-documented response to low-K is the transcriptional upregulation of *HAK5* (Ahn et al., 2004; Armengaud et al., 2004). This low-K response has actually been exploited as a K signalling reporter in several studies (Jung et al., 2009; Kim et al., 2010). Upregulation of *HAK5* was also achieved by hydrogen peroxide (H_2O_2) treatment (Shin and Schachtman, 2004) indicating that reactive oxygen species (ROS) may be involved in low-K signalling. Indeed, Shin and Schachtman (2004) showed that knockout of the NADPH oxidase RHD2 abolished *HAK5* induction by K starvation. Direct evidence was provided by measuring low-K induced ROS accumulation in the elongation zone of the main root (Kim et al., 2010). Ethylene has been shown to act upstream of ROS production (Jung et al., 2009). However, since K starvation responses were not completely absent in the central ethylene signalling mutant *ein2-1*, another ethylene-independent low-K pathway was suggested. This pathway has yet to be elucidated.

Other than ethylene, the most prominent phytohormone in K deprivation signalling is jasmonate. Microarray analysis has already revealed transcriptional regulation of many genes in the oxylipin/jasmonic acid pathway (Armengaud et al., 2004). Further transcriptional profiling using a knockout of a central oxylipin signalling gene, *COI1*, strengthened this view (Armengaud et al., 2010). The latter study also highlighted reduced damage by thrips in wildtype but not in *coi1* which supports the idea that jasmonate signalling elicited by low-K concomitantly activates jasmonate dependent defence signalling pathways. Indeed, Troufflard et al. (2010) have shown that low-K not only induced the production of jasmonates but also increased glucosinolate concentrations, a group of secondary metabolites that prevents members of the Brassicaceae family from herbivory attack.

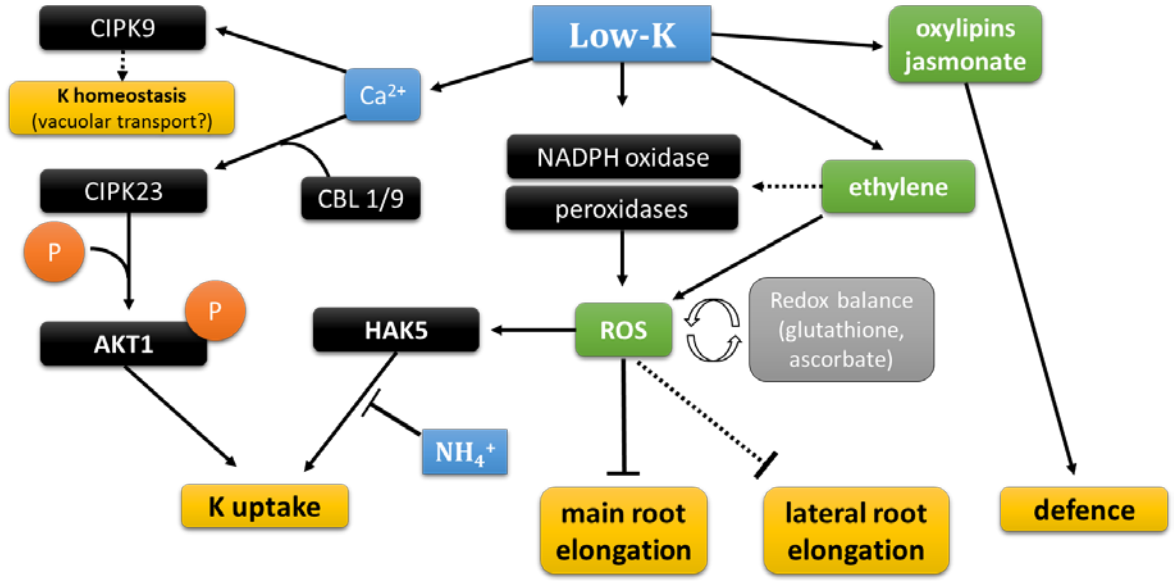

Figure 8: Simplified K starvation signalling network.
Black boxes denote proteins (or genes), white ones micro RNAs and 'P' depicts protein phosphorylation. Phenotypes are shown in yellow boxes, nutrient signals in blue and hormonal signals in green. Grey boxes highlight complex or unknown ('?') signalling pathways. Known links are indicated by solid lines and putative links by dashed lines respectively.

Despite the fact that K is not metabolised itself, K-deprivation strongly affect primary metabolism. Armengaud et al (2009) carried out a comprehensive analysis of the effects of low-K on enzyme activities and integrated these with metabolite concentrations and transcriptional profiles. The study revealed that K-deficiency uncouples glycolysis ofrom the TCA cycle in the roots leading to an accumulation of sugars and a depletion of organic acids such as malate. On the basis of these results pyruvate kinase, a K-activated enzyme, was proposed as the primary target of K-deficiency and a potential K-sensor. Importantly, the study revealed a close interaction between K and nitrate suggesting that effects of low-K on nitrate concentration, transcription of nitrate transporter genes (*NRT2.1*) and activity of nitrate-assimilating enzymes (nitrate reductase; NR) are mediated by sugar signalling (Armengaud et al. 2009). More recently, CIPK23 has been identified as a potential signalling hub linking plant responses to K and nitrate (Tsay et al., 2011). Indeed, a close relationship between K and nitrate has often been reported in the field (Gething, 1993) and provided a strong motivation for investigating K-N interactive effects on root architecture in this PhD project.

1.4.5 Sulphate signalling

Similar to other nutrient starvation responses, low-S induces the transcription of corresponding high-affinity uptake genes *SULTR1;1* and *SULTR1;2* as well as other SULTR transporter members involved in sulphate re-mobilisation and distribution (Gojon et al., 2009; see also section 1.3.2.4: Sulphate transport). However, *SULTR1;1* and *SULTR1;2* are differentially regulated by local and systemic low-S (and other) signals (Rouached et al., 2008).

Most transcriptional responses to S deprivation depend on the central transcription factor EIL3 (ETHYLENE INSENSITIVE-LIKE 3; aka SLIM1) which is the only member of this family that responds to low-S (Maruyama-Nakashita et al., 2006). The first step of sulphur assimilation is catalysed by several isoforms of chloroplastic ATP sulphurylases (*APS* genes) which are targets of miRNA 395 (Jones-Rhoades and Bartel, 2004). Hence, another micro RNA acts in response to nutrient stress. Interaction of low-S signalling with phytohormones is given by the induction of *NIT3* (Kutz et al., 2002). The encoded protein nitrilase 3 is a key enzyme in auxin biosynthesis. Not least, cytokinin pathways also seem to be involved in long-distance signalling regulating S transporter expression (Maruyama-Nakashita et al., 2004).

Surely, the summary of nutrient sensing and signalling pathways presented here is not exhaustive. It is striking though that not much information on cross-talk between nutrient signalling pathways is available. Experimental work should therefore target this knowledge gap. As mentioned before, root system architecture provides a quantifiable readout of environmental stress responses. Since nutrient acquisition is one of the root systems main function it is not surprising that many studies have investigated morphological root adaptations to nutrient starvation. Some underlying signalling components involved in these responses have already been described in this section. The following section will focus on the phenotypic outputs.

1.5 Root architecture responses to nutrient starvation

1.5.1 Morphological responses to single nutrient deficiency

Probably the first targeted analysis of morphological root plasticity to nutrient treatments was presented by Drew (1975). In his study, he locally enriched the soil around barley roots with nutrients and observed growth of primary and secondary roots of the whole root system. Drew could show that N, P and ammonium supply resulted in local proliferation of secondary roots within the nutrient rich zone. Local K supply in contrast lead to elongation of all secondary roots.

Ten years ago Lopez-Bucio et al. (2003) set out to collate the information available on Arabidopsis root architecture responses to external nutrient availability. With more than 80 Pubmed citations (as of June 2013) this review has become a benchmark in research on environmental plasticity of the root system. The authors present in this paper a diagram illustrating the main root architectural adaptations to low-N, low-P and low-S. Although not principally wrong, further research has shown that the range of phenotypic responses needs to be expanded and that some observations have to be reconsidered in the light of new results. The following paragraphs and Fig. 9 summarize the major Arabidopsis root phenotypes caused by specific N, P, K and S conditions.

Alterations in lateral branching was reported to be the main morphological consequence of nitrate supply. Very high N concentrations (≥ 10 mM) repressed the development of lateral roots after emergence (Zhang et al., 1999). Low-N combined with excessive sucrose addition similarly lead to very short LRs (Little et al., 2005). In contrast, locally higher nitrate concentrations stimulate LR elongation at the site of the nitrate rich patch (Zhang and Forde, 1998; Remans et al., 2006a). An increase of LR length and transiently higher LR emergence was also observed when seedlings were transferred from high N (10 mM) to low-N (≤ 1 mM) media (Remans et al., 2006b).

P starvation elicits a dual response: on the one hand main root growth (MR) is severely reduced (Williamson et al., 2001; Lopez-Bucio et al., 2002), on the other hand LR density was reported to be increased (Lopez-Bucio et al., 2002; Perez-Torres et al., 2008). It is not clear, however, whether MR growth arrest is the prerequisite for enhanced lateral root emergence and elongation. Another phenotypic adaptation to low-P is the proliferation of root hairs (Peret et al., 2011). However, this parameter is usually not captured in studies on RSA.

The most conspicuous low-K phenotype is a severe reduction of LR elongation (Armengaud et al., 2004; Shin and Schachtman, 2004). In fact, this phenotype of Arabidopsis fits with Drew's (1975) observations that localised K supply promotes LR growth of the whole *Hordeum vulgare* root system. Furthermore, MR growth was also reported to be reduced (Qi et al., 2008; Kim et al., 2010*)*

S deprivation is a difficult case. Both stimulation of LR growth (Kutz et al., 2002; Lopez-Bucio et al., 2003) as well as reduction of MR and LR growth (Wu et al., 2010) have been reported. A complicating issue here is the choice of the background medium: Gamborg's B5 (Kutz et al., 2002) vs. MS (Wu et al., 2010). Moreover, Kutz et al. (2002) first cultivated seedlings on S sufficient medium and subsequently transferred them to S free conditions. In contrast, Wu et al. (2010) directly germinated their seedlings on S deprived media. This illustrates the importance of the overall 'growth concept' incorporating the effect of other nutrients and short-term (i.e. transfer) vs. long-term starvation.

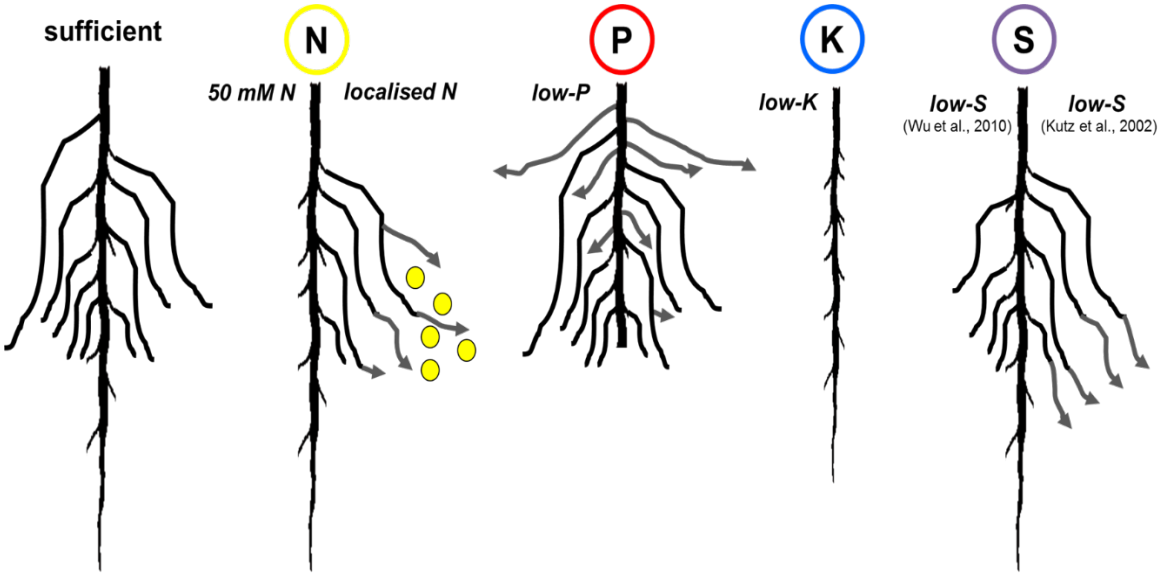

Figure 9: Arabidopsis root architecture phenotypes elicited by alterations of single nutrient supply.
'Sufficient' denotes the prototypical root phenotype observed for approx. 2 week old seedlings grown on vertical agar plates supplemented with ample amounts of nutrients. All illustrations depict RSA responses to nutrient treatments (N, P, K or S). Treatments are given in italics. For N and S two different treatments/results are shown on the left and the right hand side respectively.

Which other environmental factors have an influence on RSA? High osmotic potential was shown to repress LR elongation similarly to high N (Deak and Malamy, 2005). A later dissection of LR repression evoked by nitrate or mannitol revealed that indeed high N is the stronger signal (Roycewicz and Malamy, 2012). A comparative analysis of alternative nitrogen sources showed that L-glutamate inhibits main root elongation whilst promoting elongation of LRs close to the MR tip (Walch-Liu et al., 2006). Interestingly, this response bears high similarity to the low-K response I observed for certain Arabidopsis accessions (Kellermeier et al., 2013; see also Chapter 4). The same main authors have also shown later that the root architecture response to L-glutamate can be overcome by addition of nitrate but only when functional NRT1.1 is present (Walch-Liu and Forde, 2008). High concentrations of NH_4^+ sensed at the root tip reduce LR elongation (Li et al., 2010b). Vertical split-plate experiments have shown an inhibition of MR and LR growth by NH_4^+ whilst simultaneously increasing higher order lateral branching (Lima et al., 2010). Low-B supply reduced MR elongation and straightened the angle of the MR (Martin-Rejano et al., 2011) that typically occurs when seedlings are grown on 2-dimensional surfaces. Excess Cu repressed both MR and LR growth (Lequeux et al., 2010) whilst high levels of Zn induced LR emergence (Xu et al., 2010). Moreover, high concentrations of Fe also reduced MR growth but local, moderate supplementation of Fe stimulated LR elongation in an auxin dependent manner (Giehl et al., 2012).

1.5.2 Root architecture remodelling under multiple stresses

Root architecture responses presented in section 1.5.1 all refer to addition or elimination of a single nutrient in a complex nutritional background medium like e.g. MS (Murashige and Skoog, 1962) or Hoagland's solution (Hoagland and Arnon, 1950). Consequently, it is hard to dissect responses to a 'nutrient treatment' from the interactions that may occur a) between nutrients in the medium or b) between nutrient signalling pathways inside the plant. Case a) for instance is a well-known phenomenon in P and Fe nutrition, since the availability of either nutrients strongly depends on the presence/absence of the other (summarized in Ward et al., 2008; Abel, 2011). Case b) has been exemplified by the two opposing LR phenotypes of low-S (cf. Fig. 9; Kutz et al., 2002; Wu et al., 2010).

Very recently, Rich and Watt (2013) have pointed out that in a realistic field scenario the root system is always faced with several environmental stimuli at a time. An interesting comparison of nitrate and water availability effects on RSA was made by

Chapman et al. (2011). The authors measured RSA of seedlings grown on agar or in sand. Nitrate concentrations around the roots of sand-grown plants were directly quantified with micro-electrodes. Two main observations were made: first, RSA differed between agar and sand even when the medium was the same. Second, for seedlings grown in sand, water supply is in fact a stronger signal for MR growth than N. Hence, nitrate, water and probably oxygen supply were all important for the final RSA outcome. It should be mentioned, however, that the study was performed on very small seedlings (< 3 cm) with almost no lateral roots and thus the term 'root architecture' may be somewhat misleading here.

Interactive effects arising from multifactorial addition or withdrawal of plant nutrients were studied some 30 years ago by Wallace and co-workers. Their interest lay in the yield increase generated by addition of single vs. multiple nutrients at a time. Initially, it was shown that simultaneous Fe and Mn limitation resulted in higher vegetative yields as Mn deficiency alone (Wallace and Romney, 1980). Hence, the simple assumption of the 'one limiting factor', as proposed by *Liebig's law*, did not apply in this case. Further experiments strengthened that view as combinations of Fe, N and P application had different, non-additive effects on yield of two soybean cultivars (Wallace et al., 1981). The latter experiment also illustrates the importance of genotype-environment interactions in nutritional responses.

Interactive effects of different nutrients on RSA are so far sparsely investigated. It has been shown that reduction of MR elongation in low-P may actually be caused by Fe toxicity (Ward et al., 2008). Considering carbon as a nutrient, several studies have investigated the interplay of C and N nutrition affecting RSA (Malamy and Ryan, 2001; Little et al., 2005; MacGregor et al., 2008; Roycewicz and Malamy, 2012). Moreover, MR cessation caused by glutamate treatment was overcome by adding nitrate (Walch-Liu and Forde, 2008).

In sum, mineral nutrition has been shown to impose a strong environmental signal on root architecture formation. Yet, to date a comprehensive analysis where more than one nutritional parameter is varied at a time is still lacking. Studying the interactive phenotypic effects caused by the macronutrients N, P, K and S presents a good starting point in that respect. As a second step, it will be interesting to uncover the molecular basis of novel phenotypes by investigating genotype-environment (gen*env) interactions. This could be done by either studying mutant collections or by making use of natural variation in the species gene pool.

1.6 Natural variation in *Arabidopsis thaliana*

1.6.1 Studying natural variation in Arabidopsis

A few Arabidopsis laboratory 'strains' have been established to control the genotype factor and thus to make studies on molecular and physiological processes comparable. Common names of laboratory genotypes like Columbia (or Col-0), Landsberg erecta (Ler) or Wassilewskija (Ws) surely ring a bell for anyone interested plant molecular biology. It should not be forgotten though, that all thale cress 'wild type' strains have their origin in the wild. It was early grass-roots work by Laibach and colleagues who in the 1950s first established a collection of Arabidopsis genotypes by sampling seeds at various field sites (Alonso-Blanco and Koornneef, 2000). Sixty years down the line, the actual ecological context from which material was obtained is either lost or no longer truly significant because seed propagation in controlled environments has somewhat uncoupled the genotype from its natural environment. Hence, it is more appropriate to speak of *natural accessions* rather than ecotypes (Alonso-Blanco and Koornneef, 2000; Weigel, 2012).

Arabidopsis is a self-fertile species and consequently individuals in wild populations show a high degree of homozygosity. Although substantial genetic variation was still detected within local populations, a recent study confirmed continuous isolation by geographic distance (Platt et al., 2010). Arabidopsis occurs naturally throughout the northern hemisphere, but it is likely that the actual native range spans Europe, Northern Africa and parts of Asia. Other natural populations found in North America or the Far East have probably been anthropologically introduced as neophytes (Fig. 10; Weigel, 2012).

From an ecological perspective, natural habitats encompass riverbanks, cultivated lands or rocky ground; from sea level up to about 4500 m altitude and from tropic to subarctic latitude (Koornneef et al., 2004). It could therefore be hypothesised that natural accessions had adapted to local environments with particular geological, hydraulic, climatic and diurnal properties. Moreover, geographic and ecological separation may have advanced the genetic distance between populations and may have led to the evolution of alleles with enhanced adaptive value. At least as far as geography is concerned, Nordborg et al. (2005) and Ostrowski et al. (2006) have shown that population structure exists in European populations, generally separating east from west. Using natural accessions derived from geographically distinct populations in comparative studies therefore presents

an alternative approach to test different (but quasi-homozygous) genotypes in biologically or ecologically significant conditions.

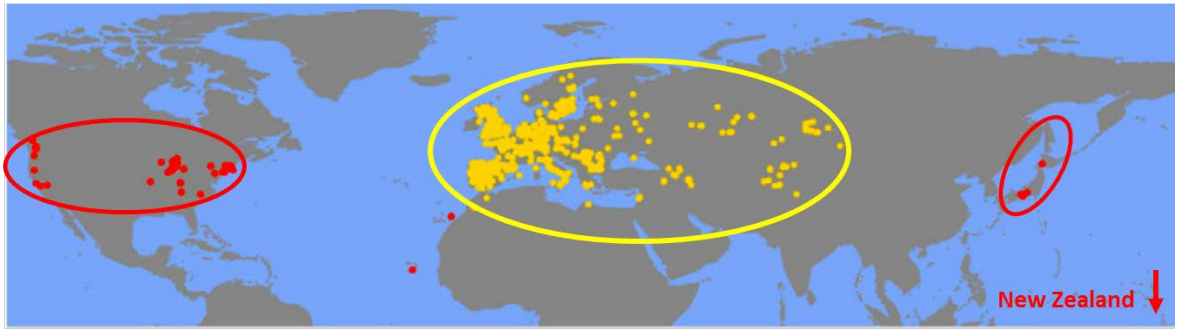

Figure 10: Geographic origin of Arabidopsis natural accessions available from common stock centres.
Native distribution is marked in yellow (circle: range; dot: individual accession). Populations that have been anthropologically introduced as neophytes are shown in red. Adapted from Weigel (2012).

Research on Arabidopsis natural variation has been done on plant development (germination, leaf morphology, flowering time or root development, etc.), primary and secondary metabolism as well as biotic and abiotic environmental stress responses. The reader shall be referred to some excellent reviews that not only give an overview of the phenotypic traits in question, but in several cases also address the genes that underlie respective polymorphisms: Koornneef et al. (2004); Alonso-Blanco et al. (2009); Weigel (2012). Some of the major natural variation studies with a focus on root growth, mineral nutrition or nutrient starvation which are (directly) relevant to this thesis will be mentioned below.

An early study investigated 26 natural accessions using two complete N-P-K fertiliser regimes and quantifying 9 shoot morphological and developmental traits (Pigliucci and Schlichting, 1995). The authors not only detected associations between traits but also demonstrated significant genotype-environmental interactions suggesting differential plasticity of genotypes in contrasting nutrient conditions.

Variation in root architecture responses to high N (30 mM) and osmotic stress (30 mM mannitol) was studied in 71 accessions by Fitz Gerald et al. (2006). A strong repression of LR elongation (cf. Deak and Malamy, 2005) was detected in 44 genotypes, including Col-0, but other accessions like Ler were able to form LRs (Fitz Gerald et al., 2006). Col-0 and Ler were consequently chosen for quantitative genetics (see below).

Root length responses to four different nitrogen sources were assessed in 56 accessions (Rauh et al., 2002). Although overall genotype-environment interactions were not significant at first sight, a close up analysis revealed that only about a quarter of all

genotypes in the total pool actually contributed to the gen*env effect detected by ANOVA. A later study also investigated shoot and root growth responses to low-N together with expression profiles of genes involved in nitrate transport and assimilation (North et al., 2009). However, only four genotypes were used for most experiments and the variation detected in root morphology was therefore rather small.

Natural variation of responses to N fertilisation is the core interest of our collaborator Fabien Chardon at INRA Versailles. His group used a core set of Arabidopsis accessions, the 'nested-core collection' (McKhann et al., 2004), to dissect genotype-, environment- and gen*env-effects of nitrate uptake efficiency (Chardon et al., 2010), seed filling (Masclaux-Daubresse and Chardon, 2011) and morphological responses to different nitrate treatments (Ikram et al., 2011). Most recently, his group was also involved in characterising root architecture responses to N availability (De Pessemier et al., 2013) using the EZ Rhizo software. Interestingly, ANOVA highlighted a strong effect of their N treatments (0.01 or 10 mM N) on MR length and LR densities but not on LR length. Yet significant gen*env effects were detected for all six RSA traits measured.

The first natural variation studies dealing with P starvation compared P uptake efficiency in 36 accessions (Narang et al., 2000) and root parameters such as MR length and LR number in 73 genotypes (Chevalier et al., 2003). Interestingly, although P concentrations used were high (1 mM) or very low (1 µM), the effect of low-P on RSA was much less pronounced in Chevalier et al. (2003) than reported earlier by Williamson et al. (2001) and Lopez-Bucio et al. (2002). In fact, Reymond et al. (2006) later observed a much stronger reduction of MR elongation in 4 out 6 accessions tested. The following identification of the P-sensor gene *LPR1* via quantitative trait loci mapping, cloning and allelic complementation (Svistoonoff et al., 2007) represents the blue-print for exploiting natural variation in the search for novel genes with adaptive significance in stress responses.

Mineral content of different plant tissues is another common theme in natural variation studies. Vreugdenhil et al. (2004) quantified seed concentrations of K, Na, Ca, Mg, Fe, Mn, Zn and P by spectrometry based on flame emission, atomic absorption or dye-formation. In a similar approach, variation of elemental distributions in seed and leaf tissue was assessed in recombinant populations generated from four different accessions (Ghandilyan et al., 2009; see section 1.6.2 for a description of recombinant populations). The shoot ionome consisting of 17 simultaneously determined elements was investigated in 12 accessions and three recombinant populations (Buescher et al., 2010) and significant genotype-effects were detected for most of the elements.

Investigating natural variation of specific mineral contents has enabled the identification of two transporter genes regulating accumulation of Mo (*MOT1*; Baxter et al., 2008a) and Cu (*HMA5*; Kobayashi et al., 2008). Baxter et al. (2010) were also able to link variation in shoot Na accumulation to polymorphisms in the *HKT1* sodium transporter gene. Interestingly, the natural distribution of a weak *HKT1* allele was significantly enriched in populations derived from coastal, saline environments, providing substantial evidence for an adaptive force driving natural selection at this particular genomic locus.

Complex phenotypic outputs are often caused by multiple loci that may also interact in their function (Kover and Mott, 2012). Dissecting the role of these loci is the main theme of *quantitative genetics*. The following section will now illustrate the concepts and methods behind it.

1.6.2 Using natural variation to search for novel genes

Quantitative genetics is usually based on two things: a) a quantifiable phenotypic reporter, i.e. a trait of interest that varies between genotypes, and b) a mapping population consisting of different genotypes. For the latter, genotype information for all individuals must be available at various positions, a.k.a. markers, along the Arabidopsis genome map.

The amount of genetic tools based on Arabidopsis natural variation is immense. Very early on, research groups have started to develop recombinant populations derived from crosses of genetically divergent natural accessions. Targeted crossing produces an F1 hybrid population in which genomic recombination takes place during meiosis. So genomes of the initially crossed, parental accession are ‘reshuffled’ in individual meiocytes of the F1 generation. Since Arabidopsis is a largely selfing species, F1 hybrids can be left to self-fertilise producing seeds of the F2 generation (Loudet et al., 2002). This resulting F2 population consists of individuals with differentially mixed genotypes inherited from both parental accessions. F2 populations are the simplest form of recombinant populations and are indeed widely applied in crop science and breeding, but they are also valuable for Arabidopsis research (Salome et al., 2011).

However, a large proportion of the genome is heterozygous at this stage and thus a large number of individuals is needed to yield statistically significant results (Loudet et al., 2002). A widely applied strategy to fix recombination events to a homozygous state is the development of recombinant inbred lines (RILs; Fig. 11A). Here, the recombinant genotype of individual F2 plants is ‘immortalised’ by propagating individuals to a more advanced generation via repeated self-fertilisation (Loudet et al., 2002). In Arabidopsis, the

common strategy of choice is single seed descent (Tuinstra et al., 1997) which is a kind of iterative process. First, a single seed from an F2 individual plant is propagated to seed stage. A single seed from this plant (now F3) is randomly chosen and again propagated to seed stage, and so on. After several generations of inbreeding, the genotype of that single ancestor has been passed 'down the line'. This process has therefore generated a *recombinant inbred line (RIL)*. Propagating many plants of the F2 generation in this manner thus generates a RIL population.

Seeds of an advanced generation (e.g. F5 to F7) are sufficiently homozygous to give more powerful results than F2s. Hence, individual RILs of this generation are genotyped at known molecular markers using the best marker technology available, e.g. single nucleotide polymorphisms (Simon et al., 2008), to distinguish the two parental alleles and hence detect the ancestry of a specific genomic fragment. An example for a genetic map of a RIL derived from a cross between accessions Col-0 and Ct-1 (Col-0 x Ct-1; Simon et al., 2008) is shown in Fig. 12. As soon as such a map has been established, the population is ready to be used for quantitative trait loci (QTL) analysis.

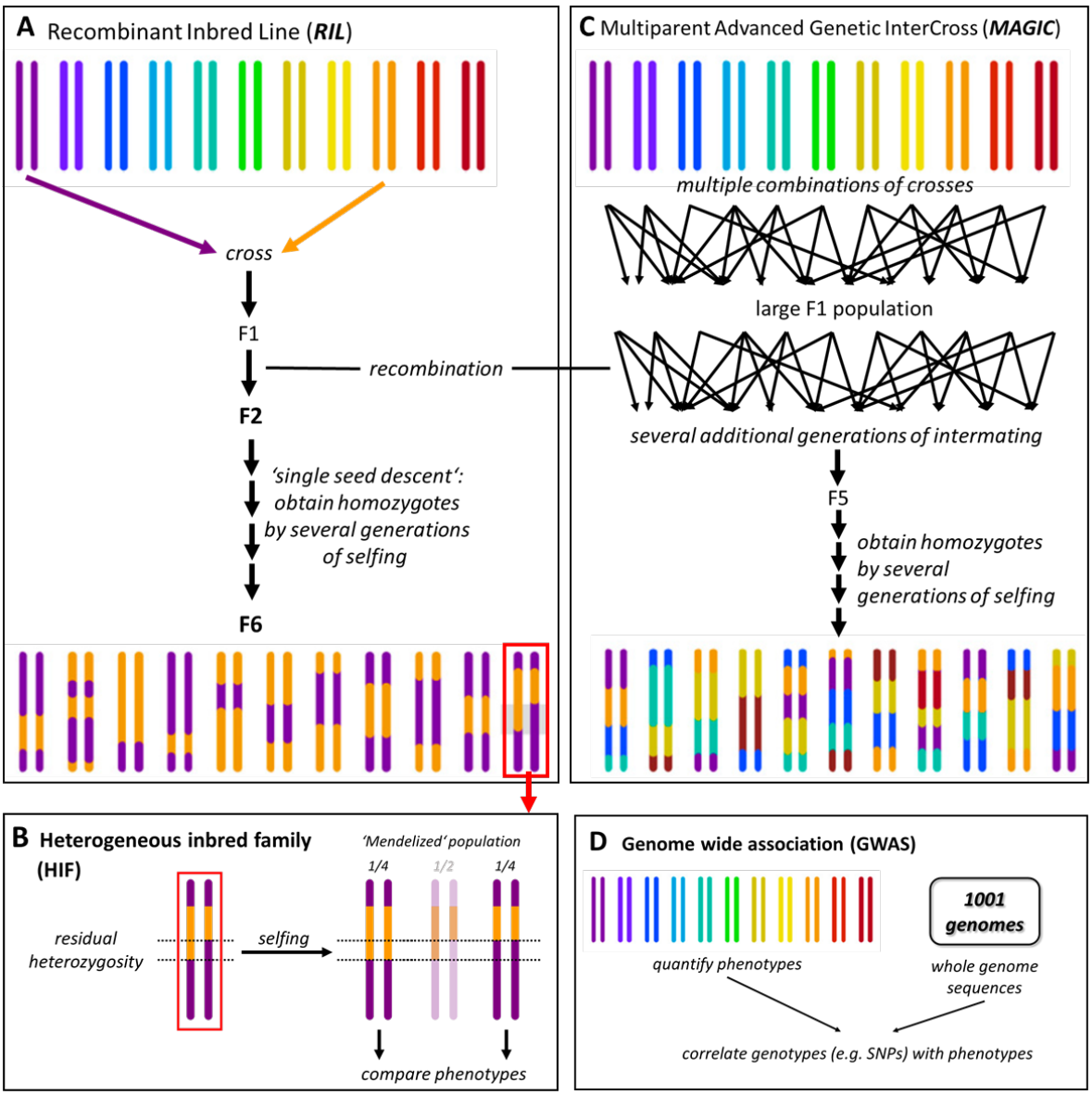

Figure 11: Overview of common quantitative genetics tools available for Arabidopsis.
A) *Recombinant inbred line populations (RILs)* are generated by initially crossing two accessions. Resulting F1 heterozygotes are subsequently self-fertilized. During meiosis, recombination events re-shuffle the genome of individual lines. Individuals from the resulting F2 population are again propagated to seed stage. At this point each selected individual forms the basis for a recombinant inbred line. To increase the rate of homozygosity, several rounds of 'single seed decent', i.e. self-fertilisation followed by propagation of a randomly selected single plant per line is performed over several generations. The whole population is usually ready for application in QTL studies F6 or F7 stage.
B) Residual heterozygosity in RILs (red box) can be exploited for QTL validation ('mendelization') and fine-mapping. So called *heterogeneous inbred families (HIFs)* are derived from a parental RIL which is heterozygous at a genomic locus of interest (an example is boxed red in A and B). This RIL is self-fertilised and seeds of the following generation either bear both alleles (on average 50% heterozygotes) or one of the two alleles in a homozygous way (~ 25 % each). Homozygous HIFs are selected and phenotypes compared. Significant differences in phenotypes confirm the involvement of a genomic locus in the mendelized interval.
Figure legend continued on next page

Fig. 11 continued

C) *Multiparent Advanced Genetic Intercross (MAGIC)* lines are a refined version of RILs (Kover et al., 2009). Here, to increase the genotypic variation, multiple genotypes are mixed via an extensive crossing strategy spanning several generations. Further steps (e.g. single seed descent) are similar to those used for the generation of RILs.

D) Next-generation sequencing technology has made it possible to sequence whole genomes of accession collections (cf. the '1001 genomes' project; Weigel and Mott, 2009). Genetic information, like the position of single nucleotide polymorphisms (SNPs), can be directly correlated with phenotypic information available for natural accessions.

Figure adapted from Weigel (2012).

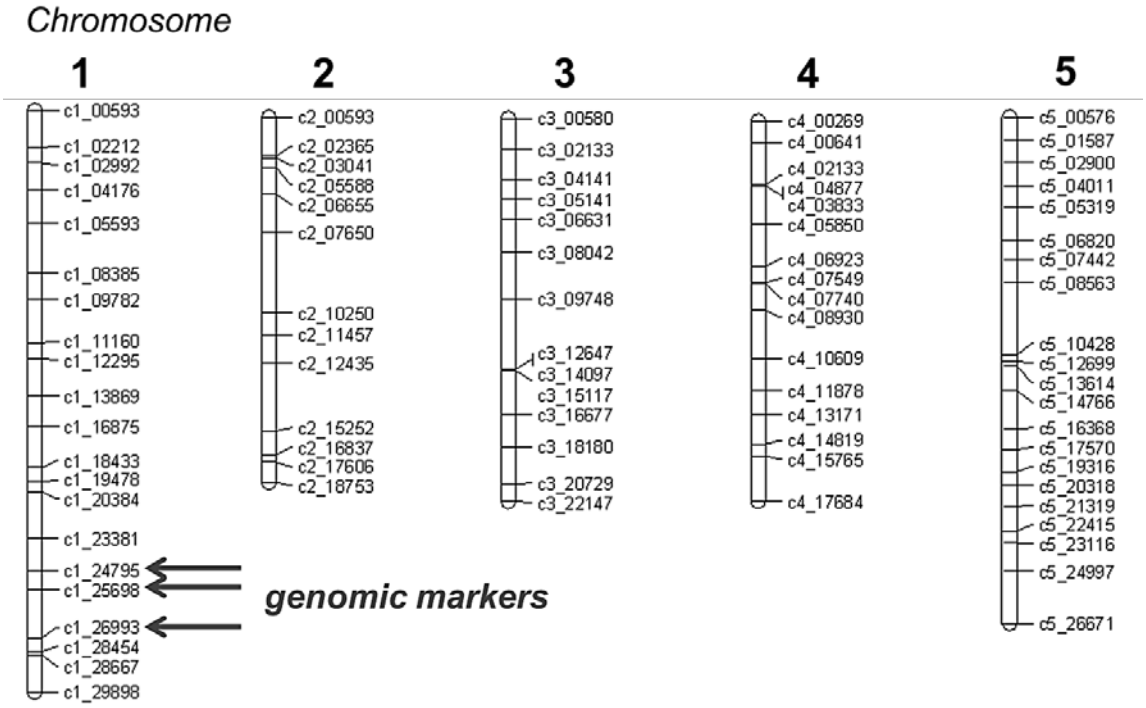

Figure 12: Example for a genetic map of an RIL population derived from the Arabidopsis natural accessions Col-0 and Ct-1.

The map shows all five chromosomes of Arabidopsis. Names of genomic markers are coded according to chromosome number (c1 to c5) followed by a 5 digit number that denotes the physical (absolute) position in kilobases (kB) measured from the top of each chromosome; e.g. marker *c1_24795* corresponds to a known polymorphism between Col-0 and Ct-1, in this case a single nucleotide polymorphism (SNP), on chromosome 1 at the physical position 24795 kB.

The map has been constructed with Map Chart 2.1 software using marker information from the Col-0 x Ct-1 recombinant inbred line population (Simon et al.; 2008).

The principle of QTL analysis is simple (Alonso-Blanco and Koornneef, 2000): a quantifiable phenotype, e.g. root length, is measured in a given experimental condition for a number of individuals originating from the same mapping population, e.g. RILs. Genotypic information at each genomic marker position is then associated, i.e. correlated, with the phenotype. High correlation rates indicate the existence of linkage between genotype and phenotype and hence denote a QTL in the respective genomic interval. In most cases several QTLs will be detected, indicating that the trait in question has a multi-genic basis (Alonso-Blanco and Koornneef, 2000). However, statistical methods are able to dissect the individual effects of each locus, separating large-effect from small-effect QTLs. Koornneef et al. (2004) give a good overview of phenotypic traits that have been investigated in early QTL studies based on F2 and RIL populations.

Of particular interest for me was research performed in Olivier Loudet's group at INRA Versailles. Not only are they at the forefront of generating new RIL populations (Loudet et al., 2002; Simon et al., 2008) but Loudet and co-workers have also performed a substantial amount QTL work themselves. The scope of analysed traits and research questions is quite diverse. QTL analysis has been performed on developmental traits like flowering time, seed size, rosette area or root architecture (Loudet et al., 2002; Loudet et al., 2005; Simon et al., 2008) with a recent shift to questions of genetic incompatibility, gene duplication and transposition as well as epigenetic inheritance (Bikard et al., 2009; Vlad et al., 2010; Durand et al., 2012).

Other groups have genetically dissected natural variation in mineral content, like K (Harada et al., 2006) or multiple elements at a time (Vreugdenhil et al., 2004; Ghandilyan et al., 2009; Buescher et al., 2010). And as mentioned above, QTL analysis also lead to the identification of the putative phosphate sensor *LPR1* (Reymond et al., 2006; Svistoonoff et al., 2007). There are many other QTL studies with important implications for plant viability, nutrition and adaptation to abiotic stress. They will be discussed later, especially in Chapter 4.

Several alternatives to QTL mapping with conventional RILs exist. For instance, a modification of the classical RIL generation protocol has led to the development of Multiparent Advanced Genetic Intercrosses, so called *MAGIC* lines (Kover et al., 2009). The backbone of this population is a sophisticated crossing scheme of 19 parental accessions which spans several generations and precedes the single seed decent procedure (Fig. 11C). Kover et al. (2009) explain the nature of *MAGIC* lines as 'between naturally occurring accessions and existing synthetic populations'. The major advantage of these lines over conventional RILs is their inherently higher genotypic variation caused by

intermating 19 instead of 2 parental accessions. Nevertheless, if individual natural genotypes show strong phenotypes by themselves, the value of biparental RILs should not be underestimated (Weigel, 2012).

Once a QTL is mapped, it is good practice to confirm the polymorphic effect by 'mendelizing' the trait. This can be done by introgression of a genomic fragment from one parent into the other which yields *near isogenic lines* (NILs; Weigel., 2012). In the case of RILs, the most straightforward way to do that is by analysing *heterogeneous inbred families* (HIFs), a special form of NILs. To generate HIFs, residual heterozygosity in the RIL set at e.g. F6 stage is exploited (Tuinstra et al., 1997). An individual RIL that is heterozygous in a genomic interval of interest (i.e. a QTL) is propagated into the next generation (Fig. 11B). Typical genomic segregation will result in approx. 50 % heterozygotes and approx. 25 % of each homozygous parental allele. The resulting homozygous HIFs only differ genetically in this interval, given that no other heterozygous intervals are present in the genome of those HIFs. When phenotypic segregation is observed for that pair of opposing HIFs, a QTL can be regarded as 'confirmed' (Loudet et al., 2005).

The most recent advance in genetic mapping makes use of the revolution caused by next-generation sequencing technology. *Genome wide association studies* (*GWAS*) compare genotype information of high density with phenomic information gathered from a large number of divergent genotypes. GWAS are based on the principle of linkage disequilibrium which expresses the physical connection of a polymorphism (linkage) with a nearby genetic variant that underlies a measurable phenotype (Weigel, 2012). The idea is that during a species' evolution recombination has not produced all possible combinations of genetic polymorphisms. In fact, linkage between polymorphisms in close physical vicinity has been largely preserved. A known molecular marker like a SNP can therefore be used as a reporter of another, causal polymorphism that flanks this polymorphism on the chromosome.

Instead of analysing 'synthetic' populations such as RILs, GWAS enables direct mapping from natural accessions (Fig. 11D), presumed that a high number of genomic markers is available for these. Atwell et al. (2010) have demonstrated the power of that approach by genotyping 191 accessions with a 250,000 Affymetrix SNP array and subsequently phenotyping an impressive 107 traits related to development, flowering, ionomics and pathogen resistance.

The best way forward, however, is to compare the whole genome sequence of all accessions in question. In Arabidopsis this has become reality by the *1001 genomes* project

(Weigel and Mott, 2009; http://www.1001genomes.org/). An international consortium of plant scientists interested in natural variation and ecological genetics has set out to sequence a large number of natural accessions and to make the sequence information available to the general public. Started in the late 'noughties', the first three sequences were published by Ossowski et al. in 2008, followed by consecutive blocks of another 80 (Cao et al., 2011) and 18 accessions three years later (Gan et al., 2011; all *MAGIC* founder accessions but Col-0). As of April 2013, a staggering 816 genomes has already been released. Unfortunately, by the time I performed my own natural variation experiments (summer 2010) this was not yet the case.

At this point, I would like to conclude with the notion that *all* genomic tools have their ups and downs. Mutant analysis allows the targeted study of individual genes in a controlled genetic background. With regard to studying environmental plasticity, mutant analysis is a viable strategy when knockouts are devoid of a strong, pleiotropic phenotype in 'control' condition but show an aberrant response to certain treatments. However, genetic redundancy restricts the number of mutants showing an obvious phenotype and hence limits the usefulness of knockouts to identify novel genes that contribute to RSA development and plasticity (Osmont et al., 2007). Classical knockout studies might also miss genes for which a full knockout results in embryo-lethal phenotypes.

Natural variation presents an alternative solution for these problems, as quantitative genetics have often revealed the function of novel genes that were functional but simply differentially expressed in natural accessions (e.g. Svistoonoff et al., 2007; Baxter et al., 2008a). Since the gene pool in the wild is subject to mutation and selection, natural variation should also provide a vast genomic resource of additional polymorphisms with potential significance in plant development and particularly stress response. On the other hand, however, studying individual genes in non-reference accessions is limited by their different genetic backgrounds, i.e. all the other polymorphisms that cannot be controlled for. In addition, many other tools in plant science, such as reporter lines for cell viability, phytohormone distribution or subcellular compartmentalisation, are not readily available in other backgrounds than Col-0, Ler or Ws.

I have therefore chosen to pursue two approaches in a complementing way: a targeted investigation of gene function in nutrient sensing and signalling pathways using the reference genotype Col-0 and a non-targeted approach to search for novel phenotypic responses to environmental signals using other natural accessions.

1.7 Objectives

A striking example for developmental plasticity in plants is the active adjustment of root system architecture (RSA) to the environment, which ensures an optimised exploitation of scarce and fluctuating resources within the soil. Whereas nutrient starvation responses to low nitrate (low-N), low phosphate (low-P), low potassium (low-K) and low sulphate (low-S) concentrations have been investigated in isolation, a comprehensive analysis of RSA in complex nutritional environments is still lacking.

The first objective of this PhD project was therefore to characterise root architecture plasticity in different binary combinations of sufficient or deficient N, P, K and S. Results obtained from this initial analysis helped to dissect the impact of individual nutrients on individual root parameters and enabled the generation of a 'nutrient impact hierarchy'. Moreover, it provided evidence for interactive effects arising from multiple nutrient starvation. And similarly important, it flagged up individual root architectural parameters that were modulated by the supply of specific nutrients and nutrient combinations.

The second objective was to use the data provided by the RSA phenotyping in different conditions to pinpoint new roles of known putative signalling components and investigate potential crosstalk between signalling pathways. To this purpose specific RSA parameters were re-analysed in knockout mutant lines grown under relevant conditions. Further assessment of regulatory networks was carried out via transcriptomic and ionomic profiling of selected conditions.

K emerged as an important nutritional factor in my initial experiments, yet natural variation in Arabidopsis root architecture responses to low-K have so far not been investigated and the molecular components mediating RSA responses to low-K remain unknown. The third objective of this project was therefore to use a non-targeted approach to identify genetic loci underlying RSA responses to low-K. Hence, I first investigated K starvation responses in a set of natural accessions. Subsequently, I performed QTL analysis to map root architecture in two contrasting environments (control vs. low-K) onto the Arabidopsis genome.

Investigation of NPKS-combinations and results obtained in natural variation experiments suggested significant overlap between low-K and low-P pathways. Iron (Fe) presented itself as a putative third component in mediating K and P starvation responses. It therefore became my next objective to investigate a potential role of Fe in the low-K root response. To address this question I subjected plants grown in low-K and/or low-P to

different Fe concentrations and measured the effects on RSA in two Arabidopsis accessions that have different response strategies to low-K. I subsequently quantified Fe distribution in K and P deprived seedlings *in situ* and *in vivo* using staining techniques as well as synchrotron X-ray fluorescence (SXRF).

The final objective of the project was to test the involvement of known K, P and Fe transport and signalling genes in RSA responses to low-K and low-P. To this end, I carried out another mutant study. A sub-selection of knockouts with aberrant phenotypes were further investigated by Fe staining and SXRF.

A particularly interesting candidate for mediating P-K-Fe crosstalk was *LPR2*. In comparison to its paralogue *LPR1*, this gene lags behind in functional characterisation. I therefore cloned the *LPR2* promoter as well as the full-length *LPR2* genomic sequence. Fusion constructs (promoter-GUS; GFP-fusion) were used to assess tissue and intracellular expression patterns. Additional transgenic material was generated to enable future LPR2 complementation and over-expression studies. Further lines will facilitate the quantification of the cellular redox status in various genetic backgrounds.

The combined results from this project have shed light on the complexity of nutritional factors that modulate environmental plasticity of the root system following a multifactorial experimental approach. I have discovered so far uncharacterised root architecture responses to nutrient treatments and collected data that supports the idea of nutrient signalling crosstalk. In selected cases, I could demonstrate the action of known signalling components in novel functional contexts. And last but not least, analysis of natural variation revealed complementing strategies of morphological adaptation to low-K.

2. Material and Methods

2.1 Plant Material

The dicotyledonous model species *Arabidopsis thaliana* (L.) Heynh. was the subject of study in all experiments described. It will be referred to as 'Arabidopsis' throughout the rest of this thesis.

Seeds of natural accessions (Akita, Alc-0, Bay-0, Bl-1, Bla-1, Bur-0, Blh-0, Col-0, Ct-1, Cvi-0, Edi-0, Ge-0, Gre-0, Jea, Kn-0, Mh-1, Mt-0, N13, Oy-0, Pyl-1, Sakata, Sha, St-0, Stw-0) and recombinant inbred lines (Col-0 x Ct-1; 7RV; Simon et al., 2008) were obtained from the Versailles stock centre (http://dbsgap.versailles.inra.fr/vnat; last viewed 30/01/2013). The accessions Ler and Ws were part of the Amtmann/Blatt laboratory stock at the University of Glasgow. See Table 3 for original Versailles stock codes.

A set of mutant seeds in Col-0 background (Table 4) was obtained from the European Arabidopsis Stock Centre (NASC; http://arabidopsis.info; last viewed 30/01/2013) and the Arabidopsis Biological Resource Centre (ABRC; https://abrc.osu.edu; last viewed 30/01/2013).

For all SALK T-DNA insertion lines, the presence of the insertion in genomic DNA was verified by PCR prior to use. For each genotype 10 – 15 plants were first grown on soil and leaf tissue collected individually about 3 to 4 weeks after germination. DNA-extraction and PCR was performed as described below (Chapter 2.4). Either a pair of primers flanking the putative insertion (denoted LP + RP in Table 4; amplifying a 'wild-type fragment') or a pair of primers amplifying part of the insertion (LBb1.3 + RP; LBb1.3: ATTTTGCCGATTTCGGAAC) were used for PCR. Suitable primers were designed for each genotype using the T-DNA Primer Design tool (http://signal.salk.edu/tdnaprimers.2.html; last viewed 30/01/2013). The amplified fragments were separated by agarose gel electrophoresis. Gel electrophoresis had three possible outcomes: a) 'wild-type' when only the primer pair LP + RP amplified a fragment of expected size, b) 'heterozygous' when both LP + RP and LBb1.3 + RP amplified expected-size fragments and c) 'homozygous insertion' when only LBb1.3 + RP yielded the fragment of interest. Adult plants were then propagated to seed production stage. Seeds were harvested from plants harbouring the 'homozygous insertion' and used for all further experiments.

Additional seeds were kindly provided by Mary Lou Guerinot (Dartmouth College, Hanover, NH, USA), Yoichiro Fukao (NAIST, Ikoma, Japan) and Hugh Nimmo (Plant Science Group, University of Glasgow, Glasgow, UK). If not otherwise stated, Col-0 is the designated wild type (WT).

Table 3: Arabidopsis natural accessions and their corresponding Versailles Stock Codes.

Natural accession	Versailles Stock Code
Akita	252 AV
Alc-0	178 AV
Bay-0	41 AV
Bl-1	42 AV
Bla-1	76 AV
Blh-1	180 AV
Bur-0	172 AV
Col-0	186 AV
Ct-1	162 AV
Cvi-0	166 AV
Edi-0	83 AV
Ge-0	101 AV
Gre-0	200 AV
Jea	25 AV
Kn-0	70 AV
Ler	
Mh-1	215 AV
Mt-0	94 AV
N13	266 AV
Oy-0	224 AV
Pyl-1	8 AV
Sakata	257 AV
Sha	236 AV
St-0	62 AV
Stw-0	92 AV
Ws	

Table 4: List of mutants in Col-0 background.

In case of T-DNA insertion lines, primer pairs used to verify the homozygous insertion are given as left border primer (LP) and right border primer (RP). References are given for previously characterised mutants.

Mutant Line	Gene ID	AtG Code	Stock Code	Source	Genotyping Primers		Reference
					LP	RP	
aha2	*AHA2*	At4g30190	SALK_022010	NASC	CTCCTGGGACAAGAATAGCAGC	CTGTTTTACTTAAGAAAAGGTTTCTCC	Haruta et al., 2010
aha7	*AHA7*	At3g60330	SALK_042485	NASC	GCCTGGTCAATCTTTAAAGGG	CCAGGTTTGTGCTTATTTTGC	Santi & Schmidt, 2009
akt1	*AKT1*	At2g26650	SALK_071803	ABRC	TCCATGTCAAGCTAAGAAGACG	TCGGTGATAGATAGTGGTGGC	Rubio et al., 2008
chl1-5	*NRT1.1*	At1g12110	N6384	NASC	n/a	n/a	Tsay et al., 1993
cipk23-1	*CIPK23*	At1g30270	SALK_036154	NASC	TTGTGATCCTCTTGCATAGGG	AATCATCCCGGACAAAGTACC	Ho et al., 2009
cipk23-2	*CIPK23*	At1g30270	SALK_112091	NASC	AGCAGAATTTACTTGCCCTCC	GTGGAATTCCAATGTGTCACC	Ho et al., 2009
cipk9	*CIPK9*	At1g01140	SALK_058629	NASC	ATTAGGGACCCACATGTCCTC	CCATCTTCCTGCATTCAAAAG	Pandey et al., 2007
fer1-3-4 (triple)	*FER1*	At5g01600		ML Guerinot	n/a	n/a	Ravet et al., 2009
	FER	At3g56090					
	FER4	At2g40300					
fer2	*FER2*	At3g11050	SALK_002947	NASC	GTTCCCTTAAACCTCTCACCG	GGCATCAAAATAGACTGCAGC	Ravet et al., 2009
fit	*FIT / FRU*	At2g28160	SALK_126020	NASC	TGATAGTGTTAGAGCCGGTGG	AGAACGGATTTGACTCACG	Colangelo & Guerinot, 2004
fpn1	*FPN1 / IREG1*	At2g38460	SALK_145458	NASC	AGAAAAGGAACCTGAGGACGG	TGAATCACAGCCACAAAACCC	Morrissey et al., 2009
fpn2	*FPN2 / IREG2*	At5g03570	SALK_074442	NASC	GGTACCTGATCATCGTTGACG	GATTTGATCAGACCTTGCACC	Morrissey et al., 2009
frd3-2	*FRD3*	At3g08040	N6585	NASC	n/a	n/a	Rogers & Guerinot, 2002
fro2	*FRO2 / FRD1*	At1g01580		ML Guerinot	n/a	n/a	Yi & Guerinot, 1996
hak5	*HAK5*	At4g13420	SALK_005604	NASC	TCACTGATATGTCGGTATGCG	CCTAGATCAGCAAACATTGCC	Rubio et al., 2008
ipk1	*IPK1*	At5g42810	SALK_065337	ML Guerinot	n/a	n/a	Stevenson-Paulik et al., 2005
ipk2ß	*IPK2ß*	At5g61760	SALK_104995	ML Guerinot	n/a	n/a	Stevenson-Paulik et al., 2005
ipk1-2ß (double)	*IPK1*	At5g42810		ML Guerinot	n/a	n/a	Stevenson-Paulik et al., 2005
	IPK2ß	At5g61760					
irt1	*IRT1*	At4g19690	SALK_054554	Y Fukao	n/a	n/a	Fukao et al., 2011
lpr1	*LPR1*	At1g23010	SALK_016297	NASC	CGAAGAATATAGGCGCCTACC	AAAGACTCATGGGTGTGAACC	Svistoonoff et al., 2007
lpr2-1	*LPR2*	At1g71040	SALK_091930	NASC	TTATAGCACCATTGCAAAGGG	GTCATAGCTCAGTCGAATCGC	Svistoonoff et al., 2007
lpr2-2	*LPR2*	At1g71040	SAIL_915_D06	ABRC	GTTCAGCAACAGTTCCTGGAC	TTTTGGAGTTTCGGTTACGG	
lpr2-3	*LPR2*	At1g71040	SALK_022690	NASC	ATTTTGCTCTCCTACCGAATG	GACCGTTTGGAGAAGCAAGAACC	
lpr2-4	*LPR2*	At1g71040	SALK_061362	NASC	TTATAGCACCATTGCAAACGG	ATTGTGAACGGTAAAGCATGG	
nrt2.1	*NRT2.1*	At1g08090	SALK_035429	NASC	GCAAGCGACTATCATCACTCC	GTTCTCCATGAGCTTCGTGAG	Little et al., 2005
pdr2	*PDR2*	At5g23630	SALK_077682	NASC	GTTTGAAGAGCGTTATGCGAC	GAAAGCGGAAATGAAAGATCC	Ticconi et al., 2009

2.2 Growth Conditions

2.2.1 Standard Growth Medium

All reagents used for media preparation were purchased from Sigma-Aldrich (Sigma-Aldrich Company Ltd, Dorset, England), Fisher Scientific (Fisher Scientific UK Ltd, Loughborough, UK) or VWR (VWR International Ltd, Lutterworth, UK). The control growth medium consisted of 0.5 mM $CaCl_2$, 0.25 mM $MgS0_4$, 2 mM KNO_3, 1 mM NaCl, 0.5 mM NaH_2PO_4, 42.5 µM Fe(III)Na-EDTA and a micronutrient mix of 1.8 µM $MnSO_4$, 45 µM H_3BO_3, 0.38 µM $ZnSO_4$, 0.015 µM $(NH_4)_6Mo_7O_{24}$, 0.16 µM $CuSO_4$, 0.01 µM $CoCl_2$. Deficiency media are described separately in the respective chapters. All media were buffered with 2 mM MES (2-(N-Morpholino)ethanesulfonic acid) and adjusted to pH 5.6 with Tris Base (Tris(hydroxymethyl)aminomethane). After addition of 0.5 % sucrose and 1 % agar (Sigma A-1296), media were autoclaved at 121 °C for 5 min.

2.2.2 Pharmacological Treatments

In some cases, media were supplemented with non-nutritional substances, such as phytohormones, hormone analogues and precursors (aminocyclopropanecarboxylic acid, indole acetic acid, kinetin, naphthalene acetic acid), hormonal antagonists (aminovinylglycine, silver nitrate) and redox active compounds (ascorbic acid, glutathione). Stock solutions were prepared and filter-sterilised (0.2 µM pore size). Respective volumes were added to media after autoclaving immediately before pouring plates (at 40 - 50 °C) to avoid pyrolysis of heat sensitive substances.

2.2.3 Seed Sterilisation

Seeds were placed in 1.5 mL tubes and immersed and 1 mL absolute EtOH for 1 min. The solution was replaced with 1 mL 2% sodium hypochlorite (bleach) solution containing 0.1% Tween-20 for 5 min. Seeds were rinsed five times with 1 mL sterile double distilled water (ddH_2O) and subsequently vernalized for 3 days in the dark at 4 °C.

2.2.4 Arabidopsis Seedling Culture

A detailed description of Arabidopsis seedling culture optimised for root architecture analysis, including helpful tips at various stages, has been published as a part of a *Methods in Molecular Biology* Edition (Kellermeier and Amtmann, 2013). In brief, media were autoclaved at 121 °C for 20 min and left to cool to approx. 40 - 50 °C. 35 mL of agar media were poured per 120 x 120 mm^2 petri dish. This low volume was chosen to limit the total amount of nutrients and thus indeed starve seedlings for the nutrients in question. For a test set of agar media I monitored the changes of nutrient concentrations and water content caused by uptake and evaporation. Cumulative water loss and nutrient uptake were roughly in balance with a slight trend towards higher water consumption/evaporation rates. An example comparing changes in P and K concentrations with changes in water volume at two time points (10 and 14 days after germination) is shown in Appendix I.

The top 2 cm of agar were removed using a sterile knife and spatula. For root architecture analysis, between 4 and 6 vernalized seeds (depending on the media used) were placed below the rim of the agar to avoid leaf contact with the media (see MacGregor et al., 2008). Plates were sealed with micropore tape (width 1.25 cm; 3M, St. Paul, MN, USA).

Sealed plates were then placed vertically in metal racks or cardboard boxes where the upper (agar-free) 2 cm protruded from the boxes (Fig. 13). Generally, cardboard boxes were preferred for root architecture quantification experiments for two reasons: 1) The light gradient generated a slight elongation of the hypocotyl and hence a better separation of roots and shoots; 2) less condensation occurred within the plates, increasing the quality of scanned images. Metal racks were only used when large amounts of plants were needed for e.g. ion or RNA extraction or when seeds were pre-germinated on control media and subsequently transferred to treatment plates. In these cases, where feasible, more than one row of seedlings was sown per plate and the number of seedlings per row was increased. To compensate faster nutrient depletion, the volume of media was also increased up to 70 mL. Controls were included in each experiment to account for variability caused by differences in growth conditions. Seedlings were grown in short day (photoperiod 9/15 h light/dark) or long day (16/8 h) at 22/18 °C with a light intensity of 160 µmol m^{-2} s^{-1} (if not otherwise stated).

Germination was scored 3 days after sowing (3 DAG) and non-germinated seedlings were discarded from further analysis. To avoid positional effects, the position of plates within the growth chamber was randomised at regular intervals.

Figure 13: Arabidopsis seedling culture on vertical plates.
Sealed petri dishes were placed vertically in metal racks (left) or cardboard boxes (right). Boxes were approx. 10 cm high so that the top 2 cm of plates (height: 12 cm) were in full light.

2.3 Phenotyping of Root System Architecture

2.3.1 Image Acquisition

Plates were scanned from the back (through the agar) with a conventional flatbed scanner (Hewlett-Packard Scanjet 4500c) at 200 dpi in bitmap (*.BMP*) format. Scanning was performed at regular intervals, usually 6-8-10-12 or 6-9-12 DAG.

2.3.2 Root Architecture Analysis with EZ Rhizo

Image analysis with the EZ Rhizo software tool (http://www.psrg.org.uk/plant-biometrics.html) was performed following the procedure described in Armengaud et al. (2009b). A description of root parameters and their corresponding abbreviations is presented in Table 5. When parts of the root system were crossing over (especially lateral roots) manual detachment was applied (see also Kellermeier and Amtmann, 2013). Detached lateral roots were re-drawn in a way that preserved their original length and original position on the main root. Since shape and angle of these roots were altered manually, lateral root angle and straightness of lateral roots were not analysed. Two other

root parameters were omitted from further analysis: *straightness* of the main root (not very reliable due to manual root detachment and low correlation with nutritional factors) and *depth* of the root system (very high positive correlation with *main root path length*).

2.3.3 **EasyPHP** ***Database Management***

All EZ Rhizo result files (*.TXT*) were loaded into the in-built EasyPHP database. Each analysed root image was supplied with the following metadata to facilitate retracing of the original images:

image name
User Name: *FK*
Experiment Name: *date of experiment in format YYMMDD [e.g. 120820]*
Box Name: *as in bottom right corner of the scanned image [e.g. C.12]*
Genotype: *as per Table 3 and Table 4*
Media: C [*for Control*]; K- [*for low-K*]; P-; K-P- [for low-KP]; etc…
[preliminary experiments carry media number codes (1000 to 1172) that can be found in the electronic appendix Ch2_number codes for media]
Age of Plants: *x* days after germination
Scale: *0.012700* (when scanned at 200 dpi)

Table 5: Root architectural parameters quantified by image analysis with *EZ Rhizo*. Abbreviations used throughout the text are shown on the left. Alternative abbreviations are shown in brackets in italics.

abbreviation	unit	description of root architecture parameters
TRS	cm	**total root size**: sum of path length of the main root and lateral roots
MRP	cm	**main root path length**
Basal	cm	**basal zone length**: main root path length from the root-hypocotyl junction to the uppermost lateral root
Branched	cm	**branched zone length**: main root path length from the first to the last lateral root
Apical	cm	**apical zone length**: main root path length from the last lateral root to the main root tip
MR angle	°	**main root angle**: angle of the vector from the root-hypocotyl junction to the main root tip
LRS	%	**lateral root size**: sum of path lengths of lateral roots as a fraction of TRS
1st order LR # *(LR #)*		**1st order lateral root number**: number of lateral roots emerging from the main root
2nd order LR #		**2nd order lateral root number**: number of lateral roots emerging from 1st order lateral roots
LRP 0.25	cm	**mean lateral root path length in the basal quarter** of the main root (0 – 25 % of the MR)
LRP 0.50	cm	**mean lateral root path length in the second quarter** of the main root (25 – 50 % of the MR)
LRP 0.75	cm	**mean lateral root path length in the third quarter** of the main root (50 – 75 % of the MR)
LRP 1.00	cm	**mean lateral root path length in the apical quarter** of the main root (75 – 100 % of the MR)
LR density / MR *(LRdensMR)*	cm^{-1}	**lateral root density along the main root**: 1st order lateral root number divided by main root path length
LR density / BZ *(LRdensBZ)*	cm^{-1}	**lateral root density within the branched zone**: 1st order lateral root number divided by branched zone length

2.4 Genotyping

2.4.1 DNA Extraction

2.4.1.1 Standard DNA Extraction

Fresh sampled leaf tissue (approx. disc of 2 cm diameter) was put into a 2 mL screw cap tube containing a steel ball bearing, snap-frozen in liquid nitrogen and ground to powder using a tissue lyser (Tissue Lyser, Qiagen, Germany) at 18 hz for 1 min. 400 µL of Edwards' DNA extraction buffer (Edwards et al., 1991; Table 6) was added. The suspension was vortexed for 1 min and left for incubation at room temperature (RT) for 10 – 30 min. Cell debris was pelleted by centrifugation at 13,200 rpm and 4 °C for 10 min. 350 µL of supernatant was transferred to a fresh 2 mL tube. An equal amount of ice-cold isopropanol was added and solutions gently mixed by inversion. Precipitated DNA was pelleted by centrifugation at 13,200 rpm and 4 °C for 20 min. The supernatant was decanted and the pellet washed with 500 µL of ice-cold 70 % ethanol by vortexing. After centrifugation (13,200 rpm, 4 °C, 5 min), the supernatant was poured off and the pellet vacuum-dried (Concentrator 5301, Eppendorf, Germany) for ca. 10 min. The DNA pellet was re-suspended in 50 µL TRIS-Buffer (10 mM TRIS-HCl; pH = 8.5) at 65 °C in a heat block for 10 min.

DNA quality and quantity was checked by spectrophotometry (BioPhotometer plus 6132, Eppendorf, Germany) and solutions stored at -20 °C longterm.

Table 6: Edwards' buffer used for DNA extraction.

Reagent	Concentration
TRIS	200 mM
NaCl	250 mM
EDTA	25 mM
SDS	0.5 %
adjust pH = 7.5 with HCl	

2.4.1.2 High Throughput DNA Extraction

Generation of recombinant heterogeneous inbred family 479 (rHIF 479) required large amounts of individual plants. Therefore, a high-throughput DNA extraction protocol was derived from the standard protocol described above. Leaf samples were harvested in 96-deep well plates (Eppendorf, Hamburg, Germany) and one steel ball bearing per plate was added. Plates were thoroughly sealed with rubber lids and frozen at -80 °C. Tissue was ground to powder using a tissue lyser (Tissue Lyser, Qiagen, Germany) at 18 hz for 1 min. DNA was then extracted following the standard DNA extraction protocol described above. To avoid cross-contamination of samples each time supernatants were discarded, a clean 96-well plate (*'sink'*) was placed head down on top of the 96-well plate containing the precipitate and solution (*'source'*) so that both holes matched exactly. In a swift movement, both plates were turned around so that the supernatant flowed from the *source* plate into the matching well of the *sink* plate.

2.4.2 Genomic Fragment Amplification via Polymerase Chain Reaction (PCR)

2.4.2.1 Standard PCR Conditions

All PCR reactions were performed in either a PTC-200 peltier thermocycler (MJ Research, St. Bruno, Canada) or a peqSTAR 96 universal gradient thermocycler (Peqlab, Erlangen, Germany). GoTaq® Flexi DNA Polymerase (Promega, Madison, WI, USA) was used for genotyping PCRs following the reaction setup described in Table 7 and the cycler conditions as per Table 8. KOD Hot Start DNA Polymerase (Novagen, Darmstadt, Germany) was used to amplify fragments in cloning reactions following the setup shown in Table 9 and cycler conditions as per Table 10. This polymerase ensures much higher precision due to its 3' to 5' exonuclease activity that allows for the excision of mismatches. In both PCRs, annealing temperatures were determined with the NetPrimer software tool (Premier Biosoft; http://www.premierbiosoft.com/netprimer/; last viewed 24/04/2013). Generally, annealing temperatures were set at 2 °C below the primer dimerization temperature given by the programme. Extension time was chosen according to fragment length: 1 min per kb of fragment in GoTaq®-based PCR, 20 s per kb in KOD-based PCR.

2.4.2.2 Primer Design for T-DNA Insertion Lines

Genotype specific PCR primers were designed using the T-DNA Primer Design software tool (http://signal.salk.edu/tdnaprimers.2.html; last viewed 24/04/13). Specificity

of primers was verified by comparison against the Arabidopsis genome sequence using the Seqviewer tool (TAIR; http://www.arabidopsis.org/; last viewed 24/04/13). Primer quality and annealing temperatures were determined with NetPrimer (see above 2.4.2.1).

Table 7: Reaction setup used for standard/genotyping PCR.

	stock conc.	**volume per reaction [µL]**
Green GoTaq® Flexi Buffer	5 X	2.5
$MgCl_2$	25 mM	0.75
dNTPs	2 mM each	0.25
Primer sense	10 µM	0.25
Primer antisense	10 µM	0.25
GoTaq® DNA Polymerase	5 U μL^{-1}	0.067
ddH_2O		8.19
DNA template		0.25
TOTAL		**12.5**

Table 8: PCR thermocycler conditions used for standard/genotyping PCR.

step	**Temp. [**°C]	**time [s]**
1) Initial denaturation	95	120
2) Denaturation	95	30
3) Annealing	*variable*	30
4) Extension	70	*variable (60 s per kb)*
repeat cycles 2) – 4) for 35 – 38 times		
5) Final extension	95	300

Table 9: Reaction setup used for high-precision PCR (cloning).

	stock conc.	**volume per reaction [µL]**
KOD reaction buffer	10 X	5
$MgSO_4$	25 mM	5
dNTPs	2 mM each	5
DMSO		2
Primer sense	10 µM	1.5
Primer antisense	10 µM	1.5
KOD DNA Polymerase	1 U μL^{-1}	1
ddH_2O		27.75
DNA template		0.25
TOTAL		**50**

Table 10: PCR thermocycler conditions used for high-precision PCR (cloning).

step		**Temp. [**°C]	**time [s]**
Initial Denaturation	Initial denaturation	95	120
3-Step Cycling	Denaturation	95	20
	Annealing	*variable*	10
	Extension	70	*variable (20 s per kb)*
	repeat 15 cycles		
2-Step Cycling	Denaturation	95	20
	Extension	70	*variable (20 s per kb)*
	repeat 20 cycles		

2.4.2.3 Simple Sequence Length Polymorphism (SSLP) Primer Design for Col-0 x Ct-1 Recombinant Inbred Lines (RILs) and Heterogenous Inbred Families (HIFs)

The whole genome sequence of Ct-1 was kindly provided pre-release in March 2011 by Dr Richard Mott, The Wellcome Trust Centre for Human Genetics, Oxford. The sequence is now available as part of the 1001 genomes project (Weigel and Mott, 2009). Whole genome sequences of Col-0 and Ct-1 were searched for insertions/deletions around regions of interest (QTL intervals) between both genotypes using CLC Genomics Workbench (CLC bio, Aarhus, Denmark). Sequences flanking the insertion/deletion which had sequence identity between both genotypes were designed accordingly. See Table 11 for a full list. Primer quality and annealing temperatures were determined with NetPrimer (see above 2.4.2.1).

2.5 Quantitative Trait Loci (QTL) Analysis

2.5.1 Experimental Design for QTL Analysis of the Low-K Response

Sterilised seeds of 154 Col-0 x Ct-1 RILs (Simon et al., 2008) and the two parental ecotypes Col-0 and Ct-1 were grown on control ([K] = 2 mM) and low-K ([K] = 0.01 mM; see Chapter 4) media. An overview of the seedling culture setup is presented in Fig. 14. Two seedlings each of all genotypes were grown on control and on low-K media. Two genotypes were mixed on each plate, up to 13 plates were mixed per box and 12 boxes were evenly spread on two shelves within the same growth chamber (at equal light intensity of approx. 160 μmol m^{-2} s^{-1}). All positions (genotypes on plates; plates within boxes) were completely randomised using a custom made random number generator. Plates were scanned 6, 8, 10 and 12 DAG and positions of plates within boxes re-randomised afterwards (using the random number generator). The whole experiment was replicated three times independently. Non-germinated seedlings (3 days after sowing) were not analysed, resulting in up to six seedlings analysed per genotype per condition.

Table 11: List of SSLP markers and primers used to genotype HIFs.
From left to right: Chromosome number (Chr), position of the marker (Pos [Mb]) in megabases along the respective chromosome and genomic marker ID (ID). Primer combinations and length of corresponding fragments (Col-0 or Ct-1 allele) are shown together with the HIF/RIL genotyped at each locus.

			primer combination		fragment length [bp]		
Chr	**Pos [Mb]**	**ID**	left border	right border	**Col-0**	**Ct-1**	**HIF**
1	26.05	c1_26053	TGACTCGGAATCATAAGACATAGTG	TATAACGTGGTCAAGGCATGG	795	656	178, 186, 353, 491
	27.08	c1_27080	CAAATTATGCGAATGAGTATCCG	TAAGTGTATTCTTGTTCTCTGTATGGC	860	558	178, 186, 353, 491
	27.16	c1_27160	TATTATTATCATTGTGGGACGGTC	TTTCCCAGTCGCTTTCCAC	454	565	178, 186, 353, 491
	28.52	c1_28515	CACAACACAATTATGGGTCAGG	AAGAACCAAAAATCACCGTAGG	965	442	178, 186, 353, 491
	29.42	c1_29422	TATTAACATAATAGTGTTGGAGTGAGGA	AGGCAAAGAGAATACAATCAGAGTC	276	337	178, 186, 353, 491
	29.77	c1_29774	TCTGTGACTGTAAAGCCAACGAG	CCTTCTGTGCCATAGATTTGTTG	1331	453	178, 186, 353, 491
2	0.57	c2_00566	GCTTGTAAGATGTATGTGTAGGGTG	ATGCAAATATAATCGTAGTGTCCG	710	443	309
	17.30	c2_17299	CTCACTTGTAGTTTTGTCTCAATCG	TATGTCTTCTACTATATTTTGACACTTGTG	1469	458	43, 122, 176, 386, 411
3	0.42	c3_00422	GCCTAGTCTCCACAGATTCAGC	ATGGAATTTGTTTGCGTTCG	1018	491	288, 476, 479
	1.50	c3_01500	TGGCGATCAAACATTGGC	AAATATACAAGGGATTAAGGACCG	285	224	479
	2.10	c3_02099	CTGAATTGGTGCTTTGGGAG	GCGAGAAAATAGGTCAACACG	269	345	479
	2.56	c3_02563	GTTGTTCATTACCGATGTTTTGAG	GGAATTTTGTCGTCTTTGATGG	264	377	479
	3.05	c3_03045	TTGAGTTTGAATATACTACAAGTTGACC	AGCATCATTATAATAATGCACCGA	336	441	479
	3.46	c3_03463	CGAAGATGCTTCATTGGGG	GAGGAGAAAAGGCTTGTGGC	273	371	479
	4.08	c3_04075	AGCAATTTCAGCATCTAATTCAAG	CATTTTGTCTATCTCTCTATTGTCCATC	278	368	479
	4.86	c3_04863	CACCTCTCCTCTGCTTATCTCAG	ATACAAAAGCATGACAATAAGCG	762	932	288, 476, 479; 306
	5.93	c3_05931	CATCAACATTTTAGCCGTATTAGAG	GCGTAAGTAATATGACATTAGCAGC	225	326	479
	6.98	c3_06977	TGGGTCTTTCTCGCTCAGG	GTGAAGACATTGGGGAGTGAAC	518	292	479
	8.07	c3_08067	ATCTAGTATTAGGGTTTCTATGGTTTAGC	AATGGGCTGAAATATACCAAGC	548	673	10, 132
	12.60	c3_12600	CTCATTTTATTTTCTCATATTCAATGC	AAGAATATGTGCAGGTTGTCAGG	763	576	49, 257
	17.03	c3_17032	TTCTTTTCTAAATCTCCAAGGTGC	AAGAAAGGTTTGGACAGAACGAG	796	362	309
	18.20	c3_18200	GCCATATAAACCAGTTCATCGA	ATGTTAATGAGAGAAACTTCCACG	881	422	309
	19.03	c3_19027	CCTACTTCTCCTTTATGATTTCTTCG	TCATGTGAGACTAGCATAAGCCG	829	472	309
	20.09	c3_20093	CTGTGGTTGATTGTTATACTGATGG	TCCAGAACACAAACCCTAGCC	630	529	309
	20.69	c3_20693	CATAACCCACAGGTCCCAAG	AAAAGGAAAATCAACACTCATGC	862	591	309
	20.95	c3_20952	TTGGTTGATTTTCGTGTCTCTG	GTTGGAAGCTGTTGGGTCTG	246	297	309
	21.25	c3_21251	AACAAACAAGAAAGAATATAGAAACCC	TAGCGTTGGGTCGTTCTCG	509	364	166, 297, 309,429
3	22.00	c3_22000	TGGTAGTTTTGGCTGAGAGACG	TGAGTGAAGTCGAAGAGCATAGC	487	1243	166, 297, 309,429
	22.61	c3_22612	TTGAGATTCAATCCATAACAGTACG	TATTTCATTGAAACCTTCTAACGG	1033	466	309
4	6.02	c4_06020	AAGGATGGCTGAAGTATATGGCT	CTTTAATCAGCGAGAGAGTAGTTCTG	429	278	434
	7.53	c4_07530	CATTGGAAGTTTATCATGTCAAGG	GAGAGATGGGGTAATGTTTTGC	1063	497	434
	9.08	c4_09078	ATTCATAAATCTCTTCAGAAGTGGC	ATGTTGTGCCTTATTGTTATCTATCTC	817	468	434
	10.02	c4_10020	GGATCGTATGAATTGACTTGTATGG	GCTATAATTTTAGTTGTTGTTGTGGC	616	433	434
	10.58	c4_10580	TTTGATGGGTACATCTTAAAGGG	TTTCATCCAGCTTTCATGGC	608	421	434
	10.97	c4_10970	TGAAATAGCACAGTATCCGAACC	GGGGCCAATTCTCACGTTAT	293	213	434
	11.41	c4_11412	TATACTACTCGACAAAACGTAACGC	GTAAGTGAATCGCTAGTCGTAAGATC	761	478	434, 469
	12.95	c4_12948	GGTAAATGATATAAGAGGACAGTTGG	CAATGAAGATTATTGGTTTTATAGAGC	873	319	434, 469
	14.93	c4_14925	AAAACGATGTCTACGACAACGG	CTGAGCAAAAAACGTAGTAGAACG	207	265	177, 245, 489
	17.68	c4_17680	CTTTTACGAATTGACAATCAGTCG	TTTGTAATAAGTCTTTTAATTCGTTGC	482	354	244
5	2.93	c5_02925	CCCTAATATCTTTTACTTTTCAATGC	AAACACGATTATATGGAGAAGTTGC	1201	311	272
	4.00	c5_04000	GAATGTGTTGTAAAAAAGAAGATGC	CAATTCTCATGCGATAACTCTCC	781	474	371
	23.30	c5_23300	CGAGTTGTGGATAATAATGTAAATCG	TACACAAGTATTTTACTTTCTAGTTGAGG	544	339	229, 406
	24.05	c5_24045	CTTCTTCCTCAAAACGACCATC	TCAGTCTAGTTTTTAGTTTCCTGGTC	807	1133	116, 297
	25.03	c5_25025	TTAAATTATGGCTTGATTGGTGC	TTTACATACGAGAAACATAAATAGAATCTG	379	621	116. 190, 297, 423
	26.70	c5_26700	CTCCTGTAACATCATCTGAAGCG	AACGAAGATCTCAGAAGCAGAGG	686	389	309, 116, 297

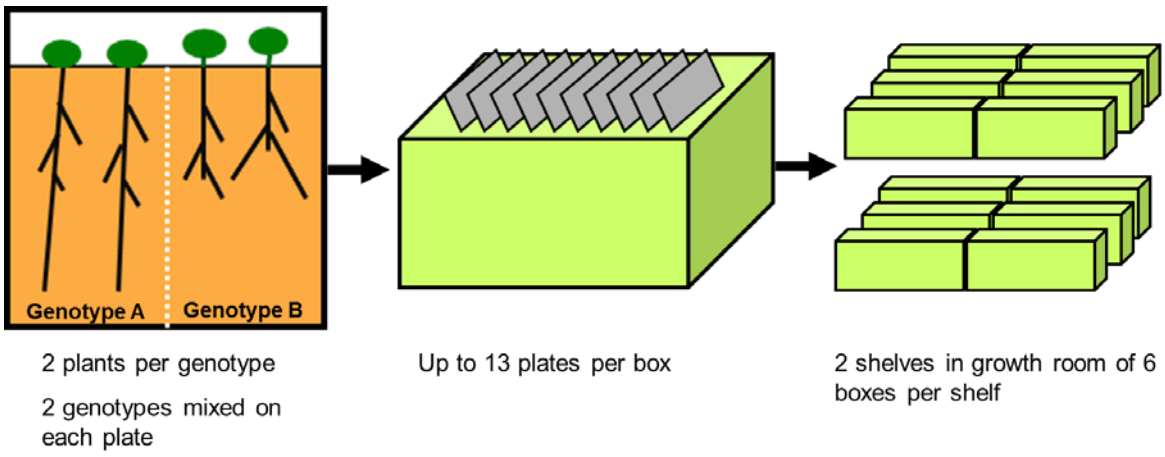

Figure 14: Experimental setup of Arabidopsis seedling culture used for QTL analysis of root architecture.
Two seedlings of two genotypes were grown on each agar plate. Up to 13 plates were randomly placed in a box and all boxes were arranged on two shelves within the same growth chamber (at equal light intensity: 160 µmol m^{-2} s^{-1}). The position of genotypes on plates (left/right) and the positions of plates within each box (position 1 to 13) were determined with a random number generator. To avoid positional effects, positions of plates within boxes were re-randomised every other day (using the random number generator).

2.5.2 QTL Mapping Procedure

A subset of 12 quantified root architectural traits was used for QTL mapping. Root parameters were quantified 10 DAG in control and 12 DAG in low-K. This represented a compromise between maximum phenotypic differences and feasibility of exact measurements with EZ Rhizo (after 10 DAG roots reached the bottom of the plate in control; after 12 DAG the rate of crossing lateral roots increased in low-K). Both datasets were cleared from outliers (95 % confidence interval) and genotype averages of individual root parameters were calculated. The *low-K/control* ratio of all root parameters was calculated for each genotype as an additional parameter characterising the 'low-K response'. Heritability h^2 of traits was estimated in collaboration with Dr Fabien Chardon, INRA Versailles, France, following the formula: $h^2 = \sigma^2_g/(\sigma^2_g + [\sigma^2_e/r])$. The genetic variance is denoted as σ^2_g, σ^2_e is the residual variance and r the number of replicates. LOD scores were calculated for each root parameter separately with Windows QTL cartographer 2.5 (Wang et al., 2011a; Silva et al., 2012). Composite interval mapping (CIM) was performed on the control dataset, the low-K dataset and the *low-K/control* dataset. The LOD threshold was determined by 1000 permutations of the respective dataset. Phenotypic

variation explained by each QTL was subsequently calculated via multiple interval mapping (MIM).

2.5.3 QTL Confirmation with Heterogeneous Inbred Families (HIFs)

Heterogeneous inbred families (HIFs) were generated to validate QTL loci previously identified with QTL mapping (Tuinstra et al., 1997). The genotypic information of Col-0 x Ct-1 RILs (Simon et al., 2008) was used to identify RILs with residual heterozygosity at QTL positions determined in the mapping procedure. A complete list of selected RILs and corresponding QTL intervals is given in Table 12, primers used for genotyping are listed in Table 11. 10 to 15 individual plants per selected RIL (F6 generation as supplied by the Versailles Stock Centre) were grown on soil and genotyped at markers corresponding to the putative heterozygous interval. Seeds were harvested from individuals harbouring the homozygous Col-0 or Ct-1 allele at the respective locus. These seeds were sown again on control and low-K plates and root architecture was quantified 12 DAG. Statistically significant differences between HIFs (containing either the Col-0 or Ct-1 allele homozygously) were scored as validated QTL.

HIFs corresponding to low K specific loci, i.e. HIF 49, 178, 434 and 479, were genotyped at multiple markers to narrow down the area of heterozygosity with higher precision. An unexpected genotypic co-segregation was observed for RILs 116, 297 and 309 (corresponding to QTL loci *CHR3.3* and *CHR5.3*; see Chapter 4).

2.5.4 Finemapping of Locus CHR3.1 with Recombinant HIF 479 (rHIF 479)

A large number (> 200) of heterozygous individuals of RIL 479 were grown on soil and genotyped at markers c3_00422 and c3_04863. Individuals that exhibited recombination within this interval (homozygous for Col-0 at one marker and homozygous for Ct-1 at the other; homozygous for either Col-0 or Ct-1 at one marker and heterozygous at the other) were selected and propagated to seed stage. This represented the parental population of *recombinant heterogeneous inbred family 479* (rHIF 479). These individuals were re-grown on soil and genotyped at a higher marker density within the genomic interval (see Table 11: markers c3_00422 to c3_04863). Seeds from individuals that were homozygous at each marker were used for phenotyping of main root path length on low-K plates. Several lines with different genotypic patterns were selected for this purpose (see Chapter 4) and statistical differences were calculated for each marker position to determine a smaller interval containing the polymorphism underlying the segregating phenotypic trait. Individuals with residual heterozygosity in this new (smaller) interval were then chosen again from the parental rHIF 479 to produce further recombinants within a smaller

genomic region of interest following the same procedure as described above. This iterative process was repeated to decrease the size of the interval.

Table 12: RILs used to produce HIFs for QTL confirmation.
Area of heterozygosity denotes the interval in which respective RILs show residual heterozygosity. Corresponding HIFs that were homozygous for either Col-0 or Ct-1 alleles in that area were phenotyped on low-K plates for the trait of interest (as per QTL analysis). Traits are only shown where phenotypic segregation was statistically significant ($p < 0.05$). LB: left border; RB: right border.

		Area of Heterozygosity				
		cM		Mb		
chromosome	RIL	LB	RB	LB	RB	Phenotypic Segregation in low-K
1	244	74	89	20.4	24.8	
	429	75	89	20.4	24.8	
	489	75	89	20.4	24.8	
	353	83	106	23.4	28.7	
	90	89	106	24.8	28.7	
	491	93	105	25.7	28.5	
	178	93	106	25.7	28.7	MRP/Apical
	186	93	113	25.7	29.9	
2	309	start	8	0.0	2.4	
	223	22	42	7.7	11.5	
	411	42	61	11.5	15.3	
	386	42	end	11.5	end	
	176	48	71	12.4	18.8	
	122	61	71	15.3	18.8	
	43	61	end	15.3	end	
	102	61	end	15.3	end	
3	191	0	6	0.0	2.1	
	332	0	6	0.0	2.1	
	476	0	16	0.0	5.1	
	288	0	20	0.0	6.6	
	479	0	26	0.0	8.0	MRP/Apical
	306	6	26	2.1	8.0	
	132	16	35	5.1	9.7	
	10	20	35	6.6	9.7	
	155	20	49	6.6	12.6	
	250	26	49	8.0	12.6	
	49	26	57	8.0	16.7	MRP/Apical
	392	35	57	9.7	16.7	
	166	57	end	15.7	end	
	297	64	end	18.1	end	
	309	71	end	20.7	end	MRP
4	434	37	52	8.9	11.9	LRP 0.25
	177	57	65	13.1	15.8	MRP
5	371	9	24	2.9	6.8	
	190	83	98	23.1	26.7	
	423	83	98	23.1	26.7	
	297	83	end	23.1	end	
	116	88	end	25.0	end	

2.5.5 Crossing of Col-0 and Ct-1 – Root Architecture Analysis of Confirmed F1 Heterozygotes

Sepals from mature flowers of Col-0 and Ct-1 plants were gently removed. Pollen from Col-0 plants was manually transferred to Ct-1 flowers and *vice versa* by rubbing stamen of excised flowers from one genotype onto pistils of intact flowers of the other genotype. Offspring of the crosses were grown on control and low-K media and root images taken 12 DAG. Tissue samples were taken from all seedlings individually and DNA was extracted following the protocol above. Heterozygous F1 individuals were identified with PCR using custom TaqMan SNP assays (Applied Biosystems, Life Technologies Corporation, Carlsbad, California) according to manufacturer's protocols. PCR was carried out using a Stratagene Mx3000P® Real-Time PCR Cycler (Agilent Technologies, Santa Clara, CA, USA) in *Allele Discrimination* mode at two markers, c2_17606 and c3_05141 (as per Simon et al., 2008), and only confirmed heterozygotes were selected for quantitative analysis of root architecture.

2.6 Analysis of Gene Expression Levels

2.6.1 RNA Extraction

Plant material was collected in screw-cap tubes containing a clean steel ball bearing and immediately snap-frozen in liquid nitrogen. The tissue was ground to powder using a tissue lyser (Tissue Lyser, Qiagen, Germany) and total RNA was extracted using the RNeasy Plant Mini Kit (Qiagen, Hilden, Germany) following manufacturer's protocols. All solutions were made with Diethylpyrocarbonate (DEPC) treated water. RNA quantity and quality was measured with a spectrophotometer (BioPhotometer plus 6132, Eppendorf, Germany) and aliquots stored at -80 °C.

2.6.2 RNA Precipitation

When RNA quality parameters were too low, a precipitation procedure was applied to increase the purity of RNA. Aliquots of RNA solution were thawed on ice. 0.1 volume of 3 M sodium acetate (pH = 5.2) and 2.5 volumes of 100% ice cold ethanol were added

and gently mixed by pipetting. The solution was stored at -20 °C overnight and subsequently centrifuged at 13.200 rpm and 4 °C for 30 min. The supernatant was removed by pipetting and the pellet washed with 70 % ethanol (made with DEPC treated ddH_2O) and centrifuged for 10 min at 13.200 rpm and 4 °C. The supernatant was discarded and the pellet air-dried for 15 min. The pellet was re-suspended in DEPC treated water and the quality and quantity of RNA re-assessed by spectrophotometry (BioPhotometer plus 6132, Eppendorf, Germany).

2.6.3 RNA Microarray Analysis

All microarray experiments were performed at the Glasgow Polyomics Facility (Sir Henry Wellcome Functional Genomics Facility, SHWFGF) using Affymetrix microarray chips. DNase Treatment and RNA quality control were performed by staff at SHWFGF prior to hybridisation of RNA to the array. Raw data normalisation was performed by Dr Pawel Herzyk at the SHWFGF using the RMA method corrected for GC probe content. Principal component analysis (PCA) of the normalised data revealed strong batch effects. Those batch effects were removed and the resulting data files used for further analysis (absolute & relative expression levels).

2.6.4 Reverse-Transcriptase PCR

Reverse transcription of RNA to produce cDNA was performed using the QuantiTect® Reverse Transcription Kit (Qiagen, Hilden, Germany) following manufacturer's instructions. cDNA was stored at -20 °C.

2.7 Histochemical Staining Techniques

2.7.1 Propidium Iodide Staining (cell wall; cell viability)

Seedlings were immersed for 10 min in 10 µg mL-1 propidium iodide (Fluka 81845, Sigma-Aldrich) solution and observed with a confocal microscope at an excitation wavelength of 543 nm.

2.7.2 Perls' Staining for Fe(III)

An analytical method to detect iron in the redox state Fe(III) is the Perls' stain. Perls' staining was performed as described in Green and Rogers (2004). To reduce staining caused by free Fe^{3+} in media sticking to the roots, excised roots or whole seedlings were immersed in 10 mM EDTA for 5 min prior to the actual staining procedure. Seedlings were washed in ddH_2O and subsequently vacuum infiltrated for 10 min in the staining solution consisting of freshly prepared 4% (v/v) HCl mixed 1:1 with 4% (w/v) potassium ferrocyanide ($K_4Fe(CN)_6$) solution. Stained seedlings were rinsed in double distilled water and observed under a regular light microscope. When possible, images were taken with an AxioCam camera (Carl Zeiss, Jena, Germany) mounted on top of the microscope. In some cases, a conventional digital camera (Canon Ixus 95) was used to take images through the lense of the microscope. In all cases, the same light settings were applied across all conditions observed.

2.7.3 Turnbull's staining for Fe(II)

Analogous to the Perls' stain, iron in the redox state Fe(II) can be detected by the Turnbull's method (Carson, 1991). Potassium ferr*o*cyanide was replaced with potassium ferr*i*cyanide ($K_3Fe(CN)_6$) solution. Otherwise, the same protocol as described in 2.7.2 was applied.

2.7.4 GUS staining

Promoter activity, and hence tissue expression levels, of genes can be visualised by transforming wild type or mutant plants fusion constructs of a promoter with the ß-glucuronidase gene (*GUS*). Here, GUS staining was used to detect tissue expression levels of the *LPR2* gene by expressing *pLPR2::GUS* fusion constructs in wild type Arabidopsis (Col-0) plants. GUS activity was demonstrated when the detection reagent *X-Gluc* (5-Bromo-4-chloro-1H-indol-3-yl β-D-glucopyranosiduronic acid) was cleaved by the GUS enzyme producing a clear blue colour.

Table 13: GUS staining solution.

	Stock conc.	Vol.(stock) per mL final solution [µL]	Final Conc.
NaH_2PO_4/ Na_2HPO4 Buffer *pH 7.0*	1 M	100	0.1 M
EDTA	0.5 M	20	10 mM
Triton X-100	10 %	10	0.1 %
$K_3Fe(CN)_6$	50 mM	20	1 mM
X-Gluc	0.1 M	20	2 mM
ddH_2O		830	

Freshly harvested Arabidopsis tissue (transformed with *pLPR2::GUS* by floral dip; see below) was immersed in the staining solution (Table 13) and vacuum infiltrated for 5 min. Tissue was incubated in the staining solution overnight at 37 °C. The following morning, the staining solution was discarded and tissue was washed by incubation in 50 % ethanol at room temperature. The washing solution (50 % ethanol) was replaced every 12 hours for 5 times and samples were observed with a light microscope.

2.8 Quantification of Ion Concentrations

2.8.1 Inductively Coupled Plasma Mass Spectrometry (ICP-MS)

Shoots of seedlings grown on vertical agar plates were separated from roots. In general, only shoot tissue was used for ionomic analysis since root tissue is prone to contamination with agar medium. Shoots from one plate were pooled and the fresh weight measured immediately. At least three plates per genotype per condition were harvested separately (three biological replicates). Pooled tissue dried in open falcon tubes at 60 °C for at least 5 days. Aliquots of approx. 5 mg dry shoot material were sent to the University of Aberdeen where ion extraction and ICP-MS was performed by Dr John Danku (group of Prof David E. Salt). Ions were extracted via in vitro digestion using 0.7 mL of concentrated nitric acid (trace metal grade, T.J. Baker) plus indium internal standard (20 ppb) per sample and incubating for 5 h at 115˚C. Samples were diluted to 6 mL final volume and elements quantified by ICP-MS (Elan DRC II, PerkinElmer). Concentrations of twenty

elements (Li, B, Na, Mg, P, S, K, Ca, Mn, Fe, Co, Ni, Cu, Zn, As, Se, Rb, Sr, Mo, Cd) were obtained using calibration standards with blanks and the external calibration method of the Elan software (version 3.4). Ion concentrations normalised to shoot dry weight (in mg per kg dry weight) were supplied by Prof D. E. Salt and statistical analysis was performed by myself .

2.8.2 Synchrotron X-Ray Fluorescence (SXRF)

Synchrotron X-Ray Fluorescence (SXRF) is routinely used by geologists, chemists and biologist alike and is becoming a more and more valuable tool in understanding metal homeostasis in plants (Punshon et al., 2009; Donner et al., 2012). SXRF has been applied to visualise metal abundance in hydrated Arabidopsis root tissue. All SXRF experiments have been carried out under supervision of Dr Tracy Punshon, Dartmouth College, and Dr Sue Wirick, University of Chicago, on Beamline X26A at the National Synchrotron Light Source (NSLS) at Brookhaven National Laboratory (BNL), Brookhaven, NY, USA. To avoid contamination with agar, Arabidopsis seedlings were grown on 20 µm pore size plastic mesh overlaying the agar growth medium (control, low-K or low-P). The mesh was lifted from the agar surface and seedlings blotted onto metal-free adhesive tape immediately prior to analysis. Shoots were removed with a sharp knife and the still hydrated roots were mounted on the experimental stage. X-Ray excitation was performed with a 10.5 keV beam passing through a Si(111) monochromator crystal before reaching the sample stage. SXRF-emission was detected in 2D map mode using detectors ME4 and 2SDD at a pixel size of 5 µm and 200 ms dwell time. For quantification of element concentration, a common standard at Beamline X26A (*SRM18333-10500*) was used for normalisation. Quantification of elements was achieved with SNRLXRF software (Sutton et al., 2002).

2.8.3 Semi-Quantitative Perls' Staining

Semi-quantitative Perls' staining of excised root tips was adapted from the Perls' staining protocol. Main roots grown on control or low-K media were cut approx. 2 mm behind the root apex. About 50-110 tips were pooled per replicate. Root tips were placed on a mesh and rinsed 5 times with cold 10 mM $CaSO_4$ solution to remove any agar sticking to the roots. Root tips were counted and blotted dry with a paper towel, put into a plastic tube and 1 mL of 4 % HCl was added as extraction solution. The suspension was vortexed

vigorously and incubated at room temperature for 5 days, vortexing at least once every day. Floating root tips were pelleted by centrifugation at 13.200 rpm for 5 min. The supernatant was diluted and used for quantification. The absorption maximum of the blue colour complex (*Prussian Blue*) at 575 nm was determined by measuring the absorption spectrum of 1 µM NaFeEDTA in a 1:1 mix of Perls' staining solution (4 % HCl and 4 % potassium ferrocyanide; see Perls' staining protocol) against 1 µM NaFeEDTA in ddH_2O (blank; Fig 15) with a PerkinElmer Lambda 45 UV/Vis monochromatic spectrophotometer (PerkinElmer, Waltham, MA, USA). All further measurements in this experiment were taken at 575 nm. Before measuring root tip samples, standard iron solutions were made from serial dilutions of NaFeEDTA in a 1:1 mixture of 4 % HCl and 4 % potassium ferrocyanide as above. Two independent series of standards were used to produce a linear standard curve (Fig. 15; R = 0.995). Supernatants of extracted root tips were mixed 1:1 with 4 % potassium ferrocyanide solution and incubated for 10 min. Absorption at 575 nm was measured and Fe(III) concentrations (normalised against number of root tips) calculated from the standard curve.

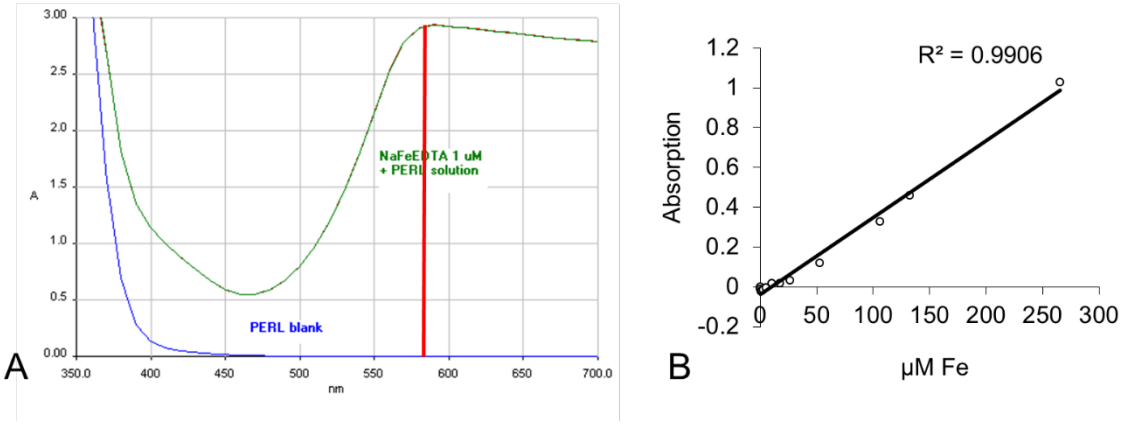

Figure 15: Standardisation of semiquantitative Perls' staining.
A) Absorption spectrum of the *Prussian Blue* ($Fe[Fe(CN)_6]$) complex formed during Perls' staining. Absorption of a 1 µM NaFeEDTA solution in ddH_2O (PERL blank) or a 1:1 mixture of 4 % HCl and 4 % potassium ferrocyanide (NaFeEDTA 1 uM + PERL solution) was measured at a 5 nm wavelength interval. The maximum absorption of Prussian Blue was detected around 575 nm (red line). **B)** Linear standard curve of absorption of standard iron solutions measured in duplicate.

2.9 Generation of Transgenic Material

2.9.1 Gateway® Cloning

DNA sequences were cloned using the Gateway® cloning technology (Invitrogen, Carlsbad, CA, USA). In this system *att* (attachment) sites mediate the site directed recombination of double stranded DNA fragments and plasmids. First, entry clones containing the sequence of interest flanked by *att* sites need to be produced. Subsequently, entry clones can be recombined with custom or commercial destination vectors to yield expression constructs that can be used to transform the organism of interest. Here, a genomic sequence of interest was first amplified by PCR (with KOD polymerase; see 2.4.2.1 high-precision PCR) using sequence specific forward and reverse primers flanked by sequences corresponding to *att* sites (Gateway forward: *GWF*; Gateway-reverse: *GWR*). Primers used for cloning are listed in Table 14. The complete PCR product was loaded onto a 1.5 % agarose gel and separated by gel electrophoresis at 100 V. The area of gel containing the DNA band of interest was excised and DNA extracted using the PureLink® Quick Gel Extraction and PCR Combo Kit (Invitrogen, Carlsbad, CA, USA) following manufacturer's instructions. The extracted PCR product was diluted to a working concentration of 150 ng μL^{-1}.

Next, BP reaction was performed to yield entry clones. 2 µL of PCR product, 2 µL of pDONR207 entry vector (150 ng μL^{-1}) and 1 µL of BP clonase II (Invitrogen, Carlsbad, CA, USA) were mixed and incubated at room temperature for 3 h. The reaction product was used to heat-shock transform chemical competent *E. coli* (TOP10 strain) cells for selection, amplification and verification of the entry clone (see below).

The LR reaction was used to generate expression constructs via recombination of entry clones with destination vectors. Per LR reaction 1 µL of entry clone, 1 µL of destination vector (both 150 ng μL^{-1}) and 0.5 µL of LR clonase II (Invitrogen, Carlsbad, CA, USA) were mixed and incubated at room temperature for at least 1 h. The reaction product was again used to heat-shock transform chemical competent *E. coli* (TOP10 strain) cells for selection, amplification and verification of the expression construct (see below). Expression constructs for *LPR2*-overexpression were generated with destination vectors pMDC32 (35S-promoter [p35S]; Curtis and Grossniklaus, 2003) and pUB-Dest (ubiquitin 10 promoter [pUBQ10]; Grefen et al., 2010). C-terminal GFP-fusions of LPR2 were produced by recombination with destination vectors p*7FWG2 (p35S; Karimi et al., 2007) and pUBC-GFP-Dest (pUBQ10; Grefen et al., 2010). For C-terminal RFP-fusion

pB7RWG2 (p35S; Karimi et al., 2007) was used. Promoter-GUS fusion constructs (*pLPR2::GUS*) were obtained by recombination of Gateway®-compatible *pLPR2* with pMDC163 (Curtis and Grossniklaus, 2003). See also Table 15 for a full list of expression constructs, incl. destination vectors used as well as bacterial (antibiotic) and plant (herbicide) resistances.

Table 14: Primers used for cloning.
Gateway® specific adaptor sequences are indicated by *GWF*- and *GWR*- and given at the bottom of the table. pDONOR primers used for sequencing were available at GATC, all other sequencing primers were custom designed and sent to the facility.

Primer Sequence	Primer Name	Used For
GWF-ACATGGAGCCTTCTCGGAGG	LPR2_GWF	Gateway®-compatible *LPR2* forward primer
GWR-TTATAGCACCATTGCAAAGGGC	LPR2_GWR_STOP	Gateway®-compatible *LPR2* reverse primer incl. stop codon
GWR-GTAGCACCATTGCAAAGGGC	LPR2_GWR_NS	Gateway®-compatible *LPR2* reverse primer without stop codon
GWF-AATAAAACTGTGGCACCGTGC	pLPR2_FOR	Gateway®-compatible LPR2-promoter forward primer (start at position -2174 bp of the *LPR2* start codon)
GWR-CTCTGGTCATTCTCCTCCGAGA	pLPR2_REV	Gateway®-compatible LPR2-promoter forward primer (stop at position +31 bp of the *LPR2* start codon)
GTGGGAGATGGGCTTTTGG	pLPR2_seq0551	sequencing of *LPR2* promoter at GATC
GACTGATGGGTTACTTTTTCGC	pLPR2_seq1229	sequencing of *LPR2* promoter at GATC
CCCCTCACTTGTTTGTCGTCT	LPR2_seq0739	sequencing of *LPR2* at GATC
TACAGAAATTCCACAGAGACTTGC	LPR2_seq1391	sequencing of *LPR2* at GATC
TAACGCTAGCATGGATCTC	pDONOR-FP	pDONR207 forward primer for sequencing (available at GATC)
GCAATGTAACATCAGAGAT	pDONOR-RP	pDONR207 reverse primer for sequencing (available at GATC)
GGGGACAAGTTTGTACAAAAAAGCAGGCT	***GWF***	Gateway® forward sequence
GGGGACCACTTTGTACAAGAAAGCTGGGT	***GWR***	Gateway® reverse sequence

Table 15: List of expression constructs used to transiently transform *N. benthamiana* and *N. tabaccum* and for stable transformation of Arabidopsis.
ID denotes the abbreviation used to label stocks in -20/-80 °C freezers. Gent: gentamycin; Hyg: hygromycin; Kan: kanamycin; Rif: rifampicin; Spec: spectinomycin.

ID	Expression Construct	Entry Clone	Destination Vector (Glasgow Stock Code)		Resistance Bacterial			Plant	References
EV01	p35S::LPR2::GFP	LPR2-N.S.	pH7FWG2	(V032)	Rif	Gent	Spec	Hyg	Karimi et al., 2007
EV02	p35S::GFP::LPR2	LPR2-STOP	pH7WGF2	(V031)	Rif	Gent	Spec	Hyg	Karimi et al., 2007
EV03	pUBI10::LPR2::GFP	LPR2-N.S.	pUBC-GFP-Dest	(V049)	Rif	Gent	Spec	Basta	Grefen et al., 2010
EV04	pUBI10::GFP::LPR2	LPR2-STOP	pUBN-GFP-Dest	(V055)	Rif	Gent	Spec	Basta	Grefen et al., 2010
EV05	pLPR2::GUS	pLPR2	pMDC163	(V043)	Rif	Gent	Kan	Hyg	Curtis and Grossniklaus, 2003
EV06	p*2x*35S::LPR2	LPR2-STOP	pMDC32	(V038)	Rif	Gent	Kan	Hyg	Curtis and Grossniklaus, 2003
EV07	pUBI10::LPR2	LPR2-STOP	pUB-Dest	(V047)	Rif	Gent	Spec	Basta	Grefen et al., 2010
EV08	p35S::RFP::LPR2	LPR2-STOP	pB7WGR2	(V030)	Rif	Gent	Spec	Basta	Karimi et al., 2007
EV09	p35S::LPR2::RFP	LPR2-N.S.	pB7RWG2	(V029)	Rif	Gent	Spec	Basta	Karimi et al., 2007
EV10	pUBI10::LPR2::RFP	LPR2-N.S.	pUBC-RFP-Dest	(V050)	Rif	Gent	Spec	Basta	Grefen et al., 2010
EV14	ER-roGFP2	roGFP2-HDEL	pWen22		Rif	Gent	Spec	Hyg	Meyer et al., 2007
EV15	mitochondrial-roGFP2	mt roGFP2	pH2GW7		Rif	Gent	Spec	Hyg	Schwarzländer et al., 2008
EV16	cytosolic-roGFP2	cyt roGFP2	pH2GW7		Rif	Gent	Spec	Hyg	Schwarzländer et al., 2008

2.9.2 Transformation of Escherichia coli

50 µL aliquots of heat-shock competent *E. coli* cells (TOP10 strain; stored at -80 °C) were thawed on ice. 5 µL of BP-product or 1.5 µL of LR-product were added and incubated on ice for a further 15 min. The mixture was incubated in a water bath equilibrated at 42 °C for 45 s. 400 µL of sterile LB medium were added and the mixture incubated in a shaker at 37 °C and 180 rpm for 1h. *E. coli* cells were sedimented by a short spin of 3-5 s, three quarters of the supernatant was removed and cells were re-suspended in the remaining solution.

For BP-products, the whole suspension was plated on LB plates containing 20 µg μL^{-1} gentamycin (pDONR207 contains a gentamycin resistance gene) and incubated at 37 °C overnight. The Gateway®-cassette of pDONR207 contains the *ccdB* gene which is toxic to TOP10 *E. coli* cells. Hence, cells transformed with the un-recombined pDONR207 vector are unable to survive (although being gentamycin resistant). Under normal circumstances, only cells transformed with the entry clone (where the Gateway®-cassette containing *ccdB* was replaced by the DNA sequence of interest) produce viable colonies. Single colonies were picked and inoculated into fresh liquid LB medium containing 20 µg mL^{-1} gentamycin. The mixture was incubated in a shaker-incubator at 37 °C and 180 rpm overnight. These cells were used for plasmid DNA extraction (see below).

For LR-products, the suspension was plated on LB plates containing antibiotics, either spectinomycin (100 µg mL^{-1}) or kanamycin (25 µg mL^{-1}) depending on the resistance gene of the destination vector (see Table 15), and incubated at 37 °C overnight. Single colonies were picked and re-cultivated overnight in liquid LB medium containing respective antibiotics in a shaker-incubator 37 °C and 180 rpm. These cells were used for plasmid DNA extraction (see below).

2.9.3 Plasmid DNA Extraction ('mini prep'*)*

E.coli cells from the liquid overnight culture (see 2.9.2) were pelleted in a 2 mL tube by centrifugation at 13.200 rpm and 4 °C for 20 s. The supernatant was discarded and the procedure repeated until all cells were pelleted. The supernatant was removed and cells were re-suspended in 400 µL of *Mini Prep Solution 1* (Table 16) by vortexing. 400 µL of *Mini Prep Solution 2* (Table 16) were added and solutions immediately mixed by inversion of the tube. After 3 - 5 min of incubation at room temperature, 400 µL of *Mini Prep Solution 3* (Table 16) were added and solutions mixed by inversion. Debris was pelleted by

centrifugation at 13.200 rpm and 4 °C for 10 min. 1000 µL of the supernatant was carefully transferred to a new 2 mL tube. For entry clones only, chloroform-isoamylalcohol purification was performed at this step. 1000 µL of a 24:1 (volume) mixture of chloroform and isoamylalcohol was added and solutions well mixed by inversion. The mixture was centrifuged at 13.200 rpm and 4 °C for 1 min to separated phases. 900 µL of upper (aqueous) phase were transferred to new 2 mL tube without disturbing the debris at the interphase. From now on, entry and expression clones were treated again in the same way. An equal amount (1000µL or 900 µL) of ice-cold 2-propanole was added to the aqueous solution and mixed by inversion. Plasmid DNA was pelleted by centrifugation at 13.200 rpm and 4 °C for 20 min. The supernatant was discarded and the pellet was washed with 500 µL 70 % ethanol (vortex) and pelleted again by centrifugation at 13.200 rpm and 4 °C for 5 min. The supernatant was decanted and the pellet vacuum-dried (Concentrator 5301, Eppendorf, Germany) for approx. 5 min. Plasmid DNA was re-suspended in 50 – 100 µL 10 mM Tris-HCl (pH = 8.0) buffer by heating the solution to 65 °C for 10 min. Plasmid DNA quality and quantity was assessed by spectrophotometry (BioPhotometer plus 6132, Eppendorf, Germany) and solutions long-term stored at -20 °C.

Table 16: Solutions used for plasmid DNA extraction.

	reagent	**conc.**
Mini Prep Solution 1	Tris-HCl	50 mM
	EDTA	10 mM
	RNase A	10 µg mL^{-1}
	Lysozyme	0.01 %
	pH adjusted to 8.0	
Mini Prep Solution 2	NaOH	0.2 M
	SDS	1 %
Mini Prep Solution 3	Potassium Acetate	3 M
	pH adjusted to 5.5 with acetic acid	

2.9.4 Plasmid Verification by Restriction-Digestion and Sequencing

To verify entry clones and expression constructs, plasmid DNA was digested with appropriate restriction enzymes and buffers. Enzyme combinations were selected by plasmid sequence analysis with *Vector NTI* software (Life Technologies, Darmstadt, Germany). Corresponding restriction buffers (NEB 1 – 4) were determined with the *Double Digest Finder* online tool (https://www.neb.com/tools-and-resources/interactive-tools/double-digest-finder; last viewed 26/04013). 1 µL of plasmid DNA was incubated with 0.25 µL of restriction enzyme 1, 0.25 µL of restriction enzyme 2, 2 µL of restriction buffer and 16.5 µL of ddH_2O for 1 h at 37 °C. The restriction product was separated by agarose (1.5 %) gel electrophoresis and DNA band patterns were compared to in silico patterns generated with *Vector NTI*.

The sequence of entry clones was also verified by sequencing at an external facility (GATC, Konstanz, Germany). Commercial sequencing primers available at the facility (pDONOR-FP, pDONOR-RP) were chosen to sequence from both ends. Sequencing reactions usually produced high quality reads of about 500 – 700 base pairs. For longer constructs, custom sequencing primers (Table 14) were designed to determine the remaining central parts of the sequence of interest.

2.9.5 Transformation of **Agrobacterium tumefaciens**

Aliquots (50 µL) of *Agrobacterium tumefaciens* (strain GV3101; Koncz and Schell, 1986) cells were thawed at room temperature for 5 min and 5 µL of plasmid DNA (from 2.9.3) was added. The mixture was first incubated on ice for 5 min, then snap-frozen in liquid nitrogen and finally incubated in a water bath at 37 °C for 5 min. 1 mL of sterile liquid LB medium was added and the culture shaken at 28 °C for 2 h. Cells were then sedimented by short (3 – 5 s) centrifugation and plated on LB plates supplied with antibiotics: gentamycin (20 µg μL^{-1}), rifampicin (50 µg μL^{-1}) and the appropriate third antibiotic (either 100 µg μL^{-1} spectinomyin or 50 µg μL^{-1} kanamycin). Plates were sealed with parafilm and incubated at 28 °C for 2 days. Single colonies were picked and re-cultured overnight in 4 mL liquid LB medium containing antibiotics. The following morning, cultures were split into three aliquots: 1) 2 mL were stored at 4 °C; this solution could be used up to 1 month for inoculation to produce fresh cultures. 2) 930 µL of culture were mixed with 70 µL of DMSO and the mixture snap-frozen in liquid nitrogen; this DMSO-stock was long-term stored at -80 °C and was used for inoculation of fresh cultures

after 1 month. 3) The rest of the culture was used for plasmid DNA extraction as described in 2.9.3.

2.9.6 Verification of A. tumefaciens *Plasmids by Re-Transformation into* E. coli

Plasmid DNA extracted from *A. tumefaciens* was used to transform *E. coli* (strain TOP10) following the protocol described in 2.9.2 to yield a higher amount of plasmid DNA. Again, plasmid DNA of transformed E. coli was extracted as in 2.9.3 and used for restriction digestion analysis as described in 2.9.4. The restriction product was separated by agarose (1.5 %) gel electrophoresis and DNA band patterns were compared to the initial pattern obtained in the first plasmid DNA extraction. Matching patterns indicated successful transformation of *A. tumefaciens*.

2.9.7 Transient Transformation of Nicotiana benthamiana *and* N. tabaccum *Leaf Epidermal Cells*

Transient transformation of *Nicotiana benthamiana* and *Nicotiana tabaccum* was achieved following the protocol described in Grefen et al. (2010). LB media with appropriate antibiotics were inoculated with *A. tumefaciens* harbouring the expression construct and grown overnight at 28 °C in a shaker-incubator (180 rpm). The next morning, 0.2 mL of this culture were used to inoculate another 5 mL fresh LB media containing antibiotics and incubated again at 28 °C and 180 rpm. During the day, samples were taken every 1 – 2 h to determine the cell density by measuring the OD_{600} with a spectrophotometer (BioPhotometer plus 6132, Eppendorf, Germany). The complete bacterial culture was pelleted after it had reached an OD_{600} of 1.0 to 1.2 by centrifugation at 13.200 rpm for 1-2 min. The pellet was washed with washing solution (1 mL of 10 mM $MgCl_2$ supplemented with 100 µM acetosyringone) by vortexing. Agrobacterium cells were pelleted again by centrifugation at 13.200 rpm for 1 min. Washing and centrifugation steps were repeated 4 times. Then, cells were re-suspended in another 1 mL of washing solution and the OD_{600} measured in a spectrophotometer. The suspensions were then diluted to reach an OD_{600} = 0.3 for single infiltration and OD_{600} = 0.2 for co-infiltration. Final solutions were incubated at room temperature for 1 – 2 h and then infiltrated into *N. benthamiana* leaf epidermis by scratching the underside of a leaf with a razor blade and injecting the bacterial suspension into the wound with a 1 mL syringe (without needle). Infiltrated plants were put back into the growth chamber (26 °C; 16/8 h light/dark) and

observed with a confocal microscope 2 to 3 days post-infiltration. All 35S-promoter based constructs where co-infiltrated with the silencing inhibitor construct P19 (Voinnet et al., 2003).

2.9.8 Stable Transformation of Arabidopsis via Floral Dip

A modified floral dip method adapted from Zhang et al. (2006) was used for stable transformation of Arabidopsis. The 5 % sucrose solution used in this protocol was replaced with 10 mM $MgCl_2$. A starter culture was produced by inoculating 5 mL liquid LB media with appropriate antibiotics with *A. tumefaciens* harbouring the expression construct and incubating overnight at 28 °C in a shaker-incubator (180 rpm). The complete starter culture was used to inoculate 400 mL of fresh liquid LB with antibiotics in a 1 L Erlenmeyer flask the next morning. This culture was grown at 28 °C and 180 rpm until an OD_{600} of 1 -1.2 was reached. The culture was sedimented by centrifugation at 4000 g and 4 °C for 20 min. Cells were washed with 400 mL ddH_2O and sedimented again by centrifugation at 4000 g and 4 °C for 20 min. Bacterial cells were re-suspended in 300 mL of 10 mM $MgCl_2$ supplemented with 0.02 % Silwet-77 (Lehle Seeds, Round Rock, TX, USA) as surfactant. The suspension was incubated in a beaker on ice for 30 min to slow down cell division (and activate the lytic cycle) and stirred again before dipping.

Arabidopsis plants were grown in long day (16/8 h light/dark) on soil for 5-6 weeks (approx. 5 plants per pot). To facilitate dipping a nylon mesh was used to cover the soil surface and the first emerging inflorescences were cut back to induce and synchronise further shoot branching. Flora dip was performed by dipping the inflorescences upside down into the bacterial suspension for 1 min. The pots were turned gently to ensure that all flowers were covered with bacterial suspension. Pots were then lifted and excess solution was drained for about 30 s. Subsequently, pots were laid on their sides into trays and covered with transparent plastic bags to keep the humidity high. These covered trays were put back into the growth chamber overnight. The next morning, the plastic bag was removed and pots brought back into vertical position. Plants were propagated to seed stage and seeds from each pot harvested separately.

2.9.9 Selection of Stable Transformants

Positive transformants obtained from floral dipping were selected with either Basta® or hygromycin. See Table 15 for a full list of expression constructs and their respective antibiotic and herbicide resistances.

Basta® selection was performed on seedlings grown on soil. Usually, a whole tray was filled with moist compost and a large number of seeds was evenly spread across the surface. After vernalisation for 3 days at 4 °C in the dark, seeds were germinated in standard long day conditions. Two weeks post-germination seedlings were sprayed with a 1:1000 dilution (in tap water) of the commercial Basta® preparation *FINALE* (Bayer Crop Science, Mannheim, Germany) until all shoots were covered with solution. Spraying was repeated twice in a 10 day interval with fresh Basta® solution. Resistant transformants were transferred to individual pots containing fresh compost and propagated to seed stage. Seeds from the T1-generation of transformants were re-sown again and Basta® selection was repeated to yield resistant T2-individuals.

Hygromycin selection was performed on plates. Half-strength MS medium was supplied with 50 µg mL^{-1} and solidified with 0.8 % agar. Vernalised seeds were sown on to the agar surface and plates were sealed with micropore tape. Plates were exposed to light for 1 day to induce germination. All plates were then wrapped in aluminium foil to avoid any further light exposure and put back into the growth chamber. After 5 days seeds had germinated and resistant plantlets had elongated, etiolated hypocotyls. The aluminium foil was removed and resistant seedlings were cultivated under normal long day conditions until they had reached four-leaf stage. Resistant seedlings were transferred to individual pots containing soil and propagated to seed stage. Hygromycin selection of T1-transformants was repeated to yield resistant T2-individuals.

At the end of my PhD project, several expression constructs were stably transformed into various Arabidopsis genotypes. For most constructs, several independent T2-lines were produced and these can now be propagated to T3- and T4-generations by further selection. Homozygous T4-individuals may be selected and used for further experiments to characterise the transgenes.

2.10 Confocal Laser Scanning Microscopy

Confocal Laser Scanning Microscopy (CLSM) was used to visualise fluorescent proteins and protein tags (GFP, YFP, RFP) in transgenic plants, as well as fluorescent dyes (propidium iodide) that had been infiltrated into plant tissue. In CLSM, a laser beam of distinct wavelength excites a specimen and fluorescence from the specimen is collected to produce 2- and 3-dimensional images of the object. This is achieved by scanning along the confocal plane in x- and y-directions to create a 2-dimensional fluorescent image of that plane. Multiple planes along the z-axis can be collected to produce a stack of planes from which a 3-dimensional representation can be remodelled.

For CLSM, a ConfoCor 2 / LSM510 confocal microscope (Carl Zeiss, Jena, Germany) was used in all experiments. In order to achieve high image quality, settings of the microscope have to be chosen correctly. Important settings to be defined by the microscope user are now briefly summarised. The excitation wavelength has to match the optimal excitation profile of the fluorescent probe of interest. GFP-constructs were excited with the argon (*Argon/2*) laser at 488 nm, YFP-constructs at 514 nm (Argon/2) and RFP-constructs with a helium-neon laser (*HeNe1*) at 543 nm. For propidium iodide staining, 543 nm (HeNe1 laser) was chosen for excitation. The intensity of the excitation laser was adjusted to the fluorescence signal intensity of the individual constructs. Negative controls were included in all experiments to avoid false-positive detection of auto-fluorescence.

The confocal aperture (the *pinhole*) determines the width of the plane from which fluorescent light is collected. A low pinhole reduces the thickness of the plane but consequently also reduces the signal intensity. Generally, the pinhole size was set to 1 *airy unit*. When bigger sizes were required due to low signal intensity, pinholes of all collected wavelengths were matched.

Dichroic mirrors are used to split the path of light of different wavelengths (e.g. *low pass*: only light below a certain wavelength will pass through the filter, light of higher wavelength will be reflected). The following mirror sets were used:

a) For GFP: MBS: HFT 488; DBS1: Mirror; DBS2: NFT 545; s: FW1.

b) For YFP: MBS: HFT 458/514; DBS1: NFT 635 VIS; DBS2: NFT 545 NFT; DBS3: Plate.

c) For GFP/RFP co-localisation: MBS: HFT UV/488/543/633; DBS1: Mirror; DBS2: NFT 545; s: FW1.

d) For propidium iodide staining: HFT 488; DBS1: Mirror; DBS2: NFT 545; NDD MBS: none.

The filter set was chosen to ensure the correct light passage to and from the specimen and to limit the range of fluorescent light collected at the photo detector. The following filter sets were used:

a) For GFP: BP 505-530.

b) For YFP: BP 530-600.

c) For GFP/RFP co-localisation: BP 505-530; BP 560-615.

d) For propidium iodide staining: LP 560.

Fluorescent light of probes was usually detected in a wavelength interval of 30 - 50 nm above the excitation wavelength. Chlorophyll in chloroplasts can be excited by a broad range of wavelengths but emits in the red area or the visible spectrum. Chlorophyll fluorescence was therefore detected above 635 nm for comparison.

The LSM510 also allows for adjustment of the detection gain and amplifier offset. To optimise the signal intensity and to reduce noise, both settings were adjusted at the beginning of an experiment. Consequently, these settings varied across experiments but they were kept constant within experiments.

2.11 Statistical Analysis

For statistical analysis the XLSTAT (Addinsoft, Paris, France) package for Excel was used in latest versions (2010 to 2013). For natural variation of root architecture and QTL analysis, outlier analysis was performed at a 95 % confidence interval and outliers respectively removed from the dataset.

Analysis of variance (ANOVA) was initially used to determine the proportion of variation within the phenotypic (root architecture) dataset explained by single environmental conditions and environmental interactions (cf. Chapter 3). ANOVA is based on variance partitioning, i.e. variances calculated as sums of deviation squares (SS) from the overall mean are split into a between-group component (here: nutrient treatment) and a within-group component (‘error’). After variances have been partitioned, between-group variabilities are compared with the within-group variabilities using a statistical test, usually an F-test. If one of the between-group variabilities is sufficiently high and hence below the significance threshold a significant proportion of the total variation in the dataset can be attributed to this group factor (here the nutrient treatment). There is generally no limit to the number of groups and for each group the between-group SS will be compared to the within-group SS.

There are several ways to calculate variance partitioning. The 'type III SS' method used here initially partititiones variances between all treatments. In a second step all treatments for which no significant effect ($p > 0.05$) was detected are discarded as group factors and ANOVA is calculated again. This process is iterated until only statistically significant treatments are left. The same analysis can be carried out between mixed types of groups/treatments. For example in Chapter 4, ANOVA was calculated for individual root architecture parameters using environmental conditions (nutrient media) and genotype factors (natural accessions) as groups. In addition to single factors, ANOVA also allows to calculate the effect of environmental interactions, or as in Chapter 4 genotype-environment interactions. The latter example is illustrated by the fact that certain genotypes show a specific root architectural phenotype only in a specific environmental condition. These interactions are particularly interesting when studying environmental responses.

For many ANOVA applications it is of interest whether means of certain groups are statistically different. In this case a post-hoc comparison is performed. Two widely used post-hoc tests are Tukey's t-test (a.k.a. Tukey's HSD) and the Bonferroni correction. Tukey's t-test essentially follows a normal Student's t-test procedure but extends it to multiple comparisons at a time. Bonferroni correction reduces type I errors (false-positives) by lowering the statistical threshold, i.e. the p-Value (e.g. 0.05) is divided by the number of groups. Post-hoc multiple comparisons were performed in Chapters 3, 4 and 6. In simple cases where only two groups were compared I used parametric tests (Student's t-test) or non-parametric tests (Mann-Whitney U) accordingly.

Cluster analysis was used to form categories of similar genotypes and genes. Arabidopsis natural accessions were grouped according to similar root phenotypes in control and low-K conditions (Chapter 4) using agglomerative hierarchical cluster analysis (AHC). AHC produces a hierarchical tree based on dissimilarity. The Euclidian distance measure used here calculates the average n-dimensional geometric distance (n = number of root architecture parameters) between individual genotypes. Ward's method was used for agglomeration of groups. Expression data was used to group genes into nutrient response clusters via k-means clustering in Chapter 3. This analysis method produces a predefined number (k) of groups with the greatest possible distinction. In principal, individual objects (genes) are moved between clusters and means of clusters are compared via statistical methods (similar to ANOVA). Computation of this procedure is repeated until an optimal distribution of genes into the k clusters is achieved.

3. Dissection of root system architecture responses to multiple environmental stresses

3.1 Introduction

Phenotypic plasticity enables plants to synchronise growth with environmental fluctuations. A good example for plasticity is the spatial configuration of the root system, i.e. root system architecture (RSA), which is highly responsive to external nutrient availability. In dicotyledonous plants, morphological adaptation generally occurs via preferential growth of the main root (MR) or lateral roots (LR), ensuring an optimised exploitation of scarce resources within the soil (Lopez-Bucio et al., 2003). In the last fifteen years, studies on the genetic model plant Arabidopsis have provided insight into the interplay between nutrient supply and RSA. So far, research has captured a small set of RSA features and the effects of single nutrients were measured in isolation. Naturally, the main objectives were those nutrients that represent the bulk of mineral uptake: nitrogen in the form of nitrate (N), phosphate (P), potassium (K), sulphate (S) and ammonium (see also Chapter 1.3: Plant mineral nutrition). Main phenotypic consequences and key genes involved in nutrient sensing and signalling underlying these morphological responses will now be summarized briefly.

N-nutrition has been associated with changes in the lateral root (LR) system. All studies mentioned in the following investigated the effect of nitrate as the sole nitrogen source. If not otherwise stated, this was also the case in the study presented in this chapter. Nitrogen deficiency transiently enhances root branching via LR emergence and elongation when transferred from high-N to low-N media (Remans et al., 2006b). In contrast, high-N and high C/N ratios repress LR elongation (Zhang et al., 1999; Lopez-Bucio et al., 2003; Little et al., 2005). Targeted colonisation of nitrate-rich patches via LR elongation is elicited via a signalling pathway that involves the nitrate transporter NRT1.1 (Remans et al., 2006a) and the MADS box transcription factor ANR1 (Zhang and Forde, 1998). NRT1.1 (aka CHL1) is phosphorylated at threonine 101 via CIPK23, a calcium-dependent CBL-interacting protein kinase (Ho et al., 2009). Phosphorylation switches NRT1.1 from low to high affinity mode and functions as the trigger for downstream signalling pathways, making NRT1.1 a putative nitrate ‘transceptor’ (Ho et al., 2009). This view has been strengthened by the discovery that NRT1.1 is also capable of transporting auxin (Krouk et al., 2010). High external nitrate concentrations repress NRT1.1 mediated auxin transport

providing a potential direct link between nitrate sensing and phytohormonal regulation of root growth. Downstream signalling also involves transcriptional upregulation of *NRT2.1* gene expression (Ho et al., 2009). NRT2.1 is the major high affinity nitrate uptake system in Arabidopsis roots and has been shown to be involved in root architecture responses to nitrogen starvation (Little et al., 2005; Remans et al., 2006b).

P-deprivation (low-P) evokes a major reduction of main root (MR) elongation (Williamson et al., 2001; Lopez-Bucio et al., 2002). It is still debated whether low-P also increases LR density in an auxin-dependent manner (Lopez-Bucio et al., 2002; Nacry et al., 2005; Perez-Torres et al., 2008; Miura et al., 2011). To date, there is no absolute consensus how to best quantify lateral branching which makes interpretation of LR data somewhat subjective (De Smet et al., 2012; Dubrovsky and Forde, 2012). Parameters that are stable across a multitude of conditions would help to dissect pure developmental phenotypes from environmentally responsive ones. As far as the main root is concerned, some molecular P-sensors have been identified (Svistoonoff et al., 2007; Ticconi et al., 2009). Local P-sensing is integrated with a system of global regulators (reviewed in Abel, 2011, and Hammond and White, 2011) in which sugar signalling plays an important role (Hammond and White, 2008; Lei et al., 2011). It is therefore of interest whether alterations in carbon input, e.g. caused by different light regimes, can influence root architecture in contrasting P environments.

K-deficiency (low-K) leads to impaired overall plant growth because K is the major osmoticum needed for cell expansion (Amtmann et al., 2006). Consequently, both main root (Qi et al., 2008; Kim et al., 2010) and lateral root elongation (Armengaud et al., 2004; Shin and Schachtman, 2004) were reduced in plants grown on low–K media. More pronounced inhibition of root growth at very low K concentrations was observed in loss of function mutants of *HAK5* and *AKT1* (Hirsch et al., 1998; Spalding et al., 1999; Rubio et al., 2008; Qi et al., 2008; Pyo et al., 2010).The shaker channel AKT1 operates in a broader range of K concentrations but is activated in low-K by CIPK23 (Xu et al., 2006; Lee et al., 2007), the same kinase that regulates NRT1.1. Hence, CIPK23 is a putative candidate for N-K crosstalk. Low-K was also shown to induce *NRT2.1* expression (Armengaud et al. 2004) and to have profound effects on root C/N metabolism (Armengaud et al. 2009a).

S-deprivation (low-S) has been reported to either enhance (Kutz et al., 2002; Lopez-Bucio et al., 2003) or reduce root growth (Wu et al., 2010). A complicating issue is the use of different nutritional backgrounds in these respective studies. Therefore the question arises: To what extent are low-S responses in fact responses to a complete 'nutrient scenario' rather than responses to S-deficiency alone.

A look at the publications cited above shows that a considerable amount of new knowledge has been gained since the start of my PhD project in autumn 2009. However, the diversity of signalling pathways and phenotypic outputs of individual nutrients that has emerged from these studies still presents a challenge for predicting RSA in a more complex nutrient environment. At this stage, we simply lack information on RSA responses to multiple environmental stresses. Are RSA responses to individual nutrients additive under multiple deficiency? Are responses to certain nutrients prioritised over others? Does each nutrient combination produce entirely new RSA outputs? Closing this knowledge gap by measuring the effects of varying nutrient combinations is essential for understanding how individual nutrient signalling pathways interact with each other and will enable the prediction of novel cross-regulatory gene networks.

To fully capture the complexity and plasticity of RSA, a comprehensive dissection of root parameters will greatly benefit this research. Novel root imaging tools (e.g. Armengaud et al., 2009b; Iyer-Pascuzzi et al., 2010; Naeem et al., 2011; Clark et al., 2013) have made this possible and are constantly being improved. Our laboratory has developed EZ Rhizo (Armengaud et al., 2009b), a root image analysis software that is well suited for fast, semi-automated quantification of up to 20 root parameters simultaneously. I have used EZ Rhizo to quantify 13 root parameters in 32 nutrient conditions resulting from all binary combinations of sufficient/deficient supply of N, P, K and S in long or short days. The obtained large dataset provides a quantitative framework for future investigation of specific nutrient combinations and specific RSA parameters over a broader concentration range. In this chapter, I can already demonstrate that this initial study can inform mutant analyses to characterise crosstalk between nutrient signalling pathways. Results presented in this chapter have initiated experiments investigating common elements of low-P and low-K response regulation which will be the topic of Chapter 5 and 6. Here, additional data was gathered by profiling the root transcriptome and quantifying the shoot ionome for a subset of conditions. Combining phenomics, transcriptomics and ionomics, I will try to embed RSA responses in a systemic understanding of molecular ‘upstream’ and physiological ‘downstream’ events.

3.2 Results

3.2.1 Dependence of root architecture parameters on N, P, K, S and day length

Arabidopsis seedlings (n = 508) were grown on vertical agar plates containing 16 different growth media that resulted from binary combinations of nitrogen (in the form of nitrate; N), phosphorus (phosphate; P), potassium (K) and sulphur (sulphate; S) supply. As a rule of thumb, sodium (Na) was used to compensate for variations in K supply and chloride (Cl) was used to alter nitrate, phosphate and sulphate concentrations. The complete composition of all 16 media used is given in Table 17. In this chapter, the two modes of nutrient supply will be referred to as *sufficient* (or *normal*) and *deficient* (or *low*; Table 18). Sufficient supply of all four nutrients (NPKS) will be termed *control* condition.

Table 17: Composition of growth media used in Chapter 3.
Combinations of N, P, K and S supply that define each medium are depicted by upper-case letters (on black background) for sufficient supply and by lower-case letters (on white background) for deficiency. Volumes (mL) of nutrient stock solutions (stock concentration in mM) needed to prepare 1 L of final medium are shown in the upper panel of the table. Resulting final ion concentrations (mM) are shown in the lower panel. Na and Cl were used to replace cations and anions respectively. Ca (0.25 mM) and Mg (0.5 mM) were constant across all conditions. The total osmolarity (values in milliosmolar) of the medium was kept as similar as possible to rule out additional osmotic effects.

		Volumes [mL] of stock solutions used to prepare 1 L of medium															
	stock conc [mM]	N P K S	N P K s	N P k S	N P k s	N p K S	N p K s	N p k S	N p k s	n P K S	n P K s	n P k S	n P k s	n p K S	n p K s	n p k S	n p k s
$CaCl_2$	125	2	2			2	2			2	2	2	2	2	2	2	2
$Ca(NO_3)_2$	125			2	2			2	2								
$MgCl_2$	500	0.5	0.95	0.5	0.95	0.5	0.95	0.5	0.95	0.5	0.95	0.5	0.95	0.5	0.95	0.5	0.95
$MgSO_4$	250	1	0.1	1	0.1	1	0.1	1	0.1	1	0.1	1	0.1	1	0.1	1	0.1
KCl	1000									1.95	1.95			1.95	1.95		
KNO_3	1000	2	2			2	2										
	50			1	1			1	1	1	1	1	1	1	1	1	1
$NaNO_3$	500			2.9	2.9			2.9	2.9								
NaCl	500			1	1	0.96	0.96	1.96	1.96			3.9	3.9	0.96	0.96	4.86	4.86
NaH_2PO_4	200	2.5	2.5	2.5	2.5	0.1	0.1	0.1	0.1	2.5	2.5	2.5	2.5	0.1	0.1	0.1	0.1

	final concentration of nutrients in media [mM]															
NO_3^-	2.00	2.00	2.00	2.00	2.00	2.00	2.00	2.00	0.05	0.05	0.05	0.05	0.05	0.05	0.05	0.05
PO_4^{3-}	0.50	0.50	0.50	0.50	0.02	0.02	0.02	0.02	0.50	0.50	0.50	0.50	0.02	0.02	0.02	0.02
K^+	2.00	2.00	0.05	0.05	2.00	2.00	0.05	0.05	2.00	2.00	0.05	0.05	2.00	2.00	0.05	0.05
SO_4^{2-}	0.25	0.025	0.25	0.025	0.25	0.025	0.25	0.025	0.25	0.025	0.25	0.025	0.25	0.025	0.25	0.025
Mg^{2+}	0.50	0.50	0.50	0.50	0.50	0.50	0.50	0.50	0.50	0.50	0.50	0.50	0.50	0.50	0.50	0.50
Ca^{2+}	0.25	0.25	0.25	0.25	0.25	0.25	0.25	0.25	0.25	0.25	0.25	0.25	0.25	0.25	0.25	0.25
Na^+	0.50	0.50	2.45	2.45	0.50	0.50	2.45	2.45	0.50	0.50	2.45	2.45	0.50	0.50	2.45	2.45
Cl^-	1.00	1.48	1.00	1.48	1.48	1.96	1.48	1.96	2.95	3.43	2.95	3.43	3.43	3.91	3.43	3.91
Osmolarity	7.00	7.00	7.00	7.25	7.00	7.25	7.00	7.25	7.00	7.25	7.00	7.25	7.00	7.25	7.00	7.25

Table 18: Nutrient concentrations used for sufficient and deficient supply in mM.
See Table C3-01 for complete compositions of all 16 resulting nutrient media.

	Nitrate (N)	Phosphate (P)	Potassium (K)	Sulphate (S)
sufficient / normal	2	0.5	2	0.25
deficient / low	0.05	0.02	0.05	0.025

On each plate, four seeds were placed on on the agar surface directly under the edge where agar has been removed with a knife and spatula (2 cm from the top of the plate). Seeds were stratified for 2 days at 4 °C in the dark and subsequently moved into growth boxes in controlled climate chambers (see also Material and Methods section 2.2.4). After three days, germination was scored and non-germinated seeds were discarded from further analysis. Seedlings were grown on at least 3 plates per media resulting in n = 10 to 26 seedlings per environmental condition (media).

Experiments were performed in two light/dark regimes (16/8 h = long day [LD]; 9/15 h = short day [SD]; light intensity in both regimes: 160 µmol m^{-2} s^{-1} ['control light']) resulting in 16 x 2 = 32 conditions in total. Plates were scanned ten days after germination (10 DAG) and thirteen selected root system architecture (RSA) parameters (see Table 5 for descriptions) were quantified with EZ Rhizo. The dataset was subjected to analysis of correlation (Table 19) and to analysis of variance (ANOVA). All raw data is deposited in the electronic appendix under *Ch3_NPKS root architecture*.

Fig. 16 displays ANOVA results from the entire dataset. Percentage of variation explained by environmental factors is plotted against individual RSA parameters. Some RSA parameters were strongly determined by the environmental factors (e.g. > 70% variation explained for total root size [TRS], main root path length [MRP], apical zone and branched zone length, 1st order lateral root number [1st order LR #]) whereas others were less so (e.g. < 25% for length of basal zone, main root angle [MR angle] and 2nd order lateral root number [2nd order LR #]). All RSA parameters depended on more than one environmental factor and each of them showed its own typical pattern of dependence. For example, apical root length was almost entirely determined by P-supply, whereas lateral root length in the basal quartile of the main root (LRP 0.25) was more equally influenced

by P, N and K. Similar patterns of dependence were also reflected in high Pearson correlation coefficients, e.g. between total root size and branched zone length (Table 19). Predominant single nutritional factors determining RSA parameters were P and N, with a stronger influence of P on main root (MR) parameters and of N on lateral root (LR) parameters. Change of K alone had a minor effect on RSA apart from main root angle and LRP 0.25. S had no effect on RSA on its own. However, both K and S contributed to RSA through interaction with other nutrients and/or day length (see below).

Table 19: Pearson correlation coefficients between root parameters quantified on 16 nutrient media in long and short day. Phenotypic data was collected 10 DAG. Correlation analysis was performed for long day (LD) and short day (SD) separately. Colour coding highlights positive (red) and negative correlations (blue) between root traits. The significance threshold was set at $p < 0.05$. n.s. not significant.

	TRS		MRP		Basal		Branched		Apical		MR angle		LRS		1st order LR #		2nd order LR #		LRP 0.25		LRP 0.50		LR density / MR		LR density / BZ	
	LD	SD	LD	SD	LD	SD	LD	SD	LD	SD	LD	SD	LD	SD	LD	SD	LD	SD	LD	SD	LD	SD	LD	SD	LD	SD
TRS																										
MRP	0.91	0.97																								
Basal	n.s.	n.s.	n.s.	n.s.																						
Branched	0.95	0.95	0.91	0.91	n.s.	n.s.																				
Apical	0.68	0.90	0.89	0.97	0.52	0.19	0.63	0.78																		
MR angle	n.s.	n.s.	n.s.	n.s.	0.50	0.35	n.s.	n.s.	n.s.	n.s.																
LRS	0.54	0.43	n.s.	n.s.	n.s.	n.s.	0.52	0.55	n.s.	n.s.	n.s.	n.s.														
1st order LR #	0.90	0.83	0.82	0.73	n.s.	n.s.	0.97	0.94	n.s.	n.s.	n.s.	n.s.	0.66	0.74												
2nd order LR #	n.s.	n.s.	n.s.	n.s.	n.s.	n.s.	n.s.	n.s.	n.s.	n.s.	n.s.	n.s.	0.82	0.52	0.64	0.72										
LRP 0.25	0.93	0.95	0.73	0.91	n.s.	n.s.	0.80	0.88	0.51	0.86	n.s.	n.s.	0.66	0.48	0.75	0.76	n.s.	n.s.								
LRP 0.50	0.57	0.39	n.s.	0.23	n.s.	n.s.	0.57	0.59	n.s.	n.s.	n.s.	n.s.	0.95	0.89	0.70	0.79	0.86	0.53	0.65	0.35						
LR density / MR	n.s.	n.s.	-0.57	-0.76	-0.64	-0.10	n.s.	n.s.	-0.81	-0.85	n.s.	n.s.	0.54	0.33	n.s.	n.s.	n.s.	n.s.	n.s.	n.s.	n.s.	n.s.				
LR density / BZ	-0.65	-0.70	-0.73	-0.76	-0.52	-0.26	-0.67	-0.65	-0.63	-0.73	n.s.	n.s.	n.s.	n.s.	-0.63	-0.47	n.s.	n.s.	-0.52	-0.70	n.s.	n.s.	0.54	0.79		

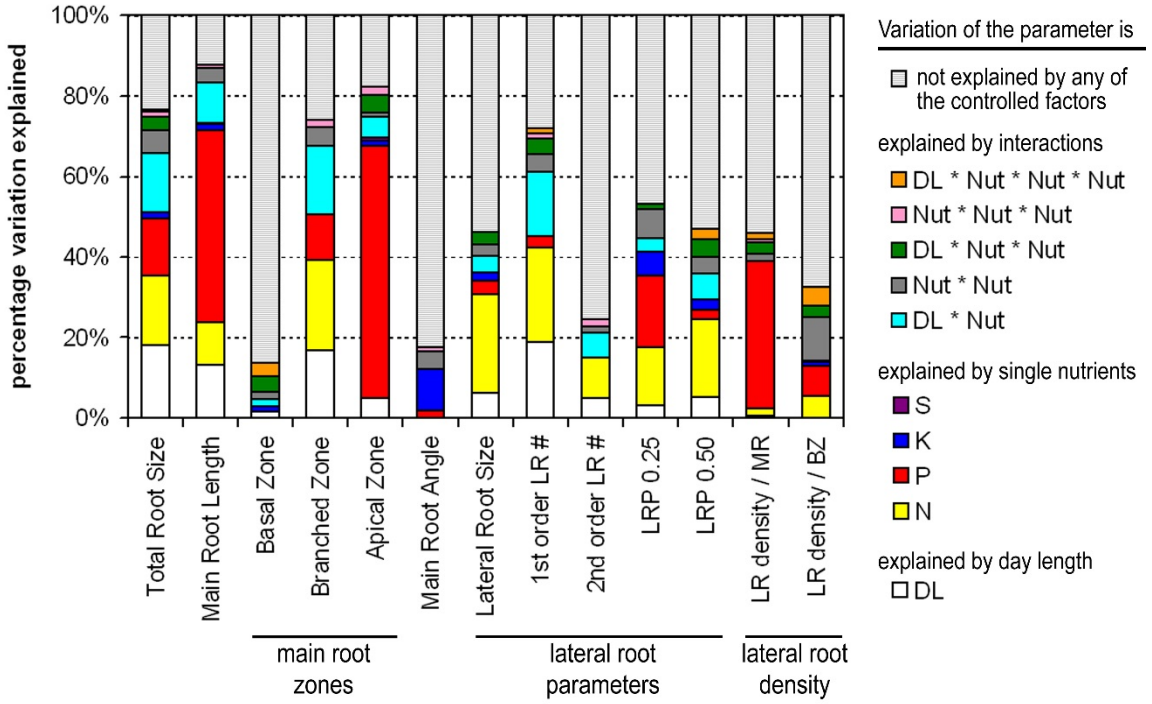

Figure 16: Variation in root parameters explained by environmental conditions obtained through global ANOVA of all nutrient and light conditions.
Independently analysed individual root parameters are given on the x-axis as per Table 5. Environmental conditions are colour coded according to the legend on the right. ANOVA was computed using type III sums of squares at a significance level of $p < 0.05$. The analysis is based on 508 plants (n = 10 to 26 plants per media) phenotyped 10 days after germination (10 DAG). Further details on growth conditions are given in the main text. DL: day length; Nut: any nutrient; *: interaction.

Interactive effects of day length and nutrient supply made an important contribution to RSA variation (Fig. 16). Especially total root size, main root and branched zone length as well as 1st order LR # depended on day length alone and on day length – nutrient interactions (DL * Nut). The dataset was therefore split into long day (LD) and short day (SD) and re-analysed separately. ANOVA was carried out for RSA parameters obtained from plants phenotyped in long day 10 days after germination (LD 10 DAG; 200 plants) and short day 10 days after germination (SD 10 DAG; 308 plants). In order to account for different root sizes of seedlings from LD 10 DAG and SD 10 DAG an additional dataset was included by analysing root images of short day grown plants again 14 DAG (SD 14 DAG; 289 plants) The number of SD 14 DAG seedlings was slightly less than in SD 10 DAG as some plants had grown into the boundaries of the plate and thus accurate analysis was no longer possible. In general, SD 14 DAG plants showed similar overall root size as LD 10 DAG plants (see also Fig. 19D).

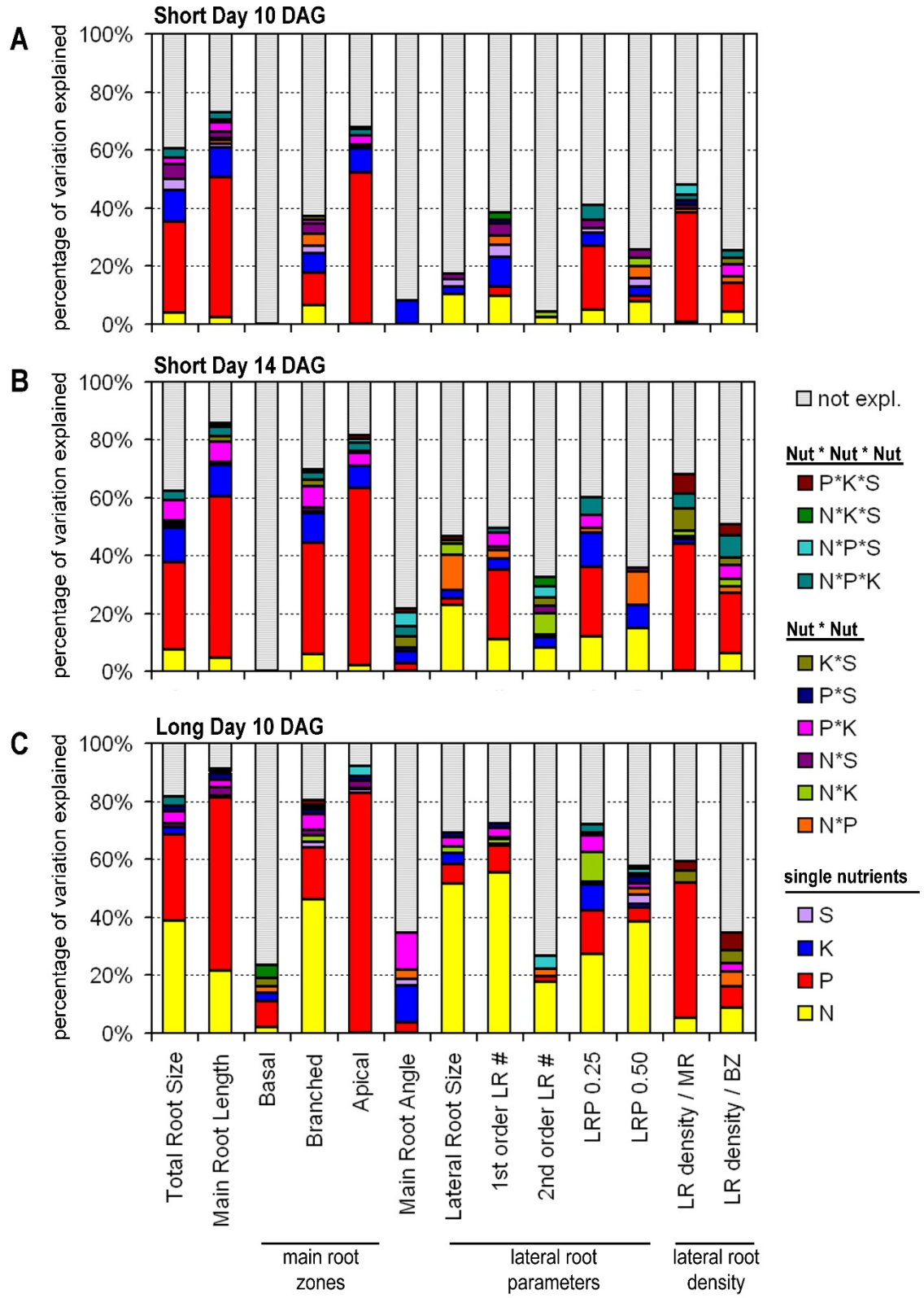

Figure 17: Variation in root parameters explained by environmental conditions obtained through ANOVA of long and short day datasets.
The analysis was performed on root data of plants grown in **A)** short day 10 DAG (number of plants: n = 308), **B)** short day 14 DAG (n = 289) and **C)** long day 10 DAG (n = 200). Independently analysed individual root parameters are given on the x-axis. Environmental conditions are colour coded according to the legend on the right. ANOVA was computed using type III sums of squares at a significance level of $p < 0.05$. *: interaction; Nut: nutrient; not expl.: not explained.

Results from this second ANOVA (Fig. 17) gave a refined picture on P- and N-effects in both light regimes. Clearly, P was the most important nutritional factor determining RSA (mainly main root parameters) in short days both at 10 DAG and at 14 DAG (Fig. 17A, B). A longer light period increased the influence of N on RSA (Fig. 17C). In particular, length and number of lateral roots were now primarily determined by N.

The importance of the carbon/nitrogen (C/N) ratio for root growth has been stressed before (Malamy and Ryan, 2001) but the strong effect of day length was surprising considering that all media were 'carbon-clamped' by addition of 0.5 % sucrose. The ratio of externally supplied C and N atoms was 88 in N-sufficient and 3509 in N-deficient media; yet this large difference in C/N ratio hardly affected RSA in short day. To investigate whether differences between SD and LD roots were caused by differences in photon input, plants were grown in SD with a higher photon flux density (280 µmol m^{-2} s^{-1} = 'high light') than used in previous experiments (160 µmol m^{-2} s^{-1} = 'control light'). Ten days after germination, 'high light' conditions in SD had produced an equal cumulative photon dosage as LD 'control light'. Sucrose was still supplied at 0.5 %. Fig. 18 shows that N-deficiency (low-N) did not alter total root size or lateral root path length in the basal quartile (LRP 0.25) in SD 'control light' (14 DAG), but reduced those parameters in both LD 'control light' and SD 'high light' (10 DAG). Moreover, low-N induced elongation of lateral roots in the second quartile (LRP 0.50) in SD 'control light', but not in LD 'control light' or SD 'high light'. These findings indicated that high photon dosage was indeed the primary co-factor eliciting low-N responses of root architecture. However, SD 'high light' reduced total root size and LRP 0.25 even in N-sufficient conditions, suggesting that high photon density had an additional, nutrient independent effect on RSA. The effects of K-deficiency (low-K) and particularly of N-K double deficiency (low-NK) were also stronger in SD 'high light' than in LD 'control light'. In conclusion, I found that increasing day length increased the influence of N on RSA and that this effect could be mimicked by higher light intensity over a shorter day length.

.

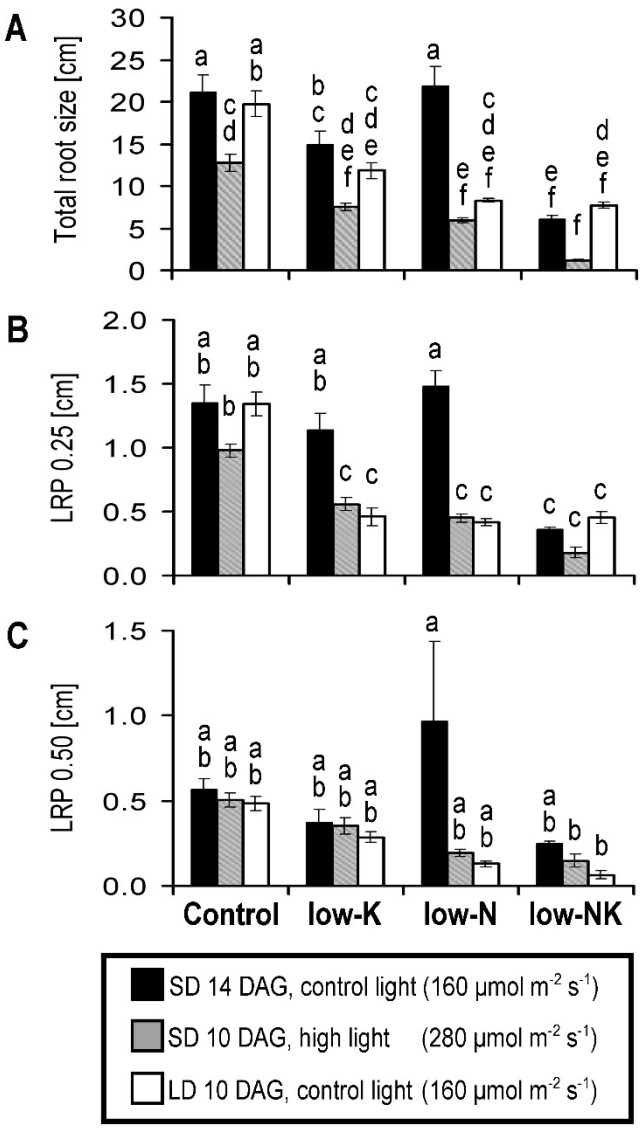

Figure 18: High light intensity in short day elicits similar root responses to nitrogen starvation as observed in long day.
A) Total root size, **B)** lateral root path length in the first quartile (LRP 0.25) and **C)** lateral root path length in the second quartile of the main root (LRP 0.50) of seedlings grown on control, single deficiency (low-K, low-N) and N-K double deficiency (low-NK) media. Plants were cultivated in three light regimes: short day (SD) with control light intensity (160 µmol m^{-2} s^{-1} as used in all other experiments; black bars), short day with a higher light intensity (280 µmol m^{-2} s^{-1}; grey bars) and in long day (LD) with control light intensity (white bars). At the time point of root architecture measurements, the total light dose perceived was the same in all three conditions (SD 14 DAG control light; SD 10 DAG high light; LD 10 DAG control light). Bars show means (n = 11 to 22) ± S.E.M. ANOVA was computed with all conditions and genotypes as input, followed by pairwise comparisons (Tukey's t-test). Different letters indicate significant differences at $p < 0.05$.

In addition to its overall effect on N-sensitivity of RSA, day length modulated several specific nutrient effects. Some examples are shown in Fig. 19. Due to similar total root size (with the exception of low-P, low-N and low-NK) root architecture quantified in LD 10 DAG was compared with SD 14 DAG (Fig. 19D). Statistical tests were performed for all conditions but for clarity only comparisons mentioned in the following text are highlighted in the figure. Apical zone length was influenced by either K or S depending on day length. In a low-N background, low-K strongly reduced apical zone length in short but not in long days while low-S reduced apical zone length in long but not in short days (Fig. 19A). Low-P reduced apical root length to a small value independent of K or S in long days whereas in short days K and S interactively modulated this parameter (Fig. 19A). An inhibitory effect of low-K on lateral root length in the basal quartile of the root (LRP 0.25) required long day conditions in sufficient N but short day conditions in low-N (Fig. 19B).

Apart from its dependence on P-supply, lateral root density within the branched zone (LRdensBZ) was quite stable across all conditions (Fig. 19C). In particular, LRdensBZ was independent of day length (no statistically significant differences between long and short day for individual media). Higher values on the right end of Fig. 19C can be regarded as an artefact of very low total root size (and hence 1st order LR # and branched zone length) that occur in NP double deficiency. Two back-to-back commentaries published in *The Plant Cell* have recently discussed the correct quantification of root parameters in studies on lateral root development (De Smet et al., 2012; Dubrovsky and Forde, 2012). It was pointed out that differences in growth conditions can lead to differences in lateral root initiation and emergence, making it hard to compare results obtained in different labs. Two ways to overcome that issue were proposed: either standardisation of growth conditions or quantification of lateral root parameters that are stable across a broad spectrum of conditions. With regard to the latter proposal, my results support the use of lateral root density within the branched zone as a reliable parameter when studying fundamental properties of LR development.

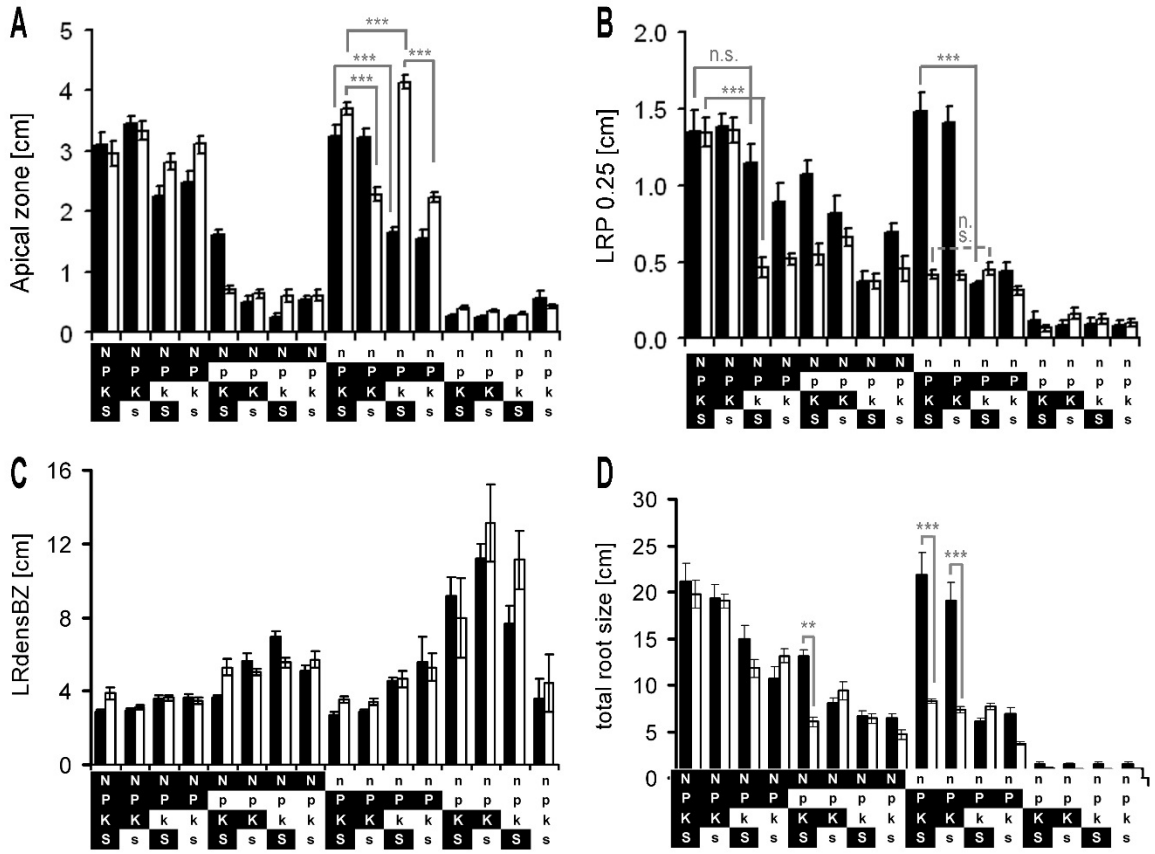

Figure 19: Interaction of day length and nutrients on root architecture parameters.
A) Apical zone length, **B)** average lateral root path length in the upper quartile of the main root (LRP 0.25), **C)** lateral root density within the branched zone (LRdensBZ) and **D)** total root size were quantified for seedlings grown in short day (black bars; 14 DAG) and long day (white bars; 10 DAG). Composition of the 16 nutrient media is depicted by capital letters for sufficient supply (also black background) and small print for deficient supply (white background). All values are means (n = 10 to 22) ± S.E.M. Grey brackets indicate comparative statistical analysis (pairwise comparisons after ANOVA; Tukey's t-test) between two conditions (only those mentioned in the text are shown). The significance level is indicated with asterisks: * $p < 0.05$; ** $p < 0.01$; *** $p < 0.001$. n.s.: not significant.

3.2.2. Nutrient-nutrient interactions shape Arabidopsis root architecture

ANOVA results shown in Fig. 16 and 17 highlight the co-regulation of root architectural features by interactive effects of two or more nutrients (indicated by asterisks). An example for N*S-interaction in long day was already discussed above; low-S had a strong inhibitory effect on apical root length in low-N but not in sufficient N (Fig. 19A). More examples of Nut*Nut interactions in short day conditions are shown in Fig.20.

N*K interaction: Inhibition of lateral root growth (LRP 0.25 and LRP 0.50) was much stronger in low-NK than in low-K alone although low-N on its own actually increased this parameter (Fig. 20A, B). In addition, low-NK also inhibited higher order lateral branching that occurred in low-K as well as low-N single deficiency (see below Fig. 21) P*K*S interaction: Both low-S and low-K decreased lateral root number and branched zone length (Fig. 20C, D); these effects were additive in P-sufficient conditions (low-KS < low-K < low-S; white bars) but not in P-deficient conditions (low-PKS ≥ low-PK, low-PKS = low-PS; grey bars). N*P interaction: The radar graph shown in Fig. 20E visualises the overall effects of low-N, low-P and low-NP on RSA, by showing relative values of several root parameters normalised to control condition (sufficient NPKS) in one single plot. Low-NP potentiated the effects of N and P single deficiency. Most notably, length and number of lateral roots were strongly reduced by NP-double deficiency while individual deficiencies had only minor (LRP 0.25) or even enhancing (LRP 0.50) effects. Low-N alone did not reduce apical root length, yet it strongly enhanced the inhibitory effect of low-P on this parameter. N*S interaction: Although being reduced in low-N and in low-S, 2^{nd} order LR number was induced by double deficiency (low-NS, Fig. 20F). The latter exemplifies an emergent property caused by interactive effects of two nutrient deficiencies. Comparing these various interactions, a clear general rule on how multiple nutrient deficiencies influence root parameters cannot be easily deduced. However, individual interactive effects provide a handle for further investigation of specific responses. This was attempted by experiments described in the following.

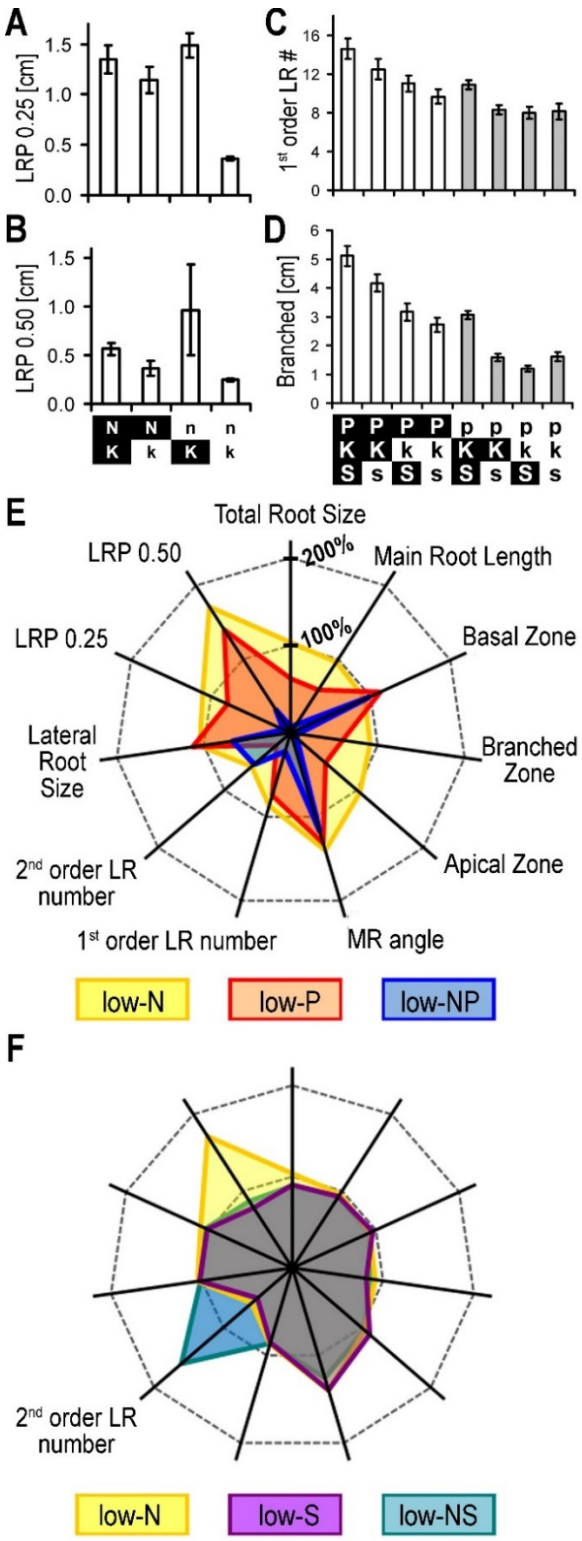

Figure 20: Nutrient-nutrient interactions affect root architectural parameters.
Bar charts show **A)** mean lateral root path length in the first (LRP 0.25) and **B)** second (LRP 0.50) quartile from the base of the main root, **C)** 1st order lateral root number and **D)** branched zone length. Media composition is depicted by capital letters for sufficient and small print for deficient concentrations of respective nutrients (if not shown nutrients were sufficient). Data shown are means (n = 14 to 22) ± S.E.M. **E and F)** Radar graphs showing means of root parameters (quantified in SD 14 DAG) normalised to the mean value of control (deficiency normalised to control). Traits and units are the same in F as in E, but are omitted for clarity.

3.2.3. Second order branching is regulated by the AKT1-CIPK23-NRT1.1 signalling module

Characterisation of root parameters in all nutrient combinations via ANOVA enabled me to generate hypotheses on the involvement of genes and pathways in controlling specific root architectural responses. An interesting starting-point was 2nd order lateral root number for which, according to ANOVA, N, K and N*K interaction emerged as main regulatory environmental factors in short day (Fig. 17B). A closer look at the data revealed, that 2nd order branching was particularly enhanced by low-K but not by low-N (Fig. 21; blue and yellow frames). Moreover, induction of 2nd order LR # by low-K was completely diminished in low-NK.

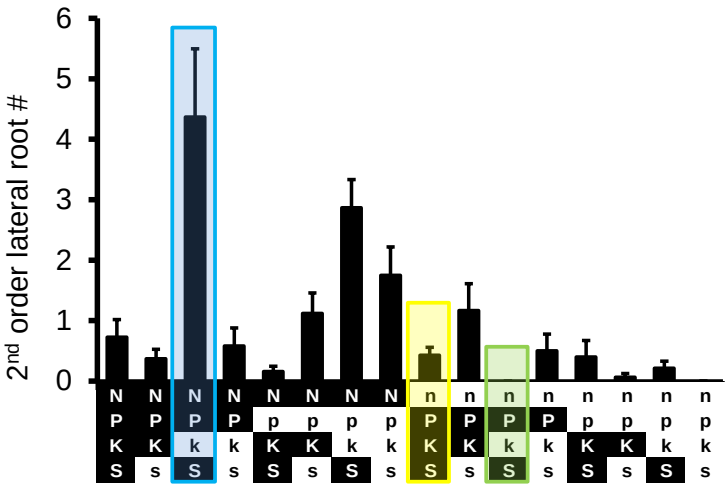

Figure 21: 2nd order lateral root number is induced by K starvation.
Number of second order lateral roots per root of plants grown on 16 nutrient media in short day (n = 289). Root architecture was quantified 14 DAG. Colour frames highlight effects of low-K (blue), low-N (yellow) and low-NK (green).

A set of knockout lines devoid in function of known K and N transport and signalling components (see 3.1 Introduction) was therefore chosen and first tested for abnormalities in the 2nd order branching response to low-K. To account for differences in 1st order lateral root growth (length) caused by either mutation or media, 2nd order LR # was normalised to average 1st order LR length (Fig. 22). Second order branching was significantly enhanced upon K-starvation in the wild type (Fig. 22A) confirming the initial results shown in Fig. 21. A similar response was observed for *hak5* and *nrt2.1* mutants,

which are defective in the main high-affinity transporters of K and nitrate respectively (Fig. 22A). In contrast, induction of 2nd order LR # by low-K was significantly reduced in knockout mutants of the K-channel AKT1 (*akt1*) and it was completely abolished in mutants defective for the kinase CIPK23 (*cipk23*), which is known to activate AKT1. These results demonstrated that CIPK23 was required for induction of LR branching in low-K, acting partly but not exclusively through AKT1.

A smaller but significant reduction of LR branching in low-K was also recorded for *chl1-5* which is a knockout line for the nitrate transceptor NRT1.1, another known target of CIPK23 regulation. This raised the question whether low nitrate concentrations can also serve as a direct branching signal which might have been masked in Fig. 21 due to the lack of nitrogen as an essential nutrient. An additional experiment was therefore designed where 2nd order LR # (normalised to average 1st order LR length) was quantified in wild type seedlings over a range of nitrate concentrations. To compensate N-nutritional effects, total nitrogen supplied was kept constant at 2 mM by replacing nitrate with either glutamate or ammonium (Fig. 22B). In this setup, 2nd order LR # showed a biphasic response with a significant increase between 0.05 and 0.1 mM nitrate as compared to control (2 mM nitrate). This concentration range corresponds to the high-affinity phase of the primary nitrate response, which is dependent on phosphorylation of NRT1.1 by CIPK23 (Liu & Tsay, 2003). It remains to be tested whether this phenotype is altered in the mutant set. Nevertheless, my results identify CIPK23 as a central regulator of LR branching acting additively through both AKT1 and NRT1.1 (see 3.3 Discussion).

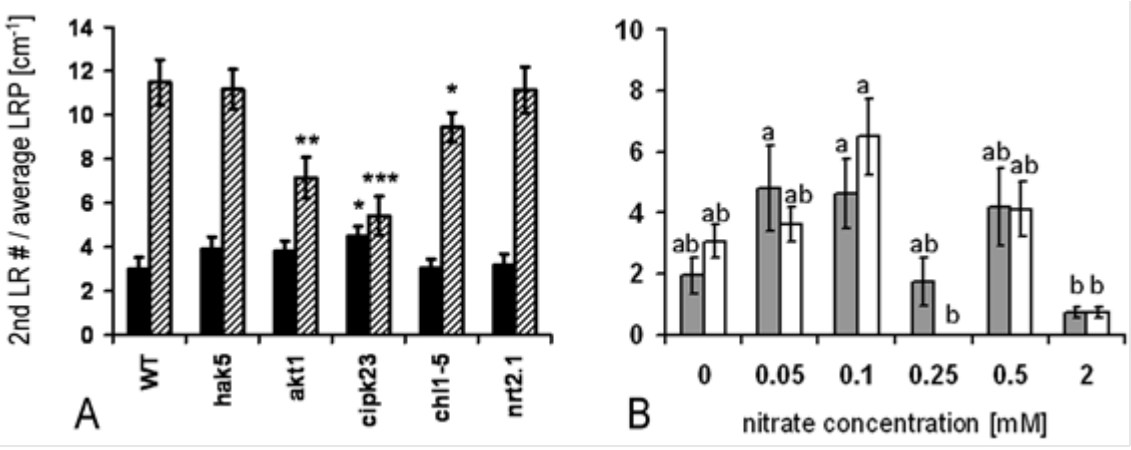

Figure 22: Higher order branching is induced by K and N starvation and is altered in K and N transport and signalling mutants.
A) Number of second order lateral roots normalised to the mean lateral root path length in control (black bars) and low-K (dashed bars). Mutant analysis is based on 19 to 29 plants per genotype and condition (n = 42 to 51 for the wild type). Statistical differences (Mann-Whitney U) are measured against the wild-type in each condition and significant differences indicated with asterisks: * $p < 0.05$; ** $p < 0.01$; *** $p < 0.001$.
B) Number of second order lateral roots per wild-type plant grown on media containing different concentrations of nitrate (seedlings per media and condition: n = 10 to 34). Total nitrogen was kept constant at 2 mM by supply of ammonium (grey bars) or glutamine (white bars). All other nutrients were added in sufficient concentration. ANOVA was computed with all conditions and genotypes as input. Different letters indicate significant differences at $p < 0.05$ (Tukey's t-test). All plants in A) and B) were phenotyped 14 DAG and means ± S.E.M are shown.

3.2.4. The main root angle: a novel low-K phenotype controlled by AKT1

When Arabidopsis wild type roots are grown on a two-dimensional surface, a typical deviation of the main root axis can be observed (Oliva and Dunand, 2007). There is no convention on how to assign the orientation of this angle. It merely depends on the direction of observation: looking from the top (through the lid of the plate) the main roots deviate to the left, looking from the back (through the agar) MRs 'slant' to the right respectively. I scanned all my plates from the back, so normally MRs skewed to the right. EZ Rhizo treats a right-oriented root angle as a *positive* angle. Although being a fairly variable trait, the root angle was influenced by K-supply as the main environmental factor according to ANOVA (Fig. 16). I therefore tested the previous set of K- and N-transport and signalling mutants for this phenotype. Low-K reduced the positive MR angle (growing more vertically) in most media or even changed the angle from right (positive) to left (negative; Fig. 23). Main root angles of all mutants displayed a wild type like negative MR

angle in low-K. However, the *AKT1* knockout line (*akt1*) displayed this behaviour already in control condition (sufficient K). In contrast, *hak5*, *cipk23* or *chl1-5* mutants all had positive MR angles in control, similar to the wild type. Surprisingly, *nrt2.1* angles were even more positive than wild type in control, but again low-K reverted the angle to negative values. The combined evidence suggests an essential role of K in imposing a positive growth angle on the main root and an essential role for AKT1 in mediating this effect, as lack of either K or AKT1 drives the angle to the left. Unlike lateral branching, the function of AKT1 in setting the MR angle is independent of its phosphorylation by CIPK23, otherwise *cipk23* should (at least partly) mimic *akt1* in this respect. AKT1 control of the angle does not involve NRT1.1 but it is counteracted by NRT2.1. Double knockouts of AKT1 and NRT2.1 would be useful tools to further dissect the molecular basis of that phenotype.

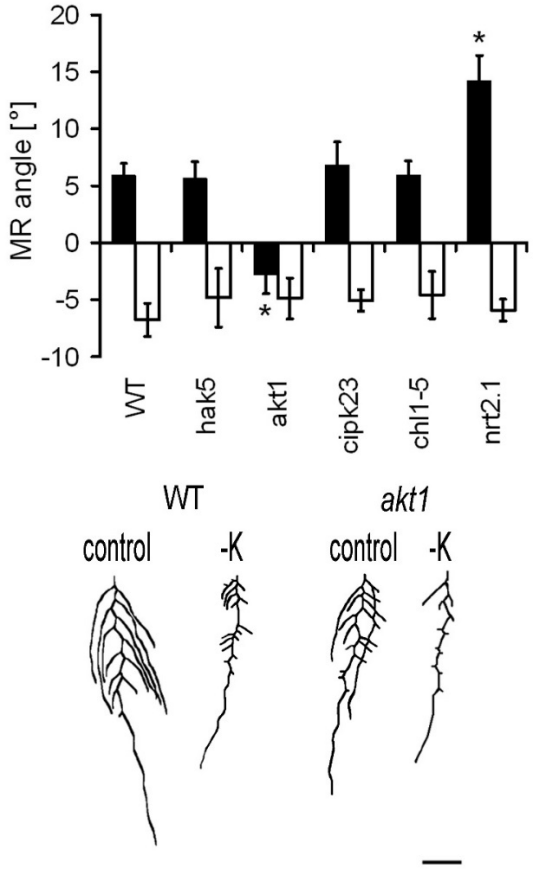

Figure 23: Change of main root angle direction on a 2D surface in response to K starvation depends on the root plasma membrane K channel AKT1.
Main root angle against full verticality was measured 10 DAG for wildtype and mutant plants (n = 13 to 21) grown in long day conditions on control (black bars) and low-K media (white bars). Corresponding representative images of root phenotypes of WT and *akt1* plants in control and -K- conditions are shown below (scale bar: 1 cm). All values are means ± S.E.M. Differences are measured against the wild-type in each condition and significant differences indicated with asterisks: * $p < 0.001$.

3.2.5 Co-regulated gene clusters match nutrient response signatures

To assess whether transcriptional action preceded the phenotypic changes caused by nutrient deficiencies, a microarray experiment was carried out on a subset of eight conditions at an early stage of RSA formation. All combinations of sufficient and deficient NPK and long day were chosen, as root parameters were most diversely influenced by different nutrients in those conditions. S was kept sufficient as it showed the least phenotypic effects (compare Fig. 16 and 17). Three independently grown batches of seedlings ('biological replicates') were harvested 6 days post-germination (6 DAG) and only root tissue was used for RNA extraction, giving a total number of 24 arrays. RNA was hybridized to Affymetrix arrays by staff at the Sir Henry Wellcome Functional Genomics Facility (SHWFGF), University of Glasgow, following their standard protocols. Normalisation of raw signal intensities was performed by Dr Pawel Herzyk at the SHWFGF with the RMA method corrected for GC probe content. Principal component analysis (PCA) of the normalised data (also performed by Pawel Herzyk) revealed a strong batch effect between biological replicates (Fig. 24A). The batch effect was computationally removed (Fig. 24B) and the resulting data files used for further analysis (absolute & relative expression levels).

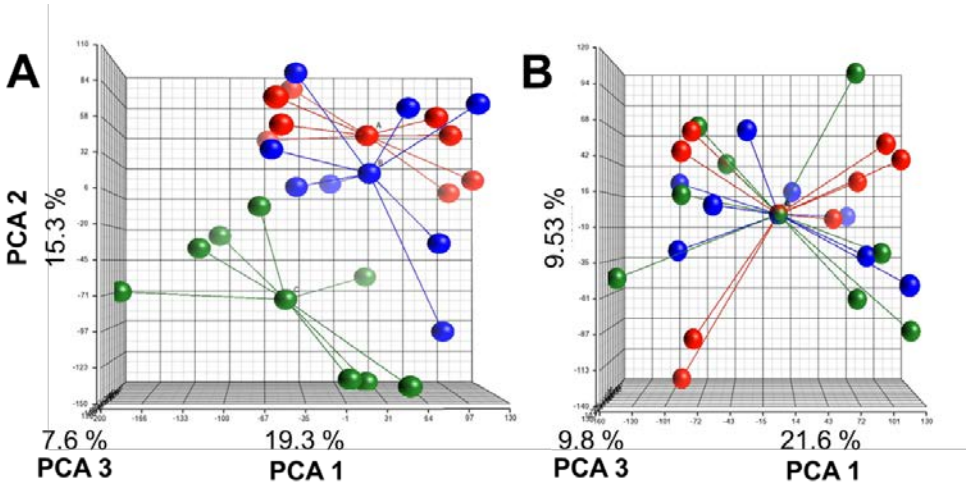

Figure 24: Principal component analysis (PCA) of normalised microarray data revealed strong batch effects.
A) PCA of normalised mRNA data generated from three independently grown batches of seedlings (green, blue and red) shows clear batch effects. Each batch is represented by eight spheres corresp, nding to eight samples each taken from a different nutritional condition (combinations of sufficient and deficient N, P and K). **B)** PCA of normalised mRNA after batch effects were computationally removed. Resulting normalised mRNA levels were used for further analysis. PCA analysis was performed by Dr Pawel Herzyk, SHWFGF, University of Glasgow.

Within each biological replicate (batch) absolute signal intensities measured in a given condition were divided by the corresponding intensity values measured in control condition (sufficient in N, P and K). The relative values were then averaged to obtain a mean 'transcriptional response' for each gene. A full list of genes including all absolute and mean relative responses (± S.E.M) can be found in the electronic appendix under *Ch3_NPKS microarray*. Relative expression levels can be misinterpreted when absolute levels are low, since small changes of absolute intensities can lead to exaggerated relative intensities (responses). To minimise the danger of generating too many false-positive responses, the dataset was subjected to a rigorous two-step filter procedure. First, genes with low mRNA levels (mean absolute signal intensity < 100 in all conditions) were discarded from further analysis. Second, a cut-off of at least 4-fold up- or (for relative intensities) in at least one condition was applied, resulting in a total number of 371 'nutrient-responsive genes' (142 up, 228 down, 1 up & down). Co-regulation of genes was assessed by hierarchical clustering based on Euclidian distance of relative expression levels. Here, genes showed a clear separation between genes that were up-regulated (142 genes) and genes that were down-regulated (228 genes) in one or several of the applied deficiency conditions (Fig. 25). In addition to individual genes, I also clustered the conditions (only 7 as relative expression was performed against control [sufficient NPK]) according to their overall expression profiles. Here, all low-N conditions were grouped against low-P and low-K. Within the four N-deficient conditions, both NP-double deficiencies were separated from single low-N and low-NK. This is in agreement with the strong low-N effect observed in the ANOVA of root architecture in long day (Fig. 17C) and the strong inhibition of root growth observed in low-NP (Fig. 19). It should be noted, that seedlings grown on different media already showed slight differences in overall growth 6 days after germination. However, in all cases merely main roots of different length (ca. 10 to 25 mm) were visible. So at this stage, no real root system *architecture* had been formed yet. I therefore conclude, that transcriptional profiles at this time point capture the onset of root architectural responses to the nutrient conditions in question.

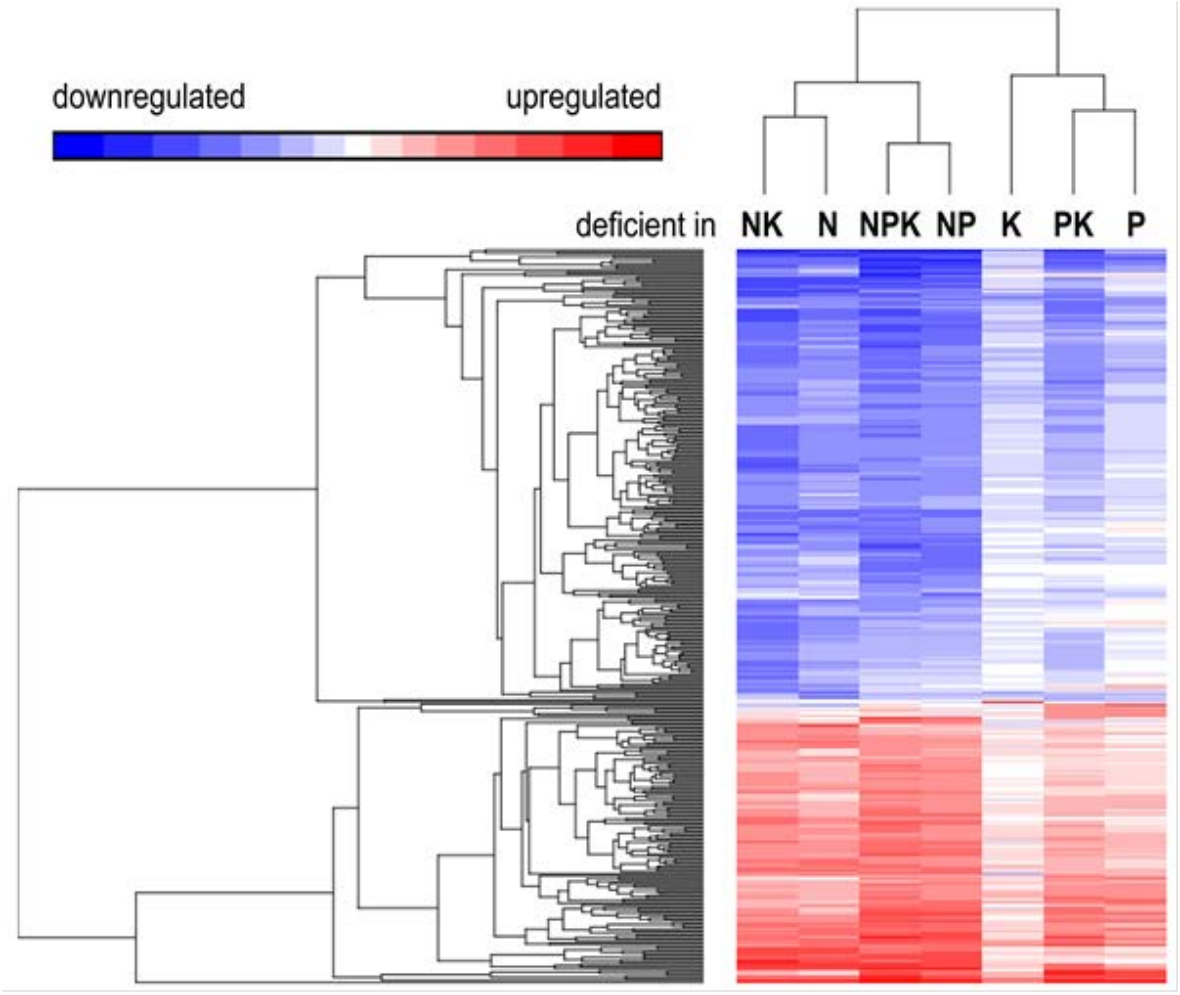

Figure 25: Heat-map resulting from hierarchical clustering of down- and up-regulated genes.
Hierarchical cluster analysis of 371 response genes (after two-step filtering) was based on Euclidian distance. Two main groups were detected: down-regulated genes (blue) and up-regulated genes (red). Clustering of conditions groups all low-N conditions against low-P and low-K conditions.

As hierarchical clustering only produced two coarse groups of up- and downregulated genes, the dataset was split into these subgroups and a second cluster analysis based on k-means was performed. Minimal Davies-Bouldin index was used to determine the optimal group numbers. Downregulated genes divided into 6 groups clusters (DOWN1 to DOWN6) and up-regulated genes into 7 groups (clusters UP1 to UP7; Fig. 26).

One gene (*AT4*) showed both (by low-P) and (by low-N) and thus formed its own cluster (UP-DOWN). An Excel file containing complete lists of response genes, including fold-changes and cluster composition, can be found in the electronic appendix under *Ch3_Microarray response genes - 4-fold cutoff*.

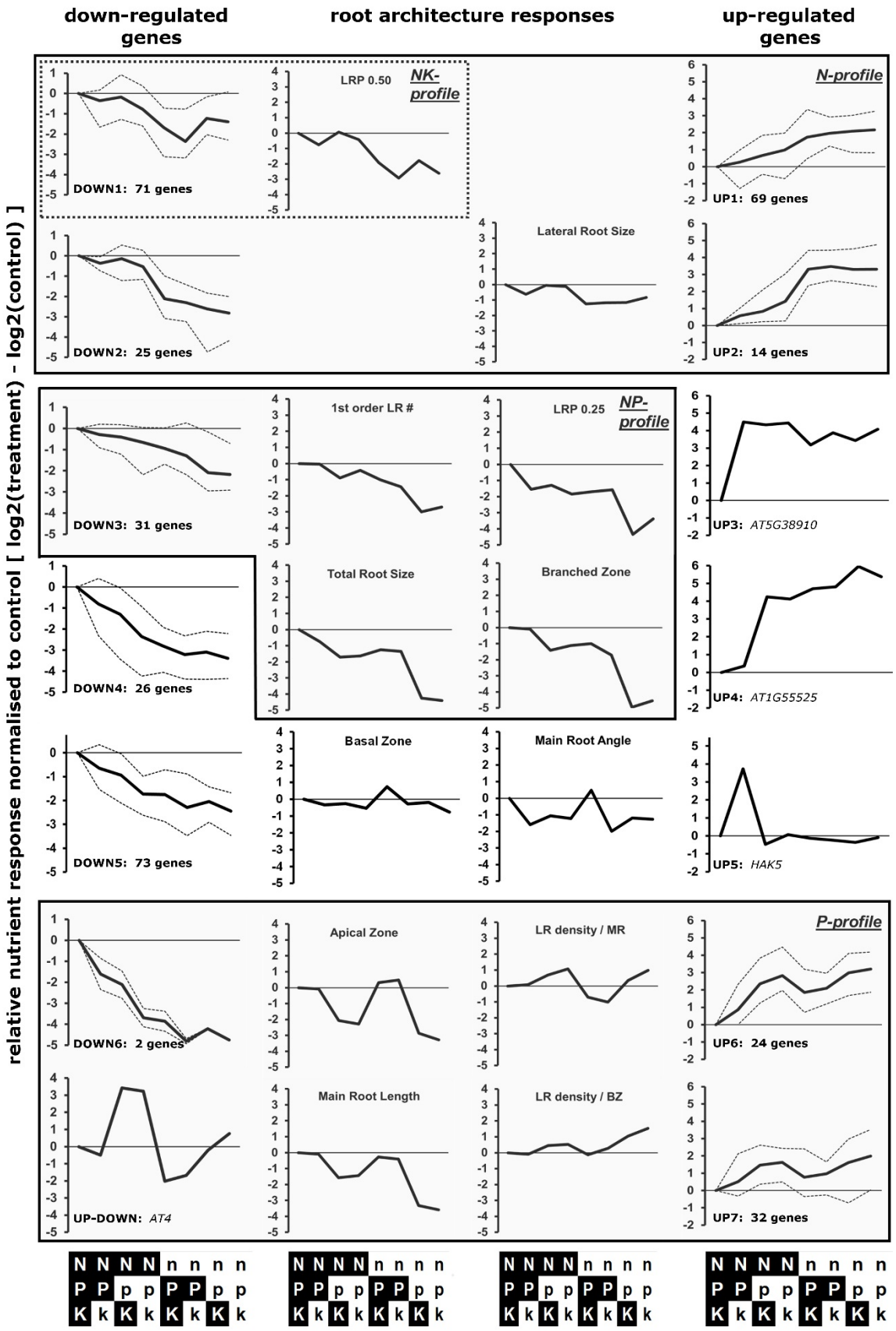

Figure 26: Response profiles of the transcriptome and root architecture in NPK-starved roots.

see *overleaf for the complete figure legend*

Figure 26: Response profiles of the transcriptome and root architecture in NPK-starved roots. Transcriptomic data is based on microarray analysis of root tissue sampled 6 DAG from seedlings grown in eight conditions of sufficient or deficient NPK-supply (sufficient: upper case letters on black background; deficient: lower case letters). Clusters of *response genes* that were down-regulated by nutrient deprivation are shown on the left and up-regulated clusters are shown on the right. The composition of *response gene clusters* was determined after a two-step filtering procedure as follows: first, only genes with an absolute mRNA level of more than 100 in at least one condition were considered. The mean mRNA levels of three independent, biological replicates in each condition were calculated and normalised against the control condition ('response'). Only genes with at least 4-fold up- or downregulation ($\Delta\log2 > 2$ or $\Delta\log2 < -2$) in at least one deficiency were selected, resulting in 371 *response genes*. Up- and down-regulated genes were k-Means clustered separately using the Euclidian distance measure. The graph shows mean transcriptional profiles of individual clusters (solid black line) plus minimal and maximal values (thin dashed line). For each transcriptional cluster ('DOWN1 to DOWN6'; 'UP-DOWN'; 'UP1 to UP7'), the number of genes within the cluster or the gene identifier (for single gene clusters) is shown below. The two mid columns show profiles of *root architecture responses*, i.e. the relative mean root parameters in deficiency conditions normalised to the mean value of the control. Grey shading highlights groups of matching transcriptional and root architectural response profiles: 'N-profile', 'NK-profile', 'NP-profile'; 'P-profile'. Overlapping groups are indicated by a dashed box ('NK-profile' within 'N-profile').

Fig. 26 displays *transcriptional response* profiles of up- and down-regulated gene clusters (left and right panel). Graphs show the mean response in each condition (as log2(treatment) – log2(control); sufficient NPK = control) as a solid black line, plus the highest (maximum) and lowest (minimum) values as dashed lines to indicate the full spread of data points. In the same way, *root architectural response* profiles [log2(mean of treatment) – log2(mean of control)] were generated from the original long day (10 DAG) dataset presented in Fig. 16 to 20. Visual and statistical comparison of early transcriptional response profiles (6 DAG) with root architectural response profiles (10 DAG) may give additional information on the involvement of genes in 'steering' root growth in response to nutrient stresses (see below).

Down-regulated genes were divided into six clusters with different response profiles (DOWN1 – DOWN6). The strongest repression was generally observed in media with low-N combined with additional and/or additive repression by low K and/or low P. The DOWN1 (71 genes) profile was characterised by low-N repression, particularly by low-NK double deficiency, but a lack of response to low-P. Another large cluster was DOWN5 containing 73 genes that were strongly down-regulated by low-N but also by low-K and low-P with each nutrient having individual and additive effects. Clusters DOWN4 (26 genes) and DOWN6 (2 genes) were steeper versions of DOWN5. Note that in

all nutritional backgrounds mRNA levels were always lower when K was deficient (low-NK < low-N; low-PK < low-P; low-NPK < low-NP), creating a small step in the profile (compare the 'stair-like' profile of DOWN5). The 25 genes in DOWN2 were specifically down-regulated by low-N, independent of P or K, while the 31 genes in DOWN 3 were particularly responsive to low-NP.

Up-regulated genes grouped into seven clusters (UP1 – UP7) of which three were single-gene clusters. *AT5G38910* (UP3) was the only gene that was strongly and almost equally up-regulated by all deficiency conditions. It belongs to the RmlC-like cupin superfamily and has high sequence similarity to germin-like proteins, which are known stress responsive elements (Bernier and Berna, 2001; Dunwell et al., 2004). *AT1G55525* (UP4) was induced by all deficiencies apart from low-K. This gene of unknown function is described as 'misc. RNA' (TAIR10). A BLAST search revealed highest sequence similarity to a RING/U-box superfamily protein (*AT5G55970*), but *AT1G55525* is probably too small to produce a functional protein. *HAK5* (UP5) showed the opposite pattern, as it was induced only by low-K (single deficiency). Interestingly, upregulation of *HAK5* expression, a well-documented root response to low-K (Ahn et al., 2004; Armengaud et al., 2004; Kim et al., 2010), was not observed in any of the multiple deficiencies (low-NK, low-PK, low-NPK). Presence/absence of N was the main factor determining the profiles of UP1 (69 genes) and UP2 (14 genes). Genes in these clusters therefore had similar nutrient-dependence as genes in DOWN2, albeit the opposite response.

UP6 (24 genes) and UP7 (32 genes) were the only profiles that displayed stronger response to low-P than to low-N. The profiles of these two clusters were very similar apart from the strength of the responses (higher in UP6). Last but not least, another single gene, *AT4* (UP & DOWN), showed P-dependent with an opposite response to low-N (downregulation). *AT4* is known to be induced by P-starvation (Shin et al., 2006) and it was shown to inhibit miR399 action by 'target mimicry', resulting in increased PHO2-mediated shoot P-concentrations (Franco-Zorrilla et al., 2007). My microarray results confirmed the induction of *AT4* by low-P. However, they also show its repression by low-N. Ultimately, up- and downregulation in NP-double deficiency cancelled each other out. Hence, *AT4* and the gene network around it are interesting targets of N-P signalling crosstalk. Further discussion of gene clusters and the putative roles of individual genes will be presented in the *Discussion* section of this chapter (section 3.3).

I also investigated whether the obtained transcriptional profiles matched RSA response profiles. In several cases this was indeed the case (profiles are grey-shaded in Fig.

26; Table 20 for Pearson correlation coefficients). For example, the 'NK-profile' of DOWN1 most strongly matched the profile of LRP 0.50. The 'N-profile' of DOWN2, (and to some extent of UP1 and UP2) was visually reminiscent of the profile displayed by the total lateral root size. However, due to the strong effect of N alone, there was a significant overlap between 'NK-' and 'N-profiles' that is reflected in similar Pearson correlation coefficients. A strong NP-effect, which determined the 'NP-profile' of DOWN3, also dominated the response of several RSA parameters: 1st order LR number, branched zone length, LRP 0.25 and consequently total root size. The 'P-profile' of UP6, UP7 and UP-DOWN matched similar profiles of apical zone and MR length as well as LR density.

I gathered all microarray data in the last months of my PhD project. Unfortunately, there was no time left to follow up on these various leads. However, in conjunction to writing up my thesis our collaborative group endeavoured to publish this dataset and thus make it available for the research community. Hence, this comparative analysis of nutrient response signatures for genes and RSA features provides a new resource for future research efforts to identify molecular sensors and signalling elements underpinning different RSA features in different nutritional conditions.

Table 20: Pearson correlation coefficients between transcriptional and root architectural response signatures.
Mean transcriptional responses of down- and up-regulated clusters (compare solid black line in Fig. C3-11) were correlated with root architectural responses (as in Fig. C3-11). Only statistically significant correlations are shown ($p < 0.01$).

	UP1	UP2	UP3	UP4	UP5	UP6	UP7	DOWN1	DOWN2	DOWN3	DOWN4	DOWN5	DOWN6	UP-DOWN
Total Root Size							-0.84			0.92				
Main Root Length							-0.87							
Basal Zone														
Branched Zone										0.95				
Apical Zone							-0.86							
Main Root Angle														
Lateral Root Size		-0.88						0.85	0.87					
1st order LR #	-0.87								0.87	0.97				
LRP 0.25										0.91				
LRP 0.50	-0.88	-0.92						0.93	0.93		0.84	0.84		
LR density / MR														0.84
LR density / BZ							0.85							

3.2.6 Single and multiple deficiencies alter shoot ionomic profiles

Until now, transcriptional and phenotypic responses of roots were the focus of investigation. When dealing with plant nutrition, it is always of interest how external nutrient conditions translate into elemental concentrations in planta. Ionomics has recently become a widely used tool in the plant research community, not least because of high-throughput, lost-cost techniques like ICP-MS that allow for precise quantification of several elements at once (Salt et al., 2008). In fact, the precision of elemental detectors often outperforms the possibility to generate high-quality samples. Root tissue grown on vertical agar plates is unsuitable for this kind of analysis as nutrient-containing agar residues can greatly disturb the measurements (David Salt, personal communication). Therefore, effects of the various nutrient treatments on growth and nutritional status of the shoot was assessed in a final experiment. Seedlings were grown as before on all 16 NPKS combinations in long day and shoots harvested 10 DAG. Fresh weight of pooled seedlings was determined immediately after harvest and the material subsequently dried for several days. Dried shoot samples were sent to Prof David Salt, University of Aberdeen, where elements were extracted and concentrations quantified with ICP-MS by Dr John Danku. Three independent, biological replicates were measured in each condition.

Generally, low-S media had the same profiles for most elements as respective conditions in sufficient S. Fig. 27 therefore only displays results from sufficient S experiments (the same conditions used in the microarray experiment). However, quantification of S concentrations in low-S media clearly demonstrated a reduced S content (Fig. 28). The reduction in S was mirrored by an increase in molybdenum (Mo), a known molecular phenotype of low-S (Alhendawi et al., 2005). Hence, the S concentration in low-S media was adequately low to induce S-deficiency symptoms albeit not promoting strong root architectural responses.

Compared to control, shoot fresh weight was reduced by about 30 % in low-K, by more than 50% in low-P and by about 90% in low-N (Fig. 27). Although low-N reduced shoot fresh weight dramatically, ion concentrations did not necessarily follow the same pattern (esp. P and micronutrients), suggesting that elemental concentrations should not be treated as artefacts. As expected, P starvation reduced shoot P concentration ($[P]_{Shoot}$) to less than half, and K starvation reduced $[K]_{Shoot}$ to about a quarter of control (Fig. 27). Low-K slightly increased $[P]_{Shoot}$ while low-P or low-N decreased $[K]_{Shoot}$. $[Ca]_{Shoot}$, $[Mg]_{Shoot}$ and $[Na]_{Shoot}$ were reduced by low-N, and to a lesser extent by low-P, but strongly increased by low-K. It has been suggested before, that Ca, Mg and Na are able to

replace K in some its physiological functions (Amtmann et al., 2006). Nevertheless, if N and P were also low, shoot accumulation of these three cations elicited by low-K was less pronounced. Micronutrient concentrations were generally lower in P- and N-deficiency, but Mn and Zn were slightly increased in low-K. The most conspicuous difference, however, was a dramatic increase of $[Fe]_{Shoot}$ caused by low-P, low-N and most notably by NP-double deficiency (15- to 20-fold). A potential explanation for this observation is presented in the following *Discussion*.

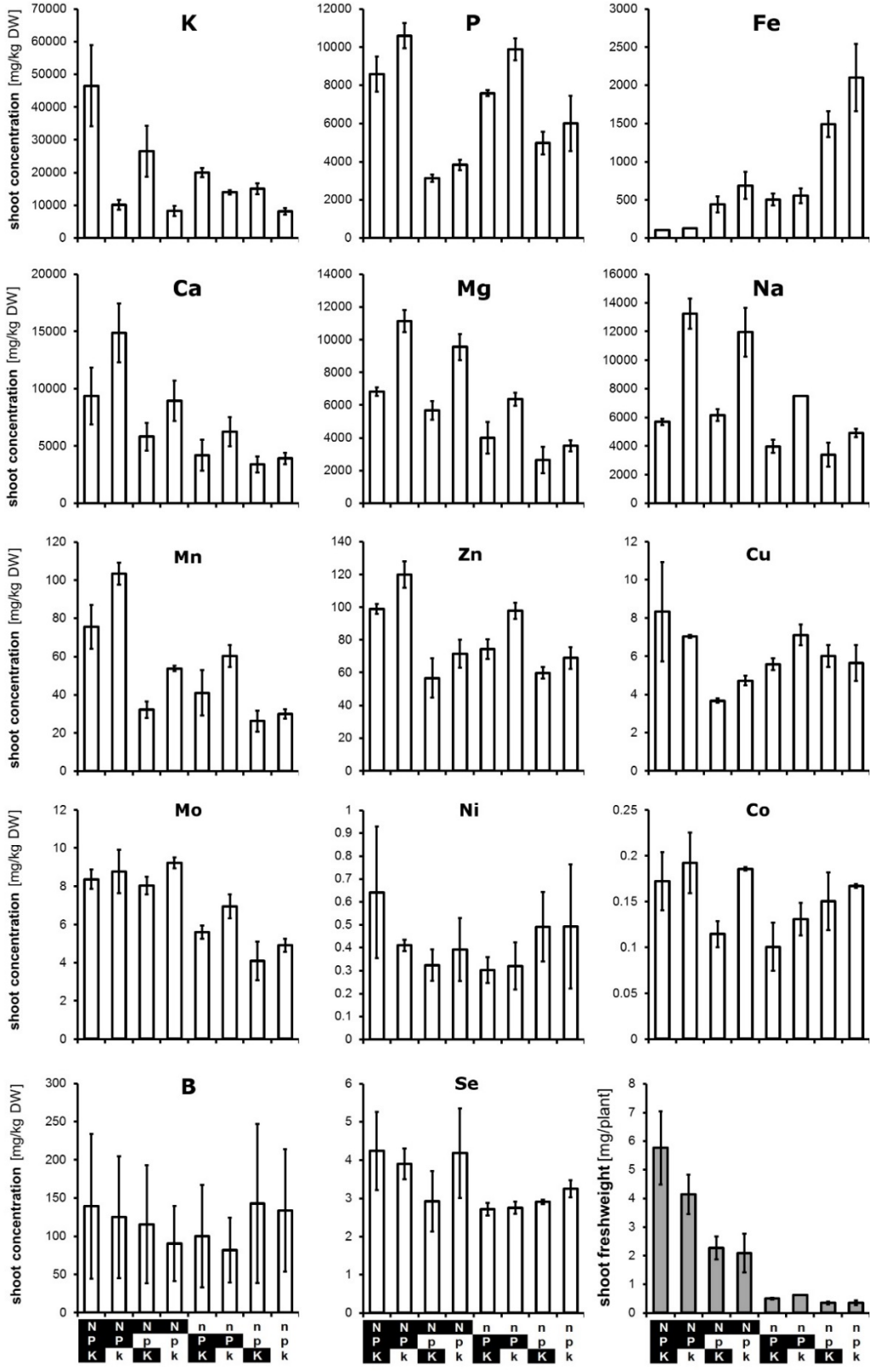

Figure 27: Quantification of shoot ion concentrations of NPK-starved seedlings with ICP-MS.

Bar charts show shoot concentrations (as mg per kg dry weight) of elements quantified with ICP-MS at the University of Aberdeen (Prof David Salt). Shoot tissue was sampled from wild-type seedlings grown on NPK-media in long day conditions and harvested 10 DAG. Plants were grown in three independent replicates. For each replicate, shoots of 30 to 100 plants were pooled, dried and ions extracted via in vitro digestion. All values are means ± S.E.M.

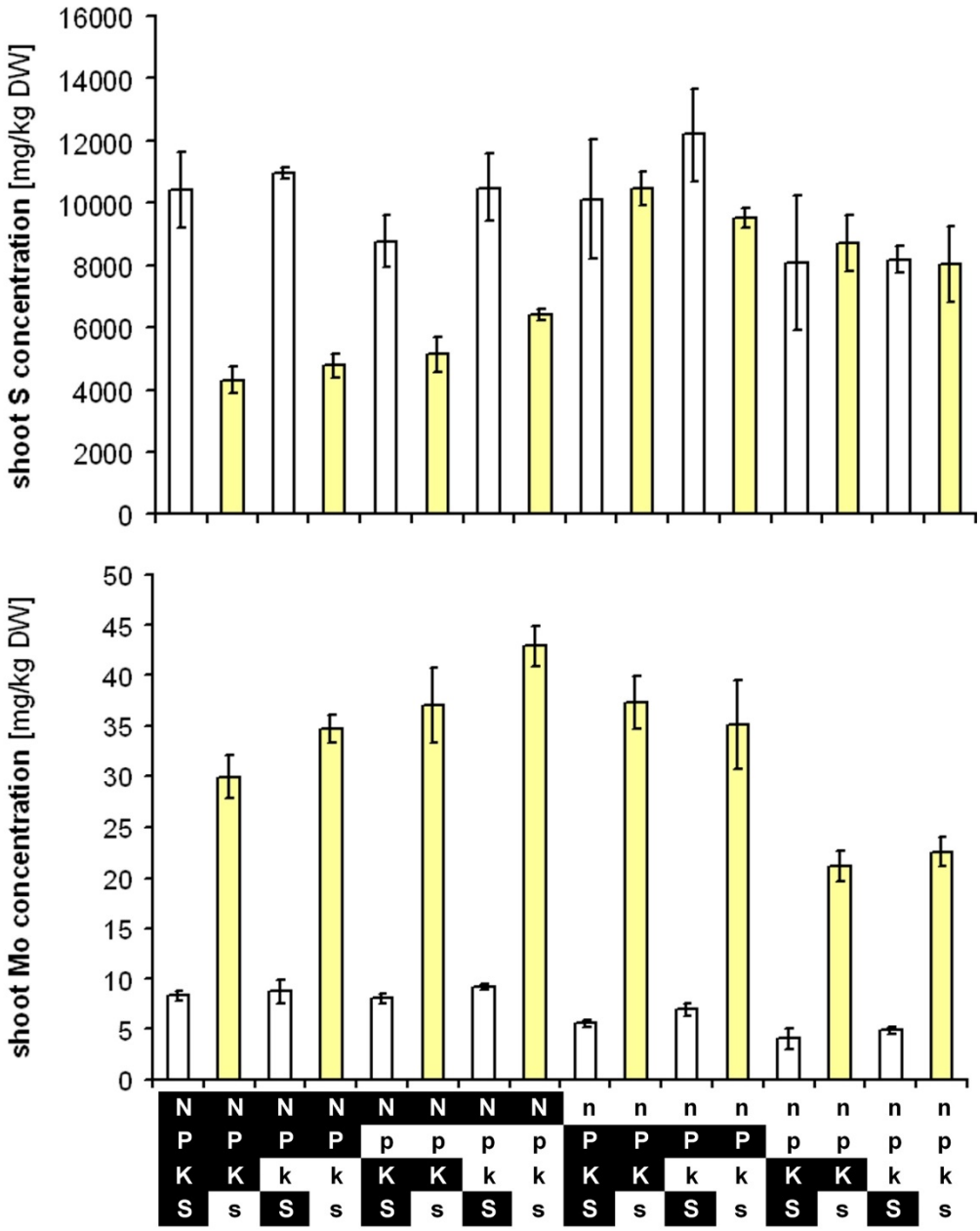

Figure 28: Shoot S and Mo concentration quantified with ICP-MS of seedlings grown in NPKS-deficiencies in long day confirm S-deficiency status of the plant.
Shoot S is greatly reduced in low-S conditions (highlighted in yellow) in sufficient N. Conversely, Mo concentrations are increased. This low-S response has been observed before (Alhendawi et al., 2005). Data shown are means ± S.E.M (n = 3 independent replicates).

3.3 Discussion

3.3.1 The need for a multifactorial experimental design to discover previously unknown nutrient interactions

Plant root systems are complex structures that act both as sensors and as effectors of soil and plant nutrient status. A detailed understanding of root responses to nutrient supply will advance the search for fundamental molecular processes that underlie plant-environment interactions and will thus generate important information for improving nutrient uptake and usage efficiency. Until now, individual nutrients have been studied in isolation. Although it has often been pointed out that the background of other nutrients is an important factor determining the effect of a specific nutrient, systematic investigations into nutrient-nutrient interactions have not been undertaken. It is empirical data that are needed to start building models that could predict RSA for a given combination of nutrients in the soil. To enable combinatorial analysis of nutrient effects, I have quantified RSA of Arabidopsis plants grown on vertical agar plates with 16 combinations of NPKS in two day length conditions (short and long day). The two concentrations tested for each nutrient were carefully selected on the basis of a literature survey to represent sufficiency (but not inhibitory over-supply) and deficiency (without being lethal). Of course a binary approach cannot cover the entire response spectrum of RSA, and future studies should extend the concentration ranges to be investigated for interactive effects. However, the obtained results show the potential of this approach to discovery previously unknown nutrient interactions both at the phenotypic and at the molecular level. In fact, ANOVA of the initial dataset has pinpointed effects of specific nutrients and nutrient-nutrient interactions on specific root architectural features (Fig. 16, 17). Two exemplary root traits (2^{nd} order lateral root number and main root angle) were then examined in more detail by further investigating the effect of nutrients (Fig. 22B) and genes (Fig. 22A, 23). Indeed, I was able to identify critical genes and/or nutrient concentrations needed to elicit phenotypic responses to the environmental conditions in question.

3.3.2 Which root features do really matter?

Dissecting nutritional responses would not have been possible without the dissection of the phenotype, i.e. quantifying a comprehensive set of root architectural parameters.

Two-dimensional projection of the root system presents a convenient macroscopic representation of RSA capturing all parts that will ultimately determine the three-dimensional root shape. Consequently, EZ Rhizo was purpose-designed to quantify as many of these parameters as possible by semi-automatic image analysis. I customized the set of root parameters for my needs by removing some traits that were always highly correlated with others (e.g. depth of the root system with main root length) and by adding some additional information via the separation of the lateral root system into quartiles (compare LRP 0.25, LRP 0.50, LRP 0.75 and LRP 1.00). It could be argued that some of the measured RSA parameters are irrelevant for the overall shape of the root in three dimensions, or are even artefacts of the growth system. However, my results provide clear proof that these parameters can still be useful (and necessary) for the discovery of signalling crosstalk (e.g. antagonistic effect of AKT1 and NRT2.1 on main root angle, Fig. 23).

Depending on the trait measured, more or less of its variation could be explained by environmental conditions (Fig. 16, 17). In some cases an apparently low environmental influence may be due to difficulties in precisely quantifying the trait. Basal zone for example is prone to measuring errors as it strongly depends on the macroscopic assignment of the root-hypocotyl border. Moreover, low absolute values can lead to higher variation within the dataset, like in the case of mean lateral root length close to the root tip (LRP 0.75 and LRP1.00). In this chapter, the latter two parameters were therefore not further characterised. Another possible reason for low 'percentage of variation explained' is inherent high stochasticity of the trait itself, which is probably the case for main root (MR) angle and second order LR number, as those parameters can be quantified with higher precision. Stochasticity, or developmental instability, has actually been proposed as an important component of root architecture formation (Forde, 2009). The author argues that developmental 'noise' of especially lateral root patterning and emergence can help the single plants to forage for nutrients more efficiently whilst belowground competition between individuals of the same species is reduced.

Nevertheless, although ANOVA only attributed small effects to environmental conditions, I was still able to identify genes responsible in controlling environmental plasticity of these two traits (compare Fig. 22, 23). In contrast, a parameter may indeed be controlled by a developmental programme that is robust against environmental fluctuations. Lateral root density within the branched zone was highlighted as a very stable parameter across all conditions, apart from low-P. In particular, LR density in the branched zone was independent of day length (Fig. 19C). I therefore propose to make use of this

parameter when studying fundamental properties of LR development (see also De Smet et al., 2012; Dubrovsky and Forde, 2012).

EZ Rhizo quantifies some commonly used root traits such as MR length, total root size and lateral root number. Those were indeed strongly associated with nutrient supply, but additional parameters measured here refined the output. For example, apical zone length, which was almost entirely determined by P, emerged as a more precise reporter of P than MR length and should therefore be used in genetic screens for P-response elements (independent of light conditions; Fig. 17). This and some other main nutritional effects on root architecture will be discussed in the following sections.

3.3.3 P is the single main factor determining main root growth

P starvation has been reported to elicit a dual response: a decrease in main root growth accompanied by an increase of lateral root growth, especially in the basal part of the root system (Williamson et al., 2001; Lopez-Bucio et al., 2002; Perez-Torres et al., 2008). My results confirmed a strong inhibitory effect of low-P on main root elongation but I did not observe an increase in lateral root elongation in the basal part of the root; instead LRP 0.25 was lower in P-deficient than in P-sufficient conditions. A possible explanation is the timing of LR initiation, which happens early on in P-starvation (Al-Ghazi et al., 2003; Perez-Torres et al., 2008) and may therefore be no longer apparent at the time points analysed here. Indeed one study reported a transient increase of lateral root initiation and elongation in low-P, followed by an overall decrease of these traits compared to control conditions (Nacry et al., 2005).

ANOVA of the entire dataset showed that P was by far the most important factor controlling main root elongation, both in terms of total main root length and length of the apical zone, regardless of other nutrients or day length (Fig. 16, 17). This argues for a prioritisation of low-P responses over other mineral nutrient responses in multiple deficiencies as far as MR growth is concerned. Under single P-deficiency, day length had an additional input into length of the apical zone and main root, as well as LRP 0.25, reducing these parameters to 50% in long days compared to short days (see NpKS in Fig. 19). Long range shoot-to-root sugar signalling has been implicated in the systemic response to low-P (Hammond and White, 2008; Lei et al., 2011) as increased root-directed transport of sucrose takes place in the phloem under P-starvation. However, the fact that MR growth was reduced in any low-P condition supports the notion that long-distance signalling is accompanied by local P-sensing at the root tip (Svistoonoff et al., 2007;

Ticconi et al., 2009) with subsequent alterations of auxin distribution and responsiveness (Perez-Torres et al., 2008; Miura et al., 2011). Two homologous genes, *LOW PHOSPHATE ROOT 1* (*LPR1*) and *LOW PHOSPHATE ROOT 2* (*LPR2*), have been proposed as central mediators of P-sensing at the root apex (Svistoonoff et al., 2007). These genes will reappear in Chapter 5 and 6 where co-regulation of P- and K-deficiency responses will be further investigated.

3.3.4 N-starvation responses depend on high photon input

External N (supplied as nitrate) was identified as the main determinant for lateral root growth, but only in long days (Fig. 17, 19). To distinguish light effects from circadian effects, an additional experiment was carried out where high photon flux density was supplied over a short day period. These conditions mimicked the effects of low-N in long day (Fig. 18) suggesting that high rates of photosynthetic carbon fixation are an important requirement for the generation of root architectural N-starvation responses. This in turn indicates that N-assimilation into carbon compounds rather than N availability *per se* is the main trigger for LR growth retardation. Indeed, the C/N ratio in the medium has been identified as a crucial factor for root growth (Zhang et al., 1999; Malamy and Ryan, 2001; Little et al., 2005; MacGregor et al., 2008; Roycewicz and Malamy, 2012).The strong dependence of low-N responsiveness on light was surprising since all growth media contained 0.5% sucrose. The calculated N/C ratio in the low-N media was 1/3509 compared to 1/88 in control thereby generating a decrease of N relative to C. Nevertheless this change of external N/C ratio did not elicit N-starvation symptoms in short days. One possibility is that only a large increase of C can produce C/N ratios that are large enough to induce N-deficiency symptoms. Another possibility is that the source-sink relationship for carbon has to be directed from shoot to root to generate a low-N stimulus in the root. It has been shown that sucrose taken up from the medium via the shoot (by shoots sticking to the agar surface) stimulates LR development (MacGregor et al., 2008). However, this study investigated only the effect of high (repressive) nitrate concentrations. I can also rule out sucrose uptake from the medium via shoots because I have removed the agar medium from these parts. Nevertheless, the view that a shoot-derived carbon signal may be required to induce LR-inhibition by low-N is favoured by the observation that high light dosage over short days reduced total root size and LR length even in N-sufficient media (Fig. 18A, B).

Microarray analysis of roots grown in long-days identified potential molecular players in C/N signalling, for example the phloem-loading sucrose transporter gene

SWEET12 (Chen et al., 2012a). *SWEET12* showed more than 2-fold upregulation by low-N and more than 4-fold upregulation by low-NP. Low-N also caused a more than 4-fold induction of the nitrate transporter gene *NRT1.8* which recovers nitrate from the xylem (Li et al., 2010a). Those two transport processes work in opposite directions, reducing sucrose and increasing nitrate concentrations in the root cortex. This regulation might reflect a strategy to reduce the LR growth-repressive effects of a high C/N ratio within the root. Krapp et al. (2011) have dissected the effect of N-starvation on roots and shoots in mature plants that were grown on sufficient nitrate (6 mM) for 5 weeks and subsequently transferred to 0 mM nitrate for up to 10 days (all in short day). The authors emphasize the importance of both organs in N-starvation and confirm the increase of the root/shoot biomass ratio in low-N (see also Linkohr et al., 2002; Ikram et al. 2011; Roycewicz and Malamy, 2012). Moreover, they identify clear differences in the transcriptome of N-starved roots and shoots. My experiments focussed on the root system only and hence no clear hypothesis on the role of individual genes in long-distance (root-shoot) C/N homeostasis can be made. Now further characterisation of the effect of external C/N (by changing nitrate and sucrose) on root architecture parameters and evaluation of shoot/root relations would help to dissect the effect of different carbon sources and sinks on low-N responses.

3.3.5 Nutrient interactions shape root architecture and provide new readouts of signalling crosstalk

Analysis of the whole dataset via ANOVA revealed significant contributions of nutrient-nutrient interactions in controlling various root architectural parameters (Fig. 16, 17). I detected two-level interactions such as N*K, N*P, P*K and N*S, as well as higher order interactions of three nutrients, indicating multiple sites of crosstalk in underlying signalling networks (Fig. 17, 20). Surprisingly, sulphur effects on RSA only appeared in the context of interactions. Based on the literature, the S concentration in my low-S media was sufficiently low to induce S-deficiency symptoms (Maruyama-Nakashima et al. 2004, 2006; Wu et al., 2010). Moreover, quantification of S (and Mo) concentrations in shoots confirmed that S nutrition was indeed impaired in low-S (Fig. 28). The lack of RSA responses to low-S therefore suggests that nutrient background and/or light conditions made an essential contribution to low-S effects observed in previous studies.

Apart from this issue, dependence of RSA parameters on nutrient interactions provided a powerful new readout for molecular studies. I tested K-N interactions using mutants for several genes with known functions in transport, sensing and/or signalling of K

and nitrate in roots. My experiments revealed new roles for the K-channel AKT1 in regulating two distinct RSA parameters (2^{nd} order LR number and MR angle) within two different signalling modules (see below). Moreover, significant P*K interactions on main root traits (such as main root length and apical zone length) gave a first hint towards potential P-K crosstalk. This finding, together with results obtained in the study on natural variation of the low-K response (Chapter 4), initiated research described in Chapter 5 and 6.

3.3.6 Higher order lateral branching is regulated by K and N through a signalling module that includes CIPK23, AKT1 and NRT1.1

I have shown that 2^{nd} order lateral root growth (LR branching) was induced by low-K and that this response depended on CIPK23 and AKT1 (Fig 21, 22). CIPK23 and associated Ca-binding proteins (CBLs 1 and 9) constitute a known cellular signalling pathway that activates K-influx through AKT1 after a rise in cytoplasmic calcium $[Ca]_{cyt}$ elicited by low external K (Li et al., 2006; Xu et al., 2006; Amtmann and Blatt, 2009). In my experiments, LR emergence emerged as a new developmental target of this signalling module. However, while *CIPK23* knockout completely abolished induction of 2^{nd} order LRs in low-K, *AKT1* knockout reduced the response only partially (Fig. 22A), indicating that CIPK23 acted through at least one other pathway. NRT1.1 presents itself as a likely candidate because it is also known to be regulated by CIPK23 (Ho et al. 2009) and *chl1-5* mutants also showed a small reduction of the low-K response. Phosphorylation by CIPK23 switches NRT1.1 from low- to high-affinity mode in the range of 0.05 -0.1 mM nitrate. A specific biphasic induction of LR branching by low nitrate (in the background of sufficient total N) with a peak around 0.1 mM nitrate was measured in additional experiments (Fig. 22B). These results further strengthened an involvement of NRT1.1 in 2^{nd} order LR induction.

NRT1.1 has previously been implicated in the root colonisation of nitrate rich patches (Remans et al., 2006a). Moreover, Krouk et al. (2010) have shown that NRT1.1 can transport auxin directly and that the presence of nitrate suppresses this transport. In their model, auxin is transported through NRT1.1 in a basipetal manner, recycling auxin from the LR tip to more basal parts of the LR. Inhibition of NRT1.1-mediated auxin transport by nitrate (via a so far unknown mechanism) leads to auxin accumulation in the tip and thus enhances lateral root elongation. Conversely, low-N increases auxin recycling and hence slows down lateral root elongation. Recycled auxin may then be available for

the promotion of higher order lateral root emergence and elongation. This opens a possible route for LR branching induced by low-K: CIPK23 may phosphorylate not only AKT1 but also to some extent NRT1.1, thereby mimicking a low-nitrate condition and leading to a halt of LR growth and branching. The question then arises whether CIPK23-phosphorylated AKT1 could also promote auxin recycling from the LR tip and how. Efflux of auxin in its acidic form is a potential target process as it will depend on the membrane potential and hence on AKT1 activity.

In summary, I have shown that LR branching in low-K is stimulated via a signalling module of AKT1, CIPK23 and NRT1.1 with CIPK23 as a central node for cross-talk of K- and nitrate signalling. This causal relationship is summarized by the model depicted in Fig. 29.

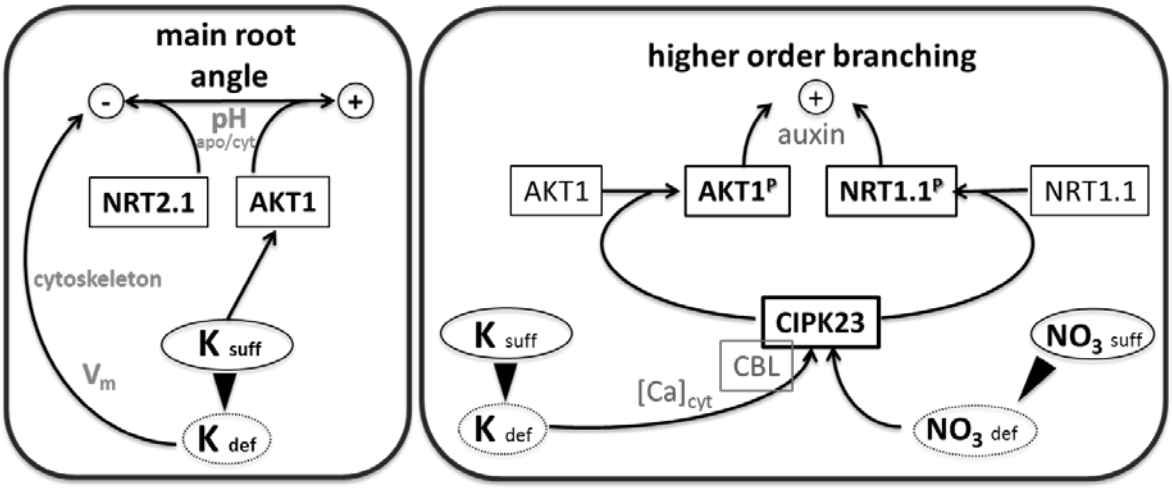

Figure 29: Working model of signalling modules controlling the main root angle and higher order branching.
Proteins are shown in square boxes, nutrient concentrations are in ovals (suff: sufficient; def: deficient). Assumed signals are in grey.
Left panel: Main root skewing is a phenomenon observed for root systems grown on a two-dimensional surface. K-deficiency (K def) promotes skewing of the main root to the left (negative), possibly directly via hyperpolarisation of the membrane potential (V_m) causing downstream alterations of the cytoskeleton. The high affinity nitrate transporter NRT2.1 and the K Shaker-type channel AKT1 act antagonistically in imposing a more negative (NRT2.1) or more positive (AKT1) angle. Note that activation of AKT1 via CIPK23 is not required. Changes in pH may act as a downstream signal of ion and proton fluxes across the membrane either through its effect on cell wall deposition and growth in the apoplast or by modulation of cytosolic pH which in turn is a major determinant for K channel activity.
Right panel: Low-K (K def) and low-N (NO_3 def) induce the emergence and elongation of second order lateral roots. The CBL-interacting kinase CIPK23 is required for this response, suggesting that a cytosolic Calcium signal ($[Ca]_{cyt}$) mediates at least the low-K status within the root. Upon stimulation, CIPK23 is able to phosphorylate both AKT1 and the nitrate transceptor NRT1.1. In their phosphorylated state ($AKT1^P$; $NRT1.1^P$), both proteins generate downstream signals that induce higher order branching. Alterations in auxin fluxes may be one of these signals, since NRT1.1 has been reported to recycle auxin

from the root tip back to basal parts in low-N (and hence probably in a phosphorylated state), slowing down lateral root elongation (Krouk et al., 2010). The increased auxin concentration in the lateral branching zone may trigger enhanced emergence of second order lateral roots. The involvement of $AKT1^{p}$ in auxin signalling, as much as the existence of any other potential downstream targets, has yet to be established.

3.3.7 Main root angle is determined by external K and antagonistic action of AKT1 and NRT2.1

Roots grown on a two-dimensional surface display a MR angle due to 'skewing' of the MR towards one side (Oliva and Dunand, 2007), typically to the right when looking at seedlings from behind (through the agar). In low-K this angle was reduced or even negative, indicating that it is the titratable product of two opposing processes (Fig. 23). So far, the exact molecular basis of the skewing phenomenon is not known but several explanations have been proposed. One possible reason is that epidermal cell file rotation (CFR) generates a twisting root (Thitamadee et al., 2002) that would normally 'drill' its way vertically into the ground. Drilling in 3D is translated into rolling over surface in 2D. Fixed at the base, the growing root produces an angle if rotation occurs in one direction only (Migliaccio and Piconese, 2001; Yuen et al., 2005). Buer et al. (2003) argued for CFR-independent differential flank growth as another possible reason for the root angle, and reported regulation by ethylene, sucrose and nitrate. At the subcellular level, the cytoskeleton has been implicated as the reason for changes in CFR (Oliva and Dunand, 2007). Alternatively, the orientation of microtubules could cause root skewing through their role in aligning cell wall deposition (Thitamadee et al., 2002; Sedbrook et al., 2004; Yuen et al., 2005).

Mutant analysis again pointed to an essential role of AKT1 in controlling the root angle (Fig. 23). In this case, however, the response was independent of CIPK23. Knockout of AKT1 led to a constitutive reduction/left-turning of the angle in control media thereby mimicking the low-K response. None of the other mutants tested showed this phenotype in control but they were all similarly responsive to low-K. In control, *nrt2.1* mutants actually showed a significantly increased root angle without reducing the effect of low-K. Taken together the results support a model in which the MR angle in nutrient sufficient condition is determined by an antagonistic action of AKT1 and NRT2.1 with the former promoting right-skewing and the latter promoting left-skewing (Fig. 29). Knockout of one of the two genes shifts the angle towards the left or right respectively.

On the basis of these results, apoplastic pH is a good candidate for representing the primary stimulus regulating the root angle. K-influx (through AKT1) promotes H^+-efflux through the proton pump (Amtmann et al., 1999), which acidifies the apoplast, while nitrate influx (through NRT2.1) is accompanied by H^+-influx (Miller et al., 2007) resulting in extracellular alkalinisation. K channel activation in turn largely depends on apoplastic pH which is set by plasmamembrane localised H-ATPases (Amtmann et al., 1999). This

activation is due to a dual effect of pH on channel gating and transportation rates (Amtmann and Blatt, 2008). Furthermore, knockout of AHA2, the major root H^+-ATPase, has previously been reported to strongly reduce ATP-induced root skewing to the right (Haruta and Sussman, 2012) thus showing a similar phenotype to knockout of AKT1. The importance of apoplastic pH for cell wall deposition and growth is well known and it will be interesting to study a potential role in nutrient responses of RSA in more detail in the future. Nevertheless, changes in apoplastic pH are coupled to changes in intracellular pH. The immediate consequence of apoplastic acidification is the (at least transient) alkalinisation of the cytosol. Cell-specific acidification/alkalinisation has been shown to be involved in gravitropic responses (Scott and Allen, 1999). In fact, intracellular pH could be regarded as a 'second messenger' in many signalling processes (Felle, 2001). Modelling signalling, transport and metabolic processes in guard cells has demonstrated diurnal changes in cytosolic pH (pH_{cyt}) albeit the cell's large static buffer capacity for protons (Chen et al., 2012b). This model was also used to test the effects of a *slac1* outward-rectifying anion channel mutant. Knocking out *SLAC1* resulted in constitutively higher pH_{cyt} and cytosolic calcium levels (Wang et al. (2012b). Cytosolic pH was the main determinant for K influx as demonstrated by clamping pH_{cyt} to wild-type levels in the knockout. However, this knowledge is so far limited to guard cells. It will be interesting to model and test the effects of transport, signalling and metabolism in other types of plant tissue, e.g. the root epidermis. In conclusion, alterations of apoplastic or cytosolic pH represent putative downstream targets of proton movements stimulated by AKT1 and NRT2.1 mediated transport and may be a signal for metabolic changes that underlie the root skewing phenomenon.

Interestingly, low-K had the same effect as AKT1-knockout but was independent of functional AKT1 or NRT2.1, which suggests a different primary signal. In this case, membrane hyperpolarisation may be a crucial factor since it occurs both in wild type plants in low-K and in *akt1* mutants in sufficient K (Spalding et al., 1999). Membrane hyperpolarisation has been shown to evoke changes in the actin cytoskeleton of mammalian cells (Nin et al., 2009; Chifflet and Hernandez, 2012) thus providing a potential link to cellular growth and shape. A hypothetical model of MR angle control could therefore be comprised of a membrane-delimited regulatory module that involves AKT1, NRT2.1 and AHA2.

Change of the main root angle is a novel phenotype for K-deprived Arabidopsis seedlings. The number of genotypes chosen for further characterisation of the phenomenon was limited to only 6, including the wild type. Within this small set, I already found two

genotypes (*akt1*, *nrt2.1*) with aberrant phenotypes in control conditions, but none with an altered response to low-K. Natural variation provides an alternative route in the search for phenotypic variants. A large genetic toolkit comprised of fully sequenced natural accessions and large mapping populations is readily available for Arabidopsis, enabling researchers to get down to the molecular base of the phenotype in question (Weigel, 2012). In that respect, a promising approach to further investigate plasticity of the main root angle would be to screen a set of Arabidopsis ecotypes in different K-conditions. I have therefore quantified the root architectural response to low-K, including the main root angle, in 26 Arabidopsis natural accessions. This study is presented in Chapter 4.

3.3.8 Transcriptional and phenotypic response signatures overlap

Transcriptional regulation of gene networks may be involved in signalling pathways that control phenotypic responses of the root system to nutrient deprivation. A microarray experiment was therefore carried out at an early stage of deficiency (6 DAG) in a subset of eight combinations of sufficient/deficient N, P and K in long day. At this stage, phenotypic differences between the conditions started to become visible but were generally quite subtle. This suggests that remobilisation of nutrients from storage compartments of the seed had reached its end and therefore sensing, signalling and uptake of external nutrients became prevalent.

Following a rigorous filtering procedure, still a large number of genes (n = 371) was detected as being responsive to the environment. Cluster analysis revealed co-regulation of gene expression resulting in transcriptional 'response profiles' of up- and downregulated genes (Fig. 25, 26). Moreover, response profiles of the root transcriptome could be matched onto response profiles of the root phenome (Fig. 26, Table 20). The 'N-profile' is characterised by a strong effect of low-N on expression levels and on lateral root size. Clusters UP1 and UP2 contained amongst others an up-regulated nitrate transporter gene (*NRT1.8*), but also a set of transcription factors (TFs): three WRKY TFs, three NAC TFs and two DREB TFs. Genes from all three TF families have been implied in abiotic stress responses (Lee et al., 2010; Nakashima et al., 2012). One of these genes, DREB2C, has also been shown to be involved in drought responses and ABA signalling (Lee et al., 2010). ABA in turn is known to repress lateral root emergence and elongation (Deak and Malamy, 2005) and hence lateral root size.

The 'NK-profile' has significant overlap with the N-profile but shows a more reduced mRNA level and less developed root architecture in low-NK than low-N alone.

Genes in the corresponding cluster DOWN1 contain amongst others three expansins and two extensins, both groups functioning in cell expansion. A set of four genes (*MRH1*, *RHS18*, *RHS19*, *LRL3*) is annotated to be involved in root hair development.

In addition, although it did not clearly match onto a root response profile visually, cluster DOWN5 was correlated with LRP 0.50 (Table 20). Downregulated genes in this cluster contained six aquaporins (*PIP1;5*, *PIP2;2*, *PIP2;3*, *PIP2;4*, *TIP1;1*, *TIP2;2*), two of which (*TIP1;1*, *TIP2;2*) were also shown to be down-regulated in mature N-starved roots (Krapp et al., 2011). Aquaporin gene expression is known to be downregulated upon water stress (Chapman et al., 2012) and hence may be a downstream signal of ABA. Summing up, reduction of lateral root elongation may be preceded by a reduced expression of cell wall modifying genes and an activation of ABA signalling pathways.

Reduced branching also defined the 'NP-profile', but here a different set of root parameters (1st order LR number, branched zone length, LRP 0.25) was concerned. The interactive effect of low-NP greatly diminished total root size and gene expression in cluster DOWN3 which contained two important auxin signalling components, *AXR3/IAA17* and *ARF18*. Members of the IAA-family act as transcriptional repressors and ARFs are known to induce auxin mediated transcription (reviewed in Leyser, 2006). Since both genes probably work in opposite directions it is not clear whether auxin signalling is reduced or enhanced if both genes are downregulated at the same time. An alternative hypothesis accounting for the strong repression of root growth in low-NP is presented in the last section of the discussion (3.3.9).

As mentioned before main root elongation was strongly P-dependent (see 3.3.3). I also observed significant overlap between profiles of P-responsive genes with P-responsive root parameters. Interestingly, upregulation of gene expression was the predominant feature of the 'P-profile' and the function of genes belonging to this profile was quite diverse. Upregulation of two phosphatases (*PAP17*, *PPSPASE1*) indicates the activation of P-remobilisation already at this stage of development (Tran et al., 2010). The involvement of cytokinin (*CKX5*) and phospholipid signalling (*PLA2A*, *PLDP2*) as well as upregulation of peroxidases suggests activation of extensive signalling networks. Last not least, an interesting pattern was observed for *AT4*. This gene is known to be induced by P-starvation (Shin et al., 2006) and it was shown to inhibit miR399 action by 'target mimicry', resulting in increased PHO2-mediated shoot P-concentrations (Franco-Zorrilla et al., 2007). My results confirmed the induction of *AT4* by low-P, however, they also show its repression by low-N. Ultimately, up- and downregulation in NP-double deficiency cancelled each other

out. This might explain the higher P concentrations measured in shoots of seedlings starved for both N and P as compared to low-P alone (Fig. 27) and opens a route for N-P crosstalk.

In summary, I have shown that nutrient-specific and nutrient-interactive signatures of transcriptional and phenotypic responses match. Surely, the next step should be to extract information from these microarrays in a more sophisticated manner and to analyse specific pathways and/or genes in more depth. Upon publication, this dataset will be made available to the research community and hence will be a valuable resource to unravel the interwoven regulatory networks controlling nutrient homeostasis and root system architecture.

3.3.9 Excessive iron accumulation in shoots of N- and P-starved seedlings is preceded by matching transcriptional responses

Ionomic profiling of NPK-starved plants revealed an increase of shoot iron (Fe) concentrations caused by single and multiple deficiencies: low-P (ca. 4-fold), low-N (ca. 5-fold), low-PK (ca. 7-fold) and low-NP (15 to 20-fold; Fig. 27). Again, a look at early transcriptomic responses already hints towards changes in Fe homeostasis. First and foremost, I detected a significant increase of MATE-efflux transporter expression: *ALMT1*, *FRD3* (more than 2-fold up, but below the 4-fold cut-off) and two other MATE-family members (AT1G71140, AT2G04050). ALMT1 promotes the secretion of malate into the rhizosphere (Delhaize et al., 2004) which helps to mobilise P but may also increases bioavailable iron (Vance et al., 2003). The synchronous upregulation of malate synthase *MLS* may account for a higher malate demand. Once inside the plant, FRD3 mediates Fe root- to shoot-translocation by secreting the Fe-chelator citrate into the xylem (Durrett et al., 2007). Although the role of the other MATE-members is unclear, these three components alone could explain a higher degree of Fe accumulation in the shoot.

Downregulation of genes belonging to the high-affinity Fe uptake machinery (reviewed in Thomine and Lanquar, 2011), namely *IRT1* (1.4-fold down), *IRT2* (2.2-fold) and *FRO2* (8.1-fold), reflect the high internal Fe status. That also suggests that an alternative, unspecific uptake mechanism that does not require FRO2-mediated Fe-reduction at the epidermal plasma membrane is responsible for Fe accumulation. Noteworthy, Krapp et al. (2011) also found a quick and stable downregulation of *IRT1* and *FRO2* in their microarray analysis of root responses to low-N. In my experiments, *CASP3* and *CASP4*, two genes involved in casparian strip formation (Roppolo et al., 2011), were downregulated in low-NP. Recent research activity in the Salt Lab at Purdue and Aberdeen

University has demonstrated a significant contribution of the casparian strip as a checkpoint in sym- and apoplastic transport to metal homeostasis (Baxter et al., 2009). Unexpectedly, I also found *NRAMP3* to be highly induced by low-N and low-P. It seems counterintuitive, as this vacuolar transporter was associated with remobilisation of Fe in seeds (Lanquar et al., 2005) rather than sequestration of excess Fe. However, a functional characterisation of *NRAMP3* in seedlings and mature plants is still lacking (Thomine and Lanquar, 2011).

All in all, the combination of transcriptomics and ionomics provides an alternative explanation of the aggravated growth phenotype caused by NP-deficiency: iron accumulation up to toxic levels rather than the simple lack of nutrients (N, P) per se.

Iron accumulation as a side-effect of nutrient deficiencies has been a recurring theme in my PhD project. Here, alterations of Fe homeostatic genes and excess Fe accumulation in NP-starved shoots (but also to some extent in low-P and low-PK; Fig 27) was the first indication for a central role of Fe homeostasis in various nutrient stresses. The following Chapter 4 will address natural variation of phenotypic responses (RSA) to low-K. Results hereof were the next step-stone that led me on to investigate P-K co-regulation in more detail. Finally, in Chapter 5 and 6, iron will be investigated in more detail as a major factor in shaping root growth under nutrient starvation.

4. Natural variation of Arabidopsis root system architecture responses to K starvation

Results published in *Plant Physiology:*

Kellermeier, F., Chardon, F., and Amtmann, A. (2013). Natural variation of Arabidopsis root architecture reveals complementing adaptive strategies to potassium starvation. Plant Physiology **161:** 1421-1432.

4.1 Introduction

My initial study on root system architecture (RSA) in single and multiple nutrient deficiency presented in Chapter 3 revealed that K supply had an impact on various root parameters. Main root and lateral root elongation as well as the main root angle orientation all responded to low concentrations of K in the growth medium. Whereas within-species natural variation has been successfully applied to characterise root responses to N-deficiency (Rauh et al, 2002; North et al., 2009; Chardon et al., 2010; Ikram et al., 2011) and P-deficiency (Reymond et al., 2006; Svistoonoff et al., 2007; Prinzenberg et al., 2010), K-deprivation (low-K) responses have so far been neglected in that respect. Only Prinzenberg et al. (2010) carried out a coarse analysis of root growth in low-K by quantifying root weight and 'root length' of 5 week old plants grown in hydroponics. Their analysis and two other studies also examined natural variation of K concentrations in shoots, roots and seeds of Arabidopsis (Vreugdenhil et al., 2004; Harada and Leigh, 2006; Prinzenberg et al., 2010).

Understanding K regulatory pathways is important as K serves as the major osmoticum for cell expansion (Leigh and Wyn Jones, 1984; Amtmann et al., 2006) and hence can be regarded as the quantitatively most important cation for plant growth. Moreover, K is essential for many cellular and tissue processes such as enzymatic activity, transport of minerals and metabolites and regulation of stomatal aperture (Amtmann et al., 2006). In the field, rapid uptake of K by the plant root system can lead to K shortage in the surrounding soil environment, especially early in the growth season. Root adaptations to low-K therefore take place at the physiological (Armengaud et al., 2004; Shin and Schachtman, 2004; Aleman et al., 2011), metabolic (Armengaud et al., 2009a) and morphological level.

In a classic study, Drew (1975) showed that growth of all lateral roots (LR) of barley seedlings responded positively to the addition of K salts, even when K supply was restricted to only a section of the root system. Conversely, a typical response of Arabidopsis (Col-0) seedlings to low-K is the drastic reduction of lateral root elongation (Armengaud et al., 2004; Shin and Schachtman, 2004). Conflicting data have been published on the effect of low-K on main root (MR) growth, ranging from no effect (Shin and Schachtman, 2004) to impaired MR elongation (Jung et al., 2009; Kim et al., 2010). A comprehensive analysis of root architecture in various genomic backgrounds (natural accessions) is still missing. However, it may reveal novel phenotypic outputs of K starvation that can be used as quantifiable reporters of K sensing and signalling pathways.

A few molecular components involved in low-K responses have already been identified, e.g. jasmonates (Armengaud et al., 2004, 2010), reactive oxygen species (Shin and Schachtman, 2004) and ethylene (Jung et al., 2009; see also Chapter 1, introduction section 1.4.4 Potassium Signalling). Nevertheless, the molecular identity of a root K sensor acting at the base of the signalling cascade is so far unknown.

Natural variation has proven a useful resource in dissecting the components of complex, multigenic phenotypes (Koornneef et al., 2004; Alonso-Blanco et al., 2009; Weigel, 2012). Many studies on plant morphology, physiology and development as well as stress response (Alonso-Blanco et al., 2009; Weigel, 2012) have built upon allelic differences in natural accessions. Natural variation of root traits such as primary root length (Mouchel et al., 2004; Loudet et al., 2005; Sergeeva et al., 2006), lateral root length (Loudet et al., 2005) and total root size (Fitz Gerald et al., 2006) have pinpointed genomic regions underlying phenotypic variation via mapping of quantitative trait loci (QTL) as a first step towards identification of novel regulatory genes (Mouchel et al., 2004). In the case of low-P, this strategy has successfully led to the identification of genes involved in local P-sensing at the root tip (Reymond et al., 2006; Svistoonoff et al., 2007).

I have therefore taken a similar two-step approach to investigate Arabidopsis root responses to low-K:

1) A set of natural accessions was phenotyped in K-sufficient and K-deficient conditions to identify differences in root system architecture responses to low-K.

2) A pair of accessions showing distinct RSA responses was subsequently chosen as the basis for QTL mapping of these responses.

In this chapter, I will show that Arabidopsis accessions have different strategies to morphologically respond to K-starvation. I have quantified a comprehensive set of root architectural parameters of Arabidopsis grown in K-sufficient and K-deficient media and identified genetic loci, each of which determines the response of a distinct subset of root architectural parameters to K-starvation. One locus was chosen for further fine-mapping and the role of target genes within that interval will be discussed.

4.2 Results

4.2.1 Choosing the genotype set and the right experimental conditions

The Arabidopsis accession set (see Table 3) was largely based on a nested core collection that has been widely used in the field (McKhann et al., 2004), plus two standard lab accessions (Ler and Ws). This collection of genotypes was generated on the basis of geographic (Fig. 30) and molecular diversity (McKhann et al., 2004).

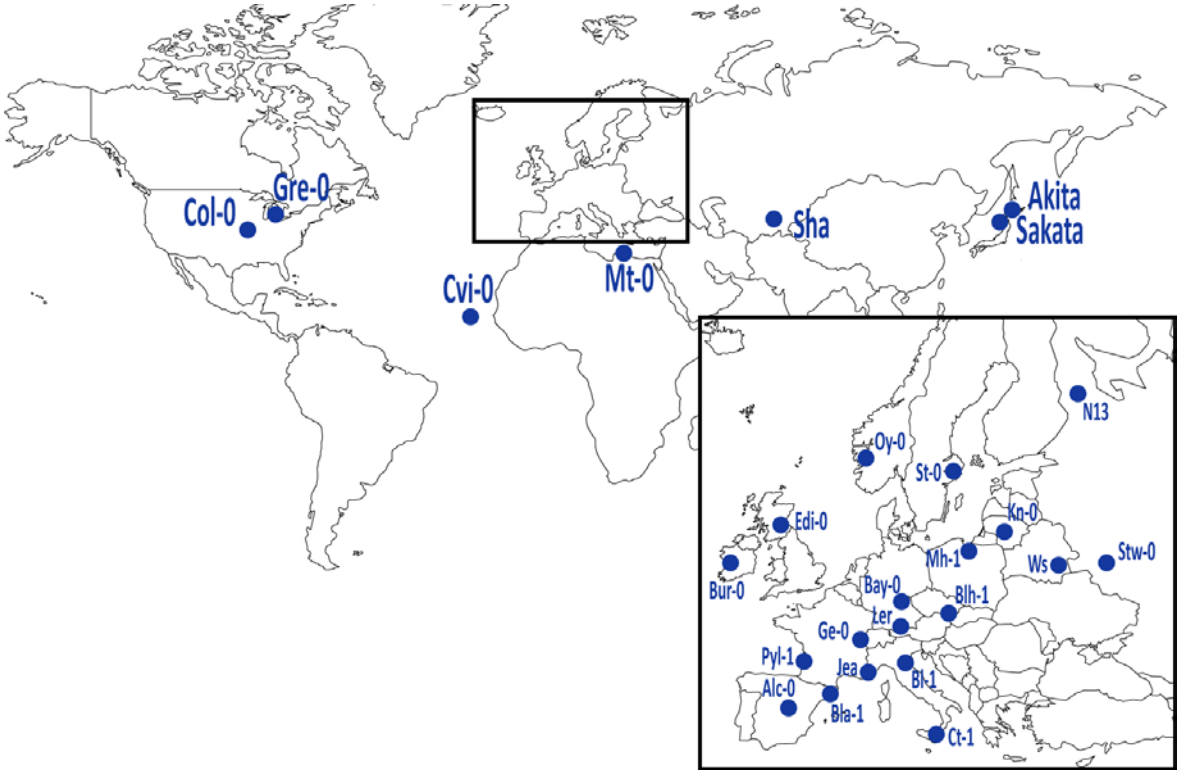

Figure 30: Geographic origin of Arabidopsis accessions used in this study.
The set of accessions was largely based on the *nested core collection 24* generated by McKhann et al. (2004). Most accessions derive from wild populations in Europe (inset) and Asia, but also genotypes from Africa and North America were part of the analysis. Columbia (Col-0), Landsberg erecta (Ler) and Wassilewskija (Ws) are commonly used laboratory 'wild types'. Because they have been 'domesticated' decades ago, the exact origin of these genotypes is not quite clear anymore. Potential origins are therefore shown on the map.

Growth conditions were based on the standard growth medium described in section 2.2.1 of the Material and Methods section. To determine the optimal low-K concentration, a randomly chosen subset of 3 accessions was phenotyped across a range of K concentrations (12 DAG; Fig. 31). Root architecture analysis indicated that an even lower K concentration (10 µM) than used in Chapter 3 (50 µM) resulted in higher variability of root parameters between the genotypes tested. In the following experiment, seedlings of all 26 accessions were grown in two contrasting environments: *control* ([K] = 2 mM; equal to the standard growth medium) and *low-K* ([K] = 0.01 mM; difference in KNO_3 compensated by addition of $NaNO_3$ and corresponding removal of NaCl)

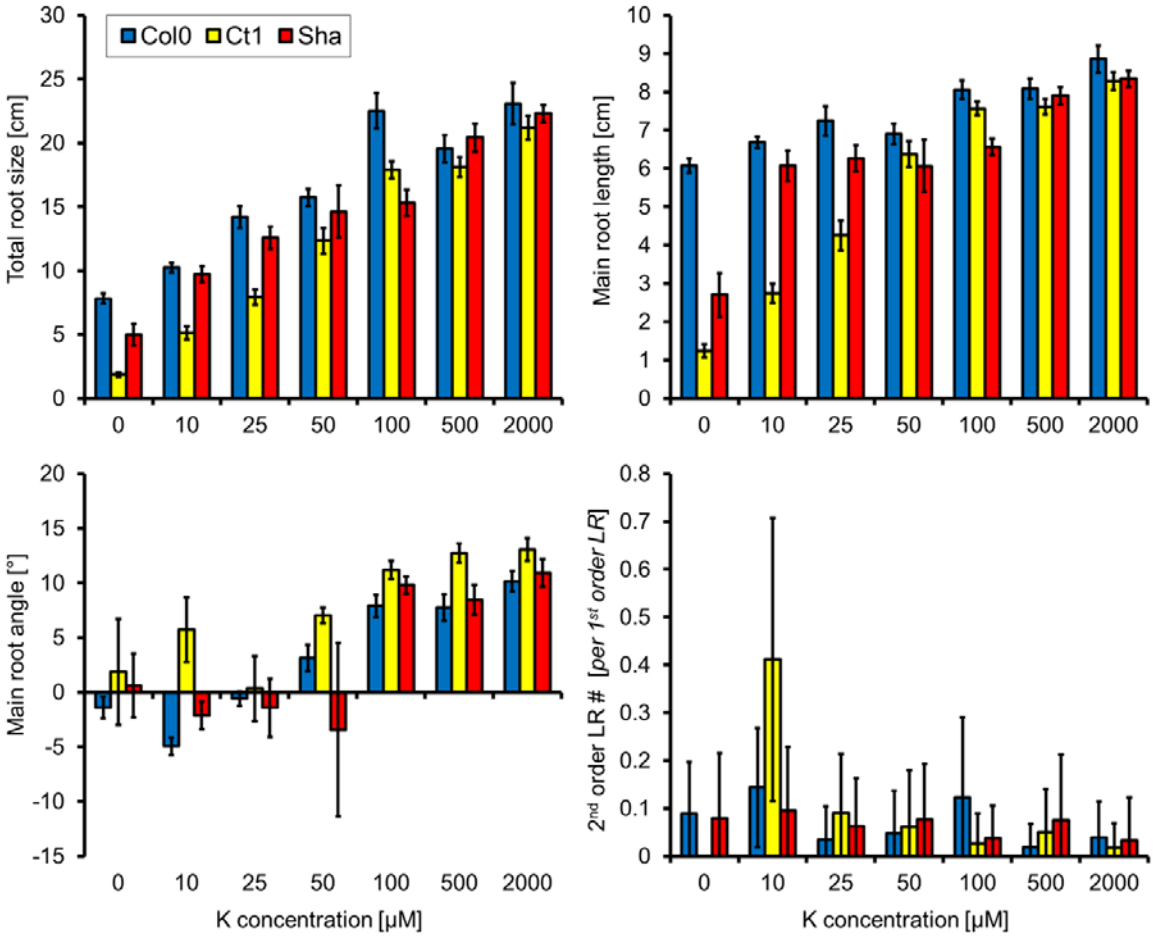

Figure 31: Preliminary RSA analysis of three accessions in various concentrations of K to determine the optimal low-K condition.
KNO_3 was replaced with $NaNO_3$ to keep nitrate concentrations constant (at 2 mM). Root parameters were quantified with EZ Rhizo 12 DAG. Values shown are means ± S.E.M. (n = 4 to 8 per genotype per condition).

4.2.2 Genotype and K-supply cause phenotypic variation of root architecture in Arabidopsis

Quantitative analysis of 14 root architectural traits was performed 12 days after germination (12 DAG) with EZ Rhizo (Armengaud et al., 2009b). For abbreviations and definitions of traits see Table 5 and Table 21. The set of traits varied slightly from those analysed in Chapter 3, partly owing to the altered low-K concentration. For example, 2nd order lateral root number was not further analysed as this trait varied too much to give meaningful results (compare also Fig. 31). 1st order LR number was therefore abbreviated as LR #. In contrast, average lateral root length in parts closer to the root tip (LRP 0.75, LRP 1.00) were included because they were important traits in distinguishing groups of accessions. Raw data generated in this experiment can be found in the electronic appendix as *Ch4_Natural variation of root architecture responses to low-K*.

Across all accessions, low-K reduced values of 11 of the 14 quantified traits compared to control (Table 21). Only lateral root path length in the third quartile from the root-shoot junction (LRP 0.75) and lateral root densities normalised to the length of the main root (LRdensMR) or branched zone (LRdensBZ) were, on average, increased in low-K. Correlation analysis revealed significant correlations between most traits (Table 22). Most correlations were similar between control and low-K conditions. To some extent, this could be interpreted as stable developmental relationships between root parameters. However, different strength of correlation on the contrary may indicate environmental plasticity. The latter is clearly the case where correlations were inverse between control and low-K, changing from positive to negative, most notably for lateral root path length, or from negative to positive as was the case for lateral root density. I also carried out correlation analysis between traits in low-K and control using all 26 pairs of accession means (Table 21 right column). Here, Pearson correlation coefficients were generally small suggesting significant variation of K-deficiency responses within the genotype pool. Exceptions were main root angle and lateral root densities with r^2 values between 0.41 and 0.49. Low-K responses of these traits are therefore less variable between genotypes. With regard to results presented in Chapter 3 (sections 3.2.4 and 3.3.7), the reduction of the main root angle as a response to low-K appears to be stable across a variety of genotypes.

Table 21: Means (± S.E.M.) of 14 root parameters across all accessions quantified in control and K deficiency.

The K response ratio (low-K/control) was calculated as mean in low-K divided by mean in control. Pearson correlation coefficients (r^2) are shown for pairwise correlation of mean low-K with mean control values of each accession. Standard errors of the mean (S.E.M.) are given in brackets.

trait ID	trait description	unit	control	low-K	low-K / control	r^2
TRS	total root size	cm	16.48	4.58	28%	0.05
			(0.33)	(0.17)		
MRP	main root path length	cm	7.11	2.72	38%	0.23
			(0.12)	(0.11)		
Apical	apical zone length	cm	3.19	1.08	34%	0.18
			(0.07)	(0.06)		
Branched	branched zone length	cm	3.65	1.44	39%	0.21
			(0.08)	(0.06)		
Basal	basal zone length	cm	0.25	0.19	76%	0.07
			(0.01)	(0.01)		
MR angle	angle of main root from full verticality	°	15.18	2.42	16%	0.41
			(0.5)	(0.48)		
LRS	lateral root system size	%	55	40	73%	0.18
	(as proportion of total root size)		(1)	(1)		
LR #	1st order lateral root number		12.65	7.17	57%	0.07
			(0.26)	(0.24)		
LRP 0.25	mean lateral root path length in the	cm	1.15	0.29	25%	0.01
	uppermost quarter of the main root		(0.03)	(0.02)		
LRP 0.50	mean lateral root path length in the	cm	0.44	0.23	52%	0.01
	2nd quarter from the top of the main root		(0.02)	(0.02)		
LRP 0.75	mean lateral root path length in the	cm	0.08	0.15	188%	0.03
	3rd quarter from the top of the main root		(0.01)	(0.01)		
LRP 1.00	mean lateral root path length in the	cm	0	0.08	n/a	0.03
	4th quarter from the top of the main root		(0)	(0.01)		
LRdensMR	lateral root density normalized to	cm^{-1}	1.82	3.16	174%	0.49
	main root length		(0.03)	(0.09)		
LRdensBZ	lateral root density normalized to	cm^{-1}	3.54	5.86	166%	0.48
	branched zone length		(0.06)	(0.17)		

Table 22: Pearson correlation coefficients between all traits quantified.
Phenotypic data was taken from all genotypes and analysed for control and low-K conditions separately. Positive correlations are highlighted in red, negative correlations in blue. Traits for which the orientation of correlation (positive or negative) changed between the two conditions are emphasised by bold print. $p < 0.05$; n.s.: not significant.

Control	MRP	TRS	LR #	LRS	LRP 0.25	LRP 0.50	LRP 0.75	LRP 1.00	MR angle	Basal	Branched	Apical	LRdens/MR
MRP													
TRS	0.67												
LR #	0.53	0.81											
LRS	n.s.	**0.34**	**0.37**										
LRP 0.25	**-0.15**	0.48	0.13	0.70									
LRP 0.50	-0.14	0.24	**0.13**	0.53	0.45								
LRP 0.75	**0.07**	**0.48**	**0.47**	0.50	n.s.	n.s.							
LRP 1.00	**0.11**	**0.21**	**0.13**	n.s.	0.16	n.s.	0.61						
MR angle	0.49	0.19	0.07	n.s.	-0.08	**0.18**	**0.12**	**0.18**					
Basal	0.63	0.12	0.06	n.s.	**-0.31**	n.s.	n.s.	n.s.	**0.65**				
Branched	0.91	0.82	0.77	-0.13	0.01	**0.09**	**0.40**	**0.22**	0.43	0.53			
Apical	0.85	0.36	0.14	n.s.	**-0.28**	-0.40	-0.36	-0.06	0.38	0.51	0.56		
LRdensMR	-0.49	**0.13**	**0.45**	n.s.	0.29	n.s.	0.43	0.03	-0.37	-0.51	-0.15	-0.75	
LRdensBZ	-0.67	-0.15	**0.17**	n.s.	0.17	0.22	0.07	**-0.13**	-0.41	-0.60	-0.45	-0.71	0.90

Low-K	MRP	TRS	LR #	LRS	LRP 0.25	LRP 0.50	LRP 0.75	LRP 1.00	MR angle	Basal	Branched	Apical	LRdensMR
MRP													
TRS	0.94												
LR #	0.82	0.83											
LRS	n.s.	**-0.16**	**-0.22**										
LRP 0.25	**0.16**	0.45	0.10	0.60									
LRP 0.50	-0.14	0.14	**-0.08**	0.74	0.69								
LRP 0.75	**-0.55**	**-0.34**	**-0.34**	0.82	n.s.	n.s.							
LRP 1.00	**-0.61**	**-0.48**	**-0.49**	n.s.	0.11	n.s.	0.65						
MR angle	0.42	0.31	0.31	n.s.	-0.17	**-0.16**	**-0.31**	**-0.33**					
Basal	0.25	0.21	0.12	n.s.	**0.03**	n.s.	n.s.	n.s.	**0.19**				
Branched	0.97	0.92	0.91	-0.39	0.14	**-0.10**	**-0.46**	**-0.56**	0.37	0.19			
Apical	0.97	0.89	0.68	n.s.	**0.19**	-0.15	-0.60	-0.62	0.44	0.24	0.87		
LRdensMR	-0.74	**-0.58**	**-0.34**	n.s.	0.00	n.s.	0.76	0.75	-0.37	-0.35	-0.59	-0.82	
LRdensBZ	-0.75	-0.60	**-0.46**	n.s.	0.10	0.32	0.74	**0.56**	-0.25	-0.19	-0.68	-0.74	0.81

Contributions of genotype, environment (low-K vs. control) and genotype-environment interactions (gen*env) to the total variation explained for each parameter were calculated via global ANOVA of the whole dataset (Fig. 32). The extent to which each of these three factors contributed to individual root parameters varied considerably, ranging from 4.5 % to 31.2 % for environment, from 3.8 % to 69.8 % for the genotype and from 5.2 % to 14.8 % for gen*env. The highest percentage explained by genotype was found amongst lateral root parameters, such as lateral root number (LR #), lateral root system size (LRS), LRdensMR and LRdensBZ. The environment (media composition) strongly influenced total root size (TRS) and main root parameters, such as main root path length (MRP), lengths of the apical zone (Apical) and branched zone (Branched), as well as MR angle. The environment also strongly affected lateral root path length in the first quartile (LRP 0.25). Genotype-environment interactions were generally less important (5.2 % for MR angle to 14.8% for LR #). They accounted for a higher proportion variation in lateral root path length in the second quartile (LRP 0.50), third quartile (LRP 0.75) and fourth quartile (LRP 1.00). Albeit their relative small contribution, the mere existence of gen*env indicates that accessions must differ in responses to low-K. A closer view on individual genotypes will give a refined picture.

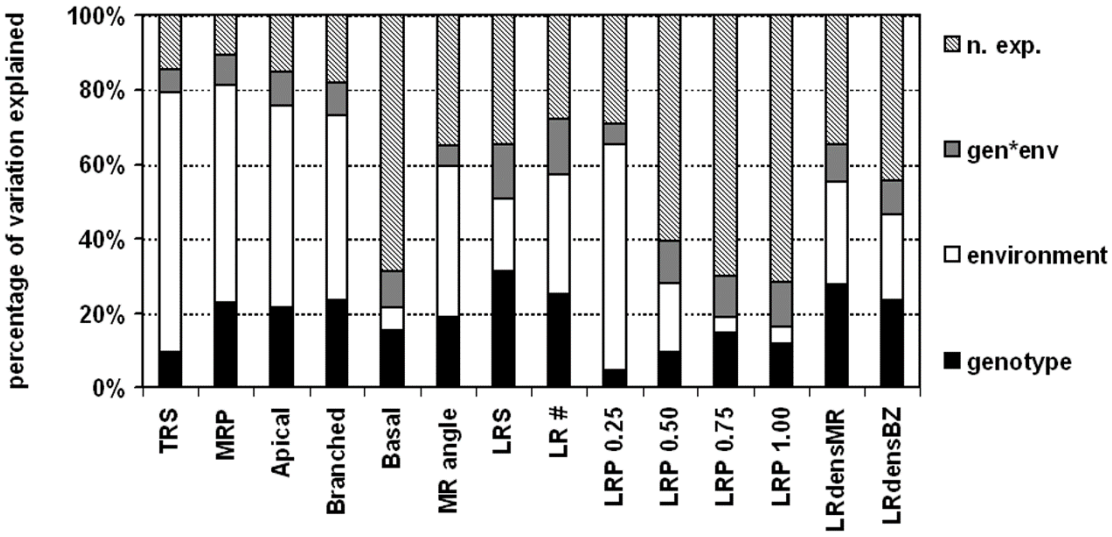

Figure 32: Variation in root parameters explained by genotype and environmental conditions obtained through global ANOVA.
Independently analysed individual root parameters, as per Table 21, are given on the x-axis. 26 Arabidopsis natural accessions (*genotype*) were grown on control and low-K media (*environment*) and root architecture parameters were quantified for 480 plants phenotyped 12 DAG (n = 7 -12 per genotype per condition). ANOVA was computed using type III sums of squares at a significance level of $p < 0.05$. n. exp.: not explained. *gen*env*: genotype-environment interaction.

4.2.3 Natural accessions adopt different strategies to adjust RSA to K supply

An overview of variation in root architecture is given in Fig. 33. Differences between accessions were already visible in control conditions. Whereas some accessions grew long main roots whilst compromising lateral root elongation (e.g. Bur-0, Ler, Pyl-1), others showed the opposite phenotype, i.e. short MRs but longer LRs (e.g. Bay-0, Stw-0). Quantitative data of selected root parameters is shown on the following page in Fig. 34.

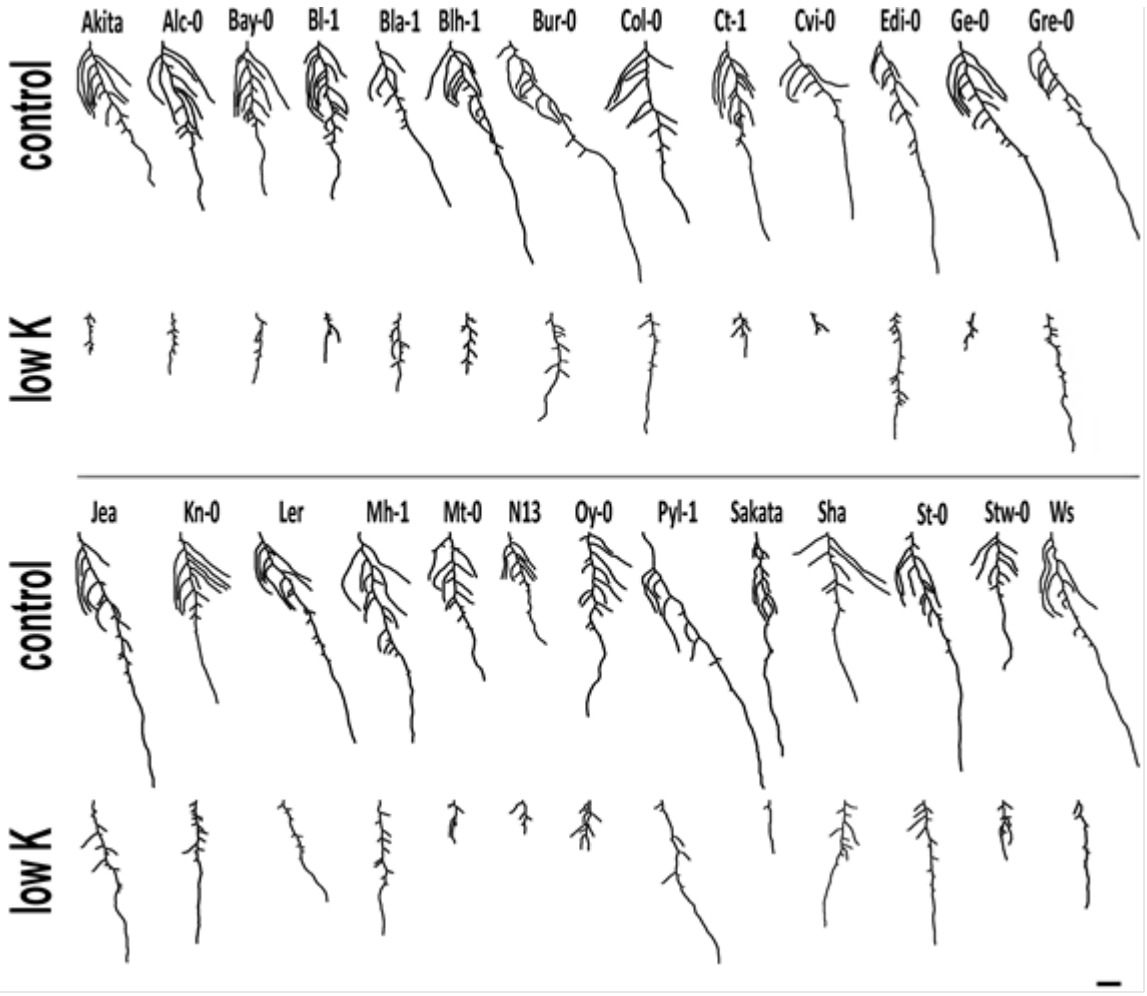

Figure 33: Typical root phenotypes of Arabidopsis accessions grown on control and low-K media.
Representative root images, obtained in the analysis with EZ Rhizo, are shown for each accession in each condition (12 DAG). Scale bar: 1cm

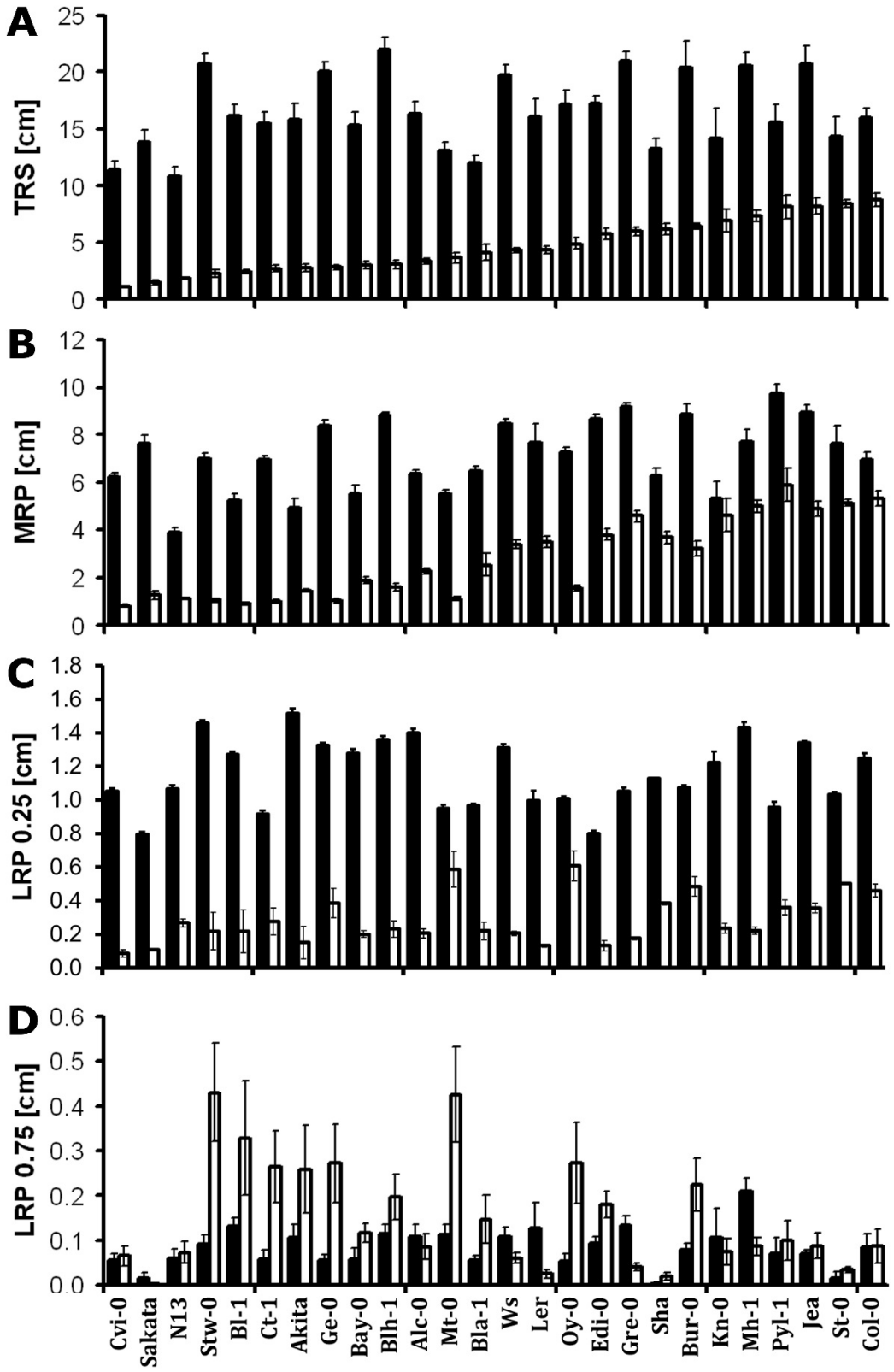

Figure 34: Low-K response of selected root parameters for individual genotypes.
Means ± S.E.M. of total root size (TRS; A), main root path length (MRP; B) and mean lateral root path length in the first (LRP 0.25; C) and third quartile of the main root (LRP 0.75; C) were calculated from plants grown in control (black bars) and low-K (white bars) condition. Accessions are sorted according to mean TRS in low-K. n = 7 – 12 plants per genotype per condition.

Low-K generally reduced total root system size (Fig. 34A) but dramatic differences occurred between genotypes in terms of main and lateral root elongation (Fig. 34B-D). Interestingly, the reference accession Col-0 had the largest total root system in low-K condition, albeit average size in control. Genotypes with a large total root size in low-K were characterized by longer main roots. Whereas low-K reduced lateral root length at the root base (LRP 0.25) in all accessions (Fig. 34C), some accessions showed a striking increase of LR length close to the root tip (LRP 0.75), e.g. Stw-0, Bl-1 Ct-1, Akita, Ge-0, Mt-0 and Oy-0 (Fig. 34D). Indeed, those lateral roots eventually outgrew the main root tip (see also representative images shown in Fig. 33). This suggested a trade-off between main and lateral root growth in K-deficient conditions, especially since these accessions were not the ones with the smallest TRS in low-K.

To identify common morphological responses amongst accessions, agglomerative hierarchical cluster analysis (AHC) was performed on the accession means of all root parameters in each condition. In both conditions, cluster-size was limited to five classes. In control conditions (classes *C1 – C5*), genotypes with a large TRS and generally longer main roots were found in *C4* and *C5* (Fig. 35). Lateral root number (LR #) was also higher in *C4* and *C5*, whereas lower LR # characterised *C1* and *C3*. Main root angle was a distinguishing feature in control, with lowest values in *C2* and highest in *C3* and *C4*. Branched zones were short in *C2* plants and long in *C4* and *C5*. In addition, *C3* members were distinguished by shorter lateral roots (small LRP 0.25) and low lateral root density (LRdensMR). In low-K (classes *K1 – K5*), length of the main root (MRP) and, more specifically, length of the apical zone were the main determinants of classification: low values were characteristic for all genotypes in *K1* and high values were characteristic for all genotypes in *K5*. Since the opposite was observed for the length of lateral roots, especially of those close to the tip, I defined two phenotypes as *response strategies* to low-K:

strategy I:	long main root	+ short lateral roots (clusters *K4* and *K5*)
strategy II:	short main root	+ long lateral roots (cluster *K1*)

K2 accessions grouped in the middle of the spectrum. High LR density and high LRP 0.75 underlie the proximity of *K1* and *K2*. The reference accession Landsberg erecta (Ler) was the only member of *K4*, characterised by its high positive main root angle. In fact, Ler and Pyl-1 showed the weakest MR angle response to low-K which grouped them closest to each other in low-K. In contrast, members of cluster *K3* had the lowest, and in fact negative, MR angles in low-K.

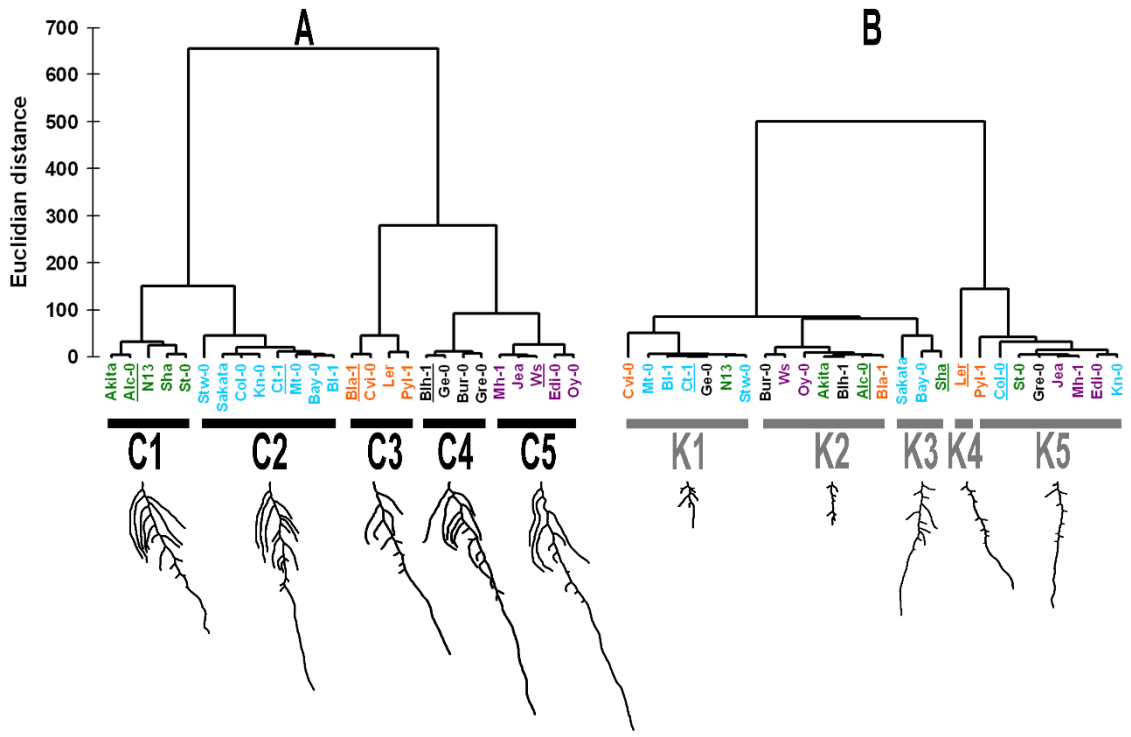

Figure 35: Agglomerative hierarchical clustering of natural accessions according to their overall root architecture highlights different response strategies to low-K.
All 14 quantified root traits of plants grown on control (A) and low-K (B) media were taken into account. Unweighted clustering was performed using Ward's method for agglomeration and Euclidian distance for dissimilarity. Genotype names are coloured according to cluster composition in control condition. For each cluster the phenotype of a representative accession (underlined) is shown below.

AHC analysis provided a refined picture on correlations between root architecture traits in control and low-K (see Table 21), showing that classes in low-K condition consisted of combinations of genotypes that differed from those in control condition. Indeed, some accessions were highly similar in control but were positioned at opposite ends of the two main branches in low-K. One such example is the pair Col-0 and Ct-1. Albeit having almost equal main root length in control condition, Col-0 is a typical low-K strategy I accession which maintains main root elongation but reduces lateral root elongation. Ct-1 on the contrary is a typical low-K strategy II accession with a small main root but elongating lateral roots.

At this point I chose this pair of accessions for further characterisation of root architectural adaptations to K deficiency. One main reason to choose these two ecotypes was the availability of a Col-0 x Ct-1 recombinant inbred line (RIL) population (Simon et al., 2008; see below) which enabled me to perform quantitative genetics. However, those

two accessions were not suitable for investigation of the main root angle response because Ct-1 main roots were just too small.

Due to its low-K insensitivity of the MR angle, this phenotype would be better studied by using Landsberg erecta (Ler) as one accession. A suitable partner (to develop mapping populations or for bulk-segregant analysis) could be Shahdara (Sha), which has been widely used in quantitative genetics studies (e.g. Loudet et al., 2005; Reymond et al., 2006). A Ler x Sha RIL population is available from the Nottingham Arabidopsis Stock Centre (NASC). This population has been used before to investigate seed germination (Clerkx et al., 2004), growth related traits and flowering time (El-Lithy et al., 2004) as well as salt stress responses (Galpaz and Reymond, 2010). Alternatively, other RIL populations with Ler as one parent, e.g. Ler x Antwerp-1, Ler x Kondara or Ler x Kashmir-2 (El-Lithy et al., 2006), could be tested. As mentioned before, I did not make any further attempts in that direction but focussed on Col-0 and Ct-1 from now on.

4.2.4 Strategies I and II are characterised by cell death around the apical meristem of main and lateral roots respectively

To investigate differences in *strategy I* (represented by Col-0) and *strategy II* accessions (represented by Ct-1) in more detail, I first followed Col-0 and Ct-1 main root growth over time. In control, MR growth continuously accelerated in both accessions. Growth rates of Col-0 main roots also slightly increased in low-K until 12 DAG, dropping significantly thereafter (Fig. 36A). In contrast, MR growth rates constantly decreased in Ct-1, reaching zero at about 9 DAG (Fig. 36B).

An immediate question arose: Can resupply of K rescue this phenotype? To answer that, I treated plants that had been exposed to K starvation for an extended period of time with 2 mM KCl solution for 1 h. Resupply of nutrients was also performed by 1h treatment with liquid control media solution (containing 2 mM K). The results of both treatments were similar, so only results of KCl-treated seedlings are shown in Fig. 36. Col-0 main roots, resupplied on any day after germination on low-K, eventually showed increased growth rates after K resupply (Fig. 36A). Main roots of Ct-1, however, only recovered when resupplied 6 DAG or earlier (Fig. 36B). Hence, after this point, MR growth in Ct-1 not only slowed down but came to an irreversible halt. In Col-0, lateral root elongation was not rescued if growth had already stopped due to K starvation (see also Fig. 34). By contrast, lateral roots close to the tip of Ct-1 continued to grow in any condition.

Since cell-cycle marker lines were not readily available in a Ct-1 background, I performed propidium iodide (PI) staining on both genotypes to test for cytological changes under K starvation. Col-0 showed no obvious aberrations at the MR apex (Fig. 36C), but cell lesions were visible around the lateral root meristem (Fig. 36E), indicated by cells completely filled with PI. The opposite was observed for Ct-1: cell death was visible around the MR meristem (Fig. 36D) while lateral roots remained undamaged (Fig. 36F). It can be concluded that K starvation causes cell death in the apical meristem of Ct-1 main roots, eventually abolishing MR growth completely. Similarly, cell death within the lateral root meristem inhibits LR elongation of Col-0.

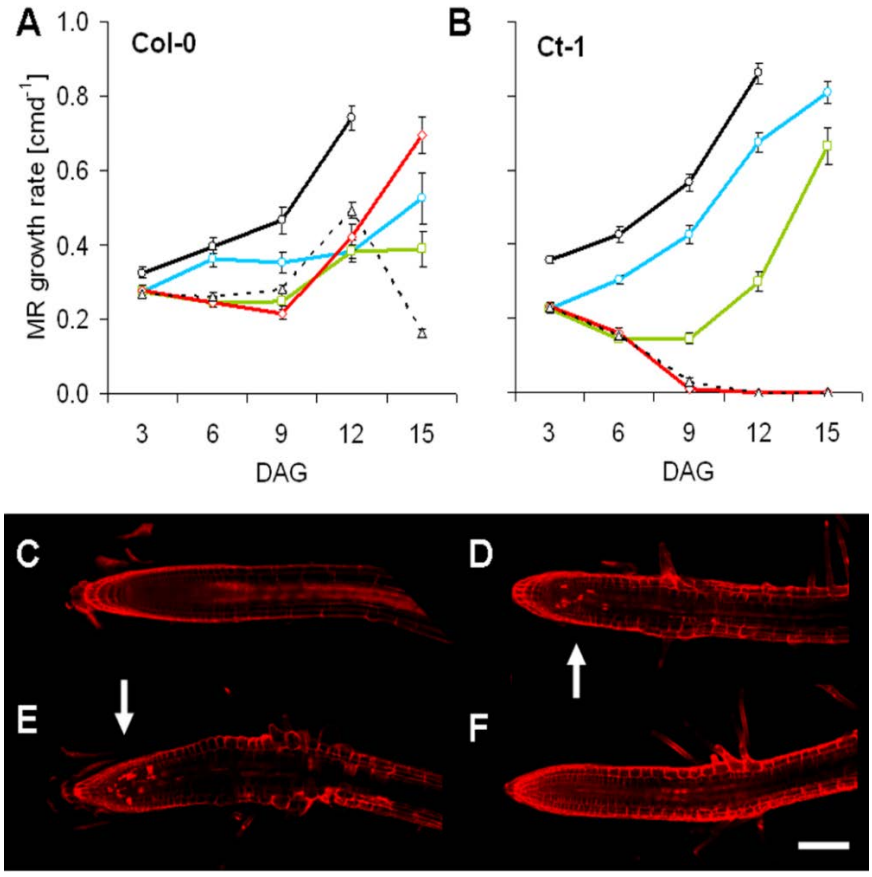

Figure 36: Irreversible main root growth arrest of Ct-1 in low-K is caused by cell death in the apical meristem.
A) Col-0 and **B)** Ct-1 seedlings (n = 8 – 15 per genotype per condition) were grown on control (black line, circles) and low-K (dashed, triangles) media or on low-K media resupplied with 2 mM KCl for 1 h at different time points: 3 days after germination (blue, circles), 6 DAG (green, squares) or 9 DAG (red, diamonds). Main root (MR) growth in Ct-1 could not be recovered when resupply occurred later than 6 DAG, whereas in Col-0 MRs continued to elongate in all conditions.
C to F) Seedlings starved for K were stained with propidium iodide (PI) solution 6 DAG and observed with a confocal microscope. Representative images are shown for main root apices of Col-0 (C) and Ct-1 (D) as well as lateral root tips (Col-0: E; Ct-1: F). Cell lesions are highlighted with white arrows. Size bar: 0.1 mm.

4.2.5 The low-K root architecture response of Col-0 is dominant over Ct-1

To get a better handle on the genetic structure of root architectural responses to low-K, I crossed Col-0 and Ct-1, both with Col-0 and Ct-1 as either male or female, and phenotyped (pooled) confirmed heterozygotes from the F1 generation (Fig. 37A for representative images). In control condition, F1 heterozygotes had Ct-1-like total root size (Fig. 37B), similar main root length as both parents but Col-0-like apical zone length. Heterozygous offspring had the largest total root size in low-K but the overall phenotype clearly resembled that of Col-0: a long main root (and apical zone) and short lateral roots. As the direction of crossing (male vs. female) did not make any difference, maternal effects can be ruled out. Interestingly, in both conditions all heterozygotes also had an elongated hypocotyl, which is typical for Ct-1. Thus Ct-1 is dominant for hypocotyl length, independent of K conditions, whereas Col-0 is dominant for root growth in low-K.

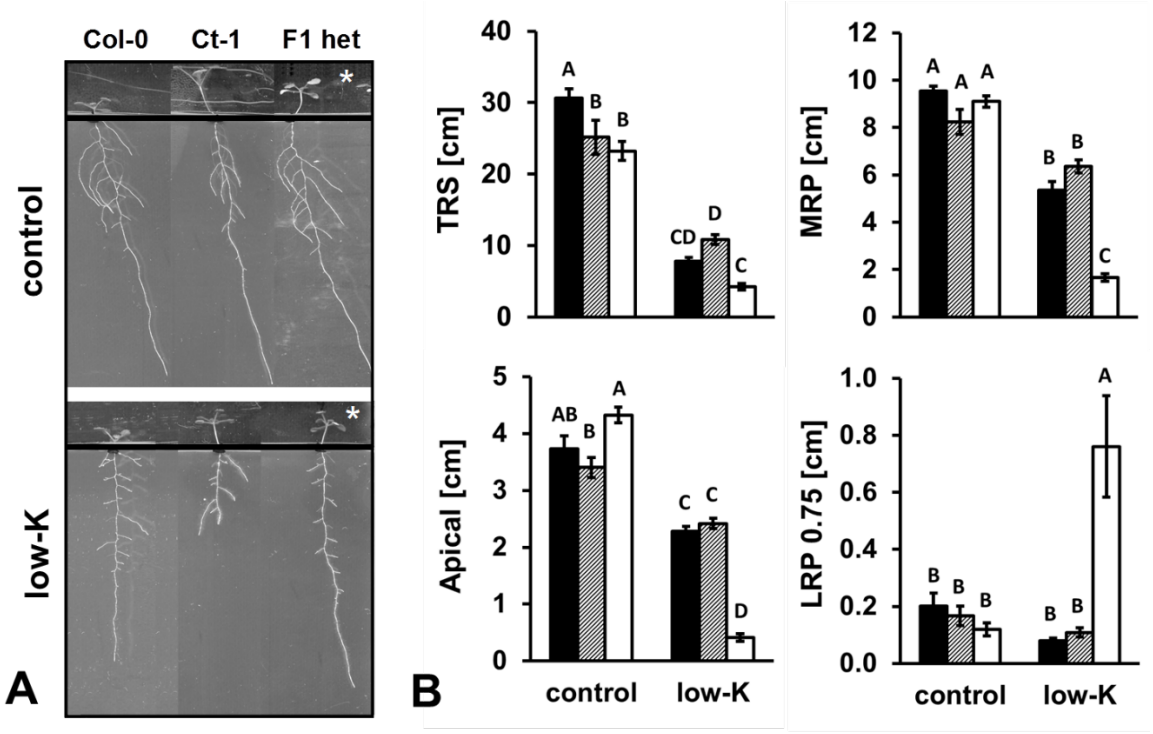

Figure 37: The K starvation response of Col-0 is dominant over Ct-1.
A) Representative images of Col-0, Ct-1 and heterozygous offspring of a Col-0 x Ct-1 cross (F1 het) grown on control or low-K (12 DAG). Note that F1 heterozygotes have elongated hypocotyls (asterisk), which is typical for Ct-1. **B)** Quantitative root parameters of F1 heterozygotes (dashed bars) confirm dominance of the Col-0 phenotype (black) over Ct-1 (white). Crosses were performed in both directions with each accession as either the male or female partner and data of both offspring was pooled for F1 heterozygotes. ANOVA was computed with all conditions and genotypes as input (n = 13 – 22 per

genotype per condition). Different letters indicate significant differences at $p < 0.05$ (Tukey's t-test)

4.2.6 QTL analysis of Col-0 x Ct-1 recombinant inbred lines (RILs) identified genetic loci for K-specific root architecture

A recombinant inbred line (RIL) population of Col-0 and Ct-1 was obtained from the Versailles stock centre (7 RV; Simon et al., 2008) as the basis for a quantitative genetics approach. A subset of 154 lines from the 7RV Core-Pop 164 were chosen and phenotyped in control and low-K conditions together with the two parental accessions (see Material and Methods section 2.5.1 for a description of the experimental setup). Raw data generated in this experiment can be found in the electronic appendix as *Ch4_QTL analysis of the low-K response*.

First, heritability of individual traits was calculated to estimate the fraction of variability within the dataset that can be explained by the genotype. This analysis was performed by Dr Fabien Chardon at INRA Versailles (France) where I performed all the remaining QTL data analysis myself as part of an academic visit under his supervision. Heritability of traits ranged from 0 to 0.85 in control and from 0.02 to 0.87 in low-K, depending on the trait in question (Fig. 38).

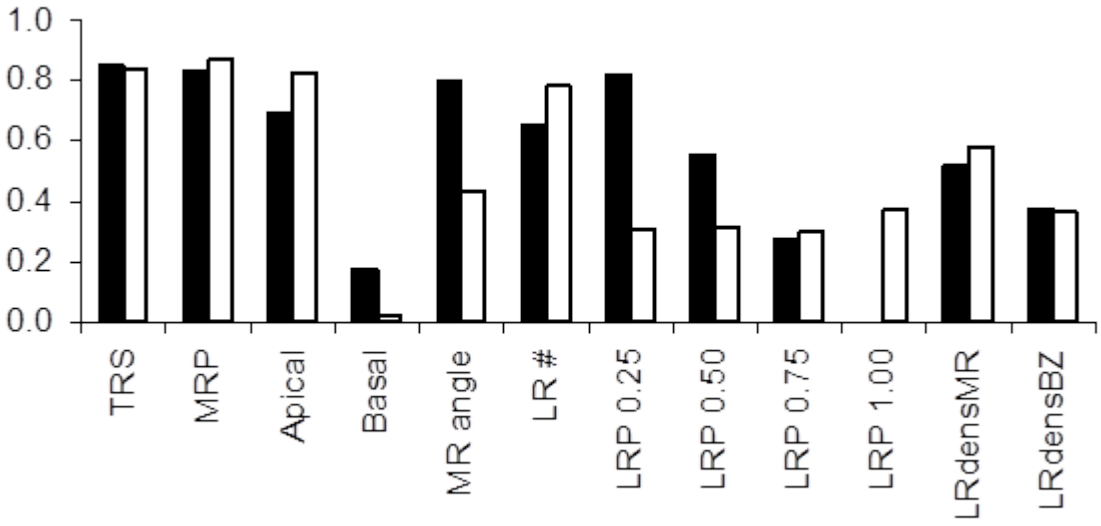

Figure 38: Heritability of traits quantified in the QTL analysis.
Heritability was calculated by Dr Fabien Chardon (INRA Versailles) from root parameter data of recombinant inbred lines (RILs) measured in control (black bars) and low-K (white bars).

Next, a look at the averages calculated for each RIL gave an idea on data spread. Fig. 39 shows RIL averages of selected root parameters, total root size (TRS), main root path length (MRP) and LRP 0.75, as the latter two previously well distinguished Col-0 from Ct-1. A more or less linear distribution of data across RILs can be observed for TRS and MRP in low-K. Although not directly visible in Fig. C4-10, due to sorting in ascending order of low-K, the distribution was equally linear in control. However, different patterns of control and low-K indicate significant variation in *responses* of the traits to low-K. LRP 0.75 displayed a distribution that was more similar to an exponential curve in low-K. For total root size and main root length, and also to some extent for LRP 0.75, a number of RILs showed higher or lower values as both parental accessions. This so called *transgression* of the trait indicates that segregating populations (like RILs) provide an even better estimate of the variation present between two genotypes (Alonso-Blanco and Koorneef, 2000). Transgression can be particularly useful when a similar phenotype is evoked by two different genetic mechanisms, e.g. the combinations of different alleles (Alonso-Blanco and Koorneef, 2000; Loudet et al., 2002). Although not absolutely necessary here, as both parental ecotypes are quite different in response to low-K, transgressive segregation may improve the quality of QTL mapping.

QTL mapping was performed with Windows QTL cartographer 2.5 software (Wang et al., 2011a). Logarithm of odds (LOD) scores were computed for each root parameter using the composite interval mapping function (CIM). 1000 permutations were used to determine the LOD threshold. LOD scores above the threshold (usually around 2.5 for each trait) indicated the existence of a genetic locus underlying a specific trait, i.e. a quantitative trait locus (QTL) For each QTL, the position of the LOD peak and the QTL interval (determined as ‘LOD minus one’ and ‘LOD minus 2’ drop) was recorded and the phenotypic variation explained by each locus was calculated. Full lists of QTL intervals detected in all conditions can be found in the electronic appendix under *Ch4_QTL positions*. Fig. 40 shows LOD score profiles of selected traits in different conditions.

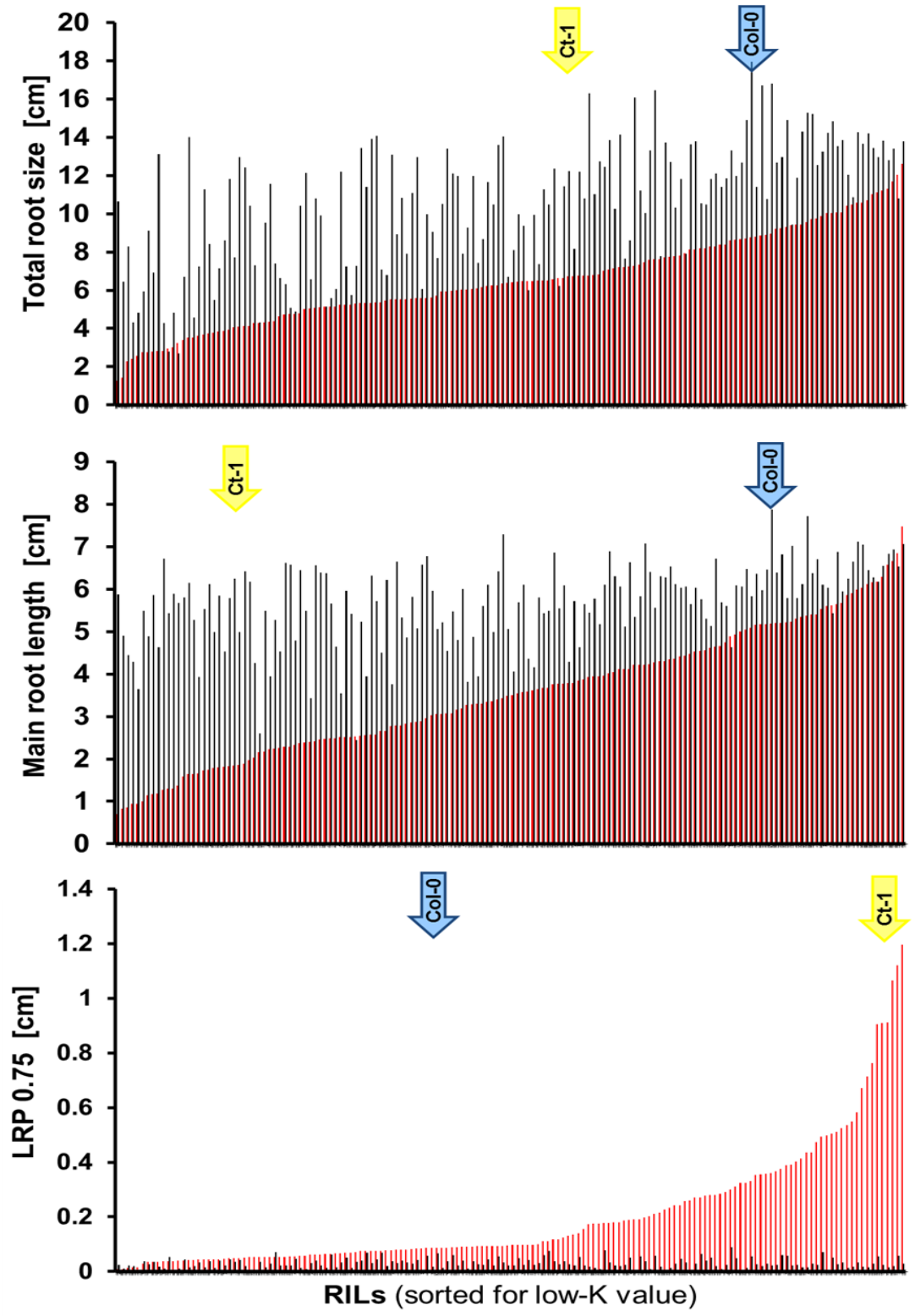

Figure 39: Distribution of root parameters of individual RILs indicates transgressive segregation of low-K traits.
Bars show mean root parameters of individual recombinant inbred lines (RILs) in control (black) and low-K (red). Each root parameter was sorted according to values in low-K (ascending). Hence, the position of each RIL is different in each plot. The low-K position of parental ecotypes Col-0 and Ct-1 is indicated by arrows. Since both ecotypes were not situated at the very extreme ends significant transgression of traits can be assumed.

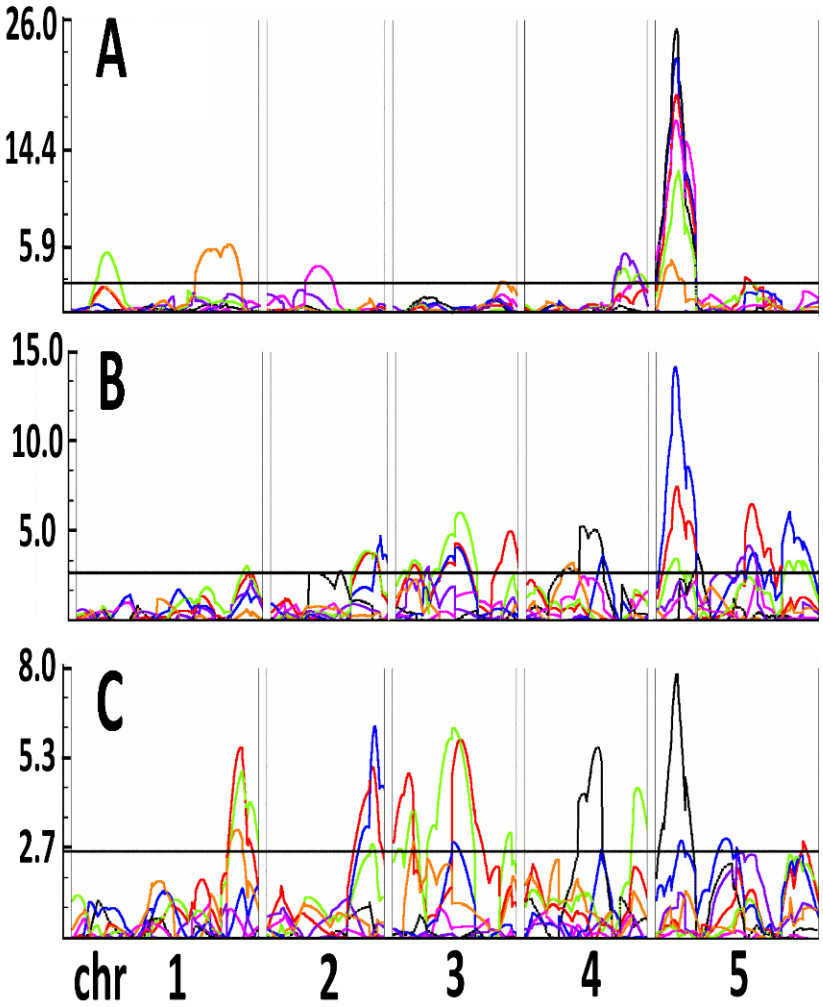

Figure 40: LOD score profiles determined via QTL mapping of the K deficiency response in a Col-0 x Ct-1 recombinant inbred line population.
LOD profiles of selected parameters: MRP (red), MR angle (pink), Apical (green), TRS (blue), LRdensBZ (purple), LRP 0.25 (black) and LRP 0.75 (orange) using root parameters quantified in **A)** control, **B)** low-K and **C)** the low-K/control ratio as input. The QTL threshold was determined with 1000 random permutations of the phenotypic dataset and is shown as a horizontal black line. Chromosomes one to five (chr 1– 5) are shown from left to right, separated by double lines. LOD score values are shown on the y-axis.

QTL analysis was carried on separated control (Fig. 40A) and low-K (Fig. 40B) datasets. To reduce redundant QTLs that were detected at similar position in both conditions, i.e. to emphasize *low-K response loci*, I also computed QTL analysis using the ratio of low-K/control for each individual RIL as input (Fig. 40C). Phenotypic variation explained by each locus is depicted by bars of different length at the respective chromosomal position in Fig. 41. For all genomic intervals with multiple QTLs (compare circles and sticks in Fig. 41), a code composed of chromosome number and an incremental identifier was assigned, for example *CHR5.1* (chromosome 5, locus 1) in this case. In some cases, two or more loci were detected within the same interval. This was usually the case when LOD profiles were steep and had shoulders near the absolute peak. In such occasions, stacked bars represent the percentage of variation explained by each of the multiple QTLs.

The *CHR5.1* multi-QTL, located on the short arm of of chromosome 5 (chr 5), was detected for all traits measured in control conditions (Fig. 40A) and largely dominated the percentage of phenotypic variation explained (Fig. 41). Additional control loci included four QTLs for apical zone length (*CHR1.1, CHR4.3, CHR5.1*) which partly co-localised with QTLs for main root angle, LRdensMR and LRdensBZ. Another MR angle QTL was located on chr 2 (*CHR2.1*). Lateral root length QTLs were located at *CHR1.2* (LRP 0.50 and 0.75) and *CHR3.3* (LRP 0.75).

CHR5.1 was also the locus with highest percentages of phenotypic variation explained in low-K (Fig. 41). Other QTLs were detected in genomic intervals not previously found in control condition. These are referred to as *low-K specific QTLs*. Low-K specific main root QTLs were located at *CHR1.3*, *CHR2.2*, *CHR3.1* and *CHR3.2*. Two MR QTLs in low-K, *CHR3.3* and *CHR5.3*, co-localised with QTLs of other traits in control. Moreover, a low-K specific lateral root path length QTL was located on chr 4 (*CHR4.2*).

Using low-K/control, for most traits no significant loci were found at *CHR5.1*, suggesting a putative role in general root development rather than stress response for this genomic region. Some other control and/or low-K QTLs ‘disappeared’ (like all QTLs at *CHR1.1*, *CHR1.2*, *CHR2.1* and *CHR5.2*) whilst other QTLs were now detected (e.g. MRP at *CHR1.2* and *CHR2.2*; LRP 0.75 at *CHR3.1*).

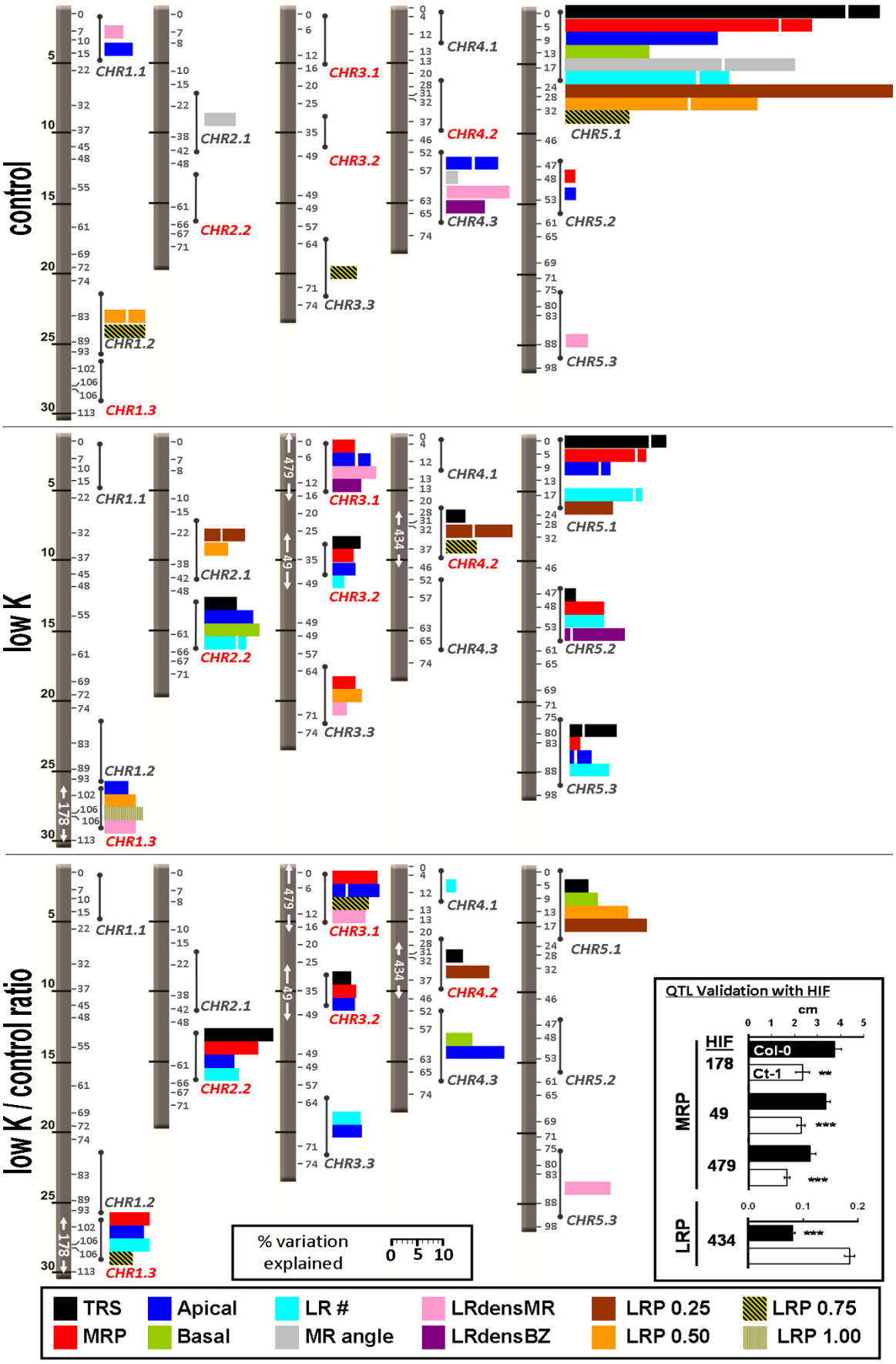

Figure 41: Positions and effects of root architecture QTLs for control and low-K conditions.

Please see overleaf for full figure legend.

Figure 41: Positions and effects of root architecture QTLs for control and low-K conditions. Results of multiple interval mapping analysis of 12 root parameters are shown for control (top panel) and low-K (middle panel) media and for the low-K/control ratio (bottom panel). The five Arabidopsis chromosomes are shown as gray bars with physical distances (Mb) on the left and genetic distances (centimorgan; cM) on the right. Coloured bars give the percentage of phenotypic variation explained by the QTLs within a certain chromosome region (indicated by circles and sticks). Each colour corresponds to a root parameter according to the legend provided at the bottom of the graph. Stacked bars of the same color (separated by white lines) show individual contributions from multiple QTLs within the region. Identifiers of low-K-specific regions (e.g. *CHR1.3*) are in red. White arrows inside the chromosomes highlight areas for which a QTL was confirmed by HIF analysis. The numbers identify the HIF for which significant (** $p < 0.01$, *** $p < 0.001$) phenotypic segregation was achieved, as shown in the box at the bottom right of the graph (Col-0 allele in black, Ct-1allele in white).

To validate the obtained loci, I developed heterogeneous inbred families (HIFs; Tuinstra et al., 1997) from RILs with residual heterozygosity within QTL intervals (see also Material and Methods section 2.5.3 and Tables 11 and 12). Three low-K specific main root path length loci were validated with HIFs 49, 178 and 479 and one low-K specific LR locus was validated with HIF 434 (Fig. 41 inset on bottom right). These HIFs can therefore be used for future fine-mapping. The low-K specific locus *CHR2.2* could not be confirmed by any HIF used.

I also observed phenotypic segregation at loci *CHR3.3* and *CHR5.3*. However, although MIM analysis identified both loci as low-K specific for most traits, phenotypic segregation of HIFs 116, 297 and 309 also persisted in control. All three RILs used to produce respective HIFs (116, 297, 309) were described as heterozygous at only one of the two loci in question (Simon et al., 2008). I genotyped all three HIFs at both loci and determined an unexpected genotypic co-segregation at both loci. It is possible that chromosomal re-arrangements could have occurred during generation of these RILs, since the corresponding genomic intervals on chromosomes 3 and chromosome 5 contain segmented duplicated genomic regions (AGI, 2000). However, genotyping via SSLP marker analysis could not resolve this question. Unfortunately, HIFs 116, 297 and 309 could therefore not be used as reliable lines for QTL validation and fine-mapping.

Due to co-localisation of QTLs for main root path length (MRP) and LRP 0.75 (at least in low-K/control), I chose locus *CHR3.1* for further fine-mapping with HIF 479.

4.2.7 Fine-mapping of the low-K specific locus CHR3.1

QTL mapping detected a low-K specific locus for main root elongation (MR length, apical zone length) in the telomeric region on the long arm of chromosome 3 (*CHR3.1*) with two peaks at approx. 5 cM (~ 1.5 Mb) and 10 cM (~ 3 Mb). Since both QTLs are very close to each other, it is possible that they in fact reflect a single locus. Residual heterozygosity of RIL 479 in the interval spanning 5 Mb from the top of chromosome 3 was exploited to generate more recombination events within that interval (for details see Material and Methods section 2.5.4). All lines were homozygous for the Col-0 allele at the next marker position (c3_06977). The resulting recombinant heterogeneous inbred family 479 (rHIF 479) was phenotyped again on low-K plates. Two rounds of rHIF generation and phenotyping were performed. In the first round, the majority of phenotyped lines were still partly heterozygous (Table 23). These lines were used to produce more, refined rHIFs which were subsequently phenotyped again (Table 24).

Table 23: Results of the first round of phenotyping rHIF479.
Main root (MR) growth rates on day 12 after germination (estimated as main root path length 12 DAG minus 10 DAG divided by 2) were determined for rHIFs and wildtypes grown on low-K media (n = 6 to 10 per genotype). Genotypes of rHIF479 are coded by their original position during selection, e.g. T1 – 6F: Tray 1, Column 6, Row F. Genotyping results are shown between markers c3-00422 and c3_04863. Empty cells denote that genotyping was omitted at this position, but colouring indicates the most likely genotype (based on genotyping before and after this position). ANOVA was computed and pairwise comparisons calculated (Bonferroni test; $p < 0.05$). Results are sorted according to mean MR growth rate. Groups are letter coded, i.e. MR growth rates were statistically different between a pair of genotypes when all letters are different. Het: heterozygous.

Genotype	c3_00422	c3_01500	c3_02099	c3_02563	c3_03045	c3_03463	c3_04075	c3_04863	mean MR growth rate (DAG12) [cm^{-1}]	Bonferroni grouping
T1 - 6F	Col-0	Col-0	Col-0	Col-0		Col-0	Col-0	Ct-1	0.39	A
Col-0	Col-0	Col-0	Col-0	Col-0		Col-0	Col-0	Col-0	0.38	**A**
T1 - 8G	Ct-1		Ct-1			Ct-1	Ct-1	Col-0	0.37	A
T2 - 3F	Ct-1		Ct-1			Ct-1	Col-0	Col-0	0.31	AB
T2 - 8A	Col-0		Col-0	Col-0	Col-0	Het		Het	0.30	ABC
T1 - 3G	Col-0		Col-0	Col-0	Het	Het	Het	Ct-1	0.29	ABC
T1 - 9H	Col-0		Col-0	Het	Het	Het		Het	0.28	ABCD
T1 - 11F	Col-0		Col-0			Col-0	Col-0	Ct-1	0.27	ABCD
T2 - 8B	Ct-1	Ct-1	Het			Het		Het	0.26	ABCD
T1 - 6H	Ct-1	Ct-1	Ct-1	?	Het	Het		Het	0.22	BCD
T2 - 7B	Ct-1		Ct-1	Ct-1	Ct-1	Het	Col-0	Col-0	0.21	BCD
T2 - 1G	Ct-1		Ct-1			Ct-1	Col-0	Col-0	0.21	BCD
T1 - 7F	Het	Het	Het	Het	Ct-1	Ct-1		Ct-1	0.17	CDE
T2 - 3H	Het	Ct-1	Ct-1	Ct-1			Ct-1	Ct-1	0.14	DE
T1 - 8F	Ct-1		Ct-1			Ct-1	Ct-1	Col-0	0.14	DE
Ct-1	Ct-1		Ct-1			Ct-1	Ct-1	Ct-1	0.06	**E**

Table 24: Results of the second round of phenotyping rHIF479.
Main root (MR) growth rates on day 18 after germination (estimated as main root path length 18 DAG minus 12 DAG divided by 6) were determined for rHIFs and wildtypes grown on low-K media (n = 6 to 14 per genotype). Genotyping results are shown between markers c3-00422 and c3_04863. Question marks denote uncertain genotyping results. ANOVA was computed and pairwise comparisons calculated (Bonferroni test; $p < 0.05$). Groups are letter coded, i.e. main root growth rates were statistically different between a pair of genotypes when all letters are different. A putative target interval is framed in red. The red arrow and dashed red line denotes a point of recombination (break between Col-0 and Ct-1 alleles) that needs to be genotyped at higher resolution by increasing the marker density.

Genotype	c3_00422	c3_01500	c3_02099	c3_02563	c3_03045	c3_03463	c3_04075	c3_04863	mean MR growth rate (DAG18) [cm^{-1}]	Bonferroni Grouping
T08-13	Col-0	Col-0	Col-0	Col-0	Ct-1	Ct-1	Ct-1	Ct-1	0.54	A
T09-15	Ct-1	?	Col-0	Col-0	Col-0	Col-0	Col-0	Ct-1	0.51	A
T07-03	Ct-1	Col-0	Col-0	Col-0	Col-0	Col-0	Col-0	Col-0	0.46	AB
T08-01	Col-0	Col-0	Col-0	Col-0	Col-0	Ct-1	Ct-1	Ct-1	0.45	AB
T15-11	Col-0	Ct-1	Ct-1	Ct-1	Ct-1	Ct-1	Ct-1	Ct-1	0.45	AB
Col-0	Col-0	Col-0	Col-0	Col-0	Col-0	Col-0	Col-0	Col-0	0.41	**ABC**
T07-07	Ct-1	Col-0	Col-0	Col-0	Col-0	Col-0	Col-0	Col-0	0.41	ABC
T07-09	Col-0	Ct-1	Ct-1	Ct-1	Ct-1	Ct-1	Ct-1	Ct-1	0.40	ABC
T10-02	Col-0	Col-0	Col-0	Col-0	Ct-1	Ct-1	Ct-1	Ct-1	0.40	ABC
T11-05	Col-0	Col-0	Col-0	Ct-1	Ct-1	Ct-1	Ct-1	Ct-1	0.39	ABC
T11-07	Col-0	Col-0	Col-0	Ct-1	Ct-1	Ct-1	Ct-1	Ct-1	0.38	ABC
T11-09	Col-0	Col-0	Col-0	Col-0	Col-0	Ct-1	Ct-1	Ct-1	0.27	BCD
T15-05	Col-0	Col-0	Col-0	Col-0	Col-0	Ct-1	Ct-1	Ct-1	0.19	CDE
T13-04	Ct-1	Col-0	Col-0	Col-0	Col-0	Col-0	Col-0	Col-0	0.15	DE
T13-10	Ct-1	Ct-1	Ct-1	Col-0	Col-0	Col-0	?	?	0.12	DE
Ct-1	Ct-1	Ct-1	Ct-1	Ct-1	Ct-1	Ct-1	Ct-1	Ct-1	0.05	**E**
T12-03	Ct-1	Ct-1	Ct-1	Ct-1	Ct-1	Col-0	Col-0	Col-0	0.02	E
T12-05	Ct-1	Ct-1	Ct-1	Ct-1	Ct-1	Col-0	Col-0	Col-0	0.00	E

After both rounds, a clear pattern separating ‘Col-0 like’ from ‘Ct-1 like’ genotypes was not achieved. In the first round, most genotypes with a high number of Col-0 alleles grouped with Col-0 and genotypes that were predominantly ‘Ct-1’ grouped with Ct-1 respectively (Table 23). However, lines T1 – 8G and T2 – 3F did not fall within this pattern.

In general, phenotyping was a very laborious task and during that period I experienced a lot of problems with the growth cabinet. Moreover, the main root phenotype of rHIF479 appeared to be rather sensitive to light conditions, making it impossible to carry out my experiments in a different growth chamber with a long day photoperiod. Consequently, I had to discard whole runs of phenotyping so that only two full sets remained to be shown here.

To improve the resolution of the MR elongation phenotype, I continued to measure MR length and MR growth rates until 18 DAG in later runs. Although still no clear

separation was observed with the second rHIF479 set (Table 24), a pattern emerged at the very top of the chromosome (markers c3_00422 and c3_01500). All lines with two Col-0 alleles at these positions grouped with Col-0 and vice versa all rHIFs with two Ct-1 alleles grouped with the Ct-1 wildtype. In addition, some lines had two different alleles at both positions. No pattern between MR growth rates and genotypes at markers c3_02563 to c3_04863 was observed. Hence, the interval from 0.4 Mb (marker c3_00422) to 1.5 Mb (c3_01500) is a putative target interval. A possible explanation for the fact that some lines had both alleles might be different recombination points that lie somewhere within that interval (highlighted with red dashed line and an arrow in Table 24). Unfortunately, my time in the lab had ended before I could carry out further genotyping within that interval. Nevertheless, by the time of submission, three additional SSLP genotyping primers had been ordered. Although I do not have solid proof that the polymorphism separating 'Col-0 like' from 'Ct-1 like' rHIF479 lies within that smaller interval, I will try to make some *informed guesses* of potential target genes in the discussion of this chapter.

4.3 Discussion

4.3.1 Natural variation of Arabidopsis root architecture reveals complementing response strategies to potassium starvation

In the study presented in this chapter, I investigated the response of Arabidopsis root architecture to changes in external K supply using a set of 26 geographically diverse natural accessions (Fig. 30). 14 root traits of seedlings grown on control and low-K media were quantified and significant contributions of genotype, environment and genotype-environment interactions to the total variation within each root parameter were detected (Fig. 32). Analysis of individual accessions (Fig. 33, 34), correlation analysis (Tables 21, 22) and cluster analysis based on phenotypic data (Fig. 35) revealed a gradient of sensitivity towards low-K. This gradient links two opposite low-K response strategies at either end of the spectrum. *Low-K response strategy I* consists of the maintenance of main root (MR) growth accompanied by a dramatic reduction of lateral root (LR) elongation (Fig. 33, 34, 35, 36E). This response has been reported previously for Col-0, the most widely used laboratory wild type accession (Armengaud et al., 2004; Shin and Schachtman, 2004). In contrast, *strategy II* accessions respond to low-K with a drastic reduction of MR growth. In fact, MR growth is completely eliminated under prolonged K deficiency (Fig. 36B) as a consequence of cell death around the apical meristem (Fig. 36D). At the same time, LR elongation is maintained, so that the MR tip is eventually outgrown by LRs originating close to the root tip (see also Fig. 37: Ct-1). In more mature plants, I also observed 2nd order lateral roots that outgrew the 1st order root from which they originated (data not shown), suggesting a preference for sequential lateral branching in strategy II accessions. I therefore conclude that both strategies allow plants to maintain elongation of certain root parts whilst saving precious resources, and as a result no differences in shoot growth were obvious in low-K.

4.3.2 Possible signalling mechanisms underlying low-K responses – potential crosstalk with low-P?

In K-starved plants, reactive oxygen species (ROS) are formed in an area close to the main root tip (Shin and Schachtman, 2004; Kim et al., 2010). However, the peak of ROS production was detected in the elongation zone rather than the meristem (Shin and

Schachtman, 2004), making ROS toxicity not a prime suspect for MR cessation observed in strategy II accessions. Nevertheless, phosphate starvation has been shown to elicit a root phenotype similar to the strategy II low-K response: short main roots and enhanced proliferation of lateral roots (Williamson et al., 2001; Lopez-Bucio et al., 2002; Perez-Torres et al., 2008; see also Chapter 3 section 3.3.3). Moreover, ROS production is also induced at the root apex in low-P (Tyburski et al., 2009). This suggests that root architecture responses elicited by low-K and low-P might share a common regulatory pathway. The root architecture response of low-P has been shown to depend largely on external iron (Fe) concentrations (Svistoonoff et al., 2007; Ward et al., 2008; Ticconi et al., 2009). The question whether K responses are equally influenced by Fe supply will be the topic of Chapter 5.

4.3.3 Natural variation of Arabidopsis in various environmental settings – comparison of low-K with other nutrient responses

The set of natural accessions used in this study was largely based on a nested core collection widely used in the field (McKhann et al., 2004). The genotypes Ct-1, Stw-0 and Mt-0 have also been shown to cluster in response to nitrogen availability (Chardon et al., 2010; Ikram et al., 2012). In fact, Mt-0 and Ct-1 have been described as 'ideotypes' for seed production in suboptimal N conditions, whereas Stw-0 and Bl-1 were among accessions with highest dry matter production in N deficiency (Chardon et al., 2012). In addition, Ge-0 clustered with the aforementioned genotypes due to low nitrate uptake efficiency and nitrogen content in contrasting environments (Chardon et al., 2010). Yet, strategy II accessions do not display a high degree of genetic similarity (Ostrowski et al., 2006; Simon et al., 2012), suggesting a central role for only a few polymorphisms in the low-K response. Moreover, Mt-0, Bl-1, Ct-1, Ge-0 and N13 were also included in a study on natural variation of drought responses (Bouchabke et al., 2008) but no clear clustering of these accessions was observed there. Thus, their phenotype in low-K is probably not the result of similarity in unspecific stress responses.

As far as K transport is concerned, Mt-0, the only strategy II member in a study by Buescher et al. (2010), had the highest shoot K concentration among 12 accessions. Interestingly, although no cluster analysis was provided, all low-K strategy II ecotypes also appear among less Zn-tolerant ecotypes (Richard et al., 2011). Supplement of surplus Zn also elicited changes in root architecture, namely a decrease in MRP at higher Zn levels and a slight increase of LRP in the lower range of concentrations. Due to K’s central role

in osmotic and ionic balance, changes in homeostasis of other metals might occur in low-K and trigger important downstream events in the root architectural response. Iron (Fe) presents itself as prime candidate, as it fulfils an essential role in physiological and metabolic processes – with a twist: Fe overload is highly toxic to most plants (Palmer and Guerinot, 2009). This was yet another reason to further investigate the influence of iron on the low-K response (see Chapter 5).

It would be interesting to investigate the soil conditions occurring at the origin of strategy I and strategy II accessions, as Poormohammad Kiani et al. (2012) have recently demonstrated a correlation between the natural distribution of a specific allele of the molybdenum transporter gene MOT1 and the Mo availability in the native range of natural accessions used. Unfortunately, data on the exact location of sampling sites is sparsely available, making it very difficult to draw such conclusions from the accession set used here. I was not able to pinpoint the exact geographic origin of Ct-1, as its sampling site coordinates were only estimated (Simon et al., 2012). The origin described is Catania, Sicily, which encompasses quite different ecosystems and soils, such as the Mediterranean seashore, alluvial floodplains (Capaccioni et al., 2005) and the volcanic slopes of Mount Etna. To generate meaningful hypotheses on the ecological driving forces behind root architecture responses to low-K (e.g. K content in native soil, other minerals on site, etc.) it would be necessary to re-sample those sites and compare the root response of populations from various ecological backgrounds.

My study also included the accessions Bay-0 and Sha, which have been extensively used in natural variation and QTL studies on e.g. flowering time (Loudet et al., 2002) root architecture (Loudet et al., 2005), partial resistance to *P. syringae* (Perchepied et al., 2006), phosphate starvation (Reymond et al., 2006; Svistoonoff et al., 2007), sulfate content (Loudet et al., 2007), shoot mineral content (Buescher et al., 2010) and growth on acidic soil (Poormohammad Kiani et al., 2012). As they cluster very closely in low-K (Fig. 35), however, it appears that responses to K availability are very similar between these two genotypes.

4.3.4 QTL analysis of root architecture in control and low-K conditions identifies regulatory hot-spots

As representatives for each low-K response strategy, I chose a Col-0 x Ct-1 RIL population for QTL analysis. Although the overall Ct-1 phenotype in low-K is recessive (Fig. 36), its genetic basis appears to be multigenic (Fig. 40, 41). To date, there is only one

published record of QTL studies performed on the Col-0 x Ct-1 RIL set with flowering time, rosette diameter and total seed weight as traits of interest (Simon et al., 2008). All seven loci mapped in this study overlap with mine. Six of them were loci identified in control condition here, plus the *CHR2.2* locus (low-K specific here but not confirmed via HIF). Since the authors of this study mapped a considerably different set of traits to similar loci, most notably *CHR5.1* and *CHR5.3*, the underlying polymorphisms might lie in the same genomic region but may actually be fundamentally different loci. Only fine-mapping can resolve this issue. An alternative explanation might be that indeed the responsible polymorphisms are the same and that the corresponding genes are key regulators of plant development rather than stress responses. However, none of the other four low-K specific loci (*CHR1.3*, *CHR3.1*, *CHR3.2*, *CHR4.2*) were detected in Simon et al. (2008).

Two loci, one on the long arm of chromosome 3 (roughly corresponding to *CHR3.2*) and one on the long arm of chr 4 *(~ CHR4.2*), affected total root size in Col-0 x Ler (Fitz Gerald et al., 2006). Within the same two regions, Reymond et al. (2006) mapped QTLs of root growth responses to phosphate deficiency in a Bay-0 x Sha RIL population. To date, only the gene corresponding to the third locus identified in this study has been mapped as *LPR1* (Svistoonoff et al., 2007). This raises the question whether putative regulatory genes that underlie root architecture responses to various stresses (e.g. low-P and low-K) are still to be discovered within those intervals. Likewise using Bay-0 x Sha RILs, lateral root QTLs were mapped on the long arm of chromosome 1, long arm of chromosome 3 and the long arm of chromosome 4 (Loudet et al., 2005), potentially equalling *CHR1.2*, *CHR3.1* and *CHR4.2*. A recent study, using 18 accessions to produce 17 F2 populations, confirmed once more the importance of flowering loci for plant growth and development (Salome et al., 2011). Indeed, three of the control QTLs might correspond to major flowering loci such as *FT* (*CHR1.2*), *FLC* (*CHR5.1*) and *MAF2* (*CHR5.3*). Another flowering locus, *FLM*, is in the low-K specific *CHR1.3* interval. However, although many QTL efforts have resulted in mapping flowering loci (Salome et al., 2011; Strange et al., 2011), one should not automatically assume that the corresponding flowering genes are crucial in this context.

In Arabidopsis, QTLs have been mapped for K accumulation in seeds (Vreugdenhil et al., 2004) and shoots (Harada and Leigh, 2006), using Cvi x Ler RILs in both occasions. One seed QTL overlaps with *CHR2.2*, two with *CHR3.1* and one with *CHR5.1* respectively (Vreugdenhil et al., 2004). The most important QTL for shoot K per dry matter also coincides with *CHR3.1* (Harada and Leigh, 2006), and the remaining two correspond to *CHR4.1* and *CHR5.3*. Moreover, loci for shoot K per fresh weight co-localise with

CHR2.1, *CHR4.1*, *CHR5.2* and *CHR5.3*. Harada and Leigh (2006) provided a list of candidate cation transporter genes within their intervals, including important K transporters such as AKT1 (*CHR2.1*), SKOR (*CHR3.1*), HAK5 (*CHR4.1*) and several members of the TPK family (*CHR5.2* and *CHR5.3*). Nevertheless, there is no written record of fine-mapping that exactly located the underlying polymorphisms. Maybe of interest in this context is a result by Rauh et al. (2002) who in a comparative study on the effect of four different nitrogen fertilizer regimes (supplementing $(NH4)_2SO_4$, NH_4NO_3, KNO_3 or no N) identified a single 'root length' QTL at *CHR3.1* only in the $(NH_4)_2SO_4$ treatment, as NH_4^+ interferes with K nutrition.

Recently, ionomics have become a standard tool in the study of natural variation and stress responses, providing researchers with data for multiple elements at a time (Salt et al., 2008; Buescher et al., 2010; Prinzenberg et al., 2010). Buescher et al. (2010) not only compared natural accessions but also mapped shoot mineral contents for several RIL populations in various environments. In a large Bay-0 x Sha population, they mapped loci for K content to regions corresponding to *CHR1.2*, *CHR1.3*, *CHR2.2* and *CHR5.3*. A K locus equivalent to *CHR3.1* was also found in a smaller population of Bay-0 x Sha and in Cvi x Ler. For all these loci, significant QTL for several ions at a time were detected, suggesting the existence of homeostatic 'hubs'. These findings are backed up by Prinzenberg et al. (2010), who measured shoot and root growth traits combined with element profiles in a Ler x Kas-2 RIL population in three conditions quite similar to mine: control (2.15 mM K, 0.15 mM P), low-K (0.15 mM K) and low-P (0.032 mM P). They identified amongst others multi-elemental loci at *CHR1.3* (K, Fe, Mg), *CHR3.1* (K, P, Mg, Co, Mn, Zn), *CHR3.2* (K, P, Zn) and *CHR5.3* (multiple elements). I also compared publicly available ionomic data of Col-0 and Ct-1 from the PiiMS database (Baxter et al., 2007). The accessions show differences in Mn and Co content but all other ions, including K, are present at similar levels. However, these data are derived from shoots of plants grown in (K-sufficient) soil and are therefore mirrored by similar root architectures of Col-0 and Ct-1 in control conditions in my experiments. To date no ionomic data are available for Col-0 and Ct-1 in K-deficient conditions. Further assessment of metal homeostasis in low-K (and low-P) root responses will be the topic of Chapter 5.

4.3.5 Some long shots: candidate genes in interval CHR3.1

Finemapping of locus *CHR3.1* did not give a clear pattern of Col-0 and Ct-1 allele distribution that overlapped with main root elongation phenotypes of rHIF479 (Tables 23

and 24). However, phenotyping the second set of rHIFs gave hints towards a smaller interval located between markers c3_00422 and c3_01500 and hence between 0.4 Mb and 1.5 Mb from the top of chromosome 3. Although more evidence is needed to back up the exact location of that finer interval, only putative target genes within that interval will be discussed in the following.

In a study on responses to K stress, genes regulating K transport are a first obvious target. Two K transporter genes could be localised within the interval: *KUP3* (AT3G02050) and *SKOR* (AT3G02850). *KUP3* belongs to the HAK/KUP/KT family of K transporters and is transcriptionally induced upon K deficiency (Wang and Wu, 2013). The gene encoding the outward rectifier SKOR has been proposed as a candidate gene in two QTL analyses investigating K content in seeds (Vreugdenhil et al., 2004) and shoots (Harada and Leigh, 2006). The authors of both studies propose *SKOR* as candidate as it is involved in K translocation from root to shoot (Gaymard et al., 1998). Yet, the Ct-1 root architecture phenotype in low-K is probably caused by cell death in the root apical meristem (RAM). A direct effect of a xylem loading K transporter on RAM maintenance seems rather unlikely.

In contrast, *WOX11* (AT3G03660), *DEL3* (AT3G01330), *RPK2* (AT3G02130), *GLV4* (AT3G02240) and *GLV8* (AT3G02242) have been shown to be important for root growth. *WOX11* is a WUSCHEL-related homeobox gene that is essential for crown-root formation in rice (Zhao et al., 2009). *DEL3* belongs to the E2F family and controls cell expansion in roots and hypocotyls (Ramirez-Parra et al., 2004). The authors have shown that *DEL3* overexpression results in severely reduced root length. GLV4 and GLV8 are CLE-Like small signalling peptides that function as growth factors in the root (Fernandez et al., 2013). Both genes are probably not involved in meristem function as they were recently demonstrated to be expressed mainly in the elongation and differentiation zone of the root (Fernandez et al., 2013). The receptor-like kinase *RPK2*, by contrast, is important for root meristem function via the CLAVATA3 pathway (Kinoshita et al., 2010).

Root meristem maintenance and cell cycle progression depends on a correct redox status (Jiang and Feldman, 2005). No less than five genes for NAD(P)-dependent oxidoreductases (AT3G01980, AT3G03330, AT3G03980, AT3G04000, AT3G05260), as well as one gene for a ubiquinone-NADH dehydrogenase (AT3G03100) and a peroxidase (AT3G01190) are located in the potential interval. Creation of an oxidising environment in the RAM has also been connected to auxin signalling (Jiang and Feldman, 2005). Auxin is always worth consideration when root and shoot growth are concerned. Four auxin responsive *SAUR* genes (AT3G03820, AT3G03830, AT3G03847, AT3G03850) and the

auxin responsive *IAA16* (AT3G04730) lie within the putative interval. Gain of function mutants of *IAA16* have longer main roots and are insensitive to exogenous auxin and abscisic acid (ABA) treatment (Rinaldi et al., 2012). Another auxin target gene is *BIG*, which promotes polar auxin transport (Gil et al., 2001) and is needed for pericycle cell activation that promotes lateral root emergence under phosphate starvation (Lopez-Bucio et al., 2005).

Gibberellin (GA) is an important hormone for cell elongation but to some extent also for cell proliferation (Ubeda-Tomas et al., 2009). Three GA related genes are located in the target interval: *GASA5* (AT3G02885), *RGL2* (AT3G03450) and *GID1A* (AT3G05120). The gibberellin receptor GID1A inactivates negative growth regulators of the DELLA family by direct interaction upon GA binding (Murase et al., 2008) and *RGL2* encodes such a DELLA protein. Nevertheless, RGL2 mainly functions in seed germination (Lee et al., 2002).

In sum, there are many potential target genes within the putatively narrowed QTL interval. And of course it cannot be ruled out that actually a so far unknown gene, or a gene with an at first sight unrelated function, may underlie the main root response QTL *CHR3.1*. Finemapping at higher resolution is needed to get closer to the polymorphism and make better ‘informed guesses’ on the targets. I used Col-0 and Ct-1 wildtypes in other experiments that further investigated the physiological basis of low-K strategy I and II responses.

5. Root responses to P and K deficiency are controlled by external Fe supply

5.1 Introduction

Phosphorus (P) and potassium (K) are two of the main nutrients needed for growth, metabolism and a variety of physiological processes (Amtmann et al., 2006). Together with nitrogen in its various forms, they represent the bulk of mineral uptake (Marschner, 1995) and are therefore widely applied in agriculture as NPK fertilizer mixes (Amtmann et al., 2006).

In Chapter 3, I have identified significant P*K interactions that influence growth of various Arabidopsis root organs, e.g. main root and apical zone length. Moreover, my study on root architecture responses to low-K presented in Chapter 4, demonstrated the existence of at least two different root architectural response strategies to overcome K limitation (see also Kellermeier et al., 2013). Interestingly, the *strategy II* accession Catania-1 (Ct-1) cedes main root growth in favour of expansion of the lateral root system. This phenotype bears high resemblance to the low-P phenotype described in the literature for agar-grown 'wild type' Arabidopsis (usually Col-0) seedlings (Williamson et al., 2001; Lopez-Bucio et al., 2002; Nacry et al., 2005; Perez-Torres et al., 2008; compare also Chapter 3 section 3.3.3). However, this characteristic low-P phenotype has been shown to be highly dependent on the concentration of iron (Fe) in the external medium (Ward et al., 2008). Inorganic phosphate has high affinity for heavy metals, particularly iron (Fe), which results in the formation of Fe-P precipitates in soils and even in commonly used growth media (Dalton et al., 1983; Hirsch et al., 2006; Ward et al., 2008). This is one of the reasons why P concentrations in soil solution are almost three orders of magnitude lower than K concentrations (approx. 0.1 to 1 mM bioavailable K; Maathuis, 2009; only 0.1 to 10 µM inorganic free phosphate; Vance, 2003; Amtmann et al., 2006). P and Fe homeostasis are also linked *in planta* as both elements co-exist in their storage forms ferritin (Fe containing proteins with a Fe-P core [Fe : P ~ 3 : 1]; Briat et al., 2010) and phytate (Fe bound to myo-inositol-hexakis-phosphate clusters; Stevenson-Paulik et al., 2005). To increase the solubility of P, plants release protons, organic acids and extracellular phosphatases into the soil (Vance, 2003), which as a side effect, also enhances Fe availability. Elemental profiling presented in Chapter 3 indeed showed an increase of shoot Fe concentrations in low-P. Surprisingly, shoot Fe was further increased in P-K double

deficiency. While interactive effects of P and Fe can be explained with the chemical interactions listed above, a potential link between K and Fe effects is less obvious and has not been reported in the literature. Nevertheless the RSA and the ionomics results obtained for low K suggested a possible role for altered root Fe homeostasis in root architectural responses not only in low-P but also in low-K.

In this chapter, I have investigated K-P-Fe interactions by two strands of experimental work. First, I have investigated root architecture of Arabidopsis seedlings grown on media containing various combinations of P, K and Fe. Second, I have applied several techniques to visualise the spatial pattern of Fe distribution in the roots of plants grown in control, low-K and low-P conditions. Two histochemical staining techniques (Perls' and Turnbull's stain; see Material and Methods sections 2.7.2 and 2.7.3) were chosen to visualise Fe localisation in fixed root tissue. In addition, synchrotron X-Ray fluorescence (Punshon et al., 2009; Donner et al., 2012; see Material and Methods section 2.8.3) was performed on hydrated root tissue.

5.2 Results

5.2.1 Main root elongation of P- and K-deficient seedlings depends on external iron supply

To investigate the effect of K, P and Fe supply on root architecture, seedlings of the Arabidopsis accessions Col-0 and Ct-1 were grown on vertical agar plates supplemented with sufficient or deficient concentrations of nutrients. Media were based on the standard growth medium (Material and Methods section 2.2.1). In low-K media ([K] = 10 µM; as in Chapter 4), KNO_3 was replaced with $NaNO_3$. For low-P ([P] = 20 µM) media, NaH_2PO_4 was reduced and original Na concentrations restored by adding NaCl. For low-PK double deficiency both KNO_3 and NaH_2PO_4 were replaced with $NaNO_3$ and NaCl respectively. Two concentrations of NaFeEDTA were supplemented: standard Fe (+Fe): 42.5 µM NaFeEDTA; low-Fe (-Fe): 4.25 µM NaFeEDTA. Root parameters were quantified with EZ Rhizo as before (see Table 5 for description of traits).

For Col-0 in standard Fe (42.5 µM), total root size (TRS) was reduced by low-K and low-P alone, but a more severe reduction was observed in P-K double deficiency (low-PK) suggesting an additive effect of low-K and low-P (Fig. 42A for representative images; Fig. 42C for quantitative data). The analysis confirmed previously shown RSA phenotypes for low-K and low-P. Thus low-K caused a reduction of lateral root path length (LRP), particularly mean LRP in the second (LRP 0.50) and third (LRP 0.75) quartile of the main root (compare *strategy I* [Col-0] phenotype in Chapter 4) while low-P decreased main root elongation, particularly in the apical zone. In low-PK double deficiency, an extremely stunted root system comprised of a short main root (much alike Ct-1 in low-K) and very few, short lateral roots was observed. When external iron was lowered to a tenth of the original concentration (-Fe: 4.25 µM), total root size was unchanged in control but it increased slightly in low-K and strongly in low-PK, reaching almost the size of root systems grown in control. Low-Fe partly restored lateral root elongation in low-K and fully restored main root growth in low-P. In fact, Fe supply determined the balance between main and lateral root growth in both control and low-P condition. Total root growth and lateral root number remained unchanged, but low-Fe favoured main root elongation over lateral root elongation.

A similar shift of main and lateral root elongation caused by low-Fe was detected for Ct-1 in control condition (Fig. 42B, C). However, low-Fe also restored main root elongation in low-K (Fig. 42C, compare apical zone length). At the same time lateral root length decreased to Col-0 like values indicating that growth arrest of the main root is the prerequisite for the expansion of the lateral root system in low-K *strategy II* accessions like Ct-1. Low-PK (in control iron) elicited a similarly atrophied architecture in Col-0 and Ct-1. Yet, the detrimental interactive effect of double low-PK on main root elongation could be overcome by lowering external Fe in both ecotypes. By contrast, lateral root elongation was not rescued by low-Fe.

In sum, Fe availability in the medium has a strong influence on root architecture, shifting the balance between main root elongation (favoured at lower Fe concentration) and lateral root elongation (favoured at higher Fe concentrations). At higher Fe concentrations main root growth is inhibited by low-P (particularly in Col-0) and low-K (particularly in Ct-1), and this inhibition appears to trigger the expansion of the lateral root system. In both cases, lowering external Fe concentrations rescues main root growth and as a consequence reduces lateral root elongation. However, in Col-0, where low K inhibits lateral root growth, low-Fe at least partly restores lateral root growth (cf. LRP 0.50 in Fig. 42C).

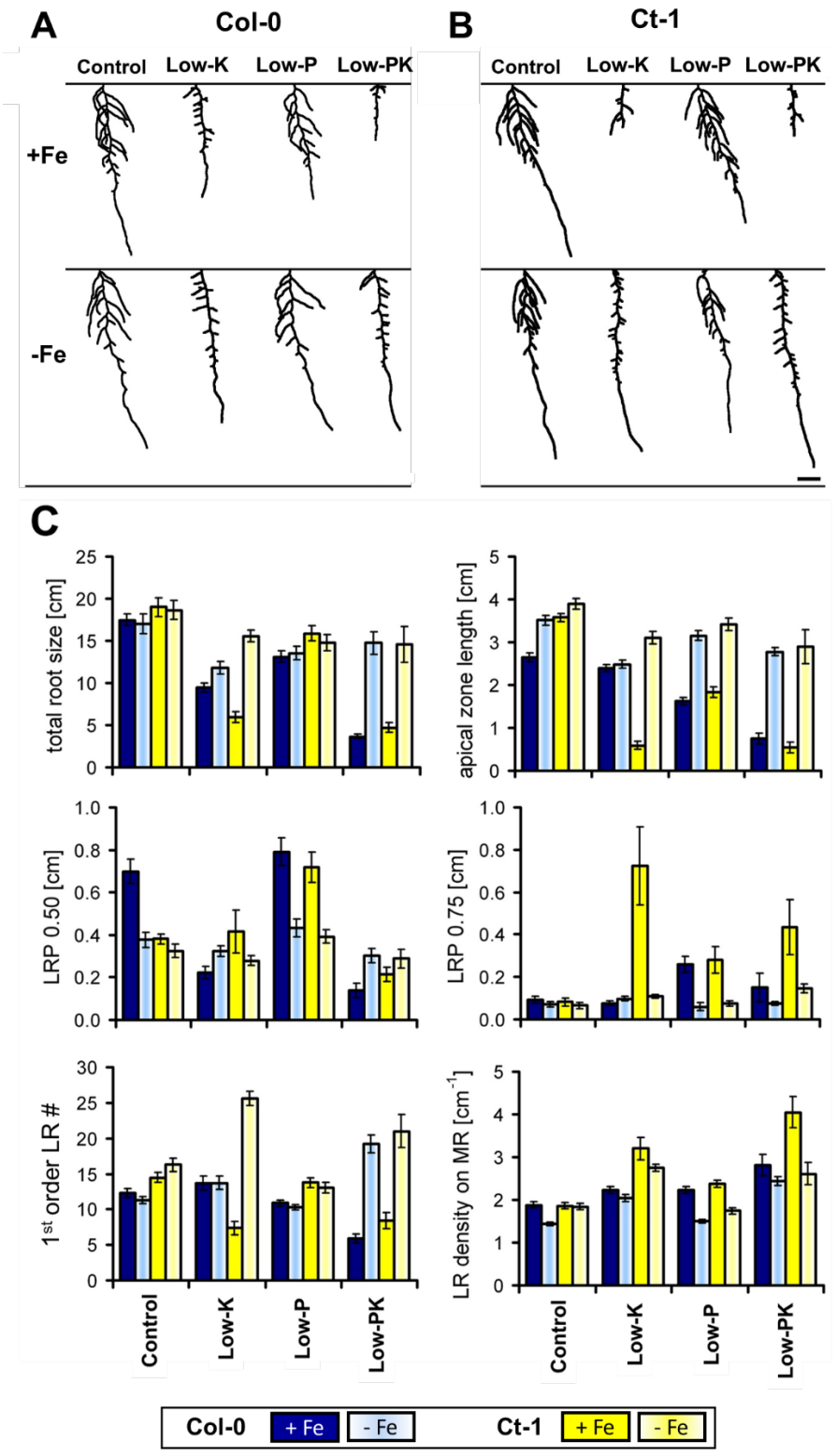

Figure 42: Reduction of Fe in the medium rescues main root growth in low-K and low-P.

Representative root phenotypes of Col-0 (A) and Ct-1 (B) seedlings grown on control, low-K, low-P and low-PK media supplemented with standard iron concentration (+Fe; 42.5 µM) or low-Fe (-Fe; 4.25 µM). (C) Quantification of root parameters in all conditions: Col-0 with standard Fe (dark blue) and low-Fe (light blue); Ct-1 with standard Fe (yellow) and low-Fe (light yellow). All values are means (n = 15 – 21; apart from 'Col-0, low-PK Fe-': n = 8) ± S.E.M.

To rule out the possibility that Fe availability within media was altered due to changes in K- or P-supply, or vice versa, I calculated the chemical equilibrium of ion speciation in all four media in question. Calculations were performed using the Visual MINTEQ 3.0 software tool (Gustafsson, 2011), with all media components and pH = 5.6 (buffered by MES-Tris) as input.

Table 25: Concentrations of ionic species present in growth solution calculated with Visual MINTEQ.
Concentrations of all added solutions (*supplied*) were used as input for each growth condition (control, single [low-K, low-P] and double deficiency [low-PK]). Calculation with Visual MINTEQ 3.0 (*calc*) shows that the bulk of all ions was present in a soluble (bioavailable) form. No major changes of ion availability occurred between media as indicated by similar *% of supplied* values. The predominant form of iron is Fe-EDTA$^-$ in all conditions. Fe-P compounds are negligible. pH = 5.6 (buffered with MES-Tris).

	Control			Low-K			Low-P			Low-PK		
	supplied [µM]	calc [µM]	% of supplied	supplied [µM]	calc [µM]	% of supplied	supplied [µM]	calc [µM]	% of supplied	supplied [µM]	calc [µM]	% of supplied
K^+	2000	1992.4	99.6	10	10.0	99.7	2000	1994.5	99.7	10	10.0	99.8
$H_2PO_4^-$	**500**	**474.7**	**94.9**	**500**	**476.5**	**95.3**	**20**	**19.0**	**95.0**	**20**	**19.1**	**95.4**
HPO_4^{2-}		**15.3**	**3.1**		**14.8**	**3.0**		**0.6**	**3.0**		**0.6**	**2.9**
$CaH_2PO_4^+$		3.68	0.74		3.88	0.78		0.152	0.76		0.16	0.80
$CaHPO_4$		1.75	0.35		1.86	0.37		0.072	0.36		0.08	0.38
Fe-EDTA$^-$	**42.5**	**42.0**	**98.9**	**42.5**	**42.0**	**98.9**	**42.5**	**42.0**	**98.9**	**42.5**	**42.0**	**98.9**
FeOH-EDTA^{2-}		0.32	0.76		0.313	0.74		0.32	0.75		0.31	0.73
$Fe(OH)^{2+}$		0.11	0.26		0.110	0.26		0.14	0.33		0.14	0.33
Fe^{3+}		**7.4E-07**	**0.00**		**6.7E-07**	**0.00**		**9.0E-07**	**0.00**		**8.2E-07**	**0.00**
$FeHPO_4^+$		**0.035**	**0.08**		**0.036**	**0.08**		**0.002**	**0.00**		**0.002**	**0.00**
$FeH_2PO_4^{2+}$		**4.1E-06**	**0.00**		**4.0E-06**	**0.00**		**2.1E-07**	**0.00**		**2.0E-07**	**0.00**
Na^+	1500	1495.6	99.7	1500	1496.4	99.8	1020	1018.1	99.8	1020	1018.5	99.9
Ca^{2+}	500	478.0	95.6	500	477.5	95.5	500	482.9	96.6	500	482.3	96.5
Mg^{2+}	250	242.4	97.0	250	242.8	97.1	250	243.7	97.5	250	243.9	97.6
NO_3^-	2000	1994.9	99.7	2000	1997.0	99.9	2000	1995.0	99.8	2000	1997.1	99.9
SO_4^{2-}	250	227.9	91.1	250	228.2	91.3	250	227.4	91.0	250	227.8	91.1
Cl^-	1500	1495.4	99.7	10	10.0	99.8	1020	1017.0	99.7	10	10.0	99.8

Calculations identified Fe(III)-EDTA$^-$ as the predominant form of Fe (98.9 % of total Fe supplied) in all conditions (Table 25). Solubilised free Fe^{3+} remains almost unchanged between conditions (ranging from 6.7 x 10^{-7} µM to 9.0 x 10^{-7} µM) and Fe-P complexes ($FeHPO_4^+$, $FeH_2PO_4^{2+}$) are negligible compared to Fe-EDTA$^-$ concentrations. Likewise, K and P are readily available in solution at the respective concentrations supplied. Thus, changes of K and P (or the accompanying changes of Na and Cl) in the external media do not alter the physicochemical availability of Fe directly. However, K : P : Fe ratios differed between the media, which may in turn affect uptake and homeostasis of Fe *in planta*. To test this hypothesis, I applied several techniques to visualise Fe in live and fixed root tissue that had been grown on various nutrient media.

5.2.2 Fe accumulates in main root apices of seedlings starved for K

Perls' staining, which specifically stains Fe in oxidation state +3 [Fe(III)], revealed accumulation of Fe in an area around the main root meristem in control condition (Fig. 43A). This 'Fe peak' was more pronounced in Ct-1 than in Col-0. No Fe was detected in the rest of the main root tip. In addition, stainable Fe concentrations were detected in more basal, and hence older, parts of the root system (Fig. 43C). This was a constant phenomenon across all genotypes and conditions tested, probably caused by slow diffusion of Fe from the medium into the apoplast or by Fe storage in older tissues. By contrast, the intensity of the Fe peak at the main root tip responded to K- and P-supply and was investigated in more detail.

Low-K caused an increase of Fe accumulation at the main root apex of Col-0 and even more so of Ct-1 (Fig. 43B). In Chapter 4, I mentioned that elongating lateral roots of Ct-1 acquired low-K sensitivity around 6 to 9 days after they emerged from the main root (which had already ceded growth). This means that, like the main root, they slowed down in growth and eventually stopped elongating altogether, giving rise to newly formed 2nd order LRs. Interestingly, this process is also accompanied by an increase of Fe around the LR meristem about 6 days after emergence (Fig. 43D). Since at this stage LRs were increasingly responsive to gravity (growing vertical), it may be possible that a developmental switch causes these LRs to become sensitive to Fe just like the main root.

Of course the next question was whether low-Fe reduced Fe accumulation in the root tip of low-K seedlings. Indeed, no Perls' staining was detected in the root tips of either of the two accessions when [Fe] in the low-K medium was lowered to a tenth of the control concentration (Fig. 43E).

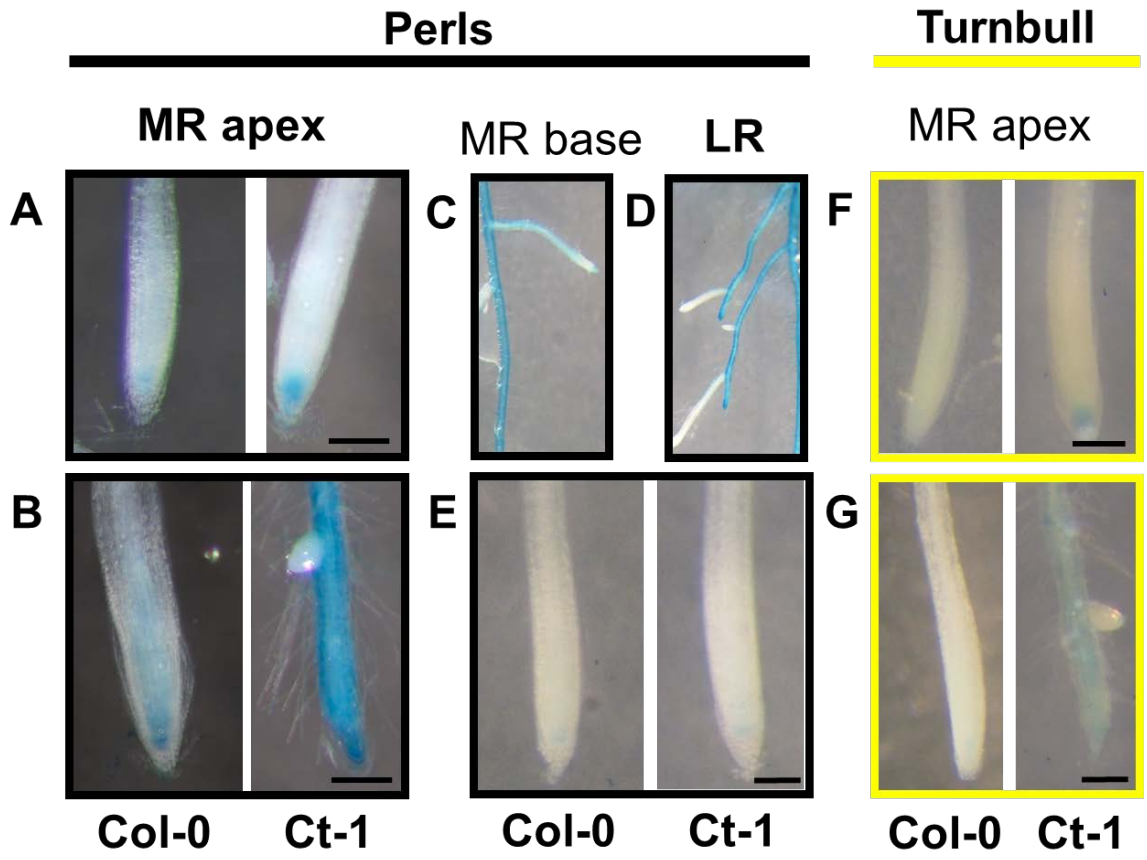

Figure 43: In low-K, Fe(III) accumulates in root apices.
A to E) Abundance of Fe(III) was visualised semi-quantitatively using the Perls' stain. **A)** In control condition, the spatial distribution of Fe(III) at the main root (MR) apex is confined to the apical meristem. The ecotype Ct-1 generally had higher Fe(III)-levels around the apex than Col-0. **B)** Fe(III)-concentrations increased in low-K, especially in low-K sensitive Ct-1. **C)** Fe(III) also accumulated to some degree in older (basal) parts of the root system. The distribution was rather uniform across all conditions (image shown is Ct-1 in control). **D)** For Ct-1 grown on low-K, lateral roots (LRs) outgrew the main root after main root growth arrest. These lateral roots in turn stopped elongating around 6-9 days after emergence, giving rise to second order lateral roots. Again, Fe(III)-accumulation at the lateral root apex preceded this event. **E)** The Fe(III)-peak in MR root tips of low-K plants was strongly reduced when external [Fe] was lowered to a 10th of the original concentration (4.25 µM).
F and G) Abundance of Fe(II) was visualised semi-quantitatively using Turnbull's staining. At the root apex, Fe(II)-concentrations were generally lower than Fe(III) and no significant increase was observed in low-K. Images shown are representatives of at least 5 independently measured samples. Bar: 0.1 mm.

Turnbull's staining, a technique analogous to Perls' staining, was used to visualise Fe in oxidation state +2 [Fe(II)]. The abundance of Fe(II) in the main root tip was much lower as compared to Fe(III), both in control and low-K (Fig. 43F, G). Hence, Fe(III) was the predominant form of stainable iron present in the main root meristem in control and low-K.

Unfortunately, neither of the two staining techniques permitted direct quantification of Fe concentrations. This was mainly due to the fact that I did not have constant access to microscopy facilities that would have enabled me to carry out all my experiments in the exact same conditions. It was therefore difficult to ensure constant light conditions, and even images taken with the AxioCam system (Zeiss) were prone to light intensity fluctuations. I therefore abstained from quantifying the stain by image analysis (e.g. with ImageJ).

Instead, I developed a quick method based on Perls' staining to quantify Fe(III) in excised and extracted root tips (see Material and Methods section 2.8.3). Briefly, main root tips of Col-0 and Ct-1 seedlings grown for 10 days on control or low-K media were excised by cutting approx. 2 mm behind the apex. Root tips from 50 – 100 plants were pooled and ions were extracted with HCl solution. After spinning down the root tissue the concentration of Fe(III) in the supernatant was determined by measuring the absorbance of the Prussian Blue complex formed after adding an appropriate amount of potassium ferrocyanide to the solution. Three independent replicates were analysed from each genotype in each condition. Fig. 44 shows that Fe concentrations (normalised to the number of root tips per sample) were higher in low-K samples of both ecotypes. However, results (control vs low-K) were not statistically different (Col-0: $p = 0.10$, Mann-Whitney U-test; Ct-1: $p = 0.29$, Student's t-test), probably due to the small sample size. It was also surprising that values measured in Ct-1 were lower than those measured in Col-0 in low-K indicating that other factors in the plant sample contribute to the signal. Another qualitative and quantitative method of Fe determination was therefore necessary to back up these results.

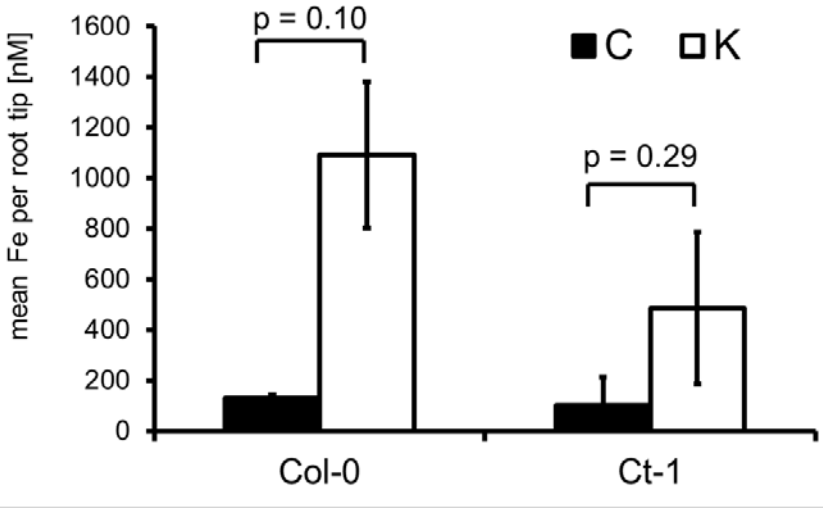

Figure 44: Quantitative Perls staining verifies low-K induced Fe accumulation in excised root tips.
Fe concentrations of excised and extracted main root tips from seedlings grown on control (black bars) or low-K media (white bars) were determined via the method described in section 2.8.3 of Material and Methods. Three independent, biological replicates were analysed from each genotype in each condition. Appropriate statistical tests were performed between data collected in control and low-K (Col-0: Mann-Whitney U-test; Ct-1: Student's t-test).

5.2.3 Synchrotron X-Ray fluorescence verifies exclusive Fe accumulation around the main root meristem in low-K

To account for potential interference of histochemical staining techniques with Fe distribution and to get a refined, multi-elemental ionic profile of the root tip, I performed synchrotron X-ray fluorescence (SXRF) measurements on hydrated root tissue. These measurements were carried out in collaboration with Prof Mary Lou Guerinot and Dr Tracy Punshon (Dartmouth College, Hanover, USA) under supervision of Dr Tracy Punshon and Dr Sue Wirick (University of Chicago) on Beamline X26A at the National Synchrotron Light Source (NSLS), Brookhaven National Laboratory (BNL), NY, USA.

Due to a very strict limit on beamtime at NSLS, I could only run a sub-selection of samples (Table 26), and not all measurements were successful (one complete overnight runt of 3 biological replicates of Col-0 control and low-K root tips failed due to an unknown error in the software). At this stage the most complete dataset is available for Ct-1 with at least 2 to 3 biological replicates for control, low-K, low-P and low-PK conditions from 12 day old roots. I also analysed Ct-1 seedlings at the onset of the low-K response (6 DAG). For other genotypes, including Col-0, it was unfortunately not possible to obtain a sufficient level of replication within the time course of this project but images obtained

from individual plants provide indicative evidence for the phenotypes described in the following.

Table 26: List of synchrotron X-ray fluorescence (SXRF) samples.
The list contains all samples, including the identifying sample code (Sample ID), the date of data collection, genotype, growth media and age of seedlings. All samples were root samples. Most of them were main root tips (MRT), some were lateral root tips (LRT) or sections of the basal part of a main root usually including a part of lateral root branch (see Details & Comments). Pixel size denotes the resolution of sample imaging and dwell time corresponds to the duration of X-ray excitation. One sample for which the overnight run failed is coloured grey.

Sample ID	Date	Genotype	Media	Age (DAG)	Details & Comments	Pixel Size (µm)	Dwell Time (ms)
Col-0_DAG12_K_01	08/08/12	Col-0	low-K	12	root # 01, main root tip (MRT)	5	200
Col-0_DAG12_K_02	08/08/12	Col-0	low-K	12	root # 01, lateral root tip (LRT)	5	200
Col-0_DAG12_K_04	08/08/12	Col-0	low-K	12	root # 02, MRT	5	200
Col-0_DAG12_P_01	08/08/12	Col-0	low-P	12	root # 03, MRT	5	200
Col-0_DAG12_P_03	08/08/12	Col-0	low-P	12	root # 04, MRT	5	200
Col-0_DAG12_P_04	08/08/12	Col-0	low-P	12	root # 04, basal part of MR (+ LR base)	5	200
Ct-1_DAG12_K_01	08/08/12	Ct-1	low-K	12	root # 05, MRT	5	200
Ct-1_DAG12_K_02	08/08/12	Ct-1	low-K	12	root # 05, LRT	5	200
lpr1_DAG12_P_02	08/08/12	*lpr1*	low-P	12	root # 06,basal part of MR (+ LR base)	5	200
lpr1_DAG12_P_03	08/08/12	*lpr1*	low-P	12	root # 07, MRT	5	200
aha2_DAG12_P_01	08/08/12	*aha2*	low-P	12	root # 08, MRT	5	200
aha2_DAG12_P_02	08/08/12	*aha2*	low-P	12	root # 08, basal part of MR (+ LR base)	5	200
Ct-1_Scanlist2	08/08/12	Ct-1	Control	12	root # 10, MRT	5	200
Ct-1_Scanlist3	08/08/12	Ct-1	Control	12	root # 11, MRT	5	200
Ct-1_Scanlist4	08/08/12	Ct-1	low-K	12	root # 12, MRT	5	200
Ct-1_Scanlist5	08/08/12	Ct-1	low-K	12	root # 13, MRT	5	200
Ct-1_Scanlist6	08/08/12	Ct-1	low-K	12	root # 14, MRT	5	200
Ct-1_Scanlist7	08/08/12	Ct-1	low-P	12	root # 15, MRT	5	200
Ct-1_Scanlist8	08/08/12	Ct-1	low-P	12	root # 16, MRT	5	200
Ct-1_Scanlist9	08/08/12	Ct-1	low-P	12	root # 17, MRT	5	200
Ct-1_Scanlist10	08/08/12	Ct-1	low-PK	12	root # 18, MRT	5	200
Ct-1_Scanlist11	08/08/12	Ct-1	low-PK	12	root # 19, MRT	5	200
Ct-1_Scanlist12	08/08/12	Ct-1	low-PK	12	root # 20, MRT	5	200
Col-0_DAG6_C and K-	08/08/12	Col-0	Control Low-K	12	2 x 3 main root tips; overnight run, experiment failed	5	500
Ct-1_DAG6_C_1b	09/08/12	Ct-1	Control	6	root # 27, MRT	5	200
Ct-1_DAG6_C_3	09/08/12	Ct-1	Control	6	root # 28, MRT	5	200
Ct-1_DAG6_C_4	09/08/12	Ct-1	Control	6	root # 29, MRT	5	200
Ct-1_DAG6_K_1b	09/08/12	Ct-1	low-K	6	root # 30, MRT	5	200
Ct-1_DAG6_K_2	09/08/12	Ct-1	low-K	6	root # 31, MRT	5	200
Ct-1_DAG6_K_3	09/08/12	Ct-1	low-K	6	root # 32, MRT	5	200
Ct-1_DAG6_K_4	09/08/12	Ct-1	low-K	6	root # 33, MRT	5	200
Ct-1_DAG6_K_5	09/08/12	Ct-1	low-K	6	root # 34, MRT	5	200
lpr2_DAG12_K_1	09/08/12	*lpr2*	low-K	6	root # 35, MRT	5	200

Fig. 45A shows relative fluorescence images of main root tips from Ct-1 seedlings grown for 12 days on control, low-K, low-P or low-PK media (root # 10 to root # 20 as per Table 26). A major advantage of SXRF over other elemental quantification techniques is the ability to simultaneously quantify the spatial pattern of several elements (particularly metals) at a time. Four images are therefore shown in Fig 45 representing Fe, K, Ca and Zn. Images are 2D projections of the root cylinder onto a plane. Therefore, if elements are distributed evenly within the cylinder, fluorescence intensity will show a gradient from the edges to the centre as seen for K or Ca.

The Fe pattern confirms tightly localised Fe accumulation in the low-K grown roots. It distinctly covers an area that might well correspond to the apical meristem (quiescent centre and surrounding cells). No Fe accumulation was observed in low-P. Low-PK samples displayed lower Fe concentrations than low-K samples but also displayed some Fe patches. It should be noted that a very high Fe peak was detected in one of the control samples. However, this is probably due to contamination of the sample with Fe-containing dust as this peak was almost at the edge of the root. Unfortunately, only two control samples were measured but images shown later also support the idea of increased, localised Fe accumulation upon low-K (see Fig. 46).

Other cations showed a different distribution (Fig 45). K was highest in control conditions and was evenly distributed throughout the root tip. Low-K and low-P reduced overall K concentrations. A similar pattern was observed for Ca but here some patchiness was observed in low-PK. Note that a Ca peak was detected outside the left-most low-PK root. In this case, it can clearly be discarded as dust contamination. Interestingly, Zn was also slightly increased by low-K. I also analysed Cu, Co and Ni, but no differences were detected between conditions (data not shown).

SXRF data can be converted into quantitative element concentrations (as µg cm^{-2} of analysed area) by comparing fluorescence intensities of samples with a standard material. Here, a standard measured at Beamline X26A (*SRM18333-10500*) was used for quantification with SNRLXRF software (Sutton et al., 2002). Average values indicated no major differences between conditions for any of the elements (Fig 45B). Slight deviations occurred (e.g. average K higher in low-K) but should not be over-interpreted. In fact, average concentrations are calculated from a large spread of data points and are corrected for the cylindrical shape of the root (Fig 45C). Nevertheless, when concentrations of elements are in a similar range across conditions, the idea of localised rather than overall changes should be favoured. Concentration maxima were two orders of magnitude higher than averages and did indeed differ, especially for Fe (Fig 45C). All in all, the results

provide strong evidence for an element-specific, localised increase of Fe in the apical meristem of K-starved main roots.

To investigate the timing of Fe accumulation in Ct-1, root tips from 6 day old seedlings grown in control and low-K were analysed. In these samples, Fe peaks around the apical meristem were detected in control condition but a significant increase of Fe accumulation occurred in low-K (Fig. 46).

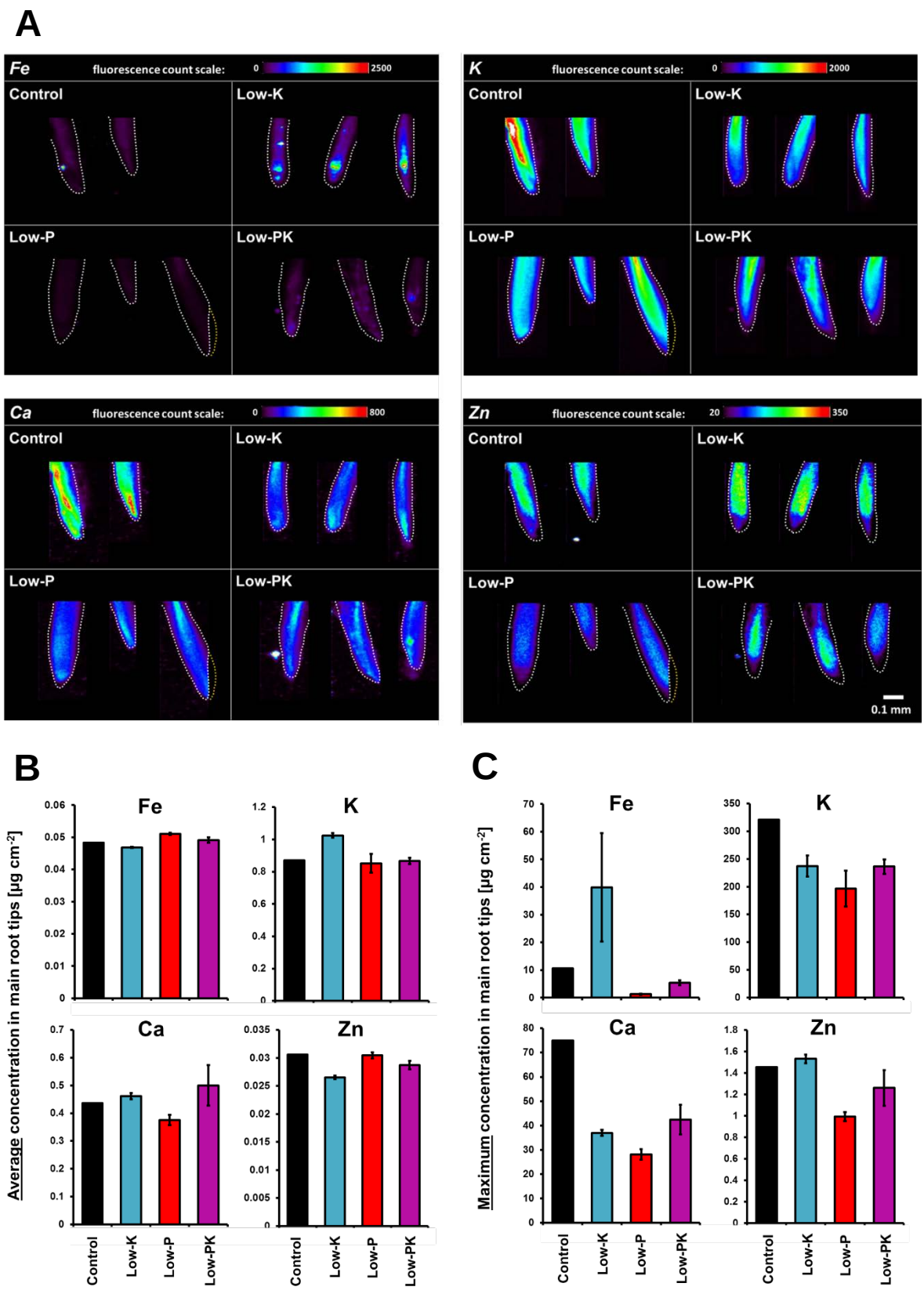

Figure 45: Synchrotron X-Ray fluorescence (SXRF) of Ct-1 main root tips verifies specific Fe accumulation in low-K

see next page for complete figure legend

Figure 45: Synchrotron X-Ray fluorescence (SXRF) of Ct-1 main root tips verifies specific Fe accumulation in low-K.
Upper panels (A): Images of relative SXRF from root apices for Ct-1 seedlings grown on control, low-K, low-P and low-PK media. Images were taken 12 DAG. Fluorescence intensities of Fe, K, Ca and Zn are shown for the same root tips. White dotted lines denote the outlines of the root (the imaging frame of the third root in low-P was slightly shifted; a yellow dotted line shows the outline of the root tip part that was not imaged).
Lower panels (B, C): Quantification of SXRF data, achieved by comparing relative fluorescence intensities with a standard (see Material and Methods section 2.8.3). Bar charts in (B) show average concentration across the whole measured area, (C) depicts the maximal values occurring within that area. Data are means ±S.E.M. (where appropriate) of samples shown in (A). In control condition, only two samples were available, hence no error bars are shown.

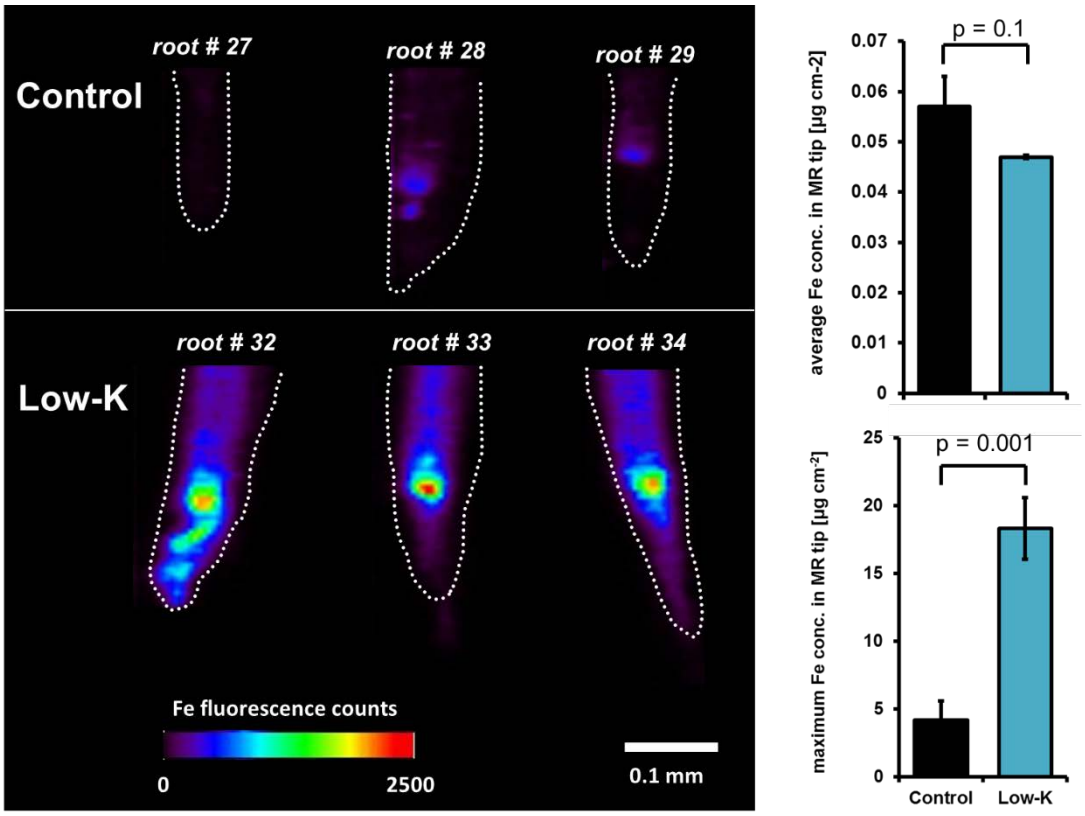

Figure 46: SXRF analysis of Ct-1 main root tips at an earlier stage of deficiency.
Main root tips (for sample descriptions see Table 26) of seedlings grown in control (upper panel) and low-K conditions (lower panel) were analysed 6 DAG. Quantification indicated no significant differences between average Fe concentrations (as per Mann-Whitney U-test) but a significant increase of Fe maxima (as per Student's t-test). Bar charts show means ±S.E.M. (n = 3 per condition).

5.2.4 In low-P, Fe accumulates in different oxidation states throughout the root system

Using the same histochemical staining approach as for low-K, I also visualised Fe distribution in P-starved root systems. At least 5 seedlings were stained with the Perls' or Turnbull's method and observed under a light microscope. Fig. 47 summarises the main findings by showing representative images.

The overview image shown in Fig. 47A provided evidence for the hypothesis of Fe accumulation in low-P (see also Ward et al., 2008). However, in contrast to low-K, Fe peaks appear throughout the root system in older parts of the main root as well as in lateral roots. No accumulation of Fe(III) occurred in the root apex (Fig. 47B). Fig. 47C depicts Fe(III) peaks or patches in close-up. The shape and distribution of Fe patches was variable but generally the size was restricted to one or two adjacent cells. The Fe maximum was often located at the cell-to-cell border, suggesting apoplastic location (see black arrowheads in Fig. 47C). Unfortunately, spatial resolution of the light microscope restricted further analysis. Consequently, staining could not fully resolve whether deposits are formed intra- or extracellularly.

Patchiness of distribution and high intensity of the stain suggested the presence of a Fe-precipitate or -complex. To test this hypothesis, knockout lines for the two most important storage forms of Fe were grown on low-P media and stained with Perls' solution: *fer1-3-4* which is deficient in all three ferritins expressed in roots (Briat et al., 2010), and *ipk1 ipk2ß* which displays an almost complete absence of phytate (inositol-6-phosphate) in seeds (Stevenson-Paulik et al., 2005). Both lines still exhibited a wildtype-like distribution of Fe (Fig. 47D for close-ups of Fe patches). So the nature of the observed Fe patches remains unclear.

Turnbull's staining suggested that the concentration of Fe(II) was increased in low-P (Fig. 47E, F) as compared to control (compare Fig. 43F). However, most of the Fe(II) was found in a region corresponding to the elongation and differentiation zone (Fig. 47F), not the apical meristem. Fe patches were also stained with the Turnbull's method, albeit at a lower intensity (Fig. 47F). This observation indicated that putative Fe clusters underlying low-P induced Fe patches probably contain Fe in both oxidation states. To further characterise the composition of Fe clusters, SXRF analysis was performed in basal parts of P-starved Col-0 seedlings. Fig. 48 shows elemental distribution of Fe, K and Zn in a representative section of a main root grown on low-P media.

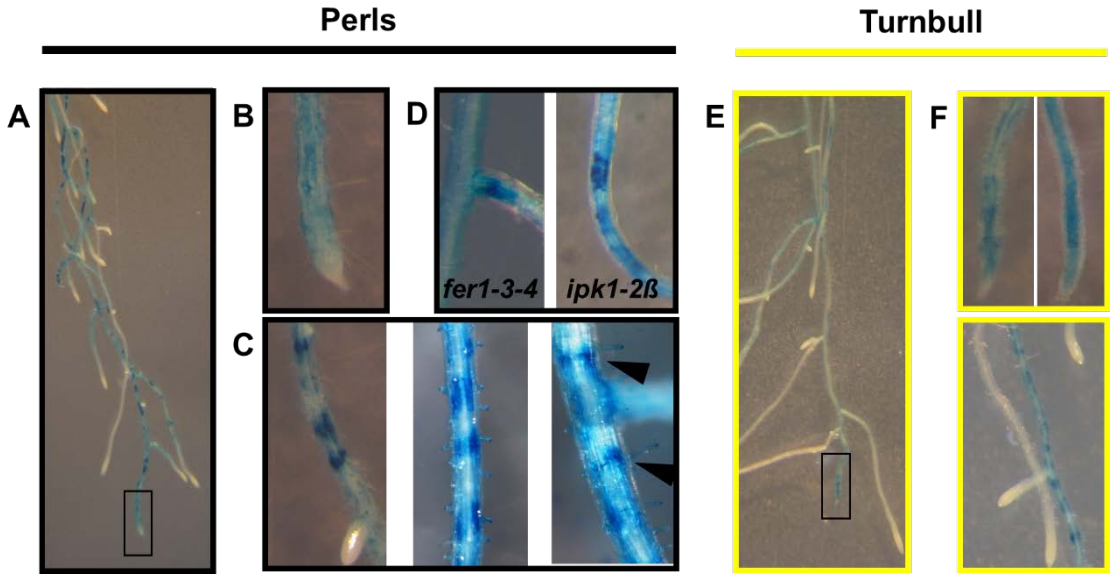

Figure 47: Patchy accumulation of Fe occurs in various parts of the root system in low-P.
A to D) Abundance of Fe(III) visualised semi-quantitatively using the Perls' method. **A)** Overview of a root grown on low-P for 12 days. The main root apical zone is highlighted with a box and a close-up is shown in **B)**. No increase of Fe(III) occurs around the main root apical meristem in low-P. **C)** Local Fe(III)-peaks were visible throughout the root system as patchy/punctate structures (left panel: branched zone of the main root; mid panel: lateral root). Right panel: At higher resolution, Fe accumulation often appeared to be at cell-to-cell borders (black arrowheads). **D)** The same pattern was observed in knockout lines devoid of the two major Fe storage forms: *fer1-3-4* (ferritin) and *ipk1-2ß* (phytate).
E and F) Abundance of Fe(II) visualised semi-quantitatively using the Turnbull's stain. **E)** Overview of a root grown on low-P for 12 days. The main root apical zone is highlighted with a box. **F)** Fe(II) accumulated in an area behind the MR apex (elongation and differentiation zone; left panel: zoom of E; right panel: another example for comparison). Lower panel: Fe patches were also stainable with Turnbull's stain. Images shown (Col-0 if not stated otherwise) are representatives of at least 5 independently measured samples.

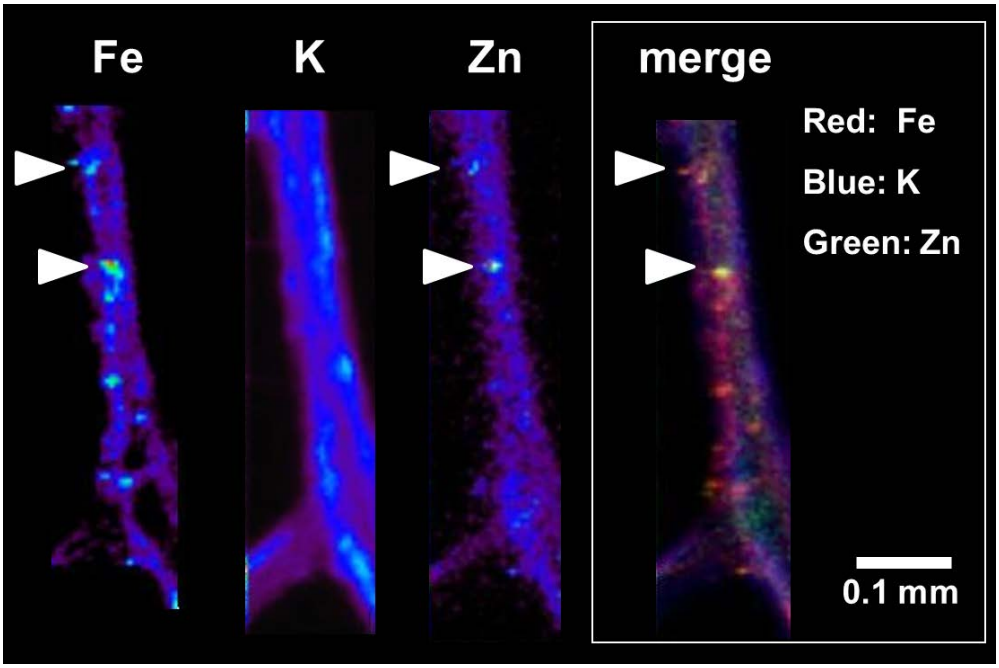

Figure 48: SXRF image of patchy element accumulation in low-P.
Fluorescence intensities are on different scales but intensity patterns indicate the spatial distribution of Fe, K and Zn concentrations. The merged image on the right depicts elemental abundances of all three metals in different colours (see figure) to facilitate visual analysis of element co-localisation. White arrowheads highlight co-localisation of Fe and Zn. Relative SXRF intensity follows a heatmap colour scale (low: blue; high: red; no flouresence: black).

Although most Fe peaks did not co-localise with any other elemental peak, two Fe peaks overlapped with Zn peaks (compare white arrowheads in Fig. 48). None of the other analysed elements had concentration peaks overlapping with those of Fe (data not shown).

In sum, P-deprivation does not enhance Fe accumulation around the apical meristem but leads to Fe patches throughout the root system. High concentrations of the typical Fe storage molecules phytate or ferritin are probably not the reason for these patches. Although the nature of these clusters is not clear, the data obtained so far suggests that they are composed of Fe(II), Fe(III) and to lesser degree Zn.

5.3 Discussion

5.3.1 Iron as a central regulator of main root growth

In this chapter I have shown that both P- and K-deficiency root phenotypes can be rescued by lowering the concentration of iron (Fe) supplied to the medium (Fig. 42). This has been previously described for low-P (Svistoonoff et al., 2007; Ward et al., 2008; Ticconi et al., 2009), but Fe-effects have not been investigated in low-K, yet. Moreover, the *low-K strategy II* phenotype of Ct-1 can be reverted to a *low-K strategy I* phenotype by reducing external Fe ($[Fe]_{ext}$), demonstrating that cessation of main root elongation caused by an Fe-dependent process is the prerequisite to lateral root elongation in Ct-1. In fact, root architecture analysis highlighted a role for $[Fe]_{ext}$ in titrating the balance between main and lateral root elongation even in P- and K-sufficient media.

It has been suggested that precipitation of Fe-P minerals in soil and commonly used growth media could induce deficiency for either of the nutrients (Dalton et al., 1983; Hirsch et al., 2006). My experiments provide strong support for the idea that reduced availability of either K, P or Fe in the medium, caused by changes of another of these three components, does not occur in my system (Table 25). However, I could show that Fe concentrations within the plant root system are altered in low-K and low-P (Fig. 17 to 22). Whilst both K- and P-deficiency responses depend on $[Fe]_{ext}$, the internal changes of Fe distribution are quite different. A straightforward postulation of a direct cross-talk mechanism between low-K and low-P signalling pathways controlled by Fe is therefore hard to make. First, both responses should be looked at in isolation.

5.3.2 Iron at the root tip in low-K and low-P

A rather simple explanation for the Ct-1 phenotype observed in low-K would be Fe accumulation up to toxic levels (Fig. 43, 44 and 45) causing cell death at the site of the main root meristem (compare Fig. 36) and consequently terminating root elongation. Additional resources (carbon and nutrients) and signalling molecules, such as auxin, would then be available to promote elongation of lateral roots. The latter is supported by the fact that only freshly formed lateral roots close to the root tip (compare LRP 0.75; Fig. 42), which have not yet stopped elongating, show enhanced growth after main root growth has ceded. In contrast, low-K induced cessation of lateral root elongation in Col-0 is much less

Fe dependent. This is supported by the fact that Ct-1 has a Col-0 like phenotype in low-K when $[Fe]_{ext}$ is reduced.

Accumulation of Fe in low K could be due to an effect of low-K on Fe uptake from the external medium, for example, as a result of changes in membrane potential or pH (Armengaud et al. 2009). Alternatively, accumulation of Fe may be caused by altered usage of Fe within the plant. For example, a redox process may use Fe(II) and consequently produce a 'dump' of Fe(III), or vice versa.

Fe is very important for cell function because it fulfils a central role as an enzymatic co-factor in many vital processes involving redox chemistry (e.g. photosynthesis and respiration), but it is also able generate reactive oxygen species (ROS) when reacting with molecular oxygen (Thomine and Lanquar, 2011). Excessive ROS production via the Fenton reaction (e.g. $Fe^{2+} + O_2 \rightarrow Fe^{3+} + \bullet O_2^-$) is a principal mechanism of Fe toxicity. In moderate concentrations, however, ROS are important signalling components of many stress responses. K starvation for example was shown to lead to ROS accumulation behind the elongation zone of the main root (Shin and Schachtman, 2004; Shin et al., 2005; Kim et al., 2010). This was associated with the reduction of main root growth.

To investigate differences in ROS accumulation between Col-0 and Ct-1, I tried to replicate ROS staining described in Kim et al. (2010) using H_2DFFDA (5-[and-6]-carboxy-2',7'-difluorodihydrofluorescein diacetate; Life Technologies, Darmstadt, Germany). The results were not informative because fluorescence of the ROS detection dye was very high in all root samples, in all root zones and in all conditions tested, even at very low excitation. I therefore did not quantify ROS activity and have not shown these data here. Published data on ROS distribution (Shin and Schachtman, 2004; Shin et al., 2005; Kim et al., 2010) do not match Fe distribution patterns recorded here in low-K, as ROS are mostly localised to the differentiation zone whilst Fe specifically accumulates in the meristem. However, the quiescent centre (QC) within the apical meristem needs an oxidative environment to function properly (Jiang et al., 2005) and Fe-dependent redox processes may be involved. Interestingly, ROS distribution is also altered in low-P (Tyburski et al., 2009). The authors of this study point out that not only the presence of ROS per se but the spatial pattern of speciation (e.g. H_2O_2 vs. $\bullet O_2^-$) are important criteria for either promoting or reducing cell division and elongation. They report reduced accumulation of both ROS species in the elongation zone and use this to explain the lack of cell elongation in low-P. I have observed accumulation of Fe(II) in the elongation and differentiation zone of low-P main roots (Fig. 47F). Maybe an increased Fe(II) availability actually mirrors the reduced production of ROS in this condition, since Fe(II) is oxidised in Fenton chemistry.

Accumulation of Fe around the QC occurred even in control condition, suggesting a functional role for Fe in apical meristem regulation. Due to its central role in biological redox chemistry, it may be speculated that stainable Fe might actually be part of enzyme complexes. However, Fe could also serve as the substrate for redox active enzymes like ferroxidases (Hoegger et al., 2006). In either case, Fe-dependent production of ROS may be the downstream consequence and hyper-accumulation of Fe may disrupt redox/ROS homeostasis. At the moment, my data do not provide the evidence to fully support this hypothesis and the actual source that feeds the root tip with Fe remains unclear. Increased uptake from the medium or alterations in homeostatic processes, like Fe transport between tissues, Fe storage or sequestration into the vacuole may be the missing link between external and internal Fe concentrations.

To elucidate which other signalling and homeostatic networks are involved in root architecture responses to low-K and low-P, a mutant study of known regulatory genes would be helpful. Therefore a selection of K, P and Fe transport and signalling knockout lines was investigated in Chapter 6.

5.3.3 Iron patches formed in low-P

Patches of Fe were found in low-P throughout the root system (Fig. 47). Staining and SXRF indicated that within these patches both Fe(III) and Fe(II) as well as Zn constitute some sort of Fe cluster/complex (Fig. 47, 48). Fe accumulation and formation of Fe clusters in chloroplasts of P-starved plants (leaves) were reported by Hirsch et al. (2006). They explained their phenotype as a shift from sequestering Fe into Fe-P clusters inside the vacuole in control condition, to relocating excess Fe into ferritins inside the chloroplast. Although I did not examine shoot tissue, I investigated the Fe distribution in a triple mutant (*fer1-3-4*) for the major ferritins expressed in Arabidopsis roots (Ravet et al., 2009; Briat et al., 2010). No difference to the wildtype was observed in low-P (Fig. 47). The same was the case for a knockout devoid of the main seed P (and consequently Fe) storage molecule phytic acid / phytate (Stevenson-Paulik et al., 2005). Hence, an alternative nature of these Fe patches should be assumed. Microscopic images often suggested localisation of Fe patches at the cell-to-cell border and thus potentially in the apoplast (Fig. 47C). Unfortunately, SXRF images do not resolve the exact location. Could it be possible that a so far uncharacterised molecular process deposits excess Fe into the apoplast? On the one hand it seems a waste, since in nature Fe deficiency is a very common phenomenon and hence many homeostatic processes tightly control the

availability of Fe within plants, saving every bit of it for 'bad times' (Morrissey and Guerinot, 2009; Palmer and Guerinot, 2009; Thomine and Lanquar, 2011). On the other hand, it is unlikely that Fe is more available to plants in low-P when using an agar-based system in which Fe is chelated and the pH is buffered. So maybe dumping Fe into the apoplast represents a strategy that is important when only one parameter in the intertwined availability of P and Fe is changed. P is needed for storing Fe as phytate (Stevenson-Paulik et al., 2005), ferritin (Briat et al., 2010) or Fe-P complexes inside the vacuole (Hirsch et al., 2006). Consequently, Fe needs to be removed from inside the plant when P is not available. Whether this has any significance in natural environments, where P and Fe availability are linked, is another question (see general discussion, Chapter 7).

6. Multicopper oxidases regulate main root growth in low-P and low-K

6.1 Introduction

In Chapter 5, iron (Fe) was identified as a central component of low-P and low-K root architecture responses. It was not clear, however, whether increased Fe uptake, altered Fe distribution or changes in redox homeostasis were responsible for that. Moreover, sites of Fe accumulation in low-K (Fe^{3+} at the main root tip) and low-P (Fe^{3+} in patches; Fe^{2+} in the elongation and differentiation zone) were not congruent. Nevertheless, similar root architecture parameters (esp. main root length, apical zone length) were affected by single K- and P-starvation and reduction of main root elongation was significantly enhanced as a result of P*K interaction (Fig. 17B, 19A, 42). A comparative root architecture analysis of knockout mutant lines devoid in components of P, K and Fe transport and signalling seemed a reasonable starting point to identify molecular component that could underly interactions of root responses to K- and P-deprivation. To follow this approach I obtained a set of publicly available T-DNA insertion lines from NASC for which a molecular or growth phenotype had been demonstrated before (see references in Table 4, Material and Methods Chapter 3). Some lines were kindly donated on request but in other cases I unfortunately did not get any response. Consequently, the mutant collection used in this study is far from being complete. The following paragraphs will briefly summarize the function of genes included here.

K: The major components of K-uptake and –signalling have already been described and respective knockouts have been used in Chapter 3. HAK5 is a high-affinity K transporter with significant contribution to K uptake at very low K concentrations (≤ 10 μM; Rubio et al., 2008; Qi et al., 2008; Rubio et al., 2010). The shaker channel AKT1 functions in a broader concentration range (Hirsch et al., 1998; Spalding et al., 1999; Qi et al., 2008; Rubio et al., 2010) and it is activated at low-K by the CBL-interacting kinase CIPK23 (Xu et al., 2006; Lee et al., 2007). In addition, the mutant for the peroxidase gene *RCI3* was included. RCI3 has recently been shown to contribute to low-K induced root responses (Kim et al., 2010).

P: Uptake at the root surface and distribution of phosphate within the plant is mainly achieved by transporters of the PHT family in Arabidopsis (Shin et al., 2004; Remy et al.,

2012), but none of these transporters was analysed here. To increase the solubility of inorganic P, protons (see below *proton pumps*), organic acids and extracellular phosphatases are released into the soil (Vance, 2003). P homeostasis in tissues and cells is tightly controlled on many levels (reviewed in Gojon et al., 2009) involving different classes of proteins like the central transcription factor PHR1 (Rubio et al., 2001), the ubiquitin conjugase PHO2/UBC24 (Aung et al., 2006) and the SUMO E3 ligase SIZ1 (Miura et al., 2005).

Two genes encoding multicopper oxidases, *LPR1* and *LPR2*, have been implicated in sensing local P concentrations and subsequently triggering downstream events (Svistoonoff et al., 2007). The authors of this study have demonstrated, that *LPR1* is expressed at the main root tip and that its expression level determines low-P sensitivity. LPR1 has been shown to be ER-localised and to work in conjunction with the ER-localised P_5-type ATPase PDR2 (Ticconi et al., 2009). Although sharing 79 % amino acid homology with *LPR1*, *LPR2* has not enjoyed similar attention. Consequently tissue and cellular expression patterns as well as *LPR2* function are so far unknown.
[please note: *LPR: LOW PHOSPHATE ROOT*; not to be confused with LRP: lateral root path length]

Fe: In Arabidopsis, Fe is taken up via the reduction based strategy (Thomine and Lanquar, 2011) which involves two components situated at the plasma membrane of the root epidermis: a) the reductase FRO2 (Yi and Guerinot, 1996; Robinson et al., 1999) which reduces extracellular Fe^{3+} to Fe^{2+} and b) the high-affinity transporter IRT1 (Vert et al., 2002) which subsequently transports Fe^{2+} across the epidermal plasma membrane. This system is particularly active at low external Fe concentrations which induce expression of both genes via the action of the transcription factor FIT (Colangelo and Guerinot, 2004). However, since *irt1* knockouts are able to produce viable plants and seeds at high external Fe supply, Fe must also be taken up by low-affinity, probably less specific, metal transporters of so far unknown nature (Thomine and Lanquar, 2011). Once inside the plant, Fe homeostasis is tightly regulated. Two transporters are involved in sequestering excess Fe into the vacuole: VIT1 (Kim et al., 2006; Roschzttardtz et al., 2009; not included in this study) and the ferroportin FPN2 (Morrissey et al., 2009). The NRAMP4 transporter works in the opposite direction, unloading Fe from the vacuole into the cytoplasm (Lanquar et al., 2005). Yet, in conjunction with its homologue NRAMP3, NRAMP4 has only been demonstrated to be important for remobilisation of Fe in germinating seeds. A role in more mature plants has yet to be established (Thomine and Lanquar, 2011). Another ferroportin,

FPN1, probably facilitates xylem loading (Morrissey et al., 2009). In addition, FRD3 helps to mobilise Fe for root-shoot transport by secreting the Fe-chelator citrate into the xylem (Rogers and Guerinot, 2002). The *frd3-2* mutant showed a range of pleiotropic, detrimental phenotypes in preliminary experiments (stunted growth, chlorosis, few lateral roots) and was therefore discarded from further analysis. Last but not least, ferritins FER1, FER3 and FER4 have been shown to buffer Fe-concentrations in roots and they have been proposed to be important for oxidative stress responses (Ravet et al., 2009; Briat et al., 2010). The corresponding triple mutant *fer1-3-4* was already shown to have a similar Fe distribution pattern in low-P (Chapter 5, Fig. 47D).

Proton pumps: Plasma membrane localised H^+-ATPases (aka proton pumps) are responsible for generating a proton gradient across the membrane which is needed to energise most solute transport processes in plants (Haruta and Sussman, 2012). As a result, cation transport (e.g. K, Ca and unspecific transport) is strongly dependent on proper function of the proton pump. Moreover, Fe- and P-deficiency promote proton extrusion to acidify the medium which helps to solubilise more of these nutrients (Vance et al., 2003; Santi and Schmidt; 2009). In total, 11 H^+-ATPases, termed AHA1 to AHA11, contribute to generating the proton gradient in Arabidopsis (Baxter et al., 2003). *AHA1* and *AHA2* are considered the most important members of the *AHA* gene family (Haruta and Sussman, 2012). Santi and Schmidt (2009) showed that in Fe deficiency AHA2 is particularly important for rhizosphere acidification whereas AHA7 is needed for proper root hair proliferation in this condition. Single knockouts for the latter two genes (*aha2*, *aha7*) were therefore obtained and investigated here.

The analysis of K-, P- and Fe-related mutants presented in this chapter revealed a role for Fe homeostatic genes as well as the multicopper oxidases *LPR1* and *LPR2* in low-P and low-K signalling. The tissue- and intracellular localisation of LPR2 are reported and the potential of multicopper oxidases to mediate crosstalk between nutrient sensing and signalling pathways is discussed.

6.2 Results

6.2.1 Root architecture analysis of mutants impaired in K, P or Fe signalling and homeostasis

A set of knockout lines with known functions in K, P or Fe transport and signalling were tested for differential root architecture responses to low-K and low-P (Fig. 49; all raw data stored in the electronic appendix under *Ch6_Mutant Analysis*). To minimize germination effects, all genotypes were first grown on control medium for 3 days and subsequently transferred to control, low-K or low-P plates. In each condition, ANOVA was computed across all genotypes followed by pairwise comparisons (Tukey's t-test). For clarity, only significant differences ($p < 0.05$) between mutants and the wildtype (Col-0) are shown by asterisks in Fig. 49.

Compared to wildtype in control condition, total root size (TRS) was significantly reduced in several mutant lines (*aha2, akt1, cipk23, hak5, fer1-3-4, fro2, phr1, pho1, pho2*; Fig. 49A) but not elevated in any other. TRS was also significantly smaller in low-K for *akt1, cipk23* and *fro2*. For most genotypes, reduced main root length (*cipk23, pho1, pho2*), reduced lateral root length (*fro2*) or both (*akt1*; Fig. 49B, C) could account for this observation. For others (*aha2, hak5, fer1-3-4*), it was the combination of smaller, in itself not significant, effects on several root parameters that lead to overall TRS reduction. Whenever root architecture parameters were significantly decreased in control condition, data on responses of these parameters to low-K and low-P were treated with caution.

In low-P, increased TRS was surprisingly observed for the low-P sensitive mutant *pdr2*, caused by an extended lateral root system. The *pdr2* mutant has been described as having a particularly short main root in P-deficiency (Ticconi et al., 2009), but I could not confirm this phenotype in my experiments. On the contrary, *lpr1* had the longest main roots in low-P in accordance with previous reports (Svistoonoff et al., 2007). *LPR1* is a nice example for gene identification via QTL analysis followed by functional characterisation. The *lpr1* mutant was shown to have much longer main roots in low-P compared to the wildtype (Svistoonoff et al., 2007). As *lpr1* showed the same phenotype in my experiments, I was also reassured that the low-P conditions used here (20 µM NaH_2PO_4, as used before in Chapter 5) were adequate.

The least P- and K-sensitive genotype in terms of TRS, however, was *lpr2*. *LPR2* (*LOW PHOSPHATE ROOT 2)* is a close paralog to *LPR1* and it has been identified as a P-sensing component in the same study (Svistoonoff et al., 2007). Confirming published

results, *lpr2* main root growth was partly rescued in low-P, although slightly less than in the case of *lpr1* (Fig. 49B). However, *lpr2* also had significantly longer main roots in low-K (142 % of WT), whereas *lpr1* behaved like wildtype in this condition. Interestingly, the other genotypes with significantly longer main roots in low-K were knockouts for three heavy metal transporters, *NRAMP4*, *FPN1* and *FPN2* as well as the aforementioned P5-type ATPase *PDR2*, which works in conjunction with *LPR1* (Ticconi et al., 2009). All three Fe transporters are involved in intracellular Fe homeostasis and distribution (Lanquar et al., 2005; Morrissey et al., 2009). In contrast, mutation of genes involved in Fe acquisition either reduced overall root growth (see *fro2*) or had no significant effect (*irt1*, *fit*) in any of my conditions.

The only mutant with enhanced lateral root growth in low-K was *aha2* suggesting an involvement of the proton pump in lateral root elongation responses under low-K. Mutation of two K-related genes (*AKT1*, *CIPK23*) resulted in higher sensitivity to low-K. Mutation of systemic P-signalling components (*PHO1, PHO2, PHR1*) impacted on root growth in control condition, but the mutants were similar to wildtype in low-P or low-K.

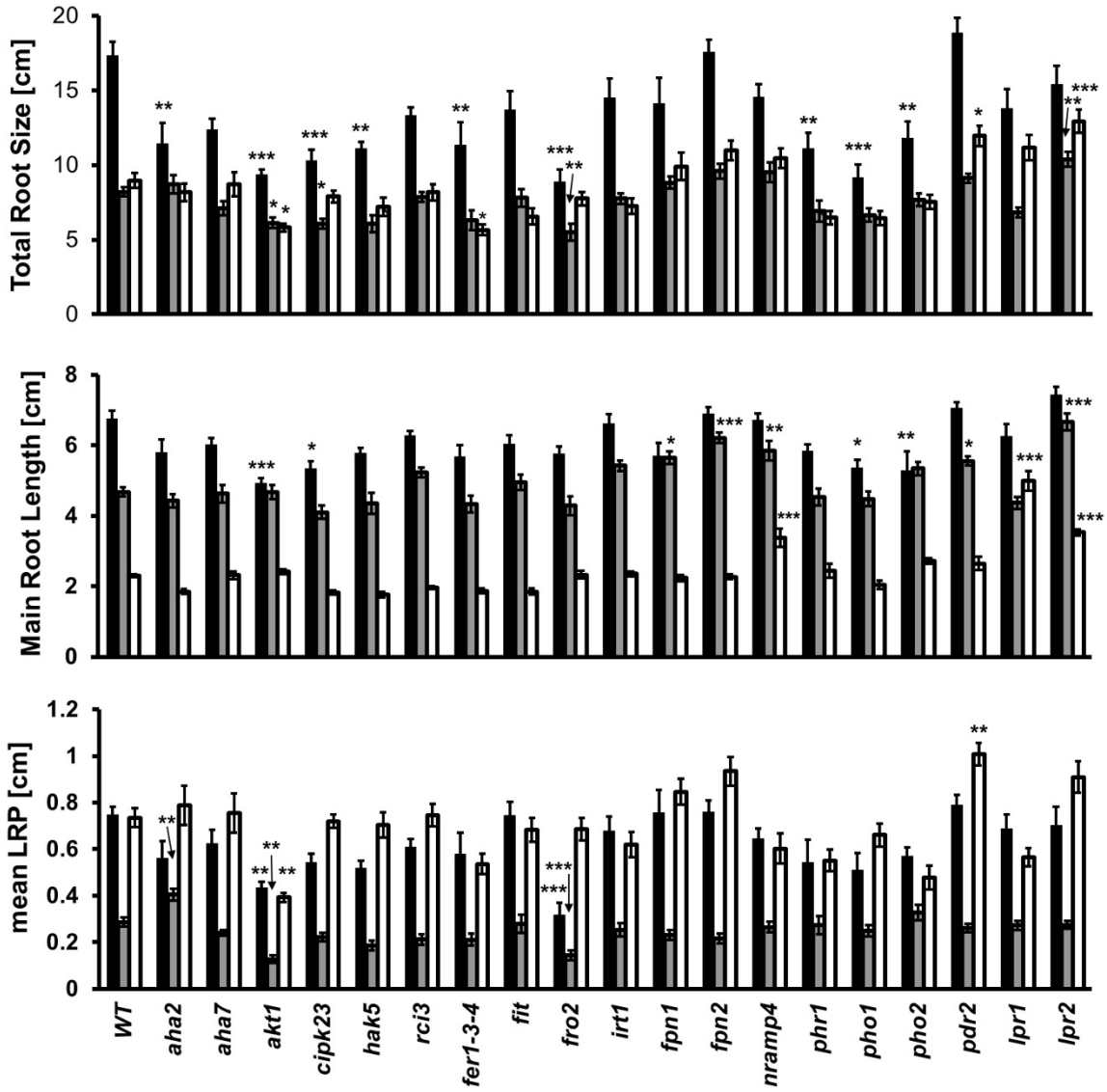

Figure 49: Root architecture analysis of K-, P- and Fe-transport and signalling mutants reveals a set of genotypes that differ in the phenotypic response to low-K and low-P.

Seedlings of all mutant lines and the wild type (Col-0) were grown on control (black bars), low-K (grey bars) and low-P media (white bars). Root architecture was quantified with EZ Rhizo 12 DAG. ANOVA was computed in each condition separately and statistically significant differences of genotypes compared to the wildtype determined via pairwise comparisons (Tukey's t-test). * $p < 0.05$; ** $p < 0.01$; *** $p < 0.001$. WT: wildtype (Col-0).

6.2.2 LOW PHOSPHATE ROOT 2 - an important signalling component in low-K

Partial rescue of main root growth in both low-P and low-K makes *LPR2* an interesting resource for the study of nutrient sensing and signalling crosstalk. To confirm the root phenotypes observed in the *lpr2* line (SALK_091930; Svistoonoff et al., 2007; in the following referred to as *lpr2-1*), I used two other homozygous T-DNA lines, termed *lpr2-3* (SALK_022690) and *lpr2-4* (SALK_061362).

Fig. 50 shows root architecture parameters normalised to control values within each genotype. ANOVA was computed within each condition and pairwise comparisons calculated between genotypes. Total root size was larger for all *lpr2* lines in low-P but also for two out of three lines (*lpr2-1*, *lpr2-4*) in low-K. All three lines also showed higher main root length in low-P and low-K. However, higher MR length was not statistically significant for *lpr2-3* ($p = 0.068$). Most notably, apical zone length was much less sensitive to low-K (and low-P) for all three *lpr2* lines and these results were consistently highly significant. In contrast, only minor variation occurred for LR number and LR density. As for LRP 0.25, all three *lpr2* genotypes had longer lateral roots than wildtype in low-P. In conclusion, although some variation occurred between the individual *lpr2* lines, all three lines displayed the same insensitivity of main root growth to low-K, suggesting that this phenotype is caused by a lack of LPR2 function. *LPR1* and *LPR2* were discovered simultaneously but only *LPR1* has been the focus of further characterisation (Svistoonoff et al., 2007, Ticconi et al., 2009; Wang et al., 2010a). Apart from phenotypic analysis of *lpr2* mutants in low-P, no further functional analysis of *LPR2* has been published so far. Based on amino acid sequence, LPR2 is a close paralogue to LPR1 (Svistoonoff et al., 2007). Since phenotypes in low-P and low-K are different between the knockouts of the two genes, I first tested whether the genes differed in tissue expression and/or intracellular localisations. For this purpose, I cloned the *LPR2* coding sequence as well as the *LPR2* promoter (2174 bp upstream of the start codon) and generated GUS- and GFP fusion constructs.

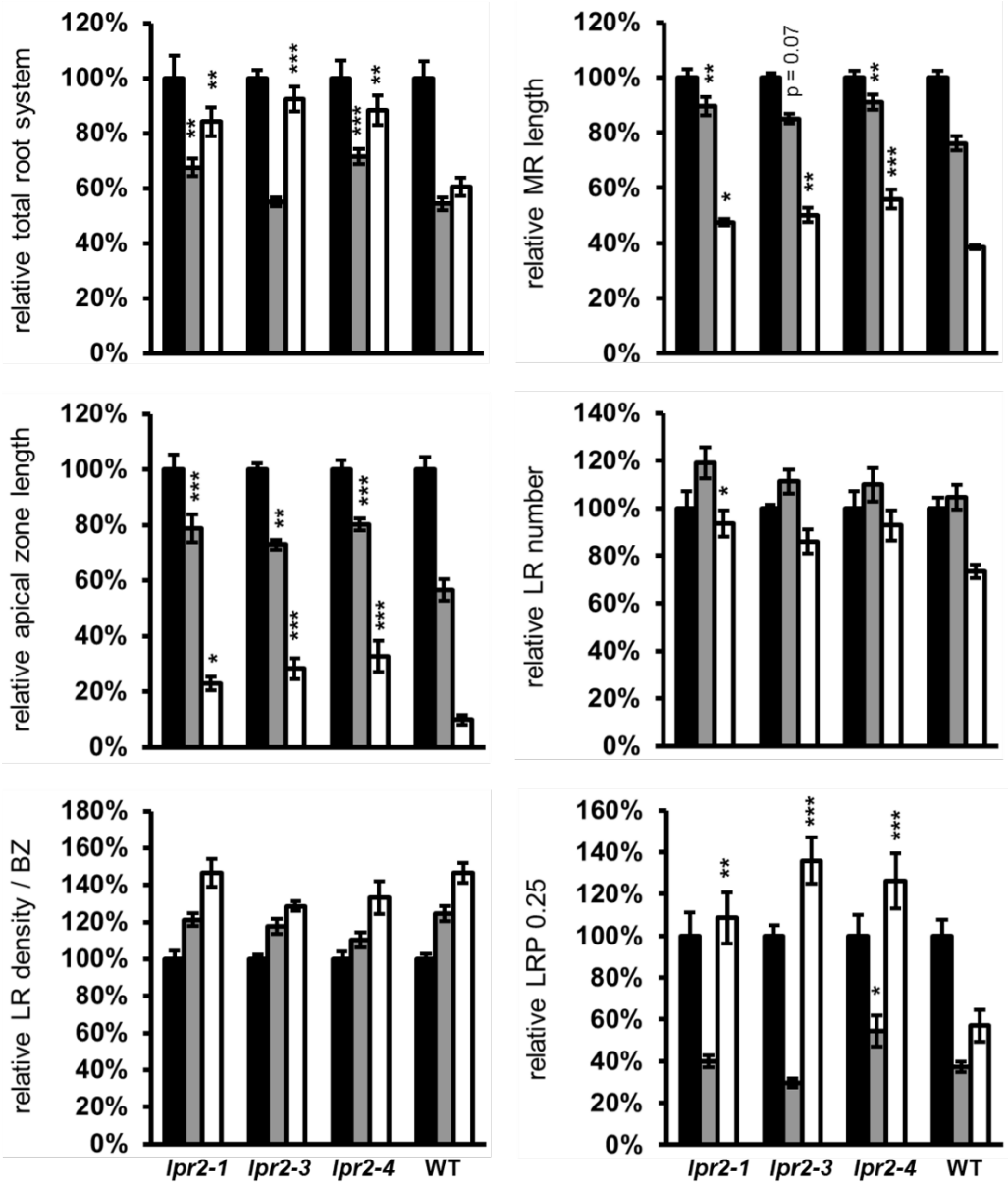

Figure 50: Confirmation of the low-K insensitive phenotype of *lpr2* with two additional *LPR2* knockout lines.
Two other homozygous T-DNA lines, termed *lpr2-3* (SALK_022690) and *lpr2-4* (SALK_061362), the original *lpr2* line (SALK_091930; now termed *lpr2-1*) and the wildtype (Col-0) were grown on control (black bars), low-K (grey bars) and low-P media (white bars). Root architecture was quantified with EZ Rhizo 12 DAG and parameters were normalised to mean control values within each genotype. Values shown are relative means ± S.E.M. (n = 10 to 18 seedlings per genotype per condition). ANOVA and pairwise comparisons (Tukey's t-test) were computed for each condition separately. Significant differences to the wildtype within each condition are denoted by asterisks: *** $p < 0.001$; ** $p < 0.01$; * $p < 0.05$. WT: wildtype (Col-0).
Absolute mean values ± S.E.M. for comparison in the order shown in the figure (*lpr2-1*; *lpr2-3*; *lpr2-4*, WT): total root system: 15.4 ± 1.2; 17.8 ± 0.5; 13.2 ± 0.8; 14.8 ± 0.9; MR length: 7.4 ± 0.2; 7.8 ± 0.1; 7.0 ± 0.2;6.0 ± 0.1; apical zone length: 3.1 ± 0.2 3.4 ± 0.1; 2.9 ± 0.1; 2.0 ± 0.1; LR number: 11 ± 1; 13 ± 0; 12 ± 1; 12 ± 1; LR density / BZ: 2.7 ± 0.1; 3.1 ± 0.1; 3.0 ± 0.1; 3.3 ± 0.1; LRP 0.25: 1.0 ± 0.1; 1.2 ± 0.1; 0.8 ± 0.1; 1.2 ± 0.1. An alternative version of this plot showing absolute values ± S.E.M. is shown in Appendix II.

The staining patterns of transgenic Arabidopsis lines (Col-0 background) stably expressing *pLPR2::GUS* (Fig. 51) indicate that *LPR2* is expressed throughout the root system, mainly in the central vasculature, but was notably absent from the elongation and differentiation zone. At the main root apex, a double peak of expression was observed around the apical meristem. GUS staining had another maximum at the root-shoot hypocotyl junction. In shoots, *pLPR2::GUS* was most active in leaf margin protrusions of cotyledons as well as true leaves. These are also the sites of auxin maxima and cell division along the leaf margin (Bilsborough et al., 2011; Wang et al., 2011b). In reproductive tissue, *LPR2* expression was detected in the vasculature of sepals, petals and stamen and in the pistil.

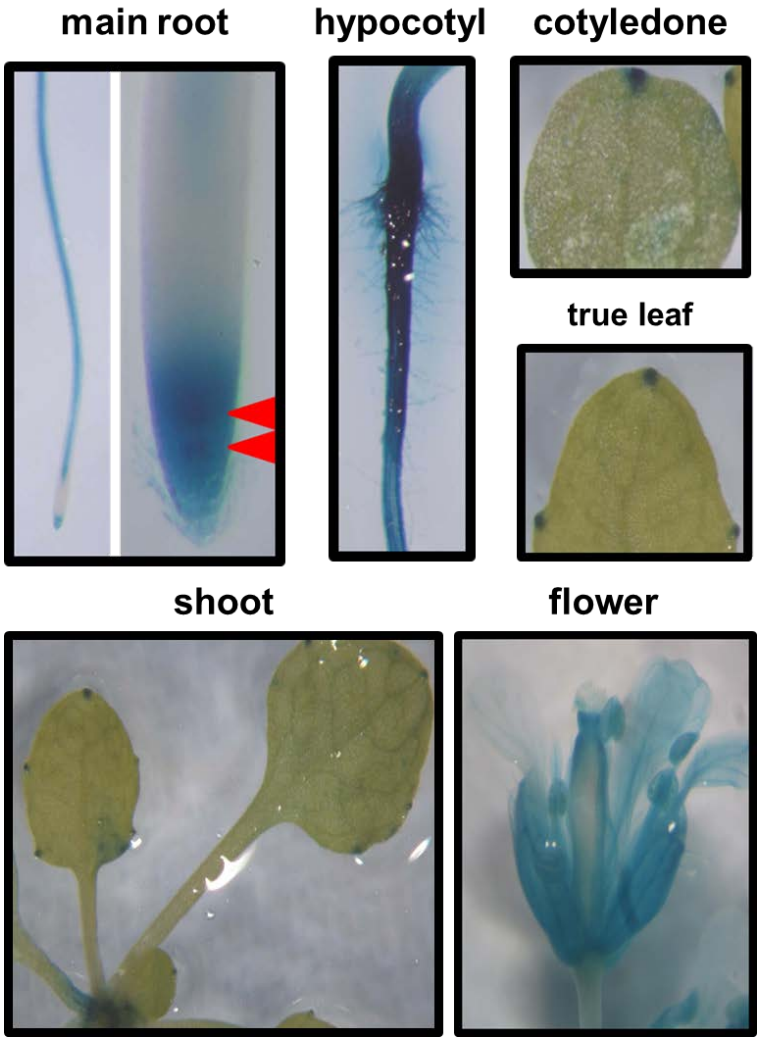

Figure 51: Tissue localisation of *LPR2* expression determined with promoter-GUS fusion constructs (*pLPR2:GUS*).
Wildtype Arabidopsis (Col-0) was stably transformed with *pLPR2:GUS* by floral dipping. Transgenic seedlings harbouring the construct were selected and GUS staining was performed on seedlings grown on agar plates (roots and shoots) and mature plants grown on soil (flowers).

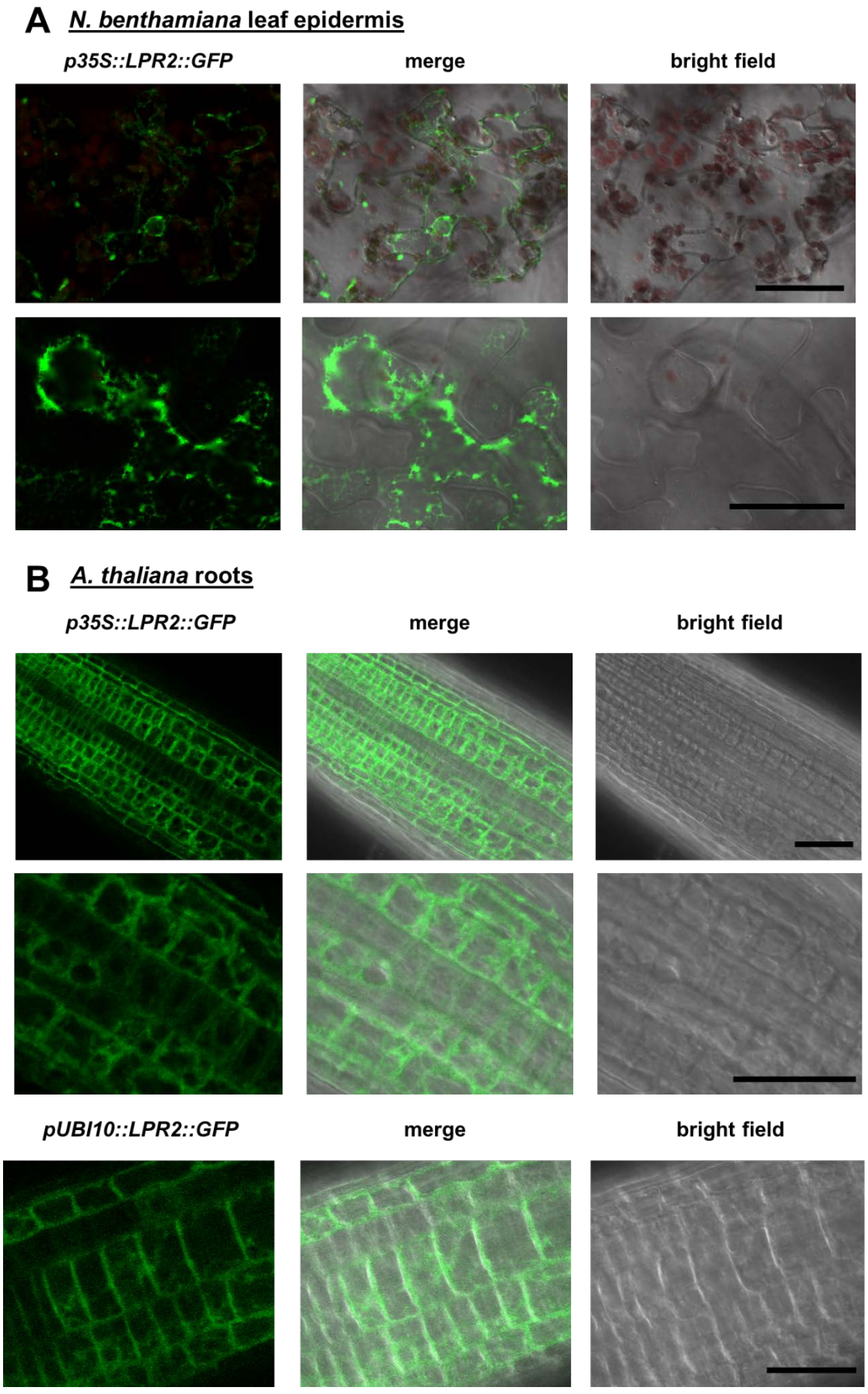

Figure 52: Intracellular localisation of LPR2.
please see next page for complete figure legend

Figure 52: Intracellular localisation of LPR2. **A)** Two examples of transient expression of *p35S::LPR2::GFP* in *Nicotiana benthamiana* leaf epidermal cells. **B)** *A. thaliana* was stably transformed with *p35S::LPR2::GFP* and *pUBI10::LPR2::GFP* by floral dip. Images shown are from offspring of T1 transformants selected with hygromycin (*p35S*) or BASTA® (*pUBI10*). Scale Bars: 50 µm.

Intracellular localisation of LPR2 was investigated by generating LPR2-GFP fusion constructs and expressing them in heterologous (*Nicotiana benthamiana*) and homologous (*A. thaliana*) systems. Transient expression of *p35S::LPR2::GFP* in *Nicotiana benthamiana* leaf epidermis suggested expression in the endoplasmic reticulum (Fig. 52A). This was confirmed by transiently co-expressing *p35S::LPR2::GFP* and *p35S::LPR2::RFP* with subcellular markers (Fig. 53). Here, qualitative and quantitative analysis of co-localisation with several endomembrane markers showed highest correlation with localisation of the composite construct *secYFP::HDEL*. This fusion construct is comprised of YFP targeted to the secretory pathway via an N-terminal signal peptide (*secYFP*; compare Karnik et al., 2013), which is retained in the ER due to the C-terminal HDEL motif (compare Gomord et al., 1997). Quality and resolution of confocal images obtained from Arabidopsis seedlings stably transformed with *p35S::LPR2::GFP* and *pUBI10::LPR2::GFP* were not as good as for *N. benthamiana*. Nevertheless the fluorescence patterns confirmed localisation to the ER (reticular structure; nuclear envelope; Fig. 52B).

In summary, LPR2 is localised in the ER as its paralogue LPR1 (Fig. 52, 53; Ticconi et al., 2009). Tissue expression patterns of both genes also agree partially, since both genes are expressed at the apical meristem (Fig. 51; Svistoonoff et al., 2007). A closer look revealed that *LPR1* is expressed within the quiescent centre and the root cap (Svistoonoff et al., 2007), and that *LPR2* may have two maxima of expression just around the QC (Fig. 51). Whereas no further expression patterns of *LPR1* were reported, I could also show that *LPR2* expression occurs inside the vasculature of the root and flowers, at the hypocotyl junction, and in leaf margin protrusions. So LPR2 seems to be active at sites of cell division (root apical meristem; leaf margin protrusions) and nutrient/water distribution (vasculature).

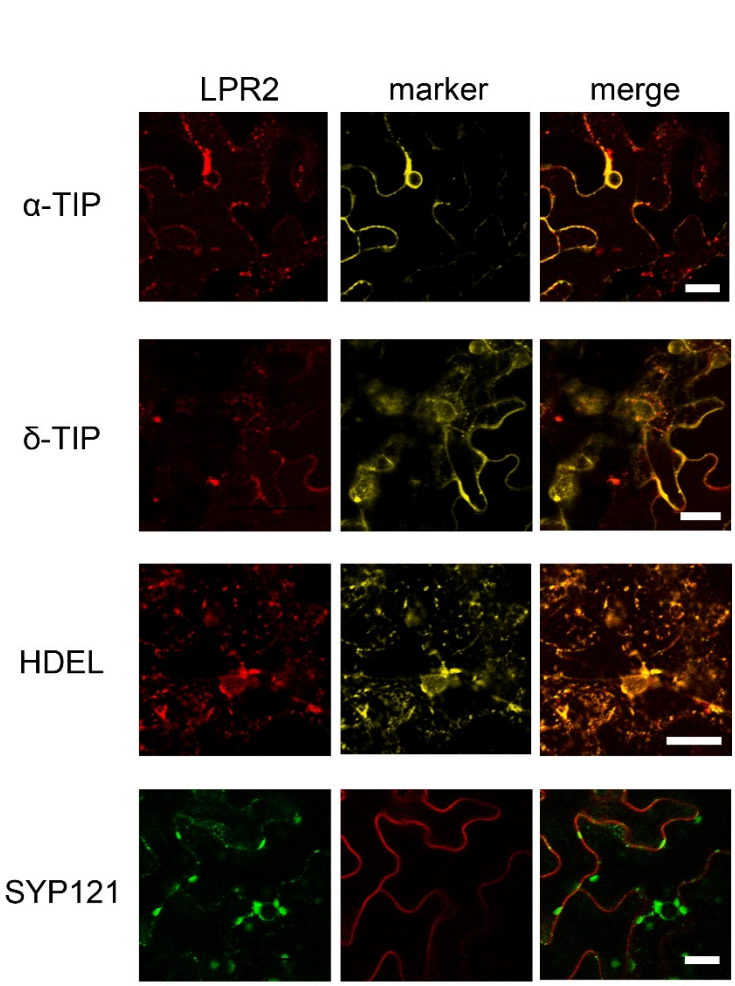

Figure 53: Co-localisation of LPR2-RFP and LPR2-GFP with subcellular markers indicates expression in the endoplasmic reticulum (ER).
Upper three panels: *p35S::LPR2::RFP* and was transiently co-expressed in *N. benthamiana* leaf epidermis cells with subcellular markers**:** *p35S::secYFP-HDEL* as an ER-marker (*secYFP*: N-terminal secretion peptide preceding YFP, targets YFP for the secretory pathway [Karnik et al, 2013]; *HDEL*: sufficient ER-retention signal [Gomord et al., 1997]); *p35S::alpha-TIP::YFP* as a marker for protein storage vesicles and autophagosomes (Jauh et al., 1999; Moriyasu et al., 2003) and *p35S::delta-TIP::YFP* marking storage vacuoles (Jauh et al., 1999).
Lower panel: *p35S::LPR2::GFP* was co-expressed with *p35S::SYP121::RFP* as a plasma membrane marker (Grefen et al., 2010). Representative images of LPR2-constructs are shown on the left and corresponding marker images are shown in the mid panel.
Co-localisation co-efficients (Pearson's R, Manders M1 and M2 co-efficients) were calculated from images of independent cells with the JaCoP plugin for Image J. (n = 6 to 10 images per condition; S.E.M in brackets). Bars: 50 µm.

6.2.3 Preliminary evidence that mutation of **LPR1** *and* **LPR2** *alters Fe accumulation patterns in the main root apex*

The data presented in Chapter 5 suggested that Fe(III) deposition at the main root apex causes the reduction of MR elongation in low-K. A logical question was, whether the relative insensitivity of *lpr2* was due to altered Fe accumulation at the root tip. Perls' staining was the first, quick method of choice. Fig. 54 shows representative images of stained MR tips. Although low-K induced Fe deposition was still apparent in *lpr2-1*, the pattern had changed. Fe accumulation appeared as a 'double peak' around the apical meristem. Comparative false colouring of the staining intensity with Photoshop suggested a slight shift of both peaks away from the centre of the wildtype peak (Fig. 54A). Unfortunately, time only permitted a single run of *lpr2-1* roots at the synchrotron X-ray facility. The image obtained from *lpr2-1* in low-K also showed a double peak. Fe(III) staining performed directly on plates by overlaying seedlings on the agar surface with staining solution further confirmed the 'double peak' in all three *lpr2* mutant alleles (Fig. 54B). No double peak was seen in low-K grown *lpr1* mutants but Fe accumulation was confined to a much smaller area than in wildtype.

These preliminary results support the hypothesis of altered Fe distribution in mutants devoid of *LPR1* and *LPR2* expression (Fig. 54C). However, more SXRF data are needed to back up this result.

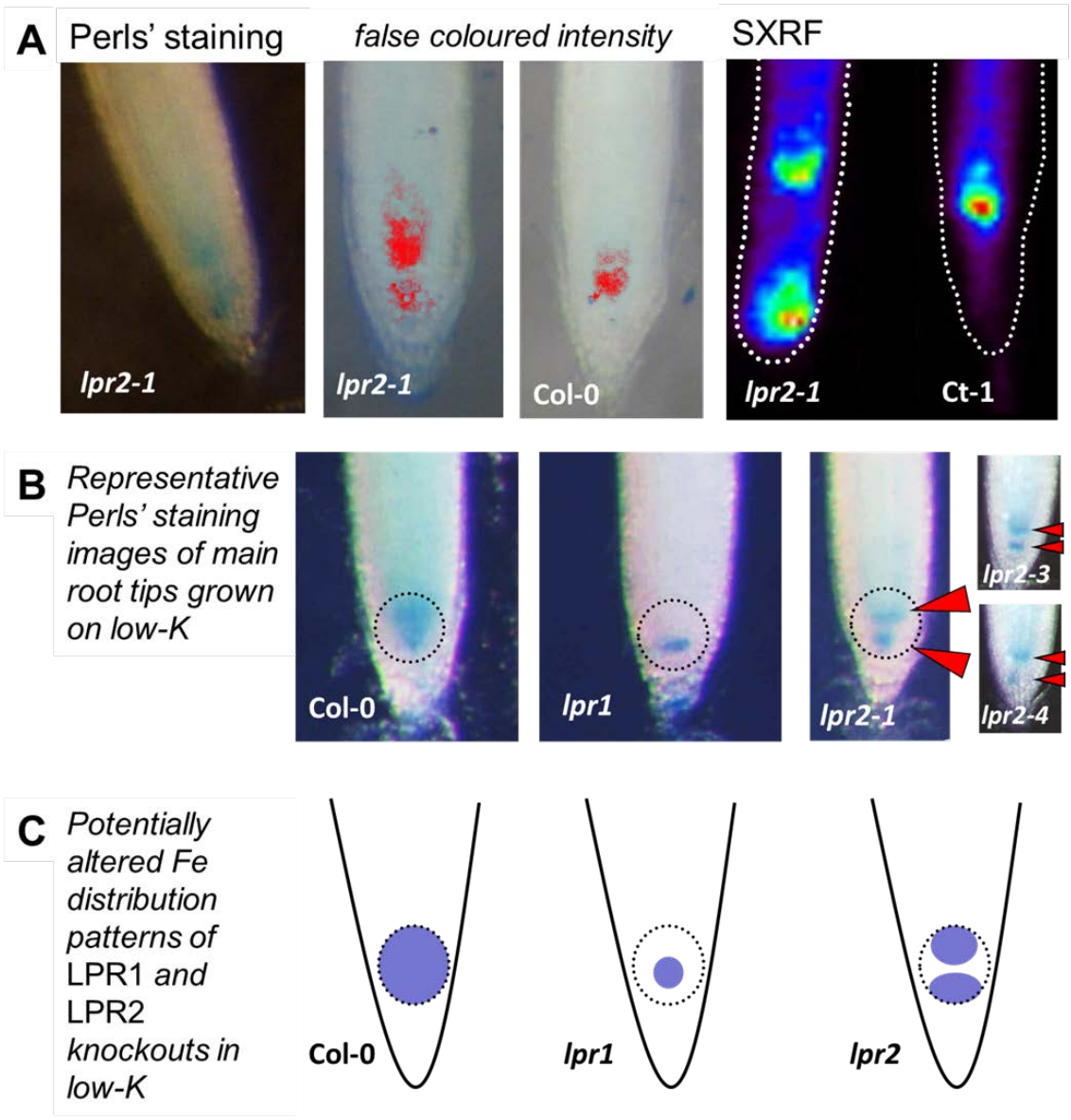

Figure 54: Preliminary staining and imaging data suggests altered Fe distribution in *lpr1* and *lpr2* knockout lines.
A) From left to right: Perls' staining of *lpr2-1* main root tips; false colouring of Perls' staining intensity of *lpr2-1* and Col-0 wildtype root tips with Photoshop; SXRF images showing Fe distribution in *lpr2-1* (root # 35 as per Table C5-02) and Ct-1 apices. **B)** Representative images of main root tips stained with the Perls' method directly on plates. Fe peaks were smaller in *lpr1* knockouts. *lpr2-1* showed a double Fe peak as in the images above (highlighted with red arrowheads). For comparison, *lpr2-3* and *lpr2-4* images are shown as insets on the right. All *lpr2* mutant alleles have a similar Perls' staining pattern. **C)** Schematic depictions of Fe distribution as observed above in (B).
All images were from main root tips of seedlings grown on low-K. Images shown are representative for usually at least 5 seedlings per genotype per condition. SXRF imaging of *lpr2-1* was only performed once.

6.2.4 Work in progress: generation of transgenic lines

By the end of my PhD project I had acquired evidence for the involvement of *LPR2* in low-K and low-P responses. Sequence analysis and functional characterisation of its paralogue *LPR1* suggest that both genes encode multicopper oxidases (MCOs; Svistoonoff et al., 2007). MCOs mediate redox reactions that couple the oxidation of various potential substrates to the reduction of molecular oxygen to water (Hoegger et al., 2006). Different subclasses of MCOs use different reducing substrates (Fig. 55). Interestingly, Fe^{2+} is the substrate of the ferroxidase subclass. Moreover, it has been suggested that some plant laccases might also be able to use Fe^{2+} as a substrate (Hoopes and Dean, 2004; Hoegger et al., 2006). This provides a direct potential link between MCO function and Fe accumulation, but to date it is unknown to which subclass *LPR1* and *LPR2* belong. Differential redox activities of LPR1 and LPR2 in low-K and low-P could explain their specific responses to the nutrients.

In order to enable the testing of these hypotheses in the future, I have started to generate transgenic plant material. In the following, I will briefly summarise the lines generated, their stage of propagation and their potential use.

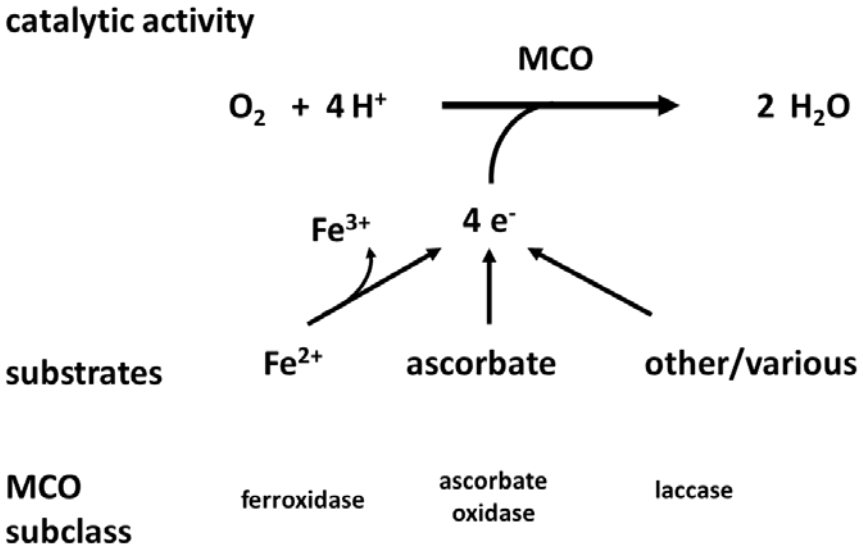

Figure 55: Overview of function and classification of multicopper oxidases (MCO).
In plants, three MCO subclasses have been described, each using a different substrate to reduce molecular oxygen (O_2) to water (Hoegger et al., 2006). To date, the subclass to which LPR1 and LPR2 belong has not been clearly determined.

LPR2 overexpression and complementation lines

The full length *LPR2* genomic sequence was put under the 35S and UBI10 promoter and introduced into Col-0 via floral dip to produce constitutive overexpression lines (*p35S::LPR2*; *pUBI10::LPR2*). I also transformed *lpr2-1* with the same constructs, to complement the knockout constitutively. These lines should be used for characterisation of the root phenotype and of Fe distribution patterns in various environmental conditions (e.g. low-K, low-P). By the time of the submission of my thesis several independent lines of all constructs and genotypes were available in T2 generation.

Redox sensitive GFP targeted to different cellular compartments in various genetic backgrounds

To directly quantify the redox state of individual living cells, a whole toolset has been developed that makes use of redox sensitive versions of GFP (Dooley et al., 2004; Meyer et al., 2007; Schwarzländer et al., 2008). The *roGFP2* version has been proven to be particularly suitable for plant purposes. I am very thankful to Dr Markus Schwarzländer (University of Bonn, Germany) who kindly provided three different *roGFP2* constructs, all driven by the constitutive 35S promoter but each containing different signal sequences that target the protein to different cell compartments: cytosol, endoplasmic reticulum (ER) or mitochondria (Meyer et al., 2007; Schwarzländer et al., 2008). I used these constructs to transform *lpr1*, *lpr2-1* and Ct-1 via floral dip. At the time of submission these lines were in T2 generation. In addition, I have also received stable Arabidopsis lines of all three *roGFP2* constructs in Col-0 background from M. Schwarzländer.

These constructs could be used in future experiments to directly monitor the redox status of cells in the apical meristem. Of particular interest will be the redox balance in the ER (compare *LPR1* and *LPR2* expression) under different conditions of K and P supply.

6.3 Discussion

6.3.1 Mutant analysis: P sensing vs. Fe homeostasis

Analysis of a set of mutants known to be involved in K, P or Fe signalling and homeostasis revealed a subset of lines that showed a differential response to low-K, low-P or both (Fig 49). Interestingly, two groups of mutants were set apart from the rest by being less sensitive to K- and/or P-starvation: 'P sensing' genes and 'Fe homeostatic' genes (Table 27). Genes belonging to the 'P sensing' group have previously been shown to be involved in local P sensing at the main root tip (Svistoonoff et al., 2007; Ticconi et al., 2009).

Table 27: Two groups of genes for which mutants showed weaker responses of root architecture to low-P and/or low-K.

			increased length in		genes
Group	**Gene**	**Function**	**low-K**	**low-P**	**described in**
P sensing	*LPR1*	Multicopper oxidase; P sensing	-	main root	Svistoonoff et al., 2007
	LPR2	Multicopper oxidase; P sensing	main root	main root	Svistoonoff et al., 2007
	PDR2	P5-type ATPase	main root	lateral roots	Ticconi et al., 2009
Fe homeostatic	*FPN1*	Fe loading into the xylem	main root	-	Morrissey et al., 2009
	FPN2	Fe sequestration into the vacuole	main root	-	Morrissey et al., 2009
	NRAMP4	Fe remobilisation from the vacuole in seeds	main root	main root	Lanquar et al., 2005

Although I could not confirm the hypersensitive main root (MR) response of the *pdr2* mutant (*PDR2*: *PHOSPHATE DEFICIENCY RESPONSE 2*) to low-P (Ticconi et al., 2009), I observed an increased lateral root (LR) system in this mutant. However, compared to Col-0, *pdr2* had relatively longer MRs in control and the expansion of the LR system may be indirect evidence for higher sensitivity of the MR (analogous to Ct-1 in low-K: slowdown of MR elongation precedes LR elongation). Nevertheless, *pdr2* main roots appeared to be less sensitive to low-K. *PDR2* was genetically shown to work in

conjunction with *LPR1* (*LOW PHOSPHATE ROOT 1*), mediating the local response of P-deficiency sensed at the MR tip (Ticconi et al., 2009). To date, the exact mechanism behind this response is not clear but Ticconi et al. (2009) argued for a common regulatory pathway via several lines of evidence. First, the expression domains of *PDR2* and *LPR1* overlap in the stem cell niche (quiescent centre; QC) and the distal meristem at the main root apex, where PDR2 is necessary for proper *SCARECROW* (*SCR*) expression. SCR is a nuclear localised transcription factor that is essential for keeping the QC in an undifferentiated state and hence controls meristem function and cell patterning. Second, both genes are expressed in the endoplasmic reticulum (ER). And third, the *lpr1 lpr2 pdr2* triple mutant was shown to be as insensitive to low-P as the *lpr1 lpr2* double mutant, whilst *pdr2* was highly sensitive to low-P in their study. The latter supports an epistatic role of the two multicopper oxidase genes *LPR1* (*LOW PHOSPHATE ROOT1*) and *LPR2* (*LOW PHOSPHATE ROOT2*) over *PDR2* (Svistoonoff et al., 2007; Ticconi et al., 2009). My results suggest that *LPR1* is a central regulator of low-P responses and *LPR2* is important in both low-P and low-K. Unfortunately, I did not have a chance to look at the *lpr1 lpr2* double or *lpr1 lpr2 pdr2* triple mutant. These lines lines have now been obtained and represent an indispensable resource to further dissect the contribution of each component to single and multiple P- and K-starvation.

The second group of mutants that showed weaker root responses to low-K and/or low-P, consisted of Fe homeostatic genes. All three genes are involved in either vacuolar Fe storage or root-to-shoot Fe distribution. This argues against a hypothetical scenario in which Fe toxicity is caused by excessive uptake at the site of Fe accumulation, i.e. main root tip. In addition, Fe transport mutants (*irt1* and *fro2*) behave like wildtype. Phenotypes of knockouts belonging to the 'Fe homeostatic' group rather favour an alternative mechanism of Fe accumulation: an internal shift of source-sink relationships concerning Fe distribution in low-K (and low-P), since both ferroportins (FPN1 and FPN2) and NRAMP4 are involved in intracellular Fe transport (Lanquar et al., 2005; Morrissey et al., 2009). Based on the phenotype observed for *nramp4*, it could be argued that *NRAMP4* may indeed fulfil an additional function in mature plants, as proposed by Thomine and Lanquar (2011). Its function may lie in the adjustment of Fe distribution in nutrient stress situations.

6.3.2 Multicopper oxidases LPR1 and LPR2 regulate root responses to P- and K-starvation

The two paralogous multicopper oxidase (MCO) genes *LPR1* and *LPR2* partly overlap in tissue expression patterns at the main root apex (Fig. 51; Svistoonoff et al., 2007). They also share the same intracellular localisation within the ER (Fig. 52, 53; Ticconi et al., 2009). No detailed data on *LPR1* tissue expression outside the main root tip was available, but eFP Browser data highlights predominant expression in flowers (Winter et al., 2007). For *LPR2*, I could also show expression in the vasculature, reproductive tissue as well as leaf margin protrusions (Fig. 51). Interestingly, the latter structure at the edge of the Arabidopsis leaf is the site of auxin maxima and cell division (Bilsborough et al., 2011; Wang et al., 2011b), just like the apical meristem of the root (Kepinski and Leyser, 2005).

In a comparative study of all 17 Arabidopsis MCOs of the laccase subgroup (*LAC1* to *LAC17*), 14 have been shown to be expressed in roots (Turlapati et al., 2011). Most of them were expressed in vascular tissues, but *LAC3*, *LAC4* and *LAC8* were also localised to the root cap and meristematic zone. Moreover, *LAC7* was mainly expressed in leaf margin protrusions (or hydathodes) in shoots.

Preliminary Fe staining results of *lpr1* and *lpr2* knockouts (several alleles *lpr2-1*, *lpr2-3*, *lpr2-4*; Fig. 54) suggest an altered pattern of Fe accumulation at the root apex. Together, these data indicate, that both multicopper oxidases are important in regulating meristem activity and in adjusting it to external cues.

As far as Fe homeostasis is concerned, MCOs have been shown to be important for Fe uptake in bacteria (Huston et al., 2002), yeast (Askwith et al., 1994), green algae (Herbik et al., 2002) and insects (Lang et al., 2012). Although further functional data on either of the MCO proteins (e.g. interaction, substrate usage) is needed for proof, it could be speculated that LPR1 and LPR2 also use Fe as a substrate, at least partially. This might explain the altered Fe accumulation patterns in respective mutant lines (Fig. 54). MCO function of LPR1 has been demonstrated by oxidising the test compound ABTS (2,2'-azinobis[3-ethylbenzothiazoline-6-sulfonate]) with total protein extracts from yeast producing the protein (Svistoonoff et al., 2007). ABTS is a typical laccase substrate (Hoegger et al., 2006), but ferroxidase activity was not tested and at least one plant laccase-like MCO has been demonstrated to have ferroxidase function (Hoopes and Dean, 2004).

Assuming ferroxidase activity for LPR2, another problem arises: Why do Fe accumulation patterns of the *lpr2* knockout match with the actual *LPR2* expression patterns as shown via *pLPR2:GUS* staining (cf. double peaks in the meristem)? If LPR2 were to produce the Fe deposits there should be double peak in situations where LPR2 is active but not in the knockout. Although it seems rather unlikely, it cannot be ruled out that LPRs also facilitate the reverse reaction of the reaction shown in Fig. 55, reducing Fe^{3+} to Fe^{2+} and using up another substrate in the process. However, the key may lie in a multicatalytic function of LPRs.

Svistoonoff et al. (2007) proposed, that LPR proteins modify the activity or distribution of a hormone-like substance. Given that *LPR2* is expressed in areas of auxin maxima (main root apex, leaf margin protrusions; Fig. 51), one could go a step further and hypothesize a direct modification of auxin signalling by LPR2, consequently inducing alterations of root meristem activity and differentiation (Stahl and Simon, 2010). The origin of Fe deposition would then lie somewhere upstream of LPR function, but would probably still require some sort of redox process, e.g. involving reactive oxygen species (Thomine and Lanquar, 2011).

So far I can only speculate on the function of *LPR1* and *LPR2* in mediating root architecture responses to low-P and low-K. Now, at the end of my PhD project, I would like to leave the reader with a few potential experiments that may shed further light on the role of multicopper oxidases in P- and K-starvation.

6.3.3 Future work

The first aim should be to investigate the low-K phenotype and Fe distribution in the *lpr1 lpr2* double mutant, and if possible also in the *lpr1 lpr2 pdr2* triple.

Improved Fe staining (Perls' and Turnbull's) with higher resolution would help in further narrowing the sites of Fe accumulation in low-K (meristem vs. root cap and elongation zone) but also in low-P (patches: intra- vs. extracellular Fe). To do that, access to a better light microscope plus the ability to stabilise light intensities at the camera would be essential. Focus should also lie on SXRF imaging of wildtype and mutant root apices in different environments. Imaging of another set of plants by Dr Tracy Punshon has already been arranged for summer 2013.

By the end of my PhD project, I have developed transgenic lines expressing *LPR2* driven by 35S and UBI10 promoters in Col-0 and *lpr2-1* backgrounds. They should be first

tested for differential phenotypes in low-K and/or low-P and could then also be used for imaging.

Direct evidence of LPR1 and LPR2 redox activity and their substrate specificity (e.g. laccase substrates, Fe^{2+}, Fe^{3+}) should be tested by in vitro assays. For a start, Gateway® compatible *LPR2* entry clones are immediately available to produce expression vectors with respective tags for protein purification (GST or HIS-tag). The full length sequence of *LPR1* needs to be cloned from genomic DNA first.

Last but not least, I have generated stable lines expressing the redox sensitive GFP-version *roGFP2* driven by the 35S-promoter and targeted to the cytosol, the ER or mitochondria (Dooley et al., 2004; Meyer et al., 2007; Schwarzländer et al., 2008). All three constructs were transformed into Ct-1, *lpr1* and *lpr2-1*. Stable lines in Col-0 background were kindly provided by M. Schwarzländer. Confocal imaging now allows for comparative analysis of the redox status within e.g. the apical meristem of these genotypes in different conditions (control, low-K, low-P). This will enable a direct measure of the involvement of redox processes controlled by either LPR1 or LPR2 in low-K and low-P responses. Moreover, it will facilitate further characterisation of the low-K strategy II response in Ct-1.

7. General Discussion

7.1 Summary

Plant roots translate a multi-factorial input of environmental cues, like concentrations of bioavailable mineral nutrients in the soil, into a multi-factorial developmental output. Whenever nutrient scarcity is encountered, a targeted proliferation of certain root organs enables the plant to counteract deficiency symptoms with optimised foraging strategies. At the same time, preferential growth inhibition in some parts of the root allows channelling of limited resources into other parts of the root. The resulting overall root system architecture (RSA) is a visible manifestation of a plant's life history belowground. Thus, RSA is a viable and quantifiable reporter system to investigate nutrient stress. By combining RSA analysis with the powerful genetic tools of Arabidopsis, I have set out to unravel nutrient sensing and signalling components that underlie environmental plasticity of root architecture with particular focus on K and on interactions between N, P, K and S.

To provide a quantitative framework of root responses to multiple environmental stimuli, I have initially measured a comprehensive set of RSA parameters in 16 binary combinations of sufficient/deficient nitrate (N), phosphate (P), potassium (K) and sulphate (S) supply in 2 light conditions. Analysis of variance showed that each RSA parameter was determined by a distinct relative contribution of individual environmental inputs. This experimental setup also enabled the creation of a nutrient response *priority list*. For example, P starvation overrides all other nutrients responses as far as the main root is concerned. A true novelty lay in the identification of environmental interactions with profound effects on root architectural parameters, amongst others N and day length, N and P or P and K. Patterns of phenotypic responses could be correlated with distinct nutrient response signatures of co-expressed genes. Unravelling the effects of nutrients and nutrient interactions on specific RSA parameters allowed the generation of hypotheses on the involvement of known signalling components in respective nutrient starvation responses. Using reverse genetics, I was able to identify two new signalling modules involving CIPK23, AKT1 and NRT1.1 that integrate K and N effects on higher order lateral root branching and main root angle.

With a dry matter content of up to 10 %, K is the quantitatively most important cationic nutrient. Hence it was no surprise that in addition to known effects of N and P, K

also emerged as an important factor controlling root architecture in my initial experiments. However, no systematic analysis of root growth responses to K deprivation had been reported so far. Within-species variation is routinely used to look for aberrant phenotypes and to subsequently correlate phenotypic differences with allelic polymorphisms of the genotypes in question, e.g. via quantitative trait loci (QTL) analysis. I have used a set of natural Arabidopsis accessions to investigate root architecture responses to low-K. A phenotypic gradient linked two extreme strategies of morphological low-K adaptations (Kellermeier et al., 2013). This gradient was based on a major trade-off between main root (MR) and lateral root (LR) elongation. S*trategy I* accessions maintained MR growth but compromised LR elongation, whereas *strategy II* genotypes arrested MR elongation in favour of lateral root emergence and elongation. QTL analysis of low-K responses in a recombinant inbred line population derived from two accessions, adopting either strategy I (Col-0) or II (Ct-1), identified genomic loci that controlled environmental plasticity of particular subsets of root architectural parameters. Comparison with other QTL analyses furthermore suggested the existence of genomic hubs that integrate multi-elemental nutrition with growth of specific root organs.

The Ct-1 phenotype in low-K strongly resembled the low-P phenotype of Col-0. In the past, main root growth arrest in low-P has been connected with iron (Fe) toxicity (Ward et al., 2008). I detected increased shoot Fe content in low-P in initial experiments. $[Fe]_{shoot}$ was even higher in P-K (and N-P) double deficiency. By varying Fe concentrations in growth media and by direct quantification of Fe abundance in planta, I could show that low-P and low-K responses were both dependent on external Fe. In fact, main root growth was restored in low-P and in low-K as well as in P-K double deficiency when external Fe concentrations were reduced. Synchrotron X-ray fluorescence and histochemical staining techniques revealed accumulation of Fe in both deficiencies, albeit in different root zones and tissues. In low-K, Fe^{3+} accumulation coincided with cell death in the apical meristem of the main root, especially in the low-K sensitive accession Ct-1. Analysis of K, P and Fe transport and signalling mutants suggested that low-K and low-P phenotypes are at least partly regulated by two processes: first, heavy metal transporters promote intracellular Fe re-distribution; second, redox signalling at the root tip conferred by a pair of paralogous, ER-localised multicopper oxidases, LPR1 and LPR2, connects P-, K- and potentially Fe-availability with meristem function.

In sum, the study presented here addressed the fundamental question of how environmental conditions interactively modulate complex developmental programs that

shape root system architecture. Novel phenotypes of nutrient starvation were identified and underlying regulatory elements have been investigated via targeted and non-targeted genetic approaches. In depth analysis revealed the co-regulation of P- and K-responses by analogous physiological reactions and shared signalling pathways.

7.2 Challenges in root phenotyping

In the past decade, root system architecture has been recognized as an essential fitness trait that enhances nutrient uptake and enables plants to deal with environmental stresses, such as drought and nutrient shortage, and thus constitutes a key trait for historic advances in crop breeding for higher yield (Hammer et al., 2009; Den Herder et al., 2010; Zhu et al., 2011). Significant efforts have been undertaken to increase the quality and quantity of root phenotypic data by implementing high-throughput phenotyping methods (reviewed in Mooney et al., 2012) as a basis for breeding and gene identification. Many techniques are based on artificial, solidified growth media where RSA is projected onto a 2D surface (Armengaud et al., 2009b; French et al., 2009; Brooks et al., 2010; Wells et al., 2012; Clark et al., 2013). Alternatively, seedlings are cultivated in gel tanks so that root systems are able to spread in 3 dimensions (Fang et al., 2009; Iyer-Pascuzzi, 2010; Clark et al., 2011). Root growth in soil can be monitored via rhizotrons (Neumann et al., 2009) or traditionally by unearthing whole root systems via so called ‘shovelomics’ (Trachsel et al., 2011). With high-end equipment, it is now also possible to reconstruct RSA of living root matter grown in soil or sand via X-ray microcomputed tomography (Mairhofer et al., 2012; Mairhofer et al., 2013).

Of course each method has its benefits and drawbacks. Agar based systems are easy to handle, and thus bear the potential for high-throughput analysis, but constitute a somewhat unphysiological growth environment. X-ray tomography on the other hand enables phenotyping in a natural scenario but is limited by cost and time. An interesting solution is the development of ‘transparent soil’ consisting of Nafion particles immersed in a nutrient solution of similar optical density (Downie et al., 2012). This platform seems particularly suitable for studying interactions between roots, soil and microorganisms.

When designing the first experiments it was clear that only high-throughput systems are feasible for screening large amounts of plants in many different conditions. Hence, I adopted an agar plate system and customized it to my needs (Kellermeier and Amtmann, 2013). To speed up growth and to limit the impact of light intensity fluctuations inside the growth chamber, I added 0.5 % sucrose to all of my media. It has been shown

that sucrose can leak into shoots sticking to the agar surface and that this can have a large influence on RSA (MacGregor et al., 2008). I avoided this effect by removing the top 2 cm of agar. Still, a major shortcoming of the plate system is the direct illumination of roots with light (Yokawa et al., 2013).

Very recently, Xu et al. (2013) have reported an 'improved agar-plate culture system' where addition of sucrose is omitted and root illumination is eliminated by shading the bottom half of the plate. They emphasize that the resulting RSA is significantly different from that of 'traditional agar-plate culture systems'. However, their setup is custom made and needs considerably more time to produce and recycle (e.g. washing, sterilisation, etc.). It has been shown that main root growth rates are higher in the dark than the light period of seedlings grown in long day (Fisahn et al., 2012). Albeit initially testing both long and short day conditions for root architecture responses to nutrient supply, I used short day conditions for all experiments investigating low-K and low-P responses. Root systems were partly shaded by placing agar plates in boxes and hence some effects of direct root illumination could be overcome (partial shading was evident by longer hypocotyls). Apart from light, Fisahn et al. (2012) speculate on the effect of the gravitational force elicited by the interplay of solar and lunar movements, i.e. the lunisolar tidal force. This is an interesting environmental factor to be considered, because it is present and changing all the time. In fact, the ANOVA analysis showed that a considerable proportion of the RSA variation could not be accounted for by the factors controlled in my experiments. While part of this variation could be stochastic some of it could be due to factors that were not controlled.

7.3 The role of genomic hubs in regulating root plasticity

By analysis of a whole set of root architectural parameters in multiple nutrient conditions, I could clearly demonstrate that distinct parts of the root system respond to the presence or absence of specific nutrients or nutrient combinations, even at the seedling stage. Moreover, QTL analysis of low-K responses revealed clusters of root traits that were co-regulated by common genomic loci (Kellermeier et al., 2013). Dissecting the root system into its subparts is therefore not only technically worthwhile (compare the potential of apical zone length as a stronger reporter of the main root response to low-P and low-K) but probably also resolves the sophisticated mechanisms that fine-tune growth in complex environmental situations with higher resolution.

Multivariate statistical analysis performed on quantified root parameters separated natural accessions according to so far largely neglected phenotypic traits, like the main root angle (Armengaud et al., 2009b; Kellermeier et al., 2013). QTL analysis of 3-dimensional rice root architecture has also pinpointed genomic hotspots that regulated more than one trait at a time, in different combinations (Topp et al., 2013). Similarly, Prinzenberg et al. (2010) have identified hotspots with overlapping QTL for shoot and root growth as well as tissue content of multiple elements in three environmental conditions (control, low-K and low-P). Unfortunately, in that study growth-related traits were limited to leaf area, relative leaf growth rate and 'root length' estimated from stretched out root systems of 32 day old plants cultivated in hydroponics.

Studies on dissected root architecture are just beginning to emerge. Some first steps have been taken by genetically mapping all individual traits (Kellermeier et al., 2013; Topp et al., 2013) or statistically transformed root data (e.g. root architecture expressed by principal component analysis; Topp et al., 2013). At the same time, many QTL studies have identified similar genomic regions that are responsible for natural variation of root growth (Fitz Gerald et al., 2006; Reymond et al., 2006; Prinzenberg et al., 2010; Kellermeier et al., 2013) and/or mineral homeostasis (Rauh et al., 2002; Vreugdenhil et al., 2004; Harada and Leigh, 2006; Buescher et al., 2010; Prinzenberg et al., 2010), suggesting an essential role of these *genomic hot-spots* or *genomic hubs* in enabling the plant to integrate growth and mineral nutrition via environmental plasticity.

Most of the underlying 'hub genes' however, have to my best knowledge not been identified yet. Surely, their central position make these hubs very interesting targets for improving plant growth in nutrient limiting conditions. I would therefore like to encourage the use of genomic resources like RILs, HIFs and whole genome sequences of natural accessions (cf. genome wide association mapping) to intensify the search for these hubs.

7.4 Root architecture in multi-factorial environments

Studying root architecture in a binary, combinatory system of sufficient and deficient N, P, K and S supply allowed to capture the effect of important macronutrient *interactions* on root growth (for effects of individual nutrients please compare results and discussion in Chapter 3). To date, research on nutrient interactions had mainly focussed on specific pairs of nutrients. Physiological and phenotypic consequences were evaluated for different nitrogen sources, e.g. nitrate, ammonium and glutamate (Bloom et al., 2002; Walch-Liu and Forde, 2008; Helali, 2010; Patterson et al., 2010), and carbon-nitrogen

interactions (Zhang et al., 1999; Malamy and Ryan, 2001; Little et al., 2005; MacGregor et al., 2008; Roycewicz and Malamy, 2012). Nitrogen and sulphur were shown to be linked metabolically (Hesse et al., 2004) as both elements are incorporated into amino acids and secondary metabolites. Ammonium nutrition improved phosphate uptake in rice which copes well with NH_4^+ as a sole nitrogen source (Kronzucker et al., 1999; Zhu et al., 2009), probably by altering the external pH and thus the proton gradient across the plasma membrane needed for P transport (Zeng et al., 2012). With regard to cation balance, several studies assessed the interplay of K nutrition and salinity (Maathuis and Amtmann 1999; Wu et al., 2009; Nieves-Cordones et al., 2010) as well as the transport interferences of K and ammonium (Cao et al., 1993; Britto et al., 2001; Qi et al., 2008; Rubio et al., 2008).

Tsay et al. (2011) had already posed the question '*whether CIPK23 serves as a connecting node for K and nitrate at an early stage of nutrient perception*'. My results on 2nd order lateral branching controlled by CIPK23, AKT1 and NRT1.1 now provide experimental evidence that supports this hypothesis (see also the model shown in Fig. 29). This finding exemplifies the value of the study presented in informing future research on specific two- and three-way interactions by picking the right phenotypic output, i.e. modulated RSA parameter, and an appropriate background condition, e.g. long or short day. Targeted analysis of mutant collections or a rather untargeted approach using natural accessions are just two possible ways to characterise the genes involved in the underlying nutrient starvation pathways.

7.5 Environmental plasticity in the field – *from Arabidops. to crops*

All my experiments dealt with RSA responses of a typical dicotyledonous species with an allorhiz root system, consisting of a main root and branching off lateral roots. It would be interesting to know, how homorhiz root systems of monocotyledons respond to similar conditions, particularly since the world's most important cereals wheat, rice and maize belong to this group. A starting point for future research may be the analysis of a monocotyledonous model species like *Brachypodium distachyon* (Bevan et al., 2010; Pacheco-Villalobos and Hardtke, 2012). Indeed, *Brachypodium* root growth could initially be quantified using very similar systems to the ones described here and genetic resources are currently being developed to enable natural variation and QTL studies (Pacheco-Villalobos and Hardtke, 2012). Ultimately, interactive effects of nutrients on root architecture should be tested in real field scenarios on true crop species to evaluate the

impact of optimized RSA in specific nutritional scenarios (e.g. single vs. multiple nutrient deficiency) on agronomic traits (e.g. biomass and yield). A vision for the future would be to actively steer root architecture by applying critical fertilizer doses with beneficial effects for root establishment at crucial time points, thus saving money, resources and the environment.

7.6 Root architecture responses to low-K: the yin and yang of main root vs. lateral root elongation

At an early stage in my PhD project, I was faced with the challenge to decide on conditions that were a promising and meaningful basis to analyse natural variation of RSA responses to environmental stress. Potassium (K) emerged as the third most important factor controlling RSA parameters, such as main root length, apical zone length and lateral root length. In fact, K was even more important than N for main root elongation in short day conditions. Most strikingly, K nutrition was more or less the single factor determining the orientation of the main root angle. Mutant analysis highlighted the regulation of the root angle by AKT1 and involvement of CIPK23, AKT1, NRT1.1 in stimulating higher order branching in low-K. Consequently, I chose to characterise K starvation responses in a set of Arabidopsis natural accessions.

In my analysis, I identified a so far unknown phenotypic gradient of main root growth retardation as a response to low-K. I could also show that main root growth arrest was a necessary prerequisite for lateral root elongation observed in low-K strategy II genotypes. Otherwise, lateral root elongation was severely impaired in K-starved Arabidopsis seedlings. Hence, by comprehensively dissecting RSA in various genetic backgrounds, I observed a whole set of novel K phenotypes. It is possible that other low-K responses might have been missed because the accession set was limited to a rather small number of genotypes. With more than 800 fully-sequenced accessions now available through the 1001 genomes project (Weigel and Mott, 2009) it would be worthwile to search again for morphological responses to low-K, and hence for additional strategies, in an extended population. Based on my results I chose a recombinant Col-0 x Ct-1 population to investigate the difference between strategy I (e.g. Col-0) and strategy II (e.g. Ct-1) genotypes as it provided a system to uncover the molecular components that govern the decision between main and lateral root elongation.

In the light of nutrient crosstalk, it is interesting to note that low-K responses display considerable overlap with root responses to excessive ammonium supply. For

instance, higher order branching was shown to be induced by localised supply of ammonium (NH_4^+) using a split-plate experimental setup (Lima et al., 2010). The authors of this study could rescue the phenotype by knocking out ammonium transporter genes, most notably *AMT1;3* which is expressed in epidermal and cortical cells of first and second order lateral roots including the lateral root cap. Emergence of 2nd or 3rd order LRs coincided with a significant reduction in 1st order or 2nd order LR elongation, leading to a 'brushy' LR phenotype similar to the one I observed in low-K (genotype Col-0).

As mentioned before, K and ammonium have long been subject of comparative research. A direction connection is blockage of K transport through HAK5 by the presence of NH_4^+ (Qi et al., 2008; Rubio et al., 2008), which at low external K concentrations restricts K uptake to AKT1. High levels of NH_4^+ were shown to reduce main and lateral root elongation by inhibiting cell elongation in the elongation zone of roots (Li et al., 2010b). Yet, five days after treatment with 60 mM NH_4^+ no significant difference to the control in meristematic cell division was detected. In contrast, Li et al. (2010b) observed an increased efflux of NH_4^+ in the elongation zone, coinciding with a reduction of cell length.

Futile NH_4^+ cycling was proposed as a potential mechanism linking NH_4^+ transport to growth defects (Britto et al., 2001; Szczerba et al., 2008), as passive NH_4^+ uptake followed by active outward pumping uses up lots of energy and consequently increases respiration rates. Influx and efflux of NH_4^+ were significantly lower at higher external K concentrations (Szczerba et al., 2008), reducing the cost of this energy-intensive process. Apart from one exception, where I substituted nitrate with NH_4^+ to investigate the branching response in different nitrate concentrations, I did not add NH_4^+ to any of my other media. However, NH_4^+ is an intermediate product of nitrate assimilation which in temperate species at low-N largely takes place in roots (Black et al., 2002).

This raises the question: Are higher order branching responses to high NH_4^+ or low-K still two sides of the same coin? Branching induced by NH_4^+ is dependent on proper ammonium transporter function and knockout of HAK5 does not alter the lateral branching response to low-K. Therefore HAK5-mediated K transport and/or signalling can be discarded as a common regulatory element. Alternatively, futile cycling of K may waste precious energy deposits, reducing cell expansion in a way that is analogous to NH_4^+ (Szczerba et al., 2006). However, futile K cycling was shown to take place predominantly at higher external K concentrations, probably via low-affinity K/proton exchange systems (Britto and Kronzucker, 2006; Szczerba et al., 2006). Moreover, leakage of K through e.g. AKT1 was proposed to be limited by interaction of AKT1 with the 'silent' K channel α-

subunit AtKC1 (Wang et al., 2010b; Tsay et al., 2011). Still, the simple lack of K as an osmoticum may limit cell expansion (Amtmann et al., 2006), resulting in reduced main root and lateral root elongation. The fact that main root growth in low-K was rescued by lowering Fe indicates that at least in the case of main roots low-K did not limit cell extension. My results also suggest that main root and lateral root responses to low-K are partly uncoupled. Because low-Fe could not fully rescue LR growth. Nevertheless, staining for cell viability demonstrated that cell death in the apical meristem of both main and lateral roots marks an irreversible growth arrest. So reduction of cell length cannot fully explain the short LR phenotype. A low-K sensitive mechanism controlling cell division in LRs should be postulated. At the moment I can make no further comment without entering the realm of pure speculation. A closer look at my QTL study may give additional hints to solve that 'mystery': a low-K specific lateral root length QTL was detected and validated on chromosome 4 (*CHR4.2*) and fine-mapping of that locus could be started immediately using HIF 434.

7.7 Root slanting is a novel phenotypic reporter of K starvation

Apart from main and lateral root growth, a novel, K-responsive trait was identified in the main root angle. This phenomenon, also referred to as root 'slanting' or 'skewing', typically occurs when a 3-dimensional root system is grown on a 2D surface (Oliva and Dunand, 2007). I demonstrated here that low-K reverts the angle from right- to leftward. Hence, I propose to use this response as a novel reporter in K starvation studies. In addition, reversion of the angle was also observed for the *akt1* knockout line in sufficient K.

Potential mechanisms involved in root slanting under sufficient and deficient K have already been discussed in Chapter 3 and will therefore not be repeated here in detail. In Chapter 3, I also speculated on the involvement of the proton pump *AHA2* as a potential regulatory gene, as knockout of AHA2 was shown to reduce ATP-induced root skewing (Haruta and Sussman, 2012) and since apoplastic pH is a critical determinant of cell wall deposition. Later in my project, I have analysed the *aha2* mutant in low-P and low-K conditions (see Chapter 6). With regard to the main root angle, I did not observe an obvious deviation from wildtype behaviour in control and low-K for *aha2*. Only a shift in absolute values was detected (WT: 4.1 ± 0.7 ° in control, -0.1 ± 0.6 ° in low-K; *aha2*: 1.6 ± 1.3 ° in control, -4.2 ± 0.8 ° in low-K; values as means ± S.E.M). Differences to values reported in Chapter 3 are probably due to differences in low-K concentrations (10 µM here

compared to 50 µM in Chapter 3). Therefore, the hypothesis of an AHA2 mediated apoplastic acidification that leads to altered root skewing should be rejected for now.

In addition, the *pdr2* mutant was identified as a second genotype that showed clear left-slanting in control conditions (-3.8 ± 0.9 °) with no further exaggeration in low-K (-3.4 ± 0.9 °). So far, only a low-P conditional main root phenotype (shorter MRs) was described for this genotype (Ticconi et al., 2004; Ticconi et al., 2009). *PDR2* encodes an ER localised P5-type ATPase, that is believed to control meristem activity by promoting proper *SCR* expression (Ticconi et al., 2009; see also below).

In Chapter 3, I have discussed a role for the polarity of membrane potential in regulating the cytoskeleton. Plasma membrane hyperpolarisation in *akt1* might be a cause for the negative growth angle. The question now arises whether analogous root slanting phenotypes of *AKT1* and *PDR2* knockouts have a similar molecular or physiological basis. Double knockouts and cross-complementation by overexpression of either gene in the other background may help to answer that.

7.8 A central role for iron and redox regulation

Iron (Fe) availability was shown to be essential for low-P responses (Hirsch et al., 2006; Svistoonoff et al., 2007; Ward et al., 2008; Ticconi et al., 2009). I could show in Chapter 5 that main root growth responses to low-K equally depended on external Fe and potential signalling mechanisms (e.g. ROS) have been proposed there. Here, I would like to discuss a general question:

Is Fe accumulation in low-P and/or low-K of any environmental significance, i.e. would it occur in the field?

Although some Fe is bound in phosphate containing minerals (Ward et al., 2008), Fe is predominantly present as iron oxides and hydroxides in nature (Marschner, 1995), actually at rather high concentrations of about 45 g per kg soil (Palmer and Guerinot, 2009). In this sense, phosphate deficiency caused by high Fe concentrations is realistic, but not vice versa. Yet, Fe deficiency is an agronomically important phenomenon (Thomine and Lanquar, 2011). $Fe(OH)_3$ for instance is highly insoluble and its mobilization into dissolved Fe^{3+} depends largely on soil pH. In fact, acidification of the external medium via plasma membrane localized proton pumps, like AHA2 and AHA7 in Arabidopsis (Santi and Schmidt, 2009), is a well-documented response to Fe starvation (Palmer and Guerinot, 2009; Thomine and Lanquar, 2011) and each unit drop of pH changes Fe solubility by about 3 orders of magnitude (Guerinot and Yi, 1994). Protons are also released into the soil

in low-P (Vance et al., 2003) thus indirectly increasing the availability of Fe. K starvation on the contrary inhibits proton fluxes because K is needed for electric counterbalance of proton movement through the H^+-ATPases (Amtmann et al., 2006). In my growth system, proton release should not have had a significant impact on Fe availability, as pH was buffered with MES/Tris at pH = 5.6.

Dicotyledons and monocotyledons have different ways to mobilise Fe^{3+} for uptake (Palmer and Guerinot, 2009). Dicots adopt a reduction based strategy, where Fe^{3+} needs to be reduced to Fe^{2+} via FRO2 (Robinson et al., 1999) before it can be taken up by heavy metal transporters, particularly the high affinity transporter IRT1 (Vert et al., 2002). Although recent research confirmed Fe^{2+} uptake by grasses, monocots primarily utilize chelating agents, so called phytosiderophores derived from methionine, to take up Fe^{3+}-phytosiderophore complexes directly (Palmer and Guerinot, 2009). Chelation of Fe^{3+} was already accomplished by supplementation of EDTA to all of my growth media (up to 99 % soluble Fe-$EDTA^-$).

In sum, changes in proton extrusion evoked by P or K starvation as well as release of chelating agents, such as organic acids, phytosiderophores or nicotianamide are probably not relevant in my study. It cannot be ruled out, however, that these mechanisms are part of a natural P-K-Fe nutritional network.

Redistribution of Fe^{3+} within the plant also demands a chelator. FRD3 for example, loads citrate into the xylem thus facilitating root-to-shoot Fe transport (Durrett et al., 2007). Consequently, the *frd3-2* mutant displays pleiotropic Fe deficiency phenotypes such as leaf chlorosis even under adequate Fe nutrition and it over-accumulates Fe in roots. Interestingly, concentrations of organic acids like malate and citrate were much higher in whole seedlings starved for P as compared to control (Morcuende et al., 2007). In contrast, K-starved roots showed a strong decrease of malate (Armengaud et al, 2009a). Citrate was not quantified in the latter study but it can be regarded as a much stronger chelator, particularly at higher (neutral) pH (Jones et al., 1996). Bringing these findings together, it could be speculated that higher organic acid concentrations facilitate Fe redistribution within plants in low-P. This would enable the plant to transport excess Fe to specialised 'sink' cells or tissues and might therefore explain the Fe patches which I observed in low-P. In contrast, Fe peaks around the apical meristem evoked by low-K might be a result of impaired chelator availability that hampers Fe-sequestration from its putative site of uptake close to the root tip. Indeed, Marschner et al. (2011) have recently hypothesized that Fe availability is particularly high at the growing root apex. They argue that root exudation

has a maximum at this localisation (Lemanceau et al., 2009) but colonisation with microorganisms that compete for soluble Fe is low.

At this point, reviewing my data and putting it into the context of published work, it is hard to make any predictions on low-P or low-K induced accumulation of Fe in roots of plants grown on natural soils. Unfortunately, comprehensive ionomic datasets in the model plant Arabidopsis are available for shoots (compare e.g. the PiiMS database; http://www.ionomicshub.org/home/PiiMS; last visited 02/06/13) but not for root tissue. In the case of Fe, it has actually been shown that shoot [Fe] is not a good predictor of a plants' Fe status because shoot [Fe] is quite stable across a 10-fold range of Fe-fertilisation (Baxter et al., 2008b). Ghandilyan et al. (2009) have measured about 50 times higher Fe concentrations in Arabidopsis roots than in shoots, but this analysis was carried out in hydroponics supplemented with 22 µM Fe^{2+} and equimolar EDTA (and hence a similar system to mine). Moreover, across a whole range of species grown on natural soils of Japan, large variation in leaf Fe content was found between species grown on alluvial soils with higher K content, but very low Fe concentrations were quantified in plants grown on serpentine and low pH soils (Osaki et al., 2003). Only the broadly accepted idea of Fe accumulation in low-P was confirmed by slightly, but statistically significantly elevated shoot Fe levels under P-limited conditions (Baxter et al., 2008b).

So at the moment there is no clear answer to the question whether Fe accumulation occurs in natural environments (soil) deprived of K or P. The best way forward is gathering more experimental evidence. A first step would be to eliminate EDTA from the growth medium. Direct, chemical interactions of Fe, P and K would be more realistically simulated in that way. Moreover, the influence of other, natural chelators like citrate and malate could be assessed. Fe concentrations need to be quantified in roots and shoots separately. Roots would simply have to be thoroughly cleaned with water prior to analysis. ICP-MS is a suitable method to measure average tissue concentrations of multiple elements. Quantification via ICP-MS might actually work better with root material grown in soil as plate-grown roots are hard to clean from agar contamination and they contain a lot of nutrients that have passively diffused into the apoplast. Of course, local Fe accumulation from soil-grown roots could also be visualised by e.g. Perls' staining or SXRF. This analysis could be performed with other species as well. The provision of a more natural growth setting unfortunately comes with a major drawback: due to its complex composition, nutrient concentrations in soil are much harder to control.

Interactions of nutrients in soil and nutrient uptake from soil may be quite different from the agar plate system used here. Still, another question remains:

Is Fe accumulation in meristematic tissues in low-K and low-P a 'nasty side effect' or in fact a regulatory signal?

I detected an iron peak in the apical meristem of the main root even in control samples, suggesting that Fe fulfils an important role in meristematic function independent of environmental conditions. Given that iron is a principal player in cellular redox processes and a co-factor of many redox enzymes, the Fe peak may be directly reflecting molecular components that provide the oxidative environment needed for stem cell maintenance (Jiang et al., 2005; Dunand et al., 2007). Variation of Fe abundance in nutritional stress situations like low-K could be regarded as an approximate reporter of altered redox status and hence meristematic activity.

The multicopper oxidases LPR1 and LPR2 have been proposed as local 'P sensors' but the mechanism is still unknown (Svistoonoff et al., 2007). Neither is it mechanistically understood, how mutation of the P5-type ATPase PDR2 results in hypersensitive low-P responses (Ticconi et al., 2009). In the discussion of Chapter 6, I have argued that redox reactions catalyzed by LPR1 and LPR2 might mediate conversion of Fe^{2+} to/from Fe^{3+} either directly (ferroxidase activity) or indirectly, since Fe patterns in the root apex are altered in both knockouts. In order to be considered central regulatory elements for root growth, LPRs should be conserved across a range of plant species. Indeed, searches of two public databases, WU-BLAST (http://www.arabidopsis.org/wublast/index2.jsp; last viewed: 31/05/13) and MIPS (http://mips.helmholtz-muenchen.de/plant/genomes.jsp; last viewed: 01/06/13), revealed the existence of homologous proteins in *Arabidopsis lyrata*, *Brassica rapa*, *Vitis vinifera*, *Glycine max*, *Ricinus communis*, *Populus trichocarpa*, *Lycopersicon esculentum*, *Picea sitchensis*, *Oryza sativa*, *Sorghum bicolor*, *Selaginella moellendorffii*, *Physcomitrella patens* and *Zea mays* (in descending order of homology score). For all species mentioned here, at least two homologs were detected. So LPR-like multicopper oxidases are found across a broad range of plant species and have probably evolved at an early stage of land plant evolution (compare higher protein similarity to homologs in the moss *P. patens* than in maize).

I could show that LPR2 localises to the ER, just like LPR1 and PDR2 (Ticconi et al., 2009). Moreover, sensitivity to the trafficking inhibitor Brefeldin A was opposite in *pdr2* and *lpr1 lpr2* mutants, i.e. *pdr2* was more and the *lpr1 lpr2* double knockout was less sensitive (Ticconi et al., 2009; Wang et al., 2010a). Both expression profiles and Brefeldin A treatments strongly suggest the involvement of the ER in sensing and signalling low-P and low-K. Interestingly, Duan et al. (2010) demonstrated that an ER-mediated pathway elicits programmed cell death in the apical meristem of roots under severe water stress.

They observed lateral root proliferation after the main root had ceded growth and showed that ROS production increased substantially in water-stressed main root meristems. That provides a sound basis to speculate that LPRs (and PDR2) may analogously adjust the oxidative environment of the meristem to nutrient availability.

It would probably be an adaptive advantage to have two paralogous systems that are differentially responsive to P and K. I therefore hypothesize that localised accumulation of Fe is indeed a regulatory signal that indirectly integrates local environmental P and K concentrations and translates them into meristematic function governing root elongation. Direct measurements of the redox status at the tissue and cell level would help to support or negate this hypothesis. Transgenic lines expressing redox-sensitive versions of GFP (roGFP2; Meyer et al., 2007; Schwarzländer et al., 2008) in various genetic backgrounds (Col-0, *lpr1*, *lpr2-1*, Ct-1) present a good resource to start with. These experiments could be complemented by analysing markers for cell cycle progression and programmed cell death.

7.9 Outlook

Like most of my fellow PhD candidates, I (sadly) had to finish my project with a lot of open questions and unexplored sidetracks. For instance, I have performed my experiments in homogenous nutrient conditions, i.e. growth media initially had equal concentrations across the whole agar-plate. It is well known, however, that plants actively respond to nutrient fluctuations, for example by colonising patches rich in nitrate (Zhang and Forde, 1998) or iron (Giehl et al., 2012) with newly formed or elongating LRs. Integration of local environmental cues with the overall nutritional status of the plant is the prerequisite for such responses. Hence, split-plates with different nutrient conditions in segments of a single plate represent a good experimental starting point to dissect local from systemic signalling pathways. Future research on nutrient interactions should take this into account and should make use of appropriate methods. In addition, multilevel datasets generated from the same material are generally more informative than ‘patchwork data’ pieced together from independent experiments. Whereas root architecture measurements can be made without disturbing the plants’ viability, many other experimental techniques are destructive and therefore prohibit the collection of complementary data. To give an example: Perls’ staining for Fe fixes the plant material with 4 % HCl and therefore does not permit subsequent RNA sampling. Non-invasive techniques should therefore be preferred in the future, allowing for full control of environmental conditions whilst

simultaneously monitoring root growth and other experimental parameters such as nutrient and metabolite concentrations or abundance of fluorescence markers (GFP-tagging, redox and pH dyes, etc.). Such platforms are beginning to emerge, like 'The RootChip' (Grossmann et al., 2011) or the 'RootArray' (Busch et al., 2012), and should become more widely spread in the research community in years to come.

I would like to conclude on an optimistic note: These are exciting times for plant science! New technologies enable us to investigate the mysteries of plant life in ever more realistic growth scenarios. Particularly root research benefits from non-invasive techniques that help to bring the 'hidden-half' into the light of day - whilst actually keeping it in the dark. Each month new whole-genome sequences are released and hence facilitate the search for novel genes involved in fundamental processes of development and stress response in model species and crops. In fact, a central task will be to *make sense* of all the large datasets generated in 'omics' studies. And of course, the time has come to transfer knowledge gained in the lab to applications out in the field. I am sure that if we manage to integrate the disciplines of science, and if we are willing to talk to computer specialists and farmers alike, we are ready to tackle the challenges ahead.

REFERENCES

Abel S. (2011). Phosphate sensing in root development. Current Opinion in Plant Biology **14:** 303-309.

Ache P., Becker D., Ivashikina N., Dietrich P., Roelfsema M. R. G., and Hedrich R. (2000). GORK, a delayed outward rectifier expressed in guard cells of *Arabidopsis thaliana*, is a K+-selective, K+-sensing ion channel. Febs Letters **486:** 93-98.

AGI (2000). Arabidopsis Genome Initiative: Analysis of the genome sequence of the flowering plant *Arabidopsis thaliana*. Nature **408:** 796-815.

Ahn S. J., Shin R., and Schachtman D. P. (2004). Expression of KT/KUP genes in arabidopsis and the role of root hairs in K+ uptake. Plant Physiology **134:** 1135-1145.

Aida M., Beis D., Heidstra R., Willemsen V., Blilou I., Galinha C., Nussaume L., Noh Y. S., Amasino R., and Scheres B. (2004). The PLETHORA genes mediate patterning of the Arabidopsis root stem cell niche. Cell **119:** 109-120.

Aleman F., Nieves-Cordones M., Martinez V., and Rubio F. (2011). Root K(+) Acquisition in Plants: The *Arabidopsis thaliana* Model. Plant and Cell Physiology **52:** 1603-1612.

Al-Ghazi Y., Muller B., Pinloche S., Tranbarger T. J., Nacry P., Rossignol M., Tardieu F., and Doumas P. (2003). Temporal responses of Arabidopsis root architecture to phosphate starvation: evidence for the involvement of auxin signalling. Plant Cell and Environment **26:** 1053-1066.

Alhendawi R. A., Kirkby E. A., and Pilbeam D. J. (2005). Evidence that sulfur deficiency enhances molybdenum transport in xylem sap of tomato plants. Journal of Plant Nutrition **28:** 1347-1353.

Alonso-Blanco C., Aarts M. G. M., Bentsink L., Keurentjes J. J. B., Reymond M., Vreugdenhil D., and Koornneef M. (2009). What Has Natural Variation Taught Us about Plant Development, Physiology, and Adaptation? Plant Cell **21:** 1877-1896.

Alonso-Blanco C., and Koornneef M. (2000). Naturally occurring variation in Arabidopsis: an underexploited resource for plant genetics. Trends in Plant Science **5:** 22-29.

Amtmann A., and Armengaud P. (2007). The role of calcium sensor-interacting protein kinases in plant adaptation to potassium-deficiency: new answers to old questions. Cell Research **17:** 483-485.

Amtmann A., and Blatt M. R. (2009). Regulation of macronutrient transport. New Phytologist **181:** 35-52.

Amtmann A., Hammond J. P., Armengaud P., and White P. J. (2006). Nutrient sensing and signalling in plants: Potassium and phosphorus. Advances in Botanical Research **43:** 209-257.

Amtmann A., Jelitto T. C., and Sanders D. (1999). K+-Selective inward-rectifying channels and apoplastic pH in barley roots. Plant Physiology **120:** 331-338.

Armengaud P., Breitling R., and Amtmann A. (2004). The potassium-dependent transcriptome of Arabidopsis reveals a prominent role of jasmonic acid in nutrient signaling. Plant Physiology **136:** 2556-2576.

Armengaud P., Breitling R., and Amtmann A. (2010). Coronatine-Insensitive 1 (COI1) Mediates Transcriptional Responses of *Arabidopsis thaliana* to External Potassium Supply. Molecular Plant **3:** 390-405.

Armengaud P., Sulpice R., Miller A. J., Stitt M., Amtmann A., and Gibon Y. (2009a). Multilevel Analysis of Primary Metabolism Provides New Insights into the Role of Potassium Nutrition for Glycolysis and Nitrogen Assimilation in Arabidopsis Roots. Plant Physiology **150:** 772-785.

Armengaud P., Zambaux K., Hills A., Sulpice R., Pattison R. J., Blatt M. R., and Amtmann A. (2009b). EZ-Rhizo: integrated software for the fast and accurate measurement of root system architecture. Plant Journal **57:** 945-956.

Askwith C., Eide D., Vanho A., Bernard P. S., Li L. T., Daviskaplan S., Sipe D. M., and Kaplan J. (1994). The Fet3 Gene of *Saccharomyces cerevisiae* Encodes a Multicopper Oxidase Required for Ferrous Iron Uptake. Cell **76:** 403-410.

Atamian H. S., Roberts P. A., and Kaloshian I. (2012). High and low throughput screens with root-knot nematodes Meloidogyne spp. Journal of visualized experiments **61:** e3629.

Atwell S., Huang Y. S., Vilhjalmsson B. J., Willems G., Horton M., Li Y., Meng D. Z., Platt A., Tarone A. M., Hu T. T., Jiang R., Muliyati N. W., Zhang X., Amer M. A., Baxter I., Brachi B., Chory J., Dean C., Debieu M., de Meaux J., Ecker J. R., Faure N., Kniskern J. M., Jones J. D. G., Michael T., Nemri A., Roux F., Salt D. E., Tang C. L., Todesco M., Traw M. B., Weigel D., Marjoram P., Borevitz J. O., Bergelson J., and Nordborg M. (2010). Genome-wide association study of 107 phenotypes in Arabidopsis thaliana inbred lines. Nature **465:** 627-631.

Aung K., Lin S. I., Wu C. C., Huang Y. T., Su C. L., and Chiou T. J. (2006). *pho2*, a phosphate overaccumulator, is caused by a nonsense mutation in a microRNA399 target gene. Plant Physiology **141:** 1000-1011.

Baluska F., Mancuso S., Volkmann D., and Barlow P. W. (2010). Root apex transition zone: a signalling-response nexus in the root. Trends in Plant Science **15:** 402-408.

Barberon M., Berthomieu P., Clairotte M., Shibagaki N., Davidian J. C., and Gosti F. (2008). Unequal functional redundancy between the two *Arabidopsis thaliana* high-affinity sulphate transporters SULTR1;1 and SULTR1;2. New Phytologist **180:** 608-619.

Bari R., Pant B. D., Stitt M., and Scheible W. R. (2006). PHO2, microRNA399, and PHR1 define a phosphate-signaling pathway in plants. Plant Physiology **141:** 988-999.

Baxter I., Brazelton J. N., Yu D. N., Huang Y. S., Lahner B., Yakubova E., Li Y., Bergelson J., Borevitz J. O., Nordborg M., Vitek O., and Salt D. E. (2010). A Coastal Cline in Sodium Accumulation in Arabidopsis thaliana Is Driven by Natural Variation of the Sodium Transporter AtHKT1;1. Plos Genetics **6:** e1001193.

Baxter I., Hosmani P. S., Rus A., Lahner B., Borevitz J. O., Muthukumar B., Mickelbart M. V., Schreiber L., Franke R. B., and Salt D. E. (2009). Root Suberin Forms an Extracellular Barrier That Affects Water Relations and Mineral Nutrition in Arabidopsis. Plos Genetics **5:** e1000492.

Baxter I., Muthukumar B., Park H. C., Buchner P., Lahner B., Danku J., Zhao K., Lee J., Hawkesford M. J., Guerinot M. L., and Salt D. E. (2008a). Variation in molybdenum content across broadly distributed populations of Arabidopsis thaliana is controlled by a mitochondrial molybdenum transporter (MOT1). Plos Genetics **4:** e1000004.

Baxter I. R., Vitek O., Lahner B., Muthukumar B., Borghi M., Morrissey J., Guerinot M. L., and Salt D. E. (2008b). The leaf ionome as a multivariable system to detect a plant's physiological status. Proceedings of the National Academy of Sciences of the United States of America **105:** 12081-12086.

Bernier F., and Berna A. (2001). Germins and germin-like proteins: Plant do-all proteins. But what do they do exactly? Plant Physiology and Biochemistry **39:** 545-554.

Bevan M. W., Garvin D. F., and Vogel J. P. (2010). *Brachypodium distachyon* genomics for sustainable food and fuel production. Current Opinion in Biotechnology **21:** 211-217.

Bikard D., Patel D., Le Mette C., Giorgi V., Camilleri C., Bennett M. J., and Loudet O. (2009). Divergent Evolution of Duplicate Genes Leads to Genetic Incompatibilities Within *A. thaliana*. Science **323:** 623-626.

Bilsborough G. D., Runions A., Barkoulas M., Jenkins H. W., Hasson A., Galinha C., Laufs P., Hay A., Prusinkiewicz P., and Tsiantis M. (2011). Model for the regulation of Arabidopsis thaliana leaf margin development. Proceedings of the National Academy of Sciences of the United States of America **108:** 3424-3429.

Bishopp A., Help H., El-Showk S., Weijers D., Scheres B., Friml J., Benkova E., Mahonen A. P., and Helariutta Y. (2011). A Mutually Inhibitory Interaction between Auxin and Cytokinin Specifies Vascular Pattern in Roots. Current Biology **21:** 917-926.

Black B. L., Fuchigami L. H., and Coleman G. D. (2002). Partitioning of nitrate assimilation among leaves, stems and roots of poplar. Tree Physiology **22:** 717-724.

Blilou I., Xu J., Wildwater M., Willemsen V., Paponov I., Friml J., Heidstra R., Aida M., Palme K., and Scheres B. (2005). The PIN auxin efflux facilitator network controls growth and patterning in Arabidopsis roots. Nature **433:** 39-44.

Bloom A. J., Meyerhoff P. A., Taylor A. R., and Rost T. L. (2002). Root development and absorption of ammonium and nitrate from the rhizosphere. Journal of Plant Growth Regulation **21:** 416-431.

Bouchabke O., Chang F. Q., Simon M., Voisin R., Pelletier G., and Durand-Tardif M. (2008). Natural Variation in *Arabidopsis thaliana* as a Tool for Highlighting Differential Drought Responses. Plos One **3:** e1705.

Briat J. F., Ravet K., Arnaud N., Duc C., Boucherez J., Touraine B., Cellier F., and Gaymard F. (2010). New insights into ferritin synthesis and function highlight a link between iron homeostasis and oxidative stress in plants. Annals of Botany **105:** 811-822.

Britto D. T., Siddiqi M. Y., Glass A. D. M., and Kronzucker H. J. (2001). Futile transmembrane NH4+ cycling: A cellular hypothesis to explain ammonium toxicity in plants. Proceedings of the National Academy of Sciences of the United States of America **98:** 4255-4258.

Brooks T. L. D., Miller N. D., and Spalding E. P. (2010). Plasticity of Arabidopsis Root Gravitropism throughout a Multidimensional Condition Space Quantified by Automated Image Analysis. Plant Physiology **152:** 206-216.

Buchner P., Takahashi H., and Hawkesford M. J. (2004). Plant sulphate transporters: co-ordination of uptake, intracellular and long-distance transport. Journal of Experimental Botany **55:** 1765-1773.

Buer C. S., Wasteneys G. O., and Masle J. (2003). Ethylene modulates root-wave responses in Arabidopsis. Plant Physiology **132:** 1085-1096.

Buescher E., Achberger T., Amusan I., Giannini A., Ochsenfeld C., Rus A., Lahner B., Hoekenga O., Yakubova E., Harper J. F., Guerinot M. L., Zhang M., Salt D. E., and Baxter I. R. (2010). Natural Genetic Variation in Selected Populations of *Arabidopsis thaliana* Is Associated with Ionomic Differences. Plos One **5**

Busch W., Moore B. T., Martsberger B., Mace D. L., Twigg R. W., Jung J., Pruteanu-Malinici I., Kennedy S. J., Fricke G. K., Clark R. L., Ohler U., and Benfey P. N. (2012). A microfluidic device and computational platform for high-throughput live imaging of gene expression. Nature Methods **9:** 1101-1106.

Bustos R., Castrillo G., Linhares F., Puga M. I., Rubio V., Perez-Perez J., Solano R., Leyva A., and Paz-Ares J. (2010). A Central Regulatory System Largely Controls Transcriptional Activation and Repression Responses to Phosphate Starvation in Arabidopsis. Plos Genetics **6:** e1001102.

Cao J., Schneeberger K., Ossowski S., Gunther T., Bender S., Fitz J., Koenig D., Lanz C., Stegle O., Lippert C., Wang X., Ott F., Muller J., Alonso-Blanco C., Borgwardt K., Schmid K. J., and Weigel D. (2011). Whole-genome sequencing of multiple *Arabidopsis thaliana* populations. Nature Genetics **43:** 956-963.

Cao Y. W., Glass A. D. M., and Crawford N. M. (1993). Ammonium Inhibition of Arabidopsis Root-Growth Can Be Reversed by Potassium and by Auxin Resistance Mutations Aux1, Axr1, and Axr2. Plant Physiology **102:** 983-989.

Capaccioni B., Didero M., Paletta C., and Didero L. (2005). Saline intrusion and refreshening in a multilayer coastal aquifer in the Catania Plain (Sicily, Southern Italy): dynamics of degradation processes according to the hydrochemical characteristics of groundwaters. Journal of Hydrology **307:** 1-16.

Carson F. L. (1991). Histotechnology: A Self-Instructional Text. American Society for Clinical Pathology Press, Chicago.

Castaings L., Camargo A., Pocholle D., Gaudon V., Texier Y., Boutet-Mercey S., Taconnat L., Renou J. P., Daniel-Vedele F., Fernandez E., Meyer C., and Krapp A. (2009). The nodule inception-like protein 7 modulates nitrate sensing and metabolism in Arabidopsis. Plant Journal **57:** 426-435.

Chapman N., Miller A. J., Lindsey K., and Whalley W. R. (2012). Roots, water, and nutrient acquisition: let's get physical. Trends in Plant Science **17:** 701-710.

Chapman N., and Miller T. (2011). Nitrate Transporters and Root Architecture. *In* Transporters and Pumps in Plant Signaling. Springer Verlag, Berlin, pp 165-190.

Chapman N., Whalley W. R., Lindsey K., and Miller A. J. (2011). Water supply and not nitrate concentration determines primary root growth in Arabidopsis. Plant Cell and Environment **34:** 1630-1638.

Chardon F., Barthelemy J., Daniel-Vedele F., and Masclaux-Daubresse C. (2010). Natural variation of nitrate uptake and nitrogen use efficiency in *Arabidopsis thaliana* cultivated with limiting and ample nitrogen supply. Journal of Experimental Botany **61:** 2293-2302.

Chardon F., Noel V., and Masclaux-Daubresse C. (2012). Exploring NUE in crops and in Arabidopsis ideotypes to improve yield and seed quality. Journal of Experimental Botany **63:** 3401-3412.

Chen C. C., Chen Y. Y., Tang I. C., Liang H. M., Lai C. C., Chiou J. M., and Yeh K. C. (2011). Arabidopsis SUMO E3 Ligase SIZ1 Is Involved in Excess Copper Tolerance. Plant Physiology **156:** 2225-2234.

Chen L. Q., Qu X. Q., Hou B. H., Sosso D., Osorio S., Fernie A. R., and Frommer W. B. (2012a). Sucrose Efflux Mediated by SWEET Proteins as a Key Step for Phloem Transport. Science **335:** 207-211.

Chen Z-H., Hills A., Bätz U., Amtmann A., Lew V.L., and Blatt M.R. (2012b). Systems dynamic modeling of the stomatal guard cell predicts emergent behaviors in transport, signaling, and volume control. Plant Physiology **159:** 1235-1251.

Chen Z. H., Nimmo G. A., Jenkins G. I., and Nimmo H. G. (2007). BHLH32 modulates several biochemical and morphological processes that respond to P-i starvation in Arabidopsis. Biochemical Journal **405:** 191-198.

Chevalier F., Pata M., Nacry P., Doumas P., and Rossignol M. (2003). Effects of phosphate availability on the root system architecture: large-scale analysis of the natural variation between Arabidopsis accessions. Plant Cell and Environment **26:** 1839-1850.

Chifflet S., and Hernandez J. A. (2012). The plasma membrane potential and the organization of the actin cytoskeleton of epithelial cells. International Journal of Cell Biology **2012:** 121424.

Chopin F., Orsel M., Dorbe M. F., Chardon F., Truong H. N., Miller A. J., Krapp A., and Daniel-Vedele F. (2007). The Arabidopsis ATNRT2.7 nitrate transporter controls nitrate content in seeds. Plant Cell **19:** 1590-1602.

Clark R. T., Famoso A. N., Zhao K. Y., Shaff J. E., Craft E. J., Bustamante C. D., McCouch S. R., Aneshansley D. J., and Kochian L. V. (2013). High-throughput two-dimensional root system phenotyping platform facilitates genetic analysis of root growth and development. Plant Cell and Environment **36:** 454-466.

Clark R. T., MacCurdy R. B., Jung J. K., Shaff J. E., McCouch S. R., Aneshansley D. J., and Kochian L. V. (2011). Three-Dimensional Root Phenotyping with a Novel Imaging and Software Platform. Plant Physiology **156:** 455-465.

Clerkx E. J. M., El-Lithy M. E., Vierling E., Ruys G. J., Blankestijin-De Vries H., Groot S. P. C., Vreugdenhil D., and Koornneef M. (2004). Analysis of natural allelic variation of Arabidopsis seed germination and seed longevity traits between the accessions Landsberg erecta and Shakdara, using a new recombinant inbred line population. Plant Physiology **135:** 432-443.

Colangelo E. P., and Guerinot M. L. (2004). The essential basic helix-loop-helix protein FIT1 is required for the iron deficiency response. Plant Cell **16:** 3400-3412.

Curtis M. D., and Grossniklaus U. (2003). A gateway cloning vector set for high-throughput functional analysis of genes in planta. Plant Physiology **133:** 462-469.

Dalton C. C., Iqbal K., and Turner D. A. (1983). Iron Phosphate Precipitation in Murashige and Skoog Media. Physiologia Plantarum **57:** 472-476.

Darwin C., and Darwin. F. (1880). The Power of movements in plants. John Murry, London.

De Angeli A., Monachello D., Ephritikhine G., Frachisse J. M., Thomine S., Gambale F., and Barbier-Brygoo H. (2006). The nitrate/proton antiporter AtCLCa mediates nitrate accumulation in plant vacuoles. Nature **442:** 939-942.

De Pessemier J., Chardon F., Juraniec M., Delaplace P., and Hermans C. (2013). Natural variation of the root morphological response to nitrate supply in *Arabidopsis thaliana*. Mechanisms of Development **130:** 45-53.

De Smet I., J. White P., Bengough A. G., Dupuy L., Parizot B., Casimiro I., Heidstra R., Laskowski M., Lepetit M., Hochholdinger F., Draye X., Zhang H., Broadley M. R., Peret B., Hammond J. P., Fukaki H., Mooney S., Lynch J. P., Nacry P., Schurr U., Laplaze L., Benfey P., Beeckman T., and Bennett M. (2012). Analyzing Lateral Root Development: How to Move Forward. Plant Cell **24:** 15-20.

De Smet I., Tetsumura T., De Rybel B., Frey N. F. D., Laplaze L., Casimiro I., Swarup R., Naudts M., Vanneste S., Audenaert D., Inze D., Bennett M. J., and Beeckman T. (2007). Auxin-dependent regulation of lateral root positioning in the basal meristem of Arabidopsis. Development **134:** 681-690.

De Tullio M. C., Jiang K. N., and Feldman L. J. (2010). Redox regulation of root apical meristem organization: Connecting root development to its environment. Plant Physiology and Biochemistry **48:** 328-336.

Deak K. I., and Malamy J. (2005). Osmotic regulation of root system architecture. Plant Journal **43:** 17-28.

Delhaize E., and Randall P. J. (1995). Characterization of a Phosphate-Accumulator Mutant of *Arabidopsis thaliana*. Plant Physiology **107:** 207-213.

Delhaize E., Ryan P. R., Hebb D. M., Yamamoto Y., Sasaki T., and Matsumoto H. (2004). Engineering high-level aluminum tolerance in barley with the ALMT1

gene. Proceedings of the National Academy of Sciences of the United States of America **101:** 15249-15254.

Dello Ioio R., Nakamura K., Moubayidin L., Perilli S., Taniguchi M., Morita M. T., Aoyama T., Costantino P., and Sabatini S. (2008). A Genetic Framework for the Control of Cell Division and Differentiation in the Root Meristem. Science **322:** 1380-1384.

Den Herder G., Van Isterdael G., Beeckman T., and De Smet I. (2010). The roots of a new green revolution. Trends in Plant Science **15:** 600-607.

Donner E., Punshon T., Guerinot M. L., and Lombi E. (2012). Functional characterisation of metal(loid) processes in planta through the integration of synchrotron techniques and plant molecular biology. Analytical and Bioanalytical Chemistry **402:** 3287-3298.

Dooley C. T., Dore T. M., Hanson G. T., Jackson W. C., Remington S. J., and Tsien R. Y. (2004). Imaging dynamic redox changes in mammalian cells with green fluorescent protein indicators. Journal of Biological Chemistry **279:** 22284-22293.

Downie H., Holden N., Otten W., Spiers A. J., Valentine T. A., and Dupuy L. X. (2012). Transparent Soil for Imaging the Rhizosphere. Plos One **7:** e44276.

Drew M. C. (1975). Comparison of Effects of a Localized Supply of Phosphate, Nitrate, Ammonium and Potassium on Growth of Seminal Root System, and Shoot, in Barley. New Phytologist **75:** 479-490.

Dreyer I., and Blatt M. R. (2009). What makes a gate? The ins and outs of Kv-like K+ channels in plants. Trends in Plant Science **14:** 383-390.

Duan Y. F., Zhang W. S., Li B., Wang Y. N., Li K. X., Sodmergen, Han C. Y., Zhang Y. Z., and Li X. (2010). An endoplasmic reticulum response pathway mediates programmed cell death of root tip induced by water stress in Arabidopsis. New Phytologist **186:** 681-695.

Dubrovsky J. G., and Forde B. G. (2012). Quantitative Analysis of Lateral Root Development: Pitfalls and How to Avoid Them. Plant Cell **24:** 4-14.

Duby G., Hosy E., Fizames C., Alcon C., Costa A., Sentenac H., and Thibaud J. B. (2008). AtKC1, a conditionally targeted Shaker-type subunit, regulates the activity of plant K+ channels. Plant Journal **53:** 115-123.

Dunand C., Crevecoeur M., and Penel C. (2007). Distribution of superoxide and hydrogen peroxide in Arabidopsis root and their influence on root development: possible interaction with peroxidases. New Phytologist **174:** 332-341.

Dunwell J. M., Purvis A., and Khuri S. (2004). Cupins: the most functionally diverse protein superfamily? Phytochemistry **65:** 7-17.

Durand S., Bouche N., Strand E. P., Loudet O., and Camilleri C. (2012). Rapid Establishment of Genetic Incompatibility through Natural Epigenetic Variation. Current Biology **22:** 326-331.

Durrett T. P., Gassmann W., and Rogers E. E. (2007). The FRD3-mediated efflux of citrate into the root vasculature is necessary for efficient iron translocation. Plant Physiology **144:** 197-205.

Edwards K., Johnstone C., and Thompson C. (1991). A Simple and Rapid Method for the Preparation of Plant Genomic DNA for PCR Analysis. Nucleic Acids Research **19:** 1349-1349.

El-Lithy M. E., Bentsink L., Hanhart C. J., Ruys G. J., Rovito D. I., Broekhof J. L. M., van der Poel H. J. A., van Eijk M. J. T., Vreugdenhil D., and Koornneef M. (2006). New Arabidopsis recombinant inbred line populations genotyped using SNPWave and their use for mapping flowering-time quantitative trait loci. Genetics **172:** 1867-1876.

El-Lithy M. E., Clerkx E. J. M., Ruys G. J., Koornneef M., and Vreugdenhil D. (2004). Quantitative trait locus analysis of growth-related traits in a new Arabidopsis recombinant inbred population. Plant Physiology **135:** 444-458.

Fang S. Q., Yan X. L., and Liao H. (2009). 3D reconstruction and dynamic modeling of root architecture in situ and its application to crop phosphorus research. Plant Journal **60:** 1096-1108.

Felle H. H. (2001). pH: Signal and Messenger in Plant Cells. Plant Biology **3:** 577-591.

Fernandez A., Drozdzecki A., Hoogewijs K., Nguyen A., Beeckman T., Madder A., and Hilson P. (2013). Transcriptional and Functional Classification of the GOLVEN/ROOT GROWTH FACTOR/CLE-Like Signaling Peptides Reveals Their Role in Lateral Root and Hair Formation. Plant Physiology **161:** 954-970.

Fisahn J., Yazdanbakhsh N., Klingele E., and Barlow P. (2012). *Arabidopsis thaliana* root growth kinetics and lunisolar tidal acceleration. New Phytologist **195:** 346-355.

Fitz Gerald J. N., Lehti-Shiu M. D., Ingram P. A., Deak K. I., Biesiada T., and Malamy J. E. (2006). Identification of quantitative trait loci that regulate Arabidopsis root system size and plasticity. Genetics **172:** 485-498.

Forde B. G. (2009). Is it good noise? The role of developmental instability in the shaping of a root system. Journal of Experimental Botany **60:** 3989–4002.

Franco-Zorrilla J. M., Martin A. C., Solano R., Rubio V., Leyva A., and Paz-Ares J. (2002). Mutations at CRE1 impair cytokinin-induced repression of phosphate starvation responses in Arabidopsis. Plant Journal **32:** 353-360.

French A., Ubeda-Tomas S., Holman T. J., Bennett M. J., and Pridmore T. (2009). High-Throughput Quantification of Root Growth Using a Novel Image-Analysis Tool. Plant Physiology **150:** 1784-1795.

Friml J., Vieten A., Sauer M., Weijers D., Schwarz H., Hamann T., Offringa R., and Jurgens G. (2003). Efflux-dependent auxin gradients establish the apical-basal axis of Arabidopsis. Nature **426:** 147-153.

Fukao Y., Ferjani A., Tomioka R., Nagasaki N., Kurata R., Nishimori Y., Fujiwara M., and Maeshima M. (2011). iTRAQ Analysis Reveals Mechanisms of Growth Defects Due to Excess Zinc in Arabidopsis. Plant Physiology **155:** 1893-1907.

Galinha C., Hofhuis H., Luijten M., Willemsen V., Blilou I., Heidstra R., and Scheres B. (2007). PLETHORA proteins as dose-dependent master regulators of Arabidopsis root development. Nature **449:** 1053-1057.

Galpaz N., and Reymond M. (2010). Natural Variation in *Arabidopsis thaliana* Revealed a Genetic Network Controlling Germination Under Salt Stress. Plos One **5:** e15198.

Gan Y. B., Bernreiter A., Filleur S., Abram B., and Forde B. G. (2012). Overexpressing the ANR1 MADS-Box Gene in Transgenic Plants Provides New Insights into its Role in the Nitrate Regulation of Root Development. Plant and Cell Physiology **53:** 1003-1016.

Gaymard F., Pilot G., Lacombe B., Bouchez D., Bruneau D., Boucherez J., Michaux-Ferriere N., Thibaud J. B., and Sentenac H. (1998). Identification and disruption of a plant shaker-like outward channel involved in K+ release into the xylem sap. Cell **94:** 647-655.

Gething P.A. (1993). Improving returns from nitrogen fertilizer. The potassium-nitrogen partnership. IPI Research Topics (International Potash Institute; Basel, CH) **13:** 51 pp.

Ghandilyan A., Barboza L., Tisne S., Granier C., Reymond M., Koornneef M., Schat H., and Aarts M. G. M. (2009). Genetic analysis identifies quantitative trait loci controlling rosette mineral concentrations in *Arabidopsis thaliana* under drought. New Phytologist **184:** 180-192.

Ghanem M. E., Hichri I., Smigocki A. C., Albacete A., Fauconnier M. L., Diatloff E., Martinez-Andujar C., Lutts S., Dodd I. C., and Perez-Alfocea F. (2011). Root-targeted biotechnology to mediate hormonal signalling and improve crop stress tolerance. Plant Cell Reports **30:** 807-823.

Giehl R. F. H., Lima J. E., and von Wiren N. (2012). Localized Iron Supply Triggers Lateral Root Elongation in Arabidopsis by Altering the AUX1-Mediated Auxin Distribution. Plant Cell **24:** 33-49.

Gifford M. L., Dean A., Gutierrez R. A., Coruzzi G. M., and Birnbaum K. D. (2008). Cell-specific nitrogen responses mediate developmental plasticity. Proceedings of the National Academy of Sciences of the United States of America **105:** 803-808.

Gil P., Dewey E., Friml J., Zhao Y., Snowden K. C., Putterill J., Palme K., Estelle M., and Chory J. (2001). BIG: a calossin-like protein required for polar auxin transport in Arabidopsis. Genes & Development **15:** 1985-1997.

Gojon A., Nacry P., and Davidian J.-C. (2009). Root uptake regulation: a central process for NPS homeostasis in plants. Current Opinion in Plant Biology **12:** 328-338.

Gomord V., Denmat L. A., Fitchette-Laine A. C., Satiat-Jeunemaitre B., Hawes C., and Faye L. (1997). The C-terminal HDEL sequence is sufficient for retention of secretory proteins in the endoplasmic reticulum (ER) but promotes vacuolar targeting of proteins that escape the ER. Plant Journal **11:** 313-325.

Green L. S., and Rogers E. E. (2004). FRD3 controls iron localization in Arabidopsis. Plant Physiology **136:** 2523-2531.

Grefen C., Donald N., Hashimoto K., Kudla J., Schumacher K., and Blatt M. R. (2010). A ubiquitin-10 promoter-based vector set for fluorescent protein tagging facilitates temporal stability and native protein distribution in transient and stable expression studies. Plant Journal **64:** 355-365.

Gregory P. J., Atkinson C. J., Bengough A. G., Else M. A., Fernandez-Fernandez F., Harrison R. J., and Schmidt S. (2013). Contributions of roots and rootstocks to sustainable, intensified crop production. Journal of Experimental Botany **64:** 1209-1222.

Grieneisen V. A., Xu J., Maree A. F. M., Hogeweg P., and Scheres B. (2007). Auxin transport is sufficient to generate a maximum and gradient guiding root growth. Nature **449:** 1008-1013.

Grossmann G., Guo W. J., Ehrhardt D. W., Frommer W. B., Sit R. V., Quake S. R., and Meier M. (2011). The RootChip: An Integrated Microfluidic Chip for Plant Science. Plant Cell **23:** 4234-4240.

Guo B., Jin Y., Wussler C., Blancaflor E. B., Motes C. M., and Versaw W. K. (2008). Functional analysis of the Arabidopsis PHT4 family of intracellular phosphate transporters. New Phytologist **177:** 889-898.

Gustafsson J. P. (2011). Visual MINTEQ 3.0. KTH, Department of Land and Water Resources Engineering, Stockholm.

Haecker A., Gross-Hardt R., Geiges B., Sarkar A., Breuninger H., Herrmann M., and Laux T. (2004). Expression dynamics of WOX genes mark cell fate decisions during early embryonic patterning in Arabidopsis thaliana. Development **131:** 657-668.

Hammer G. L., Dong Z. S., McLean G., Doherty A., Messina C., Schusler J., Zinselmeier C., Paszkiewicz S., and Cooper M. (2009). Can Changes in Canopy and/or Root System Architecture Explain Historical Maize Yield Trends in the US Corn Belt? Crop Science **49:** 299-312.

Hammond J. P., Bennett M. J., Bowen H. C., Broadley M. R., Eastwood D. C., May S. T., Rahn C., Swarup R., Woolaway K. E., and White P. J. (2003). Changes in gene expression in Arabidopsis shoots during phosphate starvation and the potential for developing smart plants. Plant Physiology **132:** 578-596.

Hammond J. P., and White P. J. (2008). Sucrose transport in the phloem: integrating root responses to phosphorus starvation. Journal of Experimental Botany **59:** 93-109.

Hammond J. P., and White P. J. (2011). Sugar Signaling in Root Responses to Low Phosphorus Availability. Plant Physiology **156:** 1033-1040.

Harada H., and Leigh R. A. (2006). Genetic mapping of natural variation in potassium concentrations in shoots of *Arabidopsis thaliana*. Journal of Experimental Botany **57:** 953-960.

Haruta M., and Sussman M. R. (2012). The Effect of a Genetically Reduced Plasma Membrane Protonmotive Force on Vegetative Growth of Arabidopsis. Plant Physiology **158:** 1158-1171.

Helali S. M., Nebli H., Kaddour R., Mahmoudi H., Lachaal M., and Ouerghi Z. (2010). Influence of nitrate-ammonium ratio on growth and nutrition of *Arabidopsis thaliana*. Plant and Soil **336:** 65-74.

Helariutta Y., Fukaki H., Wysocka-Diller J., Nakajima K., Jung J., Sena G., Hauser M. T., and Benfey P. N. (2000). The SHORT-ROOT gene controls radial patterning of the Arabidopsis root through radial signaling. Cell **101:** 555-567.

Herbik A., Bolling C., and Buckhout T. J. (2002). The involvement of a multicopper oxidase in iron uptake by the green algae *Chlamydomonas reinhardtii*. Plant Physiology **130:** 2039-2048.

Hesse H., Nikiforova V., Gakiere B., and Hoefgen R. (2004). Molecular analysis and control of cysteine biosynthesis: integration of nitrogen and sulphur metabolism. Journal of Experimental Botany **55:** 1283-1292.

Hirsch J., Marin E., Floriani M., Chiarenza S., Richaud P., Nussaume L., and Thibaud M. C. (2006). Phosphate deficiency promotes modification of iron distribution in Arabidopsis plants. Biochimie **88:** 1767-1771.

Hirsch R. E., Lewis B. D., Spalding E. P., and Sussman M. R. (1998). A role for the AKT1 potassium channel in plant nutrition. Science **280:** 918-921.

Ho C. H., Lin S. H., Hu H. C., and Tsay Y. F. (2009). CHL1 Functions as a Nitrate Sensor in Plants. Cell **138:** 1184-1194.

Hoagland D. R., and Arnon D. I. (1950). The water-culture method for growing plants without soil. California Agricultural Experiment Station, Circular **347.**

Hoegger P. J., Kilaru S., James T. Y., Thacker J. R., and Kues U. (2006). Phylogenetic comparison and classification of laccase and related multicopper oxidase protein sequences. Febs Journal **273:** 2308-2326.

Honsbein A., Sokolovski S., Grefen C., Campanoni P., Pratelli R., Paneque M., Chen Z. H., Johansson I., and Blatt M. R. (2009). A Tripartite SNARE-K+ Channel Complex Mediates in Channel-Dependent K+ Nutrition in Arabidopsis. Plant Cell **21:** 2859-2877.

Hoopes J. T., and Dean J. F. D. (2004). Ferroxidase activity in a laccase-like multicopper oxidase from *Liriodendron tulipifera*. Plant Physiology and Biochemistry **42:** 27-33.

Hubberten H. M., Drozd A., Tran B. V., Hesse H., and Hoefgen R. (2012). Local and systemic regulation of sulfur homeostasis in roots of *Arabidopsis thaliana*. Plant Journal **72:** 625-635.

Huston W. M., Jennings M. P., and McEwan A. G. (2002). The multicopper oxidase of *Pseudomonas aeruginosa* is a ferroxidase with a central role in iron acquisition. Molecular Microbiology **45:** 1741-1750.

Ikram S., Bedu M., Daniel-Vedele F., Chaillou S., and Chardon F. (2011). Natural variation of Arabidopsis response to nitrogen availability. Journal of Experimental Botany **63:** 91-105.

Iyer-Pascuzzi A. S., Symonova O., Mileyko Y., Hao Y. L., Belcher H., Harer J., Weitz J. S., and Benfey P. N. (2010). Imaging and Analysis Platform for Automatic Phenotyping and Trait Ranking of Plant Root Systems. Plant Physiology **152:** 1148-1157.

Jahnke S., Menzel M. I., van Dusschoten D., Roeb G. W., Buhler J., Minwuyelet S., Blumler P., Temperton V. M., Hombach T., Streun M., Beer S., Khodaverdi M., Ziemons K., Coenen H. H., and Schurr U. (2009). Combined MRI-PET dissects dynamic changes in plant structures and functions. Plant Journal **59:** 634-644.

Jauh G. Y., Phillips T. E., and Rogers J. C. (1999). Tonoplast intrinsic protein isoforms as markers for vacuolar functions. Plant Cell **11:** 1867-1882.

Jiang K., and Feldman L. J. (2005). Regulation of root apical meristem development. *In* Annual Review of Cell and Developmental Biology, Vol 21. ANNUAL REVIEWS, Palo Alto, pp 485-509.

Johansson I., Wulfetange K., Porée F., Michard E., Gajdanowicz P., Lacombe B., Sentenac H., Thibaud J.-B., Mueller-Roeber B., Blatt M. R., and Dreyer I. (2006). External K+ modulates the activity of the Arabidopsis potassium channel SKOR via an unusual mechanism. Plant Journal **46:** 269–281.

Jones D. L., Darrah P. R., and Kochian L. V. (1996). Critical evaluation of organic acid mediated iron dissolution in the rhizosphere and its potential role in root iron uptake. Plant and Soil **180:** 57-66.

Jones-Rhoades M. W., and Bartel D. P. (2004). Computational identification of plant MicroRNAs and their targets, including a stress-induced miRNA. Molecular Cell **14:** 787-799.

Jung J. Y., Shin R., and Schachtman D. P. (2009). Ethylene Mediates Response and Tolerance to Potassium Deprivation in Arabidopsis. Plant Cell **21:** 607-621.

Karimi M., Depicker A., and Hilson P. (2007). Recombinational cloning with plant gateway vectors. Plant Physiology **145:** 1144-1154.

Karnik R., Grefen C., Bayne R., Honsbein A., Kohler T., Kioumourtzoglou D., Williams M., Bryant N. J., and Blatt M. R. (2013). Arabidopsis Sec1/Munc18 Protein SEC11 Is a Competitive and Dynamic Modulator of SNARE Binding and SYP121-Dependent Vesicle Traffic. Plant Cell **25:** 1368-1382.

Kataoka T., Hayashi N., Yamaya T., and Takahashi H. (2004a). Root-to-shoot transport of sulfate in Arabidopsis. Evidence for the role of SULTR3;5 as a component of low-affinity sulfate transport system in the root vasculature. Plant Physiology **136:** 4198-4204.

Kataoka T., Watanabe-Takahashi A., Hayashi N., Ohnishi M., Mimura T., Buchner P., Hawkesford M. J., Yamaya T., and Takahashi H. (2004b). Vacuolar sulfate transporters are essential determinants controlling internal distribution of sulfate in Arabidopsis. Plant Cell **16:** 2693-2704.

Kellermeier F., and Amtmann A. (2013). Phenotyping jasmonate regulation of root growth. Methods in molecular biology (Clifton, N.J.) **1011:** 25-32.

Kellermeier F., Chardon F., and Amtmann A. (2013). Natural variation of Arabidopsis root architecture reveals complementing adaptive strategies to potassium starvation. Plant Physiology **161:** 1421-1432.

Kepinski S., and Leyser O. (2005). Plant development: Auxin in loops. Current Biology **15:** R208-R210.

Kiba T., Feria-Bourrellier A. B., Lafouge F., Lezhneva L., Boutet-Mercey S., Orsel M., Brehaut V., Miller A., Daniel-Vedele F., Sakakibara H., and Krapp A. (2012). The Arabidopsis Nitrate Transporter NRT2.4 Plays a Double Role in Roots and Shoots of Nitrogen-Straved Plants. Plant Cell **24:** 245-258.

Kim M. J., Ciani S., and Schachtman D. P. (2010). A Peroxidase Contributes to ROS Production during Arabidopsis Root Response to Potassium Deficiency. Molecular Plant **3:** 420-427.

Kim S. A., Punshon T., Lanzirotti A., Li L. T., Alonso J. M., Ecker J. R., Kaplan J., and Guerinot M. L. (2006). Localization of iron in Arabidopsis seed requires the vacuolar membrane transporter VIT1. Science **314:** 1295-1298.

Kinoshita A., Betsuyaku S., Osakabe Y., Mizuno S., Nagawa S., Stahl Y., Simon R., Yamaguchi-Shinozaki K., Fukuda H., and Sawa S. (2010). RPK2 is an essential receptor-like kinase that transmits the CLV3 signal in Arabidopsis. Development **137:** 3911-3920.

Knappe S., Flugge U. I., and Fischer K. (2003). Analysis of the plastidic phosphate translocator gene family in Arabidopsis and identification of new phosphate translocator-homologous transporters, classified by their putative substrate-binding site. Plant Physiology **131:** 1178-1190.

Kobayashi Y., Kuroda K., Kimura K., Southron-Francis J. L., Furuzawa A., Iuchi S., Kobayashi M., Taylor G. J., and Koyama H. (2008). Amino acid polymorphisms in strictly conserved domains of a P-type ATPase HMA5 are involved in the mechanism of copper tolerance variation in Arabidopsis. Plant Physiology **148:** 969-980.

Koncz C., and Schell J. (1986). The Promoter of Tl-DNA Gene 5 Controls the Tissue-Specific Expression of Chimeric Genes Carried by a Novel Type of Agrobacterium Binary Vector. Molecular & General Genetics **204:** 383-396.

Koornneef M., Alonso-Blanco C., and Vreugdenhil D. (2004). Naturally occurring genetic variation in *Arabidopsis thaliana*. Annual Review of Plant Biology **55:** 141-172.

Kopittke P. M., de Jonge M. D., Menzies N. W., Wang P., Donner E., McKenna B. A., Paterson D., Howard D. L., and Lombi E. (2012). Examination of the Distribution of Arsenic in Hydrated and Fresh Cowpea Roots Using Two- and Three-Dimensional Techniques. Plant Physiology **159:** 1149-1158.

Korshunova Y. O., Eide D., Clark W. G., Guerinot M. L., and Pakrasi H. B. (1999). The IRT1 protein from *Arabidopsis thaliana* is a metal transporter with a broad substrate range. Plant Molecular Biology **40:** 37-44.

Kover P. X., and Mott R. (2012). Mapping the genetic basis of ecologically and evolutionarily relevant traits in *Arabidopsis thaliana*. Current Opinion in Plant Biology **15:** 212-217.

Kover P. X., Valdar W., Trakalo J., Scarcelli N., Ehrenreich I. M., Purugganan M. D., Durrant C., and Mott R. (2009). A Multiparent Advanced Generation Inter-Cross to Fine-Map Quantitative Traits in *Arabidopsis thaliana*. Plos Genetics **5:** e1000551.

Krapp A., Berthome R., Orsel M., Mercey-Boutet S., Yu A., Castaings L., Elftieh S., Major H., Renou J. P., and Daniel-Vedele F. (2011). Arabidopsis Roots and Shoots Show Distinct Temporal Adaptation Patterns toward Nitrogen Starvation. Plant Physiology **157:** 1255-1282.

Kronzucker H. J., Siddiqi M. Y., Glass A. D. M., and Kirk G. J. D. (1999). Nitrate-ammonium synergism in rice. A subcellular flux analysis. Plant Physiology **119:** 1041-1045.

Krouk G., Lacombe B., Bielach A., Perrine-Walker F., Malinska K., Mounier E., Hoyerova K., Tillard P., Leon S., Ljung K., Zazimalova E., Benkova E., Nacry P., and Gojon A. (2010). Nitrate-Regulated Auxin Transport by NRT1.1 Defines a Mechanism for Nutrient Sensing in Plants. Developmental Cell **18:** 927-937.

Kutschera L. (1960). Wurzelatlas mitteleuropäischer Ackerunkräuter und Kulturpflanzen. DLG Verlag, Frankfurt am Main.

Kutz A., Muller A., Hennig P., Kaiser W. M., Piotrowski M., and Weiler E. W. (2002). A role for nitrilase 3 in the regulation of root morphology in sulphur-starving *Arabidopsis thaliana*. Plant Journal **30:** 95-106.

Lahner B., Gong J. M., Mahmoudian M., Smith E. L., Abid K. B., Rogers E. E., Guerinot M. L., Harper J. F., Ward J. M., McIntyre L., Schroeder J. I., and Salt D. E. (2003). Genomic scale profiling of nutrient and trace elements in *Arabidopsis thaliana*. Nature Biotechnology **21:** 1215-1221.

Lang M. L., Braun C. L., Kanost M. R., and Gorman M. J. (2012). Multicopper oxidase-1 is a ferroxidase essential for iron homeostasis in *Drosophila melanogaster*. Proceedings of the National Academy of Sciences of the United States of America **109:** 13337-13342.

Lanquar V., Lelievre F., Bolte S., Hames C., Alcon C., Neumann D., Vansuyt G., Curie C., Schroder A., Kramer U., Barbier-Brygoo H., and Thomine S. (2005). Mobilization of vacuolar iron by AtNRAMP3 and AtNRAMP4 is essential for seed germination on low iron. Embo Journal **24:** 4041-4051.

Laskowski M., Grieneisen V. A., Hofhuis H., ten Hove C. A., Hogeweg P., Maree A. F. M., and Scheres B. (2008). Root System Architecture from Coupling Cell Shape to Auxin Transport. Plos Biology **6:** 2721-2735.

Laugier E., Bouguyon E., Mauries A., Tillard P., Gojon A., and Lejay L. (2012). Regulation of High-Affinity Nitrate Uptake in Roots of Arabidopsis Depends Predominantly on Posttranscriptional Control of the NRT2.1/NAR2.1 Transport System. Plant Physiology **158:** 1067-1078.

Lee S. C., Cheng H., King K. E., Wang W. F., He Y. W., Hussain A., Lo J., Harberd N. P., and Peng J. R. (2002). Gibberellin regulates Arabidopsis seed germination via RGL2, a GAI/RGA-like gene whose expression is up-regulated following imbibition. Genes & Development **16:** 646-658.

Lee S. C., Lan W. Z., Kim B. G., Li L. G., Cheong Y. H., Pandey G. K., Lu G. H., Buchanan B. B., and Luan S. (2007). A protein phosphorylation/dephosphorylation network regulates a plant potassium channel. Proceedings of the National Academy of Sciences of the United States of America **104:** 15959-15964.

Lee S. J., Kang J. Y., Park H. J., Kim M. D., Bae M. S., Choi H. I., and Kim S. Y. (2012). DREB2C Interacts with ABF2, a bZIP Protein Regulating Abscisic Acid-Responsive Gene Expression, and Its Overexpression Affects Abscisic Acid Sensitivity. Plant Physiology **153:** 716-727.

Lei M. G., Liu Y. D., Zhang B. C., Zhao Y. T., Wang X. J., Zhou Y. H., Raghothama K. G., and Liu D. (2011). Genetic and Genomic Evidence That Sucrose Is a Global Regulator of Plant Responses to Phosphate Starvation in Arabidopsis. Plant Physiology **156:** 1116-1130.

Leigh R. A., and Jones R. G. W. (1984). A Hypothesis Relating Critical Potassium Concentrations for Growth to the Distribution and Functions of This Ion in the Plant-Cell. New Phytologist **97:** 1-13.

Lemanceau P., Bauer P., Kraemer S., and Briat J. F. (2009). Iron dynamics in the rhizosphere as a case study for analyzing interactions between soils, plants and microbes. Plant and Soil **321:** 513-535.

Lequeux H., Hermans C., Lutts S., and Verbruggen N. (2010). Response to copper excess in *Arabidopsis thaliana*: Impact on the root system architecture, hormone distribution, lignin accumulation and mineral profile. Plant Physiology and Biochemistry **48:** 673-682.

Leyser O. (2006). Dynamic integration of auxin transport and signalling. Current Biology **16:** R424-R433.

Li J. Y., Fu Y. L., Pike S. M., Bao J., Tian W., Zhang Y., Chen C. Z., Li H. M., Huang J., Li L. G., Schroeder J. I., Gassmann W., and Gonga J. M. (2010a). The Arabidopsis Nitrate Transporter NRT1.8 Functions in Nitrate Removal from the Xylem Sap and Mediates Cadmium Tolerance. Plant Cell **22:** 1633-1646.

Li L. G., Kim B. G., Cheong Y. H., Pandey G. K., and Luan S. (2006). A Ca2+ signaling pathway regulates a K+ channel for low-K response in Arabidopsis. Proceedings of the National Academy of Sciences of the United States of America **103:** 12625-12630.

Li Q., Li B. H., Kronzucker H. J., and Shi W. M. (2010b). Root growth inhibition by NH4+ in Arabidopsis is mediated by the root tip and is linked to NH4+ efflux and GMPase activity. Plant Cell and Environment **33:** 1529-1542.

Lima J. E., Kojima S., Takahashi H., and von Wiren N. (2010). Ammonium Triggers Lateral Root Branching in Arabidopsis in an AMMONIUM TRANSPORTER1;3-Dependent Manner. Plant Cell **22:** 3621-3633.

Lin S. H., Kuo H. F., Canivenc G., Lin C. S., Lepetit M., Hsu P. K., Tillard P., Lin H. L., Wang Y. Y., Tsai C. B., Gojon A., and Tsay Y. F. (2008). Mutation of the Arabidopsis NRT1.5 Nitrate Transporter Causes Defective Root-to-Shoot Nitrate Transport. Plant Cell **20:** 2514-2528.

Linkohr B. I., Williamson L. C., Fitter A. H., and Leyser H. M. O. (2002). Nitrate and phosphate availability and distribution have different effects on root system architecture of Arabidopsis. Plant Journal **29:** 751-760.

Little D. Y., Rao H. Y., Oliva S., Daniel-Vedele F., Krapp A., and Malamy J. E. (2005). The putative high-affinity nitrate transporter NRT2.1 represses lateral root initiation in response to nutritional cues. Proceedings of the National Academy of Sciences of the United States of America **102:** 13693-13698.

Liu K. H., and Tsay Y. F. (2003). Switching between the two action modes of the dual-affinity nitrate transporter CHL1 by phosphorylation. Embo Journal **22:** 1005-1013.

Lopez-Bucio J., Cruz-Ramirez A., and Herrera-Estrella L. (2003). The role of nutrient availability in regulating root architecture. Current Opinion in Plant Biology **6:** 280-287.

Lopez-Bucio J., Hernandez-Abreu E., Sanchez-Calderon L., Nieto-Jacobo M. F., Simpson J., and Herrera-Estrella L. (2002). Phosphate availability alters architecture and causes changes in hormone sensitivity in the Arabidopsis root system. Plant Physiology **129:** 244-256.

Lopez-Bucio J., Hernandez-Abreu E., Sanchez-Calderon L., Perez-Torres A., Rampey R. A., Bartel B., and Herrera-Estrella L. (2005). An auxin transport independent pathway is involved in phosphate stress-induced root architectural alterations in Arabidopsis. Identification of BIG as a mediator of auxin in pericycle cell activation. Plant Physiology **137:** 681-691.

Loudet O., Chaillou S., Camilleri C., Bouchez D., and Daniel-Vedele F. (2002). Bay-0 x Shahdara recombinant inbred line population: a powerful tool for the genetic dissection of complex traits in Arabidopsis. Theoretical and Applied Genetics **104:** 1173-1184.

Loudet O., Gaudon V., Trubuil A., and Daniel-Vedele F. (2005). Quantitative trait loci controlling root growth and architecture in *Arabidopsis thaliana* confirmed by heterogeneous inbred family. Theoretical and Applied Genetics **110:** 742-753.

Lynch J. (1995). Root Architecture and Plant Productivity. Plant Physiology **109:** 7-13.

Ma Z., Baskin T. I., Brown K. M., and Lynch J. P. (2003). Regulation of root elongation under phosphorus stress involves changes in ethylene responsiveness. Plant Physiology **131:** 1381-1390.

Maathuis F. J. M. (2009). Physiological functions of mineral macronutrients. Current Opinion in Plant Biology **12:** 250-258.

Maathuis F. J. M., and Amtmann A. (1999). K+ nutrition and Na+ toxicity: The basis of cellular K+/Na+ ratios. Annals of Botany **84:** 123-133.

MacGregor D. R., Deak K. I., Ingram P. A., and Malamy J. E. (2008). Root system architecture in Arabidopsis grown in culture is regulated by sucrose uptake in the aerial tissues. Plant Cell **20:** 2643-2660.

Mairhofer S., Zappala S., Tracy S., Sturrock C., Bennett M. J., Mooney S. J., and Pridmore T. P. (2013). Recovering complete plant root system architectures from soil via X-ray mu-Computed Tomography. Plant Methods **9**

Mairhofer S., Zappala S., Tracy S. R., Sturrock C., Bennett M., Mooney S. J., and Pridmore T. (2012). RooTrak: Automated Recovery of Three-Dimensional Plant Root Architecture in Soil from X-Ray Microcomputed Tomography Images Using Visual Tracking. Plant Physiology **158:** 561-569.

Malamy J. E., and Ryan K. S. (2001). Environmental regulation of lateral root initiation in Arabidopsis. Plant Physiology **127:** 899-909.

Marschner H. (1995). Mineral nutrition of higher plants. Academic Press Ltd, London.

Marschner P., Crowley D., and Rengel Z. (2011). Rhizosphere interactions between microorganisms and plants govern iron and phosphorus acquisition along the root axis - model and research methods. Soil Biology & Biochemistry **43:** 883-894.

Martin-Rejano E. M., Camacho-Cristobal J. J., Herrera-Rodriguez M. B., Rexach J., Navarro-Gochicoa M. T., and Gonzalez-Fontes A. (2011). Auxin and ethylene are involved in the responses of root system architecture to low boron supply in Arabidopsis seedlings. Physiologia Plantarum **142:** 170-178.

Maruyama-Nakashita A., Nakamura Y., Tohge T., Saito K., and Takahashi H. (2006). Arabidopsis SLIM1 is a central transcriptional regulator of plant sulfur response and metabolism. Plant Cell **18:** 3235-3251.

Maruyama-Nakashita A., Nakamura Y., Yamaya T., and Takahashi H. (2004). Regulation of high-affinity sulphate transporters in plants: towards systematic analysis of sulphur signalling and regulation. Journal of Experimental Botany **55:** 1843-1849.

Masclaux-Daubresse C., and Chardon F. (2011). Exploring nitrogen remobilization for seed filling using natural variation in *Arabidopsis thaliana*. Journal of Experimental Botany **62:** 2131-2142.

McKhann H. I., Camilleri C., Berard A., Bataillon T., David J. L., Reboud X., Le Corre V., Caloustian C., Gut I. G., and Brunel D. (2004). Nested core collections maximizing genetic diversity in *Arabidopsis thaliana*. Plant Journal **38:** 193-202.

Meyer A. J., Brach T., Marty L., Kreye S., Rouhier N., Jacquot J. P., and Hell R. (2007). Redox-sensitive GFP in *Arabidopsis thaliana* is a quantitative biosensor for the redox potential of the cellular glutathione redox buffer. Plant Journal **52:** 973-986.

Migliaccio F., and Piconese S. (2001). Spiralizations and tropisms in Arabidopsis roots. Trends in Plant Science **6:** 561-565.

Miller A. J., Fan X. R., Orsel M., Smith S. J., and Wells D. M. (2007). Nitrate transport and signalling. Journal of Experimental Botany **58:** 2297-2306.

Miller A. J., Shen Q. R., and Xu G. H. (2009). Freeways in the plant: transporters for N, P and S and their regulation. Current Opinion in Plant Biology **12:** 284-290.

Misson J., Raghothama K. G., Jain A., Jouhet J., Block M. A., Bligny R., Ortet P., Creff A., Somerville S., Rolland N., Doumas P., Nacry P., Herrerra-Estrella L., Nussaume L., and Thibaud M. C. (2005). A genome-wide transcriptional analysis using *Arabidopsis thaliana* Affymetrix gene chips determined plant responses to phosphate deprivation. Proceedings of the National Academy of Sciences of the United States of America **102:** 11934-11939.

Miura K., Lee J., Gong Q. Q., Ma S. S., Jin J. B., Yoo C. Y., Miura T., Sato A., Bohnert H. J., and Hasegawa P. M. (2011). SIZ1 Regulation of Phosphate

Starvation-Induced Root Architecture Remodeling Involves the Control of Auxin Accumulation. Plant Physiology **155:** 1000-1012.

Miura K., Rus A., Sharkhuu A., Yokoi S., Karthikeyan A. S., Raghothama K. G., Baek D., Koo Y. D., Jin J. B., Bressan R. A., Yun D. J., and Hasegawa P. M. (2005). The Arabidopsis SUMO E3 ligase SIZ1 controls phosphate deficiency responses. Proceedings of the National Academy of Sciences of the United States of America **102:** 7760-7765.

Mooney S. J., Pridmore T. P., Helliwell J., and Bennett M. J. (2012). Developing X-ray Computed Tomography to non-invasively image 3-D root systems architecture in soil. Plant and Soil **352:** 1-22.

Morcuende R., Bari R., Gibon Y., Zheng W., Pant B. D., Bläsing O., Usadel B., Czechowski T., Udvardi M. K., Stitt M., Scheible W. R. (2012). Genome-wide reprogramming of metabolism and regulatory networks of Arabidopsis in response to phosphorus. Plant Cell and Environment **30:** 85-112.

Moriyasu Y., Hattori M., Jauh G. Y., and Rogers J. C. (2003). Alpha tonoplast intrinsic protein is specifically associated with vacuole membrane involved in an autophagic process. Plant and Cell Physiology **44:** 795-802.

Morrissey J., Baxter I. R., Lee J., Li L. T., Lahner B., Grotz N., Kaplan J., Salt D. E., and Guerinot M. L. (2009). The Ferroportin Metal Efflux Proteins Function in Iron and Cobalt Homeostasis in Arabidopsis. Plant Cell **21:** 3326-3338.

Morrissey J., and Guerinot M. L. (2009). Iron Uptake and Transport in Plants: The Good, the Bad, and the Ionome. Chemical Reviews **109:** 4553-4567.

Mouchel C. F., Briggs G. C., and Hardtke C. S. (2004). Natural genetic variation in Arabidopsis identifies BREVIS RADIX, a novel regulator of cell proliferation and elongation in the root. Genes & Development **18:** 700-714.

Müller B., and Sheen J. (2008). Cytokinin and auxin interaction in root stem-cell specification during early embryogenesis. Nature **453:** 1094-1097.

Murase K., Hirano Y., Sun T. P., and Hakoshima T. (2008). Gibberellin-induced DELLA recognition by the gibberellin receptor GID1. Nature **456:** 459-463.

Murashige T., and Skoog F. (1962). A Revised Medium for Rapid Growth and Bio Assays with Tobacco Tissue Cultures. Physiologia Plantarum **15:** 473-497.

Nacry P., Canivenc G., Muller B., Azmi A., Van Onckelen H., Rossignol M., and Doumas P. (2005). A role for auxin redistribution in the responses of the root system architecture to phosphate starvation in Arabidopsis. Plant Physiology **138:** 2061-2074.

Naeem A., French A. P., Wells D. M., and Pridmore T. P. (2011). High-throughput feature counting and measurement of roots. Bioinformatics **27:** 1337-1338.

Nagarajan V. K., Jain A., Poling M. D., Lewis A. J., Raghothama K. G., and Smith A. P. (2011). Arabidopsis Pht1;5 Mobilizes Phosphate between Source and Sink Organs and Influences the Interaction between Phosphate Homeostasis and Ethylene Signaling. Plant Physiology **156:** 1149-1163.

Nakashima K., Takasaki H., Mizoi J., Shinozaki K., and Yamaguchi-Shinozaki K. (2012). NAC transcription factors in plant abiotic stress responses. Biochimica Et Biophysica Acta - Gene Regulatory Mechanisms **1819:** 97-103.

Narang R. A., Bruene A., and Altmann T. (2000). Analysis of phosphate acquisition efficiency in different Arabidopsis accessions. Plant Physiology **124:** 1786-1799.

Neumann G., George T. S., and Plassard C. (2009). Strategies and methods for studying the rhizosphere - the plant science toolbox. Plant and Soil **321:** 431-456.

Nibau C., Gibbs D. J., and Coates J. C. (2008). Branching out in new directions: the control of root architecture by lateral root formation. New Phytologist **179:** 595-614.

Nieves-Cordones M., Aleman F., Martinez V., and Rubio F. (2010). The *Arabidopsis thaliana* HAK5 K+ Transporter Is Required for Plant Growth and K+ Acquisition from Low K+ Solutions under Saline Conditions. Molecular Plant **3:** 326-333.

Nikiforova V., Freitag J., Kempa S., Adamik M., Hesse H., and Hoefgen R. (2003). Transcriptome analysis of sulfur depletion in *Arabidopsis thaliana*: interlacing of biosynthetic pathways provides response specificity. Plant Journal **33:** 633-650.

Nin V., Hernandez J. A., and Chifflet S. (2009). Hyperpolarization of the Plasma Membrane Potential Provokes Reorganization of the Actin Cytoskeleton and Increases the Stability of Adherens Junctions in Bovine Corneal Endothelial Cells in Culture. Cell Motility and the Cytoskeleton **66:** 1087-1099.

Nishida S., Tsuzuki C., Kato A., Aisu A., Yoshida J., and Mizuno T. (2011). AtIRT1, the Primary Iron Uptake Transporter in the Root, Mediates Excess Nickel Accumulation in *Arabidopsis thaliana*. Plant and Cell Physiology **52:** 1433-1442.

Nordborg M., Hu T. T., Ishino Y., Jhaveri J., Toomajian C., Zheng H. G., Bakker E., Calabrese P., Gladstone J., Goyal R., Jakobsson M., Kim S., Morozov Y., Padhukasahasram B., Plagnol V., Rosenberg N. A., Shah C., Wall J. D., Wang J., Zhao K. Y., Kalbfleisch T., Schulz V., Kreitman M., and Bergelson J. (2005). The pattern of polymorphism in *Arabidopsis thaliana*. Plos Biology **3:** 1289-1299.

North K. A., Ehlting B., Koprivova A., Rennenberg H., and Kopriva S. (2009). Natural variation in Arabidopsis adaptation to growth at low nitrogen conditions. Plant Physiology and Biochemistry **47:** 912-918.

Nussaume L., Kanno S., Javot H., Marin E., Pochon N., Ayadi A., Nakanishi T. M., and Thibaud M.-C. (2011). Phosphate Import in Plants: Focus on the PHT1 Transporters. Frontiers in plant science **2:** 83.

Oliva M., and Dunand C. (2007). Waving and skewing: how gravity and the surface of growth media affect root development in Arabidopsis. New Phytologist **176:** 37-43.

Osaki M., Watanabe T., Ishizawa T., Nilnond C., Nuyim T., Shinano T., Urayama M., and Tuah S. J. (2003). Nutritional characteristics of the leaves of native plants growing in adverse soils of humid tropical lowlands. Plant Foods for Human Nutrition **58:** 93-115.

Osmont K. S., Sibout R., and Hardtke C. S. (2007). Hidden branches: Developments in root system architecture. Annual Review of Plant Biology **58:** 93-113.

Ossowski S., Schneeberger K., Clark R. M., Lanz C., Warthmann N., and Weigel D. (2008). Sequencing of natural strains of *Arabidopsis thaliana* with short reads. Genome Research **18:** 2024-2033.

Ostrowski M. F., David J., Santoni S., McKhann H., Reboud X., Le Corre V., Camilleri C., Brunel D., Bouchez D., Faure B., and Bataillon T. (2006). Evidence for a large-scale population structure among accessions of *Arabidopsis thaliana*: possible causes and consequences for the distribution of linkage disequilibrium. Molecular Ecology **15:** 1507-1517.

Pacheco-Villalobos D., and Hardtke C. S. (2012). Natural genetic variation of root system architecture from Arabidopsis to Brachypodium: towards adaptive value. Philosophical Transactions of the Royal Society B - Biological Sciences **367:** 1552-1558.

Palmer C. M., and Guerinot M. L. (2009). Facing the challenges of Cu, Fe and Zn homeostasis in plants. Nature Chemical Biology **5:** 333-340.

Pandey G. K., Cheong Y. H., Kim B. G., Grant J. J., Li L. G., and Luan S. (2007). CIPK9: a calcium sensor-interacting protein kinase required for low-potassium tolerance in Arabidopsis. Cell Research **17:** 411-421.

Pant B. D., Buhtz A., Kehr J., and Scheible W. R. (2008). MicroRNA399 is a long-distance signal for the regulation of plant phosphate homeostasis. Plant Journal **53:** 731-738.

Park B. S., Song J. T., and Seo H. S. (2011). Arabidopsis nitrate reductase activity is stimulated by the E3 SUMO ligase AtSIZ1. Nature Communications **2:** 400.

Patterson K., Cakmak T., Cooper A., Lager I., Rasmusson A. G., and Escobar M. A. (2010). Distinct signalling pathways and transcriptome response signatures

differentiate ammonium- and nitrate-supplied plants. Plant Cell and Environment **33:** 1486-1501.

Peret B., Clement M., Nussaume L., and Desnos T. (2011). Root developmental adaptation to phosphate starvation: better safe than sorry. Trends in Plant Science **16:** 442-450.

Peret B., De Rybel B., Casimiro I., Benkova E., Swarup R., Laplaze L., Beeckman T., and Bennett M. J. (2009). Arabidopsis lateral root development: an emerging story. Trends in Plant Science **14:** 399-408.

Perez-Torres C. A., Lopez-Bucio J., Cruz-Ramirez A., Ibarra-Laclette E., Dharmasiri S., Estelle M., and Herrera-Estrella L. (2008). Phosphate Availability Alters Lateral Root Development in Arabidopsis by Modulating Auxin Sensitivity via a Mechanism Involving the TIR1 Auxin Receptor. Plant Cell **20:** 3258-3272.

Perilli S., Mambro R., and Sabatini S. (2012). Growth and development of the root apical meristem. Current Opinion in Plant Biology **15:** 17-23.

Petricka J. J., Winter C. M., and Benfey P. N. (2012). Control of Arabidopsis Root Development. *In* Annual Review of Plant Biology, Vol 63. ANNUAL REVIEWS, Palo Alto, pp 563-590.

Pigliucci M., and Schlichting C. D. (1995). Reaction Norms of Arabidopsis (Brassicaceae). III. Response to Nutrients in 26 Populations from a Worldwide Collection. American Journal of Botany **82:** 1117-1125.

Platt A., Horton M., Huang Y. S., Li Y., Anastasio A. E., Mulyati N. W., Agren J., Bossdorf O., Byers D., Donohue K., Dunning M., Holub E. B., Hudson A., Le Corre V., Loudet O., Roux F., Warthmann N., Weigel D., Rivero L., Scholl R., Nordborg M., Bergelson J., and Borevitz J. O. (2010). The Scale of Population Structure in *Arabidopsis thaliana*. Plos Genetics **6:** e1000843.

Poormohammad Kiani S., Trontin C., Andreatta M., Simon M., Robert T., Salt D. E., and Loudet O. (2012). Allelic heterogeneity and trade-off shape natural variation for response to soil micronutrient. PLoS genetics **8:** e1002814.

Prinzenberg A. E., Barbier H., Salt D. E., Stich B., and Reymond M. (2010). Relationships between Growth, Growth Response to Nutrient Supply, and Ion Content Using a Recombinant Inbred Line Population in Arabidopsis. Plant Physiology **154:** 1361-1371.

Punshon T., Guerinot M. L., and Lanzirotti A. (2009). Using synchrotron X-ray fluorescence microprobes in the study of metal homeostasis in plants. Annals of Botany **103:** 665-672.

Punshon T., Hirschi K., Yang J., Lanzirotti A., Lai B., and Guerinot M. L. (2012). The Role of CAX1 and CAX3 in Elemental Distribution and Abundance in Arabidopsis Seed. Plant Physiology **158:** 352-362.

Pyo Y. J., Gierth M., Schroeder J. I., and Cho M. H. (2010). High-Affinity K(+) Transport in Arabidopsis: AtHAK5 and AKT1 Are Vital for Seedling Establishment and Postgermination Growth under Low-Potassium Conditions. Plant Physiology **153:** 863-875.

Qi Z., Hampton C. R., Shin R., Barkla B. J., White P. J., and Schachtman D. P. (2008). The high affinity K+ transporter AtHAK5 plays a physiological role in planta at very low K+ concentrations and provides a caesium uptake pathway in Arabidopsis. Journal of Experimental Botany **59:** 595-607.

Ramirez-Parra E., Lopez-Matas M. A., Frundt C., and Gutierrez C. (2004). Role of an atypical E2F transcription factor in the control of Arabidopsis cell growth and differentiation. Plant Cell **16:** 2350-2363.

Rauh B. L., Basten C., and Buckler E. S. (2002). Quantitative trait loci analysis of growth response to varying nitrogen sources in *Arabidopsis thaliana*. Theoretical and Applied Genetics **104:** 743-750.

Ravet K., Touraine B., Boucherez J., Briat J. F., Gaymard F., and Cellier F. (2009). Ferritins control interaction between iron homeostasis and oxidative stress in Arabidopsis. Plant Journal **57:** 400-412.

Remans T., Nacry P., Pervent M., Filleur S., Diatloff E., Mounier E., Tillard P., Forde B. G., and Gojon A. (2006a). The Arabidopsis NRT1.1 transporter participates in the signaling pathway triggering root colonization of nitrate-rich patches. Proceedings of the National Academy of Sciences of the United States of America **103:** 19206-19211.

Remans T., Nacry P., Pervent M., Girin T., Tillard P., Lepetit M., and Gojon A. (2006b). A central role for the nitrate transporter NRT2.1 in the integrated morphological and physiological responses of the root system to nitrogen limitation in Arabidopsis. Plant Physiology **140:** 909-921.

Remy E., Cabrito T. R., Batista R. A., Teixeira M. C., Sa-Correia I., and Duque P. (2012). The Pht1;9 and Pht1;8 transporters mediate inorganic phosphate acquisition by the *Arabidopsis thaliana* root during phosphorus starvation. New Phytologist **195:** 356-371.

Reymond M., Svistoonoff S., Loudet O., Nussaume L., and Desnos T. (2006). Identification of QTL controlling root growth response to phosphate starvation in *Arabidopsis thaliana*. Plant Cell and Environment **29:** 115-125.

Rich S. M., and Watt M. (2013). Soil conditions and cereal root system architecture: review and considerations for linking Darwin and Weaver. Journal of Experimental Botany **64:** 1193-1208.

Richard O., Pineau C., Loubet S., Chalies C., Vile D., Marques L., and Berthomieu P. (2011). Diversity analysis of the response to Zn within the *Arabidopsis thaliana* species revealed a low contribution of Zn translocation to Zn tolerance and a new role for Zn in lateral root development. Plant Cell and Environment **34:** 1065-1078.

Rinaldi M. A., Liu J., Enders T. A., Bartel B., and Strader L. C. (2012). A gain-of-function mutation in IAA16 confers reduced responses to auxin and abscisic acid and impedes plant growth and fertility. Plant Molecular Biology **79:** 359-373.

Robinson N. J., Procter C. M., Connolly E. L., and Guerinot M. L. (1999). A ferric-chelate reductase for iron uptake from soils. Nature **397:** 694-697.

Rogers E. E., and Guerinot M. L. (2002). FRD3, a member of the multidrug and toxin efflux family, controls iron deficiency responses in Arabidopsis. Plant Cell **14:** 1787-1799.

Roppolo D., De Rybel B., Tendon V. D., Pfister A., Alassimone J., Vermeer J. E. M., Yamazaki M., Stierhof Y. D., Beeckman T., and Geldner N. (2011). A novel protein family mediates Casparian strip formation in the endodermis. Nature **473:** 380-383.

Rouached H., Wirtz M., Alary R., Hell R., Arpat A. B., Davidian J. C., Fourcroy P., and Berthomieu P. (2008). Differential regulation of the expression of two high-affinity sulfate transporters, SULTR1.1 and SULTR1.2, in arabidopsis. Plant Physiology **147:** 897-911.

Roycewicz P., and Malamy J. E. (2012). Dissecting the effects of nitrate, sucrose and osmotic potential on Arabidopsis root and shoot system growth in laboratory assays. Philosophical Transactions of the Royal Society B - Biological Sciences **367:** 1489-1500.

Rubin G., Tohge T., Matsuda F., Saito K., and Scheible W. R. (2009). Members of the LBD Family of Transcription Factors Repress Anthocyanin Synthesis and Affect Additional Nitrogen Responses in Arabidopsis. Plant Cell **21:** 3567-3584.

Rubio F., Aleman F., Nieves-Cordones M., and Martinez V. (2010). Studies on Arabidopsis *athak5*, *atakt1* double mutants disclose the range of concentrations at which AtHAK5, AtAKT1 and unknown systems mediate K plus uptake. Physiologia Plantarum **139:** 220-228.

Rubio F., Nieves-Cordones M., Aleman F., and Martinez V. (2008). Relative contribution of AtHAK5 and AtAKT1 to K+ uptake in the high-affinity range of concentrations. Physiologia Plantarum **134:** 598-608.

Rubio V., Bustos R., Irigoyen M. L., Cardona-Lopez X., Rojas-Triana M., and Paz-Ares J. (2009). Plant hormones and nutrient signaling. Plant Molecular Biology **69:** 361-373.

Rubio V., Linhares F., Solano R., Martin A. C., Iglesias J., Leyva A., and Paz-Ares J. (2001). A conserved MYB transcription factor involved in phosphate starvation signaling both in vascular plants and in unicellular algae. Genes & Development **15:** 2122-2133.

Ruffel S., Krouk G., Ristova D., Shasha D., Birnbaum K. D., and Coruzzi G. M. (2011). Nitrogen economics of root foraging: Transitive closure of the nitrate-cytokinin relay and distinct systemic signaling for N supply vs. demand. Proceedings of the National Academy of Sciences of the United States of America **108:** 18524-18529.

Sabatini S., Heidstra R., Wildwater M., and Scheres B. (2003). SCARECROW is involved in positioning the stem cell niche in the Arabidopsis root meristem. Genes & Development **17:** 354-358.

Salome P. A., Bomblies K., Laitinen R. A. E., Yant L., Mott R., and Weigel D. (2011). Genetic Architecture of Flowering-Time Variation in *Arabidopsis thaliana*. Genetics **188:** 421-433.

Salt D. E., Baxter I., and Lahner B. (2008). Ionomics and the study of the plant ionome. Annual Review of Plant Biology **59:** 709-733.

Sanchez-Calderon L., Lopez-Bucio J., Chacon-Lopez A., Gutierrez-Ortega A., Hernandez-Abreu E., and Herrera-Estrella L. (2006). Characterization of low phosphorus insensitive mutants reveals a crosstalk between low phosphorus-induced determinate root development and the activation of genes involved in the adaptation of Arabidopsis to phosphorus deficiency. Plant Physiology **140:** 879-889.

Santi S., and Schmidt W. (2009). Dissecting iron deficiency-induced proton extrusion in Arabidopsis roots. New Phytologist **183:** 1072-1084.

Sarkar A. K., Luijten M., Miyashima S., Lenhard M., Hashimoto T., Nakajima K., Scheres B., Heidstra R., and Laux T. (2007). Conserved factors regulate signalling in *Arabidopsis thaliana* shoot and root stem cell organizers. Nature **446:** 811-814.

Schachtman D. P., and Shin R. (2007). Nutrient sensing and signaling: NPKS. *In* Annual Review of Plant Biology, Vol 58. ANNUAL REVIEWS, Palo Alto, pp 47-69.

Scheible W. R., Morcuende R., Czechowski T., Fritz C., Osuna D., Palacios-Rojas N., Schindelasch D., Thimm O., Udvardi M. K., and Stitt M. (2004). Genome-wide reprogramming of primary and secondary metabolism, protein synthesis, cellular growth processes, and the regulatory infrastructure of Arabidopsis in response to nitrogen. Plant Physiology **136:** 2483-2499.

Schlereth A., Moller B., Liu W. L., Kientz M., Flipse J., Rademacher E. H., Schmid M., Jurgens G., and Weijers D. (2010). MONOPTEROS controls embryonic root initiation by regulating a mobile transcription factor. Nature **464:** 913-916.

Schwarzländer M., Fricker M. D., Muller C., Marty L., Brach T., Novak J., Sweetlove L. J., Hell R., and Meyer A. J. (2008). Confocal imaging of glutathione redox potential in living plant cells. Journal of Microscopy **231:** 299-316.

Scott A. C. and Allen N. S. (1999). Changes in cytosolic pH within Arabidopsis root columella cells play a key role in the early signaling pathway for root gravitropism. Plant Physiology **121:** 1291–1298.

Sedbrook J. C., Ehrhardt D. W., Fisher S. E., Scheible W. R., and Somerville C. R. (2004). The Arabidopsis SKU6/SPIRAL1 gene encodes a plus end-localized microtubule-interacting protein involved in directional cell expansion. Plant Cell **16:** 1506-1520.

Sergeeva L. I., Keurentjes J. J. B., Bentsink L., Vonk J., van der Plas L. H. W., Koornneef M., and Vreugdenhil D. (2006). Vacuolar invertase regulates elongation of *Arabidopsis thaliana* roots as revealed by QTL and mutant analysis. Proceedings of the National Academy of Sciences of the United States of America **103:** 2994-2999.

Shin H., Shin H. S., Chen R., and Harrison M. J. (2006). Loss of At4 function impacts phosphate distribution between the roots and the shoots during phosphate starvation. Plant Journal **45:** 712-726.

Shin H., Shin H. S., Dewbre G. R., and Harrison M. J. (2004). Phosphate transport in Arabidopsis: Pht1;1 and Pht1;4 play a major role in phosphate acquisition from both low- and high-phosphate environments. Plant Journal **39:** 629-642.

Shin R., Berg R. H., and Schachtman D. P. (2005). Reactive oxygen species and root hairs in Arabidopsis root response to nitrogen, phosphorus and potassium deficiency. Plant and Cell Physiology **46:** 1350-1357.

Shin R., and Schachtman D. P. (2004). Hydrogen peroxide mediates plant root cell response to nutrient deprivation. Proceedings of the National Academy of Sciences of the United States of America **101:** 8827-8832.

Silva L. D. C. E., Wang S., and Zeng Z.-B. (2012). Composite interval mapping and multiple interval mapping: procedures and guidelines for using Windows QTL Cartographer. Methods in molecular biology (Clifton, N.J.) **871**

Simon M., Loudet O., Durand S., Berard A., Brunel D., Sennesal F. X., Durand-Tardif M., Pelletier G., and Camilleri C. (2008). Quantitative trait loci mapping in five new large recombinant inbred line populations of *Arabidopsis thaliana* genotyped with consensus single-nucleotide polymorphism markers. Genetics **178:** 2253-2264.

Simon M., Simon A., Martins F., Botran L., Tisne S., Granier F., Loudet O., and Camilleri C. (2012). DNA fingerprinting and new tools for fine-scale discrimination of *Arabidopsis thaliana* accessions. Plant Journal **69:** 1094-1101.

Sitte P., Weiler E. W., Kadereit J. W., Bresinsky A., and Koerner C. (2002). Strasburger - Lehrbuch der Botanik, Ed 35. Spektrum Akademischer Verlag, Heidelberg.

Spalding E. P., Hirsch R. E., Lewis D. R., Qi Z., Sussman M. R., and Lewis B. D. (1999). Potassium uptake supporting plant growth in the absence of AKT1 channel activity - Inhibition by ammonium and stimulation by sodium. Journal of General Physiology **113:** 909-918.

Stahl Y., and Simon R. (2010). Plant primary meristems: shared functions and regulatory mechanisms. Current Opinion in Plant Biology **13:** 53-58.

Stahl Y., Wink R. H., Ingram G. C., and Simon R. (2009). A Signaling Module Controlling the Stem Cell Niche in Arabidopsis Root Meristems. Current Biology **19:** 909-914.

Stevenson-Paulik J., Bastidas R. J., Chiou S. T., Frye R. A., and York J. D. (2005). Generation of phytate-free seeds in Arabidopsis through disruption of inositol polyphosphate kinases. Proceedings of the National Academy of Sciences of the United States of America **102:** 12612-12617.

Strange A., Li P., Lister C., Anderson J., Warthmann N., Shindo C., Irwin J., Nordborg M., and Dean C. (2011). Major-Effect Alleles at Relatively Few Loci Underlie Distinct Vernalization and Flowering Variation in Arabidopsis Accessions. Plos One **6:** e19949.

Sutton S. R., Bertsch P. M., Newville M., Rivers M., Lanzirotti A., and Eng P. (2002). Microflourescence and microtomography analyses of heterogeneous earth and environmental materials. *In* PA Fenter, ML Rivers, NC Sturchio, SR Sutton, eds, Reviews in Mineralogy and Geochemistry, Vol 49. Mineralogical Society of America, Chantilly, VA, pp 429-483.

Svistoonoff S., Creff A., Reymond M., Sigoillot-Claude C., Ricaud L., Blanchet A., Nussaume L., and Desnos T. (2007). Root tip contact with low-phosphate media reprograms plant root architecture. Nature Genetics **39:** 792-796.

Swarup K., Benkova E., Swarup R., Casimiro I., Peret B., Yang Y., Parry G., Nielsen E., De Smet I., Vanneste S., Levesque M. P., Carrier D., James N., Calvo V., Ljung K., Kramer E., Roberts R., Graham N., Marillonnet S., Patel K., Jones J. D. G., Taylor C. G., Schachtman D. P., May S., Sandberg G., Benfey P., Friml J., Kerr I., Beeckman T., Laplaze L., and Bennett M. J. (2008). The auxin influx carrier LAX3 promotes lateral root emergence. Nature Cell Biology **10:** 946-954.

Swarup R., Kramer E. M., Perry P., Knox K., Leyser H. M. O., Haseloff J., Beemster G. T. S., Bhalerao R., and Bennett M. J. (2005). Root gravitropism requires lateral root cap and epidermal cells for transport and response to a mobile auxin signal. Nature Cell Biology **7:** 1057-1065.

Szczerba M. W., Britto D. T., Ali S. A., Balkos K. D., and Kronzucker H. J. (2008). NH4+-stimulated and -inhibited components of K+ transport in rice (*Oryza sativa* L.). Journal of Experimental Botany **59:** 3415-3423.

Szczerba M. W., Britto D. T., and Kronzucker H. J. (2006). Rapid, futile K+ cycling and pool-size dynamics define low-affinity potassium transport in barley. Plant Physiology **141:** 1494-1507.

Takabatake R., Hata S., Taniguchi M., Kouchi H., Sugiyama T., and Izui K. (1999). Isolation and characterization of cDNAs encoding mitochondrial phosphate transporters in soybean, maize, rice, and Arabidopsis. Plant Molecular Biology **40:** 479-486.

Tejada-Jimenez M., Galvan A., Fernandez E., and Llamas A. (2009). Homeostasis of the micronutrients Ni, Mo and Cl with specific biochemical functions. Current Opinion in Plant Biology **12:** 358-363.

Thibaud M. C., Arrighi J. F., Bayle V., Chiarenza S., Creff A., Bustos R., Paz-Ares J., Poirier Y., and Nussaume L. (2010). Dissection of local and systemic transcriptional responses to phosphate starvation in Arabidopsis. Plant Journal **64:** 775-789.

Thitamadee S., Tuchihara K., and Hashimoto T. (2002). Microtubule basis for left-handed helical growth in Arabidopsis. Nature **417:** 193-196.

Thomine S., and Lanquar V. (2011). Iron Transport and Signaling in Plants. *In* Transporters and Pumps in Plant Signaling. Springer Verlag, Berlin, pp 99-131.

Ticconi C. A., Lucero R. D., Sakhonwasee S., Adamson A. W., Creff A., Nussaume L., Desnos T., and Abel S. (2009). ER-resident proteins PDR2 and LPR1 mediate the developmental response of root meristems to phosphate availability. Proceedings of the National Academy of Sciences of the United States of America **106:** 14174-14179.

Topp C. N., Iyer-Pascuzzi A. S., Anderson J. T., Lee C. R., Zurek P. R., Symonova O., Zheng Y., Bucksch A., Mileyko Y., Galkovskyi T., Moore B. T., Harer J., Edelsbrunner H., Mitchell-Olds T., Weitz J. S., and Benfey P. N. (2013). 3D phenotyping and quantitative trait locus mapping identify core regions of the rice genome controlling root architecture. Proceedings of the National Academy of Sciences of the United States of America **110:** E1695-E1704.

Trachsel S., Kaeppler S. M., Brown K. M., and Lynch J. P. (2011). Shovelomics: high throughput phenotyping of maize (*Zea mays* L.) root architecture in the field. Plant and Soil **341:** 75-87.

Tran H. T., Hurley B. A., and Plaxton W. C. (2010). Feeding hungry plants: The role of purple acid phosphatases in phosphate nutrition. Plant Science **179:** 14-27.

Troufflard S., Mullen W., Larson T. R., Graham I. A., Crozier A., Amtmann A., and Armengaud P. (2010). Potassium deficiency induces the biosynthesis of oxylipins and glucosinolates in *Arabidopsis thaliana*. BMC Plant Biology **10:** 172.

Tsay Y. F., Chiu C. C., Tsai C. B., Ho C. H., and Hsu P. K. (2007). Nitrate transporters and peptide transporters. Febs Letters **581:** 2290-2300.

Tsay Y. F., Ho C. H., Chen H. Y., and Lin S. H. (2011). Integration of Nitrogen and Potassium Signaling. *In* Annual Review of Plant Biology, Vol 62. ANNUAL REVIEWS, Palo Alto, pp 207-226.

Tsay Y. F., Schroeder J. I., Feldmann K. A., and Crawford N. M. (1993). The Herbicide Sensitivity Gene Chl1 of Arabidopsis Encodes a Nitrate-Inducible Nitrate Transporter. Cell **72:** 705-713.

Tsukagoshi H., Busch W., and Benfey P. N. (2010). Transcriptional Regulation of ROS Controls Transition from Proliferation to Differentiation in the Root. Cell **143:** 606-616.

Tuinstra M. R., Ejeta G., and Goldsbrough P. B. (1997). Heterogeneous inbred family (HIF) analysis: a method for developing near-isogenic lines that differ at quantitative trait loci. Theoretical and Applied Genetics **95:** 1005-1011.

Turlapati P. V., Kim K. W., Davin L. B., and Lewis N. G. (2011). The laccase multigene family in *Arabidopsis thaliana*: towards addressing the mystery of their gene function(s). Planta **233:** 439-470.

Tyburski J., Dunajska K., and Tretyn A. (2009). Reactive oxygen species localization in roots of *Arabidopsis thaliana* seedlings grown under phosphate deficiency. Plant Growth Regulation **59:** 27-36.

Ubeda-Tomas S., Beemster G. T. S., and Bennett M. J. (2012). Hormonal regulation of root growth: integrating local activities into global behaviour. Trends in Plant Science **17:** 326-331.

Ubeda-Tomas S., Swarup R., Coates J., Swarup K., Laplaze L., Beemster G. T. S., Hedden P., Bhalerao R., and Bennett M. J. (2008). Root growth in Arabidopsis requires gibberellin/DELLA signalling in the endodermis. Nature Cell Biology **10:** 625-628.

Van As H. (2007). Intact plant MRI for the study of cell water relations, membrane permeability, cell-to-cell and long distance water transport. Journal of Experimental Botany **58:** 743-756.

Vance C. P., Uhde-Stone C., and Allan D. L. (2003). Phosphorus acquisition and use: critical adaptations by plants for securing a nonrenewable resource. New Phytologist **157:** 423-447.

Versaw W. K., and Harrison M. J. (2002). A chloroplast phosphate transporter, PHT2;1, influences allocation of phosphate within the plant and phosphate-starvation responses. Plant Cell **14:** 1751-1766.

Vert G., Grotz N., Dedaldechamp F., Gaymard F., Guerinot M. L., Briat J. F., and Curie C. (2002). IRT1, an Arabidopsis transporter essential for iron uptake from the soil and for plant growth. Plant Cell **14:** 1223-1233.

Vidal E. A., Araus V., Lu C., Parry G., Green P. J., Coruzzi G. M., and Gutierrez R. A. (2010). Nitrate-responsive miR393/AFB3 regulatory module controls root system architecture in *Arabidopsis thaliana*. Proceedings of the National Academy of Sciences of the United States of America **107:** 4477-4482.

Vlad D., Rappaport F., Simon M., and Loudet O. (2010). Gene Transposition Causing Natural Variation for Growth in *Arabidopsis thaliana*. Plos Genetics **6:** e1000945.

Voinnet O., Rivas S., Mestre P., and Baulcombe D. (2003). An enhanced transient expression system in plants based on suppression of gene silencing by the p19 protein of tomato bushy stunt virus. Plant Journal **33:** 949-956.

Vreugdenhil D., Aarts M. G. M., Koornneef M., Nelissen H., and Ernst W. H. O. (2004). Natural variation and QTL analysis for cationic mineral content in seeds of *Arabidopsis thaliana*. Plant Cell and Environment **27:** 828-839.

Walch-Liu P., and Forde B. G. (2008). Nitrate signalling mediated by the NRT1.1 nitrate transporter antagonises L-glutamate-induced changes in root architecture. Plant Journal **54:** 820-828.

Walch-Liu P., Liu L., Remans T., Tester M., and Forde B. G. (2006). Evidence that L-glutamate can act as an exogenous signal to modulate root growth and branching in *Arabidopsis thaliana*. Plant and Cell Physiology **47:** 1045-1057.

Wallace A., Berry W. L., and Alexander G. V. (1981). Iron, Nitrogen and Phosphorus Interactions in 2 Cultivars of Soybeans Grown in a Calcareous Soil. Journal of Plant Nutrition **3:** 625-635.

Wallace A., and Romney E. M. (1980). Some Problems in the Study of Simultaneous Multiple Nutrient Deficiencies in Plants. Journal of Plant Nutrition **2:** 213-216.

Wang L. S., Dong J. S., Gao Z. Y., and Liu D. (2012a). The Arabidopsis gene HYPERSENSITIVE TO PHOSPHATE STARVATION 3 encodes ETHYLENE OVERPRODUCTION 1. Plant and Cell Physiology **53:** 1093-1105.

Wang R. C., Okamoto M., Xing X. J., and Crawford N. M. (2003). Microarray analysis of the nitrate response in Arabidopsis roots and shoots reveals over 1,000 rapidly responding genes and new linkages to glucose, trehalose-6-phosphate, iron, and sulfate metabolism. Plant Physiology **132:** 556-567.

Wang S., Basten C. J., and Zeng Z.-B. (2011a). Windows QTL Cartographer 2.5. Department of Statistics, North Carolina State University, Raleigh, NC.

Wang W., Xu B., Wang H., Li J. Q., Huang H., and Xu L. (2011b). YUCCA Genes Are Expressed in Response to Leaf Adaxial-Abaxial Juxtaposition and Are Required for Leaf Margin Development. Plant Physiology **157:** 1805-1819.

Wang X. M., Du G. K., Meng Y. J., Li Y. Y., Wu P., and Yi K. K. (2010a). The Function of LPR1 is Controlled by an Element in the Promoter and is Independent of SUMO E3 Ligase SIZ1 in Response to Low Pi Stress in *Arabidopsis thaliana*. Plant and Cell Physiology **51:** 380-394.

Wang Y., He L., Li H. D., Xu J. A., and Wu W. H. (2010b). Potassium channel alpha-subunit AtKC1 negatively regulates AKT1-mediated K+ uptake in Arabidopsis roots under low-K+ stress. Cell Research **20:** 826-837.

Wang Y., Papanatsiou M., Eisenach C., Karnik R., Williams M., Hills A., Lew V.L., and Blatt M.R. (2012b). Systems dynamic modeling of a guard cell Cl- channel mutant uncovers an emergent homeostatic network regulating stomatal transpiration. Plant Physiology **160:** 1956-1967.

Wang Y., and Wu W.-H. (2013). Potassium transport and signaling in higher plants. Annual Review of Plant Biology **64:** 451-476.

Wang Y. Y., and Tsay Y. F. (2011). Arabidopsis Nitrate Transporter NRT1.9 Is Important in Phloem Nitrate Transport. Plant Cell **23:** 1945-1957.

Ward J. T., Lahner B., Yakubova E., Salt D. E., and Raghothama K. G. (2008). The effect of iron on the primary root elongation of Arabidopsis during phosphate deficiency. Plant Physiology **147:** 1181-1191.

Weaver J. E. (1925). Investigations on the root habits of plants. American Journal of Botany **12:** 502-509.

Weigel D. (2012). Natural Variation in Arabidopsis: From Molecular Genetics to Ecological Genomics. Plant Physiology **158:** 2-22.

Weigel D., and Mott R. (2009). The 1001 Genomes Project for Arabidopsis thaliana. Genome Biology **10:** 107.

Weijers D., Schlereth A., Ehrismann J. S., Schwank G., Kientz M., and Jurgens G. (2006). Auxin triggers transient local signaling for cell specification in Arabidopsis embryogenesis. Developmental Cell **10:** 265-270.

Wells D. M., French A. P., Naeem A., Ishaq O., Traini R., Hijazi H., Bennett M. J., and Pridmore T. P. (2012). Recovering the dynamics of root growth and development using novel image acquisition and analysis methods. Philosophical Transactions of the Royal Society B - Biological Sciences **367:** 1517-1524.

White P. J., and Brown P. H. (2010). Plant nutrition for sustainable development and global health. Annals of Botany **105:** 1073-1080.

Williamson L. C., Ribrioux S., Fitter A. H., and Leyser H. M. O. (2001). Phosphate availability regulates root system architecture in Arabidopsis. Plant Physiology **126:** 875-882.

Winter D., Vinegar B., Nahal H., Ammar R., Wilson G. V., and Provart N. J. (2007). An "Electronic Fluorescent Pictograph" Browser for Exploring and Analyzing Large-Scale Biological Data Sets. Plos One **2:** e718.

Wirth J., Chopin F., Santoni V., Viennois G., Tillard P., Krapp A., Lejay L., Daniel-Vedele F., and Gojon A. (2007). Regulation of root nitrate uptake at the NRT2.1 protein level in *Arabidopsis thaliana*. Journal of Biological Chemistry **282:** 23541-23552.

Wu Y., Hu Y., and Xu G. (2009). Interactive effects of potassium and sodium on root growth and expression of K/Na transporter genes in rice. Plant Growth Regulation **57:** 271-280.

Wu Y., Zhao Q., Gao L., Yu X. M., Fang P., Oliver D. J., and Xiang C. B. (2010). Isolation and characterization of low-sulphur-tolerant mutants of Arabidopsis. Journal of Experimental Botany **61:** 3407-3422.

Xu J., Li H. D., Chen L. Q., Wang Y., Liu L. L., He L., and Wu W. H. (2006). A protein kinase, interacting with two calcineurin B-like proteins, regulates K+ transporter AKT1 in Arabidopsis. Cell **125:** 1347-1360.

Xu J., Yin H. X., Li Y. L., and Liu X. J. (2010). Nitric Oxide Is Associated with Long-Term Zinc Tolerance in *Solanum nigrum*. Plant Physiology **154:** 1319-1334.

Xu W. F., Ding G. C., Yokawa K., Baluska F., Li Q. F., Liu Y. G., Shi W. M., Liang J. S., and Zhang J. H. (2013). An improved agar-plate method for studying root growth and response of *Arabidopsis thaliana*. Scientific Reports **3:** 1273.

Yi Y., and Guerinot M. L. (1996). Genetic evidence that induction of root Fe(III) chelate reductase activity is necessary for iron uptake under iron deficiency. Plant Journal **10:** 835-844.

Yokawa K., Kagenishi T., and Baluska F. (2013). Root photomorphogenesis in laboratory-maintained Arabidopsis seedlings. Trends in Plant Science **18:** 117-119.

Yong Z. H., Kotur Z., and Glass A. D. M. (2010). Characterization of an intact two-component high-affinity nitrate transporter from Arabidopsis roots. Plant Journal **63:** 739-748.

Yoshimoto N., Takahashi H., Smith F. W., Yamaya T., and Saito K. (2002). Two distinct high-affinity sulfate transporters with different inducibilities mediate uptake of sulfate in Arabidopsis roots. Plant Journal **29:** 465-473.

Yuen C. Y. L., Sedbrook J. C., Perrin R. M., Carroll K. L., and Masson P. H. (2005). Loss-of-function mutations of ROOT HAIR DEFECTIVE3 suppress root waving, skewing, and epidermal cell file rotation in Arabidopsis. Plant Physiology **138:** 701-714.

Zeng H. Q., Liu G., Kinoshita T., Zhang R. P., Zhu Y. Y., Shen Q. R., and Xu G. H. (2012). Stimulation of phosphorus uptake by ammonium nutrition involves plasma membrane H+ ATPase in rice roots. Plant and Soil **357:** 205-214.

Zhang H. M., and Forde B. G. (1998). An Arabidopsis MADS box gene that controls nutrient-induced changes in root architecture. Science **279:** 407-409.

Zhang H. M., Jennings A., Barlow P. W., and Forde B. G. (1999). Dual pathways for regulation of root branching by nitrate. Proceedings of the National Academy of Sciences of the United States of America **96:** 6529-6534.

Zhang X. R., Henriques R., Lin S. S., Niu Q. W., and Chua N. H. (2006). Agrobacterium-mediated transformation of *Arabidopsis thaliana* using the floral dip method. Nature Protocols **1:** 641-646.

Zhao Y., Hu Y. F., Dai M. Q., Huang L. M., and Zhou D. X. (2009). The WUSCHEL-Related Homeobox Gene WOX11 Is Required to Activate Shoot-Borne Crown Root Development in Rice. Plant Cell **21:** 736-748.

Zhu J. M., Ingram P. A., Benfey P. N., and Elich T. (2011). From lab to field, new approaches to phenotyping root system architecture. Current Opinion in Plant Biology **14:** 310-317.

Zhu Y., Di T., Xu G., Chen X., Zeng H., Yan F., and Shen Q. (2009). Adaptation of plasma membrane H+-ATPase of rice roots to low pH as related to ammonium nutrition. Plant Cell and Environment **32:** 1428-1440.

APPENDIX I

Day 10 **Day 14**

P [mM]

0.80	0.70	0.76	0.95
0.72	0.68	0.75	0.84
0.79	0.72	0.72	0.77

1.36	0.94	0.90	1.07
1.24	0.79	0.88	1.08
0.88	0.82	0.86	1.01

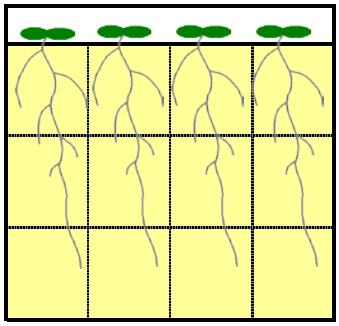

K [mM]

2.28	1.99	2.07	2.38
2.13	1.96	2.04	2.11
2.12	2.01	1.99	2.13

3.53	2.61	2.34	2.56
3.49	2.31	2.54	2.89
2.50	2.49	2.32	2.62

H_2O [% of initial]

53%	55%	52%	41%
85%	80%	74%	66%
99%	92%	85%	83%

56%	61%	56%	40%
74%	74%	68%	57%
79%	75%	69%	62%

Supplemental Figure I: A gradient of phosphate and potassium concentrations builds up on agar plates during seedling growth. Phosphate (P) and potassium (K) was extracted from squares of agar sampled on DAG 10 (left) or DAG 14 (middle) using 1 M HCl and quantified with ICP-MS (upper row). All concentrations were higher than the original (0.5 mM P; 2 mM K) supplemented to the medium. Water content on plates was approximated by weight of agar squares as % of the original weight of the square. Water loss can explain the increase in concentration, especially in the upper part of the plate. A sketch of a typical plate with four plants grown on the agar surface on DAG 14 is shown on the top right. P and K concentrations and water contents are averages of two independent experiments. In each experiment, samples taken from corresponding squares of three plates were pooled before analysis.

APPENDIX II

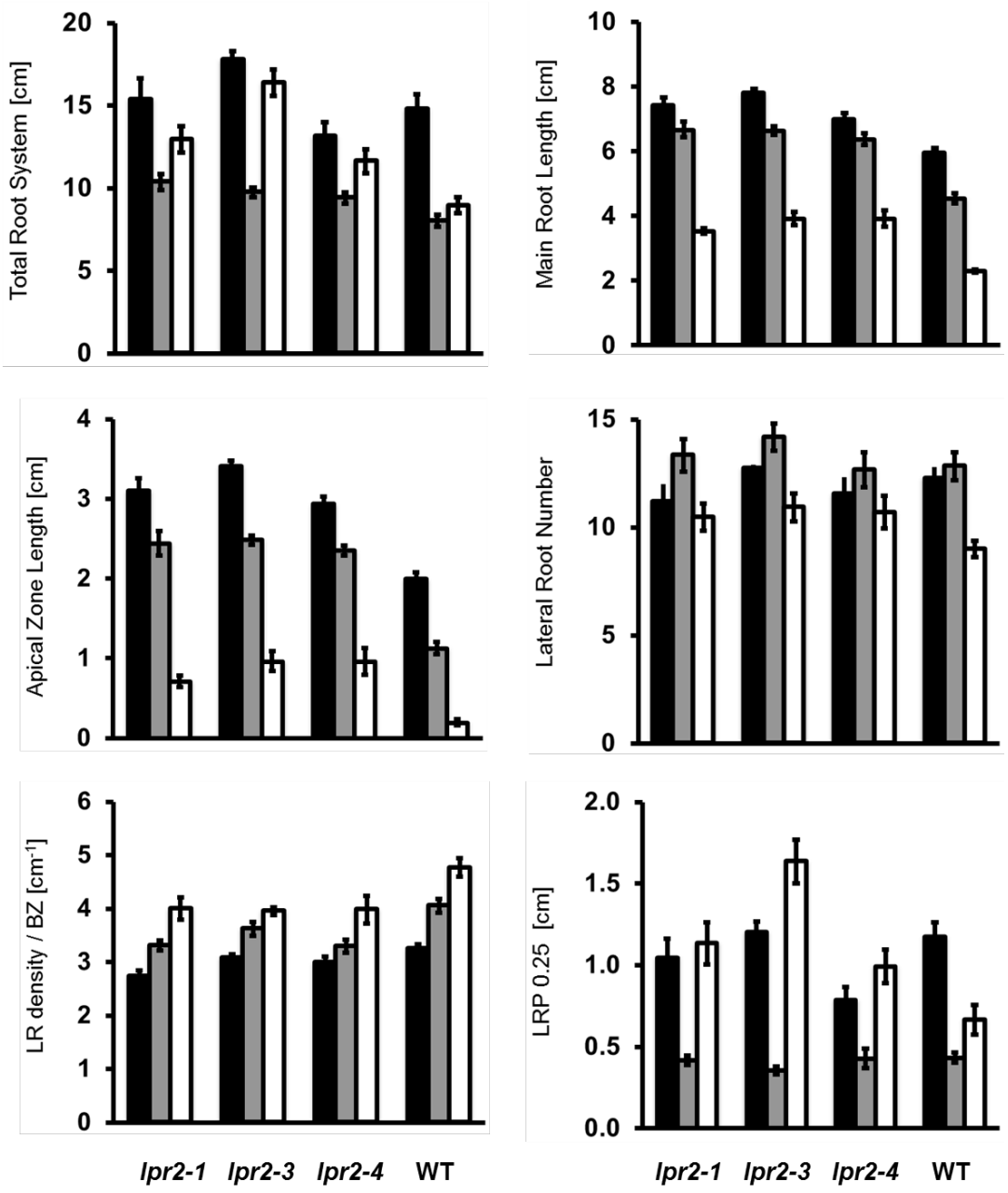

Supplemental Figure II: Confirmation of the low-K insensitive phenotype of *lpr2* with two additional LPR2 knockout lines.
Absolute means ± S.E.M. (n = 10 to 18 seedlings per genotype per condition) corresponding to relative data shown in Figure 50.

APPENDIX III

Publication:

Kellermeier, F., Chardon, F., and Amtmann, A. (2013). Natural variation of Arabidopsis root architecture reveals complementing adaptive strategies to potassium starvation. Plant Physiology **161:** 1421-1432.

APPENDIX IV

Publication:

Kellermeier F., and Amtmann A. (2013). Phenotyping jasmonate regulation of root growth. Methods in Molecular Biology (Clifton, N.J.) **1011:** 25-32.

[proof version]

ELECTRONIC APPENDIX

The electronic appendix contains raw data (Excel spreadsheets) which can be accessed upon request.

email: **f.kellermeier.1@research.gla.ac.uk**

List of electronic documents

Chapter 2

Ch2_number codes for media.xls

Chapter 3

Ch3_Microarray response genes - 4-fold cutoff.xlsx

Ch3_NPKS microarray.xls

Ch3_NPKS root architecture.xls

Chapter 4

Ch4_Natural variation of root architecture responses to low-K.xls

Ch4_QTL analysis of the low-K reponse.xls

Ch4_QTL positions.xls

Chapter 6

Ch6_Mutant Analysis